Journal of Polymer Science: Part C, Polymer Symposia, No. 5

Rheo-optics of Polymers

Held under the auspices of the
Polymer Research Institute
Amherst, Massachusetts, August 24, 1963

edited by *Richard S. Stein*

Polymer Research Institute, Amherst, Massachusetts

published 1964 by INTERSCIENCE PUBLISHERS a division of John Wiley & Sons, Inc.

No. 5

Journal of Polymer Science, Part C, POLYMER SYMPOSIA

Rheo-optics of Polymers

edited by RICHARD S. STEIN

Polymer Research Institute,
Amherst, Massachusetts

Held under the auspices of the
Polymer Research Institute
Amherst, Massachusetts, August 24, 1963

published by INTERSCIENCE PUBLISHERS,
a division of John Wiley

JOURNAL ON POLYMER SCIENCE, PART C, *Polymer Symposia*

Editors: H. MARK C. G. OVERBERGER R. S. STEIN

Editorial Board: R. M. FUOSS J. J. HERMANS

H. W. MELVILLE G. SMETS

Published at irregular intervals by Interscience Publishers, a Division of John Wiley & Sons, Inc. Publication Office at 20th and Northampton Streets, Easton, Pennsylvania. Executive, Editorial, and Circulation Offices at 605 Third Avenue, New York, New York 10061. Subscription price, $225.00 per volume (including Part A: General Papers; and Part B: Polymer Letters). Foreign postage, $5.00 per volume (including Parts A and B).

Copyright © 1964, by John Wiley & Sons, Inc., Printed in U.S.A.

Introductory Remarks

A conference on "Rheo-optics of Polymers" was held on Saturday, August 24 at the University of Massachusetts. This conference, jointly sponsored by the Division of High Polymer Physics of the American Physical Society and the Polymer Research Institute of the University of Massachusetts, was attended by over 100 representatives of universities and industry from this country and abroad. It was jointly organized by Professor Rodney D. Andrews of the Massachusetts Institute of Technology, Dr. Donald G. LeGrand of the General Electric Research Laboratories, and Professor Richard S. Stein, Director of the Polymer Research Institute of the University.

"Rheo-optics" is a new term designating the use of optical methods to study flow. This conference was concerned with the use of these methods for the study of the flow and deformation of polymers. Methods used included birefringence, x-ray diffraction, dichroism, and light scattering.

The association of these optical methods with standard rheological methods aids in the elucidation of mechanisms responsible for their behavior. The study of the time-dependence of the optical behavior often permits a determination of the rates of the contributing mechanisms.

Samples studied in the papers presented at this symposium included polymers in the form of solutions, melts, and amorphous and crystalline solids. These were studied under conditions of flow, rotational and vibrational strain, steady state deformation, relaxation, and creep.

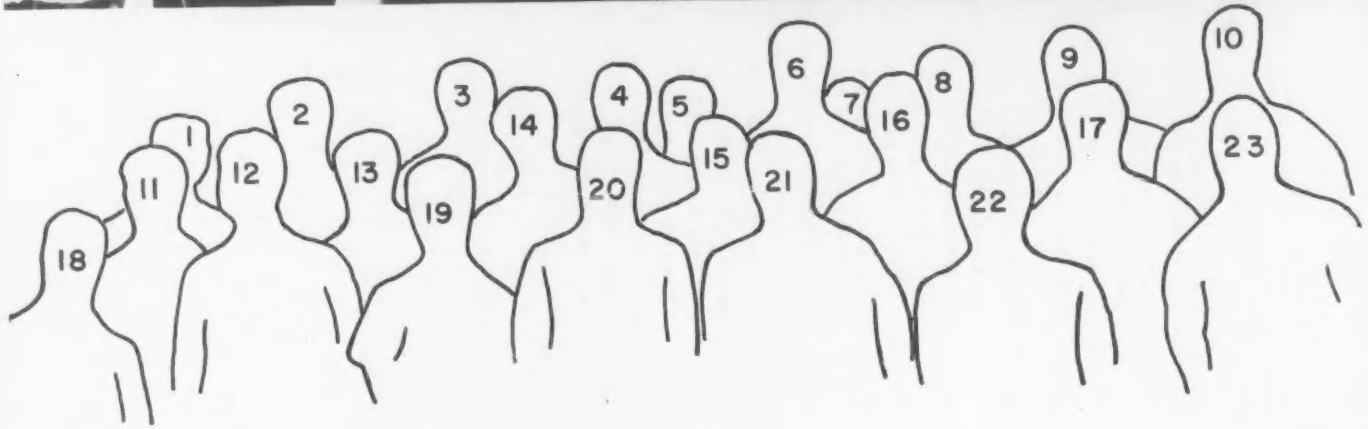
1
2
3
4
5
6
7
8
9
10
11
12
13
14
15
16
17
18
19
20
21
22
23

1. Makoto Hachiboshi
Toyobo New York, Inc.
New York, New York

2. Kigen Kawai
Kurashiki Rayon Company
Umeda, Kita-Ku
Osaka, Japan

3. Bryan Read
Basic Physics Division
National Physical Laboratory
Teddington, Middlesex, England

4. Peter Erhardt
Polymer Research Institute
University of Massachusetts
Amherst, Massachusetts

5. Daniel Sullivan
Shawinigan Resins
Springfield, Massachusetts

6. Ellis H. Dill
College of Engineering
University of Washington
Seattle, Washington

7. Unidentified

8. Ernest E. Lindsey
Engineering Department
University of Massachusetts
Amherst, Massachusetts

9. T. J. Hammack
Department of Mechanical Engineering
Massachusetts Institute of Technology
Cambridge, Mass.

10. W. Philippoff
Esso Research and Engineering Co.
Linden, New Jersey

11. Y. Ohyanagi
Kurashiki Rayon Company
Umeda, Kita-Ku
Osaka, Japan

12. Masao Horio
Department of Polymer Chemistry
Kyoto University
Kyoto, Japan

13. M. Takayanagi
Kyushu University
Fukuoka-Shi, Japan

14. James Lyons
Textile Research Institute
Princeton, New Jersey

15. Harold Wayland
California Institute of Technology
Pasadena, California

16. John Tordella
Electrochemicals Department
DuPont Experimental Station
Wilmington, Delaware

17. Robert Moore
Bell Telephone Laboratory, Inc.
Murray Hill, New Jersey

18. Richard S. Stein
Polymer Research Institute
University of Massachusetts
Amherst, Massachusetts

19. Hiromichi Kawai
Department of Polymer Chemistry
Kyoto University
Kyoto, Japan

20. Donald LeGrand
General Electric Research Laboratory
Schenectady, New York

21. Rodney Andrews
Textile Division
Department of Mechanical Engineering
Massachusetts Institute of Technology
Cambridge, Massachusetts

22. Shiro Matsuoka
Bell Telephone Laboratory, Inc.
Murray Hill, New Jersey

23. Donald C. Bogue
Department of Chemical Engineering
University of Tennessee
Knoxville, Tennessee

Contents

W. Philippoff: Streaming Birefringence of Polymer Solutions 1

Harold Wayland: Streaming Birefringence as a Rheological Research Tool 11

F. N. Peebles, J. W. Prados, and E. H. Honeycutt, Jr.: Birefringent and Rheologic Properties of Milling Yellow Suspensions 37

E. E. Lindsey, D. C. Chappelear, D. M. Sullivan, and V. A. Augstkalns: Particle Size Distribution in Dilute Liquid/Liquid Dispersions by Light Scattering 55

Ellis Harold Dill: On Phenomenological Rheo-Optic Constitutive Relations 67

Chintakindi L. Amba-Rao: Stress-Strain-Time-Birefringence Relations in Photoelastic Plastics with Creep 75

B. E. Read: Dynamic Birefringence of Amorphous Polymers 87

R. D. Andrews and T. J. Hammack: Temperature Dependence of Orientation Birefringence of Polymers in the Glassy and Rubbery States 101

Motowo Takayanagi, Shinsaku Uemura, and Shunsuke Minami: Application of Equivalent Model Method to Dynamic Rheo-Optical Properties of Crystalline Polymer 113

R. Yamada, C. Hayashi, S. Onogi, and M. Horio: Dynamic Birefringence of Several High Polymers 123

K. Sasaguri and R. S. Stein: Dynamic Birefringence of Polyolefins 139

D. G. Legrand and W. R. Haaf: Rheo-Optical Properties of Polymers. X. Relaxation 153

Robert S. Moore and Shiro Matsuoka: Morphological and Rheological Studies of Polyethylene by Light Scattering 163

Peter Erhardt, K. Sasaguri, and R. S. Stein: Studies of Rates of Spherulite Deformation by Low-Angle Light Scattering 179

Author Index 191

Subject Index 192

JOURNAL OF POLYMER SCIENCE: PART C NO. 5, PP. 1-9

Streaming Birefringence of Polymer Solutions

W. PHILIPPOFF, *Products Research Division, Esso Research and Engineering Co., Linden, New Jersey*

Synopsis

Streaming or flow-birefringence is the optical anisotropy induced by laminar flow in liquids. The optical anisotropy can be described by an optical tensor which is coaxial with the stress tensor in an elastic material In a tension experiment this is obvious. In laminar flow this has been proved by investigating the distribution of the birefringence in three directions of space. The amount of anisotropy, usually described by the degree of birefringence Δn, is proportional to the difference in principal stresses of the mechanical stress tensor in a very large range of variables, therefore giving the possibility of using optical measurements for the determination of mechanical stresses. However, the relationship is valid either for concentrated solutions or for conditions where the solvent and the polymer have essentially the same index of refraction n—a condition usually termed matching solvent. The proportionality constant between the difference in principal stresses and Δn—the stress-optical coefficient C—is, as also follows from theory, independent of concentration, shear stress temperature, molecular weight and its distribution, only determined by the structure of the monomer unit and its n. Another quantity in flow birefringence is the so-called extinction angle which is measured between the direction of the principal optical axis and the direction of flow. A reasonable amount of experimental data has been obtained to show that this angle can be quantitatively correlated with the so-called "recoverable shear" that is the shear component of the elastic strain tensor in laminar flow. Therefore, the experimental determination of the angle gives a measure of the elastic strain. A survey of the experimental results in the field shows the generalities of this approach in a variety of polymer and solvent systems.

The birefringence induced by mechanical stresses in transparent solids has been used for more than half a century as a tool for determining stress distributions in models of structures under steady loading.[1-3] The basis of such studies lies in the observance that the amount of birefringence Δn is exactly proportional to the tensile stress in the sample or more exactly Δn is proportional to the difference in principal stresses, and is oriented in the direction of the principal tensile stress. This relationship is called the stress-optical law, the proportionality constant is called the stress-optical coefficient C, and is measured in Brewsters (10^{-13} cgs). A similar birefringence occurs during the flow of liquids and is usually termed streaming or flow birefringence. It has been widely ascribed to the orientation and deformation of the coiled molecules in a polymer solution. In this review, a molecular origin of the birefringence will not be discussed, but the continuum-mechanical aspects of the problem will be described in order to

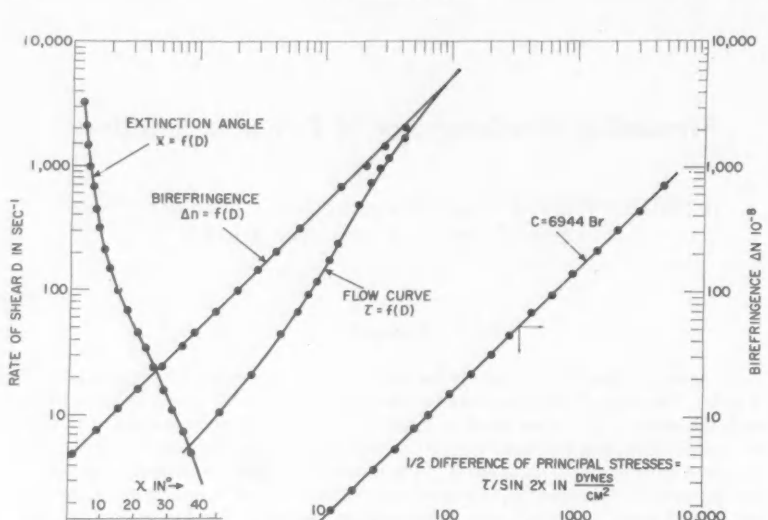

Fig. 1. Flow-birefringence experiments (Δn and χ) as well as flow curve (τ) for a 1 vol. % solution of polystyrene ($M = 9 \times 10^6$) in bromoform. Flow curve recalculated for concentric cylinder device from capillary data. $\eta_{rel} = 88$; right curve Δn versus Δp.

emphasize the possibility of applying stress-optical analysis to liquids, whereas up to now it has predominantly been used for solids.

The main difficulty is that the stressing of a liquid is a three dimensional phenomenon, distinct from the case of solids, in which the stress is in one direction only. In order to overcome the difficulties the stressing is usually performed experimentally in two dimensions (comparable to the method used in solid models) with the third dimension of the sample in the direction of the beam of light being very large compared to the others. The description of the optical phenomenon has generally been made using the tensor of polarizability of the material. The difference of the principal axes of this tensor determines a quantity called the degree of birefringence, Δn and the orientation of the principal axis of the polarizability tensor towards the direction of flow is called the extinction angle χ. With solids the direction of the principal axis of stress is given directly by the direction of the applied stress, but with the flowing solution, this is not generally the case. To obtain the direction of the principal tensile stress in flowing viscoelastic liquids Lodge[4] suggested the application of the stress-optical law, used hitherto only for solids. The direction of the principal stress is therefore coincident with that of the polarizability tensor. Both are inclined to the direction of flow at the extinction angle χ which changes with the rate of shear. The major axis of the tensor of the rate of

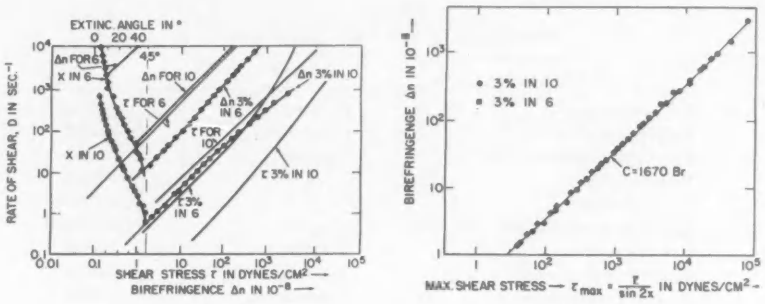

Fig. 2. (*a*) Flow-birefringence experiments and flow curve for 3% solution of Vistanex B-100 polyisobutylene in matching solvents: 6-Decalin 10-White oil of 150 cp; (*b*) plot of Δn versus Δp for experiments in Figure 2*a*.

deformation in liquids, however, is always inclined to the direction of flow by an angle of 45°. There exists therefore between the axes of these tensors a finite angle, as was emphasized by Weissenberg[5] some years ago. A derivation showing that the direction of the principal axis of deformation is inclined under the same angle χ has been formulated using the theory of finite elastic deformations.[6] This, of course, requires that the streaming solutions acquire elastic properties. The fact that a polymer solution does indeed have an elastic energy in flow is not widely accepted even though it was suggested many years ago. A physical explanation for its origin has been suggested by Mooney:[7] relaxation of a viscoelastic material occurs at a rate dependent on the material, and when it is stressed at a rate determined by the instrument this leads to a condition of elastic stress. The resultant elastic state of stress can then be described by the use of the theory of finite elastic deformations of elastic bodies.

The investigation of polymer solutions using this general idea leads to (*a*) the determination of the relation between Δn and the difference in principal stresses Δp and (*b*) the correlation of the extinction angle χ with the degree of elastic strain.

The application of the stress-optical law requires a proportionality of Δn and Δp for a flowing solution, Δp being equal to $2\tau/\sin 2\chi$, where τ is the shear stress applied. This has been proved in very numerous experiments, as shown in Figures 1 and 2 for polystyrene and polyisobutylene[8] solutions. It is quite important to note that in the case of polymer solutions τ, χ, and Δn can all be nonlinear functions of the rate of shear D; but in all cases the proportionality of Δn and Δp, (i.e., a constant stress optical coefficient C) has been obtained. This proportionality is valid over 3–4 decades of Δp or Δn. It must be emphasized that the $D - \Delta n$ curves, dependent on concentration, molecular weight, and solvent for one and the same polymer, may be linear, rising over-proportionally, or saturating to a limit in the range of investigation. This statement is important, for conclusions as to

TABLE I
Stress-Optical Coefficients C, in Brewsters

Polymer	Solvent	C
Polyisobutylene	Decalin	+1600
Polyvinylacetate	Chloroform	+1000
Polymethylmethacrylate	Benzene	+1000
Polyethylene	—	+2200
Natural rubber	—	+2000
Liquid polyisobutylene	—	+1000–1500
Polybutadiene	Toluene	+3500
Isotactic polystyrene	Bromoform	−10300
Atactic polystyrene	Bromoform	−6800
Poly *p*-chlorostyrene	Bromoform	−12000
Poly 3-4 dichlorostyrene	Bromoform	−12900
Poly 2-5 dichlorostyrene	Bromoform	−6900
Poly 2-5 dimethylstyrene	Bromoform	−8100

the softness or rigidity of dissolved molecules have been made from these curves. Sometimes, as seen in Figure 1, two influences (for example χ and τ) compensate each other so that Δn is proportional to D; when the non-Newtonian behavior ($\tau - D$ curve) is very pronounced a saturation is observed; when the solution is nearly Newtonian a change in χ causes an over-proportional rise of Δn with D (see 3% Vistanex in 10 Fig. 2*a*).

The equation of Kuhn and Kuhn[9] for the molecular origin of the flow birefringence predicts, and experiments have confirmed, that for a given combination of polymer and solvent, C is independent of molecular weight, concentration, and rate of shear within the wide range cited above, and the only important property is the structure of the monomer unit. However, a restriction is imposed in that these simple conditions are valid only when the index of refraction of the polymer is essentially equal to that of the solvent, a condition usually termed matching solvent. Values for C of a variety of polymers are shown in Table I.

The second step, namely the correlation of the extinction angle χ with the degree of elastic strain, has been achieved by the equation $s = 2 \cot 2\chi$ where s is the so-called recoverable shear.[4] The deformation of a spherical volume element of an elastic body in simple shear (similar to laminar flow) to an ellipsoid in a state of elastic strain (affine transform) leads to a difference of the principal axis of strain: $s = \lambda - (1/\lambda)$, or $\lambda = s/2 + \sqrt{s^2/4 + 1} = \cot \chi$ where λ is the ratio of the major axis of the ellipsoid to the diameter of the initial sphere. It is obvious that as soon as the extinction angle χ differs from 45°—the value observed for normal low-molecular-weight liquids—an elastic energy appears. The proof that this is indeed the case is shown in Figure 3[10] where the recoverable shear s for two solutions is measured with three entirely different methods giving it an unquestionable physical reality: (*1*) the flow birefringence—using the extinction angle; (*2*) the Weissenberg Rheogoniometer, using the relations $P_{11} - P_{22} = \tau s$ where $P_{11} - P_{22}$ is the difference of

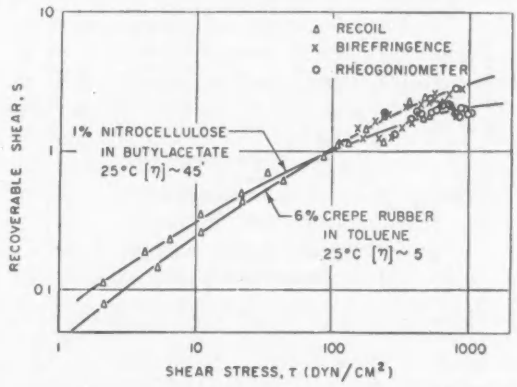

Fig. 3. Recoverable shear $s = f(\tau)$ for a 1% solution of nitrocellulose in butylacetate and for 6% natural rubber in toluene measured by three different methods.

normal stresses along the flow lines and perpendicular to them; (3) the direct measurement of s by the so-called recoil in a rotational viscometer. It is seen that $s = f(\tau)$ is a nonlinear function beginning as a linear relation and saturating at higher values of τ. Many more experimental cases exist where the first two methods were employed in wide ranges of polymers and concentrations, rates of shear, etc., with excellent agreement between the two.

The investigation of a stress distribution in flow using liquids gives, in certain respects, more experimental possibilities than the investigation of solids using the stress-optical law.

The occurrence of a polarizability tensor in the flowing solution, whose main axis is inclined by the angle χ toward the direction of flow leads theoretically to a birefringence to be observed in the three planes:[6] in the 1-2 plane (the one usually observed), the birefringence Δn_{12} and the angle χ_{12} are measured; in the 1-3 plane $\Delta n_{13} = \Delta n_{12} \cos 2\chi_{12}$ and $\chi_{13} = 0$; in the 2-3, Δn_{23} and χ_{23} are both zero. Experiments made in observing the birefringence between two transparent rotating parallel plates indeed showed,[13] see Figure 4, that not only does the expected effect (Δn_{13}) occur but its value is equal to the value precalculated by means of the results obtained in the 1-2 plane, i.e., from Δn_{12} and χ_{12}.

In the theory of the mechanical behavior of polymers the symmetry present in laminar flow leads to an equation $P_{22} = P_{33}$[11] meaning that the stresses normal to the direction of the flow lines are equal. An experimental proof of this relation has been carried out in a fairly complicated instrument by Roberts.[12] Experiments have also been carried out in a capillary,[13] where the flow birefringence looking axially down the capillary in the direction of flow Δn_{23} was observed. The mentioned equality of normal stresses must lead according to the "stress optical law" to an optically isotropic material, i.e., $\Delta n_{23} = 0$. This was indeed the case in all solutions

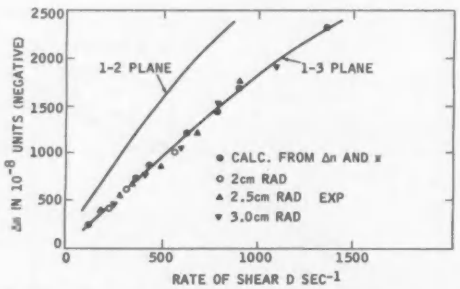

Fig. 4. Flow-birefringence experiments in the 1-2 and 1-3 planes; 30% polystyrene in toluene.

used, whereas the birefringence in the other two planes was considerable, meaning that $P_{22} - P_{33}$ is in any case less than 0.1% of $P_{11} - P_{22}$. In other cases this method gives indeed observable results: solutions or suspensions of solid particles gave a very noticeable optical anisotropy which is observable as a cross of isoclines, giving a qualitative distinction between soft and hard particles. These last two types of experiments have definitely shown that the usual flow-birefringence Δn_{12} adequately describes the polarizability tensor in laminar flow and therefore can alone be considered.

All these relations have been derived for a solution in which the solvent does not contribute to the viscosity or the flow birefringence. When one goes to more dilute solutions, in which the viscosity is commensurable with that of the solvent and the contribution of the birefringence of the solvent is not negligible, the conditions become considerably more complicated but can be analyzed (as has been done in a series of publications[8]).

Reviewing the whole field one sees the flow birefringence of solutions of a viscoelastic material (such as polymer solutions) can be described by the following tensors: (*a*) the rate-of-shear tensor, whose principal axis is 45° to the flow direction; (*b*) the stress tensor, whose shear component is directed in the direction of flow and whose principal tensile axis is directed at the angle χ to the direction of flow; (*c*) the tensor of elastic response or elastic deformation, whose shear component (the recoverable shear s) is the direction of flow and whose principal axis is inclined at the same angle χ as the stress tensor; (*d*) the tensor of polarizability, whose principal axis is also inclined by the angle χ to the direction of flow. In the theory of the flow birefringence of coiled molecules, beginning with Kuhn and Grün[14] the shape of the molecule, deformed in laminar flow, is used to calculate the polarizability tensor of the solution, introducing as a constant the difference of polarizabilities of the statistical element. However, the ratios of axes of these tensors vary widely. The polarizability tensor is nearly spherical because the birefringence is very small as compared to the mean index of refraction or the change in polarizability is negligible as compared to the mean polarizability. The elastic

deformation tensor, as well as the shape of the deformed sphere it describes, deviate strongly from the spherical shape. The ratio of the principal axes of the tensor is: $p = \lambda^2 = \cot^2 \chi$, or for large values of s: $p \div s^2$. The values of p can be quite large, as the following calculation shows: for $s = 1$, $\chi = 31°43'$ and $p = 2.62$; for $s = 2$, $\chi = 22°30'$, and $p = 5.82$. In Figure 1, the smallest χ measured was 3°, which leads to $s = 19$ and $p = 360$. Even under such extremely large deformations, as can be seen in Figure 1, the stress-optical law remains valid. From Figure 2 it is seen that $\Delta p_{max} \sim 10^5$ dynes/cm.^{2} has been experimentally achieved, which corresponds to a tensile stress in the polymer (3%) of 3.3 kg./cm.^{2}. For rubbers (as quoted in Treloar's book) stresses up to 50 and 85 kg./cm.^{2} have been used, still complying to the linear Δn versus Δp relation. These facts emphasize the generality of this law. The mentioned equality of the recoverable shear s as measured by three different methods allows one to measure the normal stress P_{11} and P_{22} using flow birefringence alone.[6] If the C is known, as is the case, and the relation $P_{22} = P_{33}$ is used, as has been experimentally proved above, then:

$$(P_{11} - P_{22})\, C = \Delta n_{13} = \Delta n_{12} \cos 2\chi$$

When C is not known, a measurement of the viscosity at the same rate of shear gives τ and:

$$P_{11} - P_{22} = \tau s = 2\tau \cot 2\chi$$

Further the analysis of laminar flow has been attempted in still another way. Gill[15] suggested the use of a plastic tube in an elliptical guide. The tube and its liquid contents are rotated and the optical phenomena are observed by axially transmitting polarized light. This approximates the stressing with rotating axes and gives rise to a cross of isoclines determining a birefringence Δn and the extinction angle χ. A calibration with Newtonian liquids[16] (liquid polyisobutylenes) gave an exact quantitative correlation with the usually measured flow-birefringence. In viscoelastic liquids the χ diminished with rate as predicted, but due to experimental difficulties, no exact correlation was as yet possible. Such a stressing is similar to a dynamic experiment with $\omega = D$. Then $\chi = {}^1/_2\, \delta$, when δ is the loss angle and $\tan \delta = G''/G'$ calculated from the complex modulus $G^* = G' + jG''$. The stress optical behavior of polymer solutions is, as far as could be ascertained, exactly parallel—even quantitatively so—to the one of rubberlike polymers or elastomers. For these materials, as described, Δn is determined by the stress. Therefore, in a dynamic experiment the phase of Δn and τ should be expected to be identical—this is indeed the case as subsequent results presented at this symposium have shown. Concerning the suspensions of rigid particles—such as the micellar solution of milling yellow—and crystalline polymers no such prediction is possible—the experimental results are the only answer.

References

1. Coker, E. G., and L. N. G. Filon, *A Treatise on Photo-elasticity*, Cambridge, London, 1931.
2. Frocht, M. M., *Photoelasticity, Vol. I*, Wiley, New York, 1941.
3. Treloar, L. R. G., *The Physics of Rubber Elasticity*, Oxford, London, 1949.
4. Lodge, A. S., *Nature*, **176**, 838 (1955); *Trans. Faraday Soc.*, **52**, 120 (1956).
5. Weissenberg, K., *Arch. Geneve*, **17**, 1 (1935).
6. Philippoff, W., *Trans. Soc. Rheol.*, **5**, 163 (1961).
7. Mooney, M., *J. Colloid Sci.*, **6**, 96 (1951).
8. Philippoff, W., *J. Polymer Sci.*, **57**, 141 (1962).
9. Kuhn, W., and H. Kuhn, *Helv. Chim. Acta.*, **26**, 1394 (1943).
10. Philippoff, W., F. H. Gaskins, and J. G. Brodnyan, *J. Appl. Phys.*, **28**, 1118 (1957); W. Philippoff, *Acta Rheologica*, **1**, 371 (1961).
11. Weissenberg, K., Conf. British Rheologists Club, 1946.
12. Roberts, J. R., *Proc. 2nd Intern. Congress Rheology*, Oxford, London, 1953, p. 91.
13. Philippoff, W., *Trans. Soc. Rheol.*, **5**, 149 (1961).
14. Kuhn, W., and F. Grün, *Kolloid-Z.*, **101**, 248 (1942).
15. Gill, S. J., *J. Appl. Polymer Sci.*, **1**, 17 (1959); S. J. Gill and F. R. Dintzis, *J. Polymer Sci.*, **57**, 251 (1962).
16. Philippoff, W., and S. J. Gill, *Trans. Soc. Rheol.*, **7**, 33 (1963).

Résumé

La biréfringence d'écoulement consiste dans l'anisotropie optique induite par un flux laminaire dans les liquides. On décrit l'anisotropie optique par un tenseur optique qui est coaxial avec le tenseur d'élongation dans un matériel élastique. Ceci est évident dans une expérience de tension. En flux laminaire, ceci a été prouvé en étudiant la distribution de la biréfringence dans trois directions de l'espace. La quantité d'anisotropie, habituellement décrite par le degré de biréfringence Δn est proportionnelle à la diffusion de tension principale du tenseur d'élongation mécanique dans un très grand domaine de variables, donnant par là la possibilité d'utiliser les mesures optiques pour la détermination des tensions mécaniques. Cependant, la relation est valable pour les solutions concentrées et pour des conditions où le solvant et le polymère ont essentiellement le même indice de réfraction n—, condition habituellement appelée solvant de comparison. La constante de préportionnalité entre la différence en tension principale et Δn—le coefficient de tension optique C—est, comme prévu par la théorie, indépendante des concentrations, température de tension de cisaillement, poids moléculaire et sa distribution, et uniquement déterminée par la structure de l'unité monomérique et son n. Une autre quantité en biréfringence d'écoulement est l'angle d'extinction qui est mesuré entre la direction de l'axe optique principal et la direction du flux. On a obtenu un nombre suffisant de résultats expérimentaux pour montrer qu'un angle peut être quantitativement mis en corrélation avec le cisaillement récupérable, qui est le composant de cisaillement du tenseur d'élongation élastique en flux laminaire. De plus, la détermination expérimentale de l'angle donne une mesure de la tension élastique. Une étude de résultats expérimentaux obtenus dans ce domaine montre les généralités de cette approximation dans une variété de systèmes de polymère et solvants.

Zusammenfassung

Strömungs- oder Fliessdoppelbrechung ist die optische Anisotropie, die durch laminare Strömung in Flüssigkeiten verursacht wird. Die optische Anisotropie kann durch einen optischen Tensor, der zum Verformungstensor in elastischem Material koaxial ist, beschrieben werden. Dies wird in einem Spannungsexperiment offensichtlich. Bei Laminarströmung wurde dies durch Untersuchung der Doppelbrechungsverteilung in den drei Richtungen das Raumes bewiesen. Der Anteil der Anisotropie, der gewöhnlich durch den Grad der Doppelbrechung Δn ausgedrückt wird, ist der Differenz der Hauptspannungen des mechanischen Spannungstensors in einem sehr grossen Variablenbereich proportional, und gibt daher die Möglichkeit, optische Messungen zur Bestimmung mechanischer Spannungen zu verwenden. Die Beziehung ist entweder für konzentrierte Lösungen oder für Bedingungen, bei denen das Lösungsmittel und das Polymere im wesentlichen denselben Brechungsindex n haben, eine Bedingung, die gewöhnlich "Lösungsmittel-Angleichung" genannt wird, gültig. Der Proportionalitätsfaktor zwischen der Hauptspannungsdifferenz und Δn—der spannungs-optische Koeffizient C—ist, wie auch aus der Theorie folgt, unabhängig von der Konzentration, Schubspannung, Temperatur, Molekulargewicht und seiner Verteilung, und ist nur durch die Struktur der Monomereinheit und ihres n bestimmt. Eine weiter Grösse bei der Strömungsdoppelbrechung ist der sogenannte Auslöschungswinkel, der zwischen der Richtung der optischen Hauptachse und der Fliessrichtung gemessen wird. Eine beträchtliche Anzahl experimenteller Daten zeigt, dass dieser Winkel quantitativ zu der sogenannten "reversiblen Scherung," nämlich der Schubkomponente des elastischen Verformungstensor bei laminarem Fliessen in Beziehung gesetzt werden kann. Daher gibt die experimentelle Bestimmung des Winkels ein Mass für die elastische Verformung. Ein Überblick über die experimentellen Ergebnisse zeigt die allgemeinen Merkmale dieser Methode bei einer Reihe von Polymer- und Lösungsmittelsystemen.

JOURNAL OF POLYMER SCIENCE: PART C NO. 5, PP. 11–36

Streaming Birefringence as a Rheological Research Tool

HAROLD WAYLAND, *Division of Engineering and Applied Science, California Institute of Technology, Pasadena, California*

Synopsis

This paper reviews the theoretical and experimental evidence currently available to establish criteria to aid the experimenter who wishes to use streaming birefringence as a tool for studying fluid flow. Instrumental techniques are reviewed, and the possibilities for both qualitative and quantitative flow visualization by streaming birefringence in pure Newtonian liquids, colloidal suspensions and dilute and concentrated polymer solutions are discussed. Methods of reconstruction of the velocity and stress fields from birefringence data are outlined.

I. Introduction

If a pencil of plane polarized light is passed through a flowing liquid which exhibits streaming birefringence (SBR), two pieces of experimental information can, in general, be obtained: (*1*) the orientation (with respect to some preassigned set of axes) of the isoclinic axes, and (*2*) the amount of birefringence (i.e., the relative shift in phase between a beam polarized along one of the isoclinic axes to a beam polarized along the other. This retardation is usually measured as the fraction of a wavelength retardation per centimeter of path length for the particular wavelength used, although theoretically it is more apt to be expressed as the ratio of the index of refraction difference for light polarized along these two axes to the mean index of refraction of the medium for this wavelength.) The relationship between the direction of the isoclinic axes and the streamlines of the flow will depend on the mechanism which gives rise to the double refraction. It is the purpose of this paper to review the theoretical and experimental evidence currently available to try to establish useful criteria to aid the experimenter who wishes to use SBR as a tool for studying fluid flow. In particular it is important to ascertain whether or not quantitative interpretation is possible and to set criteria to permit the choice of the method of interpretation applicable to the system under consideration.

The fact that, in shear flow, certain liquids exhibit different indices of refraction for light polarized in different directions was first observed by Clerk Maxwell[1] in 1866. The first published suggestion of its use as a flow visualization tool followed a demonstration by Humphrey[2] at the

London Physical Society in 1923. It is interesting to note that at this demonstration one of the audience raised the warning that it would be unwise to use Dr. Coker's method of analysis of photoelastic systems for interpreting flowing systems. This warning has too often passed unheeded! In spite of early interest, SBR became a useful qualitative tool for flow studies only during World War II, and a solid basis for quantitative studies—both theoretical and instrumental—has been laid only during the past eight or ten years.

Except for the early work of Sadron[3] and Alcock and Sadron,[4] which will be discussed in detail in Sections II and III, attempts at systematic interpretation of flow patterns by means of SBR seem to have first been published by Hauser and Dewey.[5,6] They used bentonite solutions in concentrations of the order of 1%. Dewey went into some detail on possible quantitative interpretation in his doctoral thesis,[7] but lacking a suitable theoretical basis his results were inconclusive. Hauser and Dewey's work on use of SBR for studies of flow separation and transition to turbulence did lead to some useful results. They made both still and motion pictures of the flow around two-dimensional models of automobiles, although this appears to have been done as a demonstration of the method rather than for design purposes. Taking advantage of personal advice from Dewey, Knapp and his co-workers[8,9] at the California Institute of Technology developed a polarized light flume early in World War II. This used a 0.2% solution of white Hector bentonite for the optically active medium. It was used to study flow separation at the nose and tail of underwater weapons, such as torpedoes and depth charges. The models were three dimensional, the fluid was not strictly Newtonian, and essentially nothing was known about how to make a quantitative interpretation even of two-dimensional data. But the method was extremely fruitful in improving body shapes on a cut and try basis. The work, unfortunately, received little publicity outside of military circles since it carried security classification at the time.

In 1945 Leaf[10] used the SBR of a bentonite solution to study flow separation in a firebox and was successful in improving the design with the aid of this method. In the same year Binnie[11] published his first paper on studies of the onset of turbulence in pipe flow using a solution of the dye, benzopurpurin. The use of SBR techniques has contributed considerably to the studies of the onset of turbulence in pipe flow in the hands of Binnie,[11] Binnie and Fowler,[12] and Lindgren,[13] using visual, photographic, and photocell observation of the presence and magnitude of turbulence and turbulent flashes. Lindgren found that a concentration of bentonite as small as 0.062% gave a measurable influence on the velocity of a turbulent slug. Although it is fair to say that the usefulness of SBR of colloidal solutions for studying flow separation and the onset of turbulence is well established, Lindgren's work demonstrates that great care must be exercised to avoid effects due to the presence of the colloid when fundamental flow mechanisms are being studied.

As far as I know, SBR techniques have not been used with viscoelastic liquids to study qualitative differences in their behavior *vis à vis* Newtonian liquids. For example, such techniques should be useful in observing the type of secondary flow predicted by Ericksen[14,15] in the flow of viscoelastic fluids in elliptic cylinders. For this type of observation a precise knowledge of the mechanism giving rise to the SBR is not necessary.

For quantitative interpretation three types of systems will be considered: pure liquids with Newtonian viscosity behavior, colloidal solutions and solutions of polymers. The physical mechanism giving rise to SBR in each case is quite different, and it is only since adequate theories have been developed and experimentally verified that it has been possible to put flow visualization by SBR on a sound footing. The state of the theoretical knowledge on SBR as of about 1958 is summarized in the excellent review article by Jerrard.[16]

It should be made clear in the beginning that quantitative studies will be limited to two-dimensional flow situations. It is theoretically possible to predict the amount of SBR associated with a given shear rate or stress pattern (depending on the appropriate mechanism) for complicated flows. However, the tensor nature of the optical properties of a birefringent system makes the inverse problem extremely difficult, if not impossible. It is not clear that such a solution is unique even for cylindrically symmetric flows such as Poiseuille flow.

II. Instrumental Techniques

1. Photographic Methods

The simplest method of collecting data on the optical properties of a two-dimensional flow field is to use the well established photographic techniques employed in viscoelastic studies in solids. These are well documented in the literature, as in the classic work by Frocht,[17] and will only be briefly sketched here. The conventional physical arrangement is shown in Figure 1. First let us consider the case in which monochromatic light from the source is rendered parallel by the lens, plane polarized by the polarizer, passed through the flow field and viewed through the analyzer crossed to the polarizer (with the quarter wave plates out of the system). In this case there will be no light transmitted through those portions of the flow (a) in which the retardation between the fast and slow

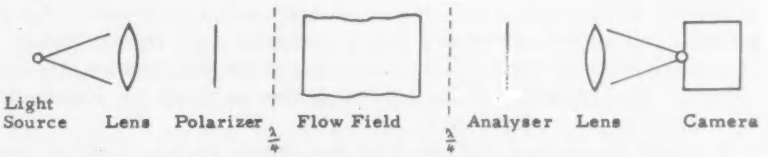

Fig. 1. Flow polarimeter.

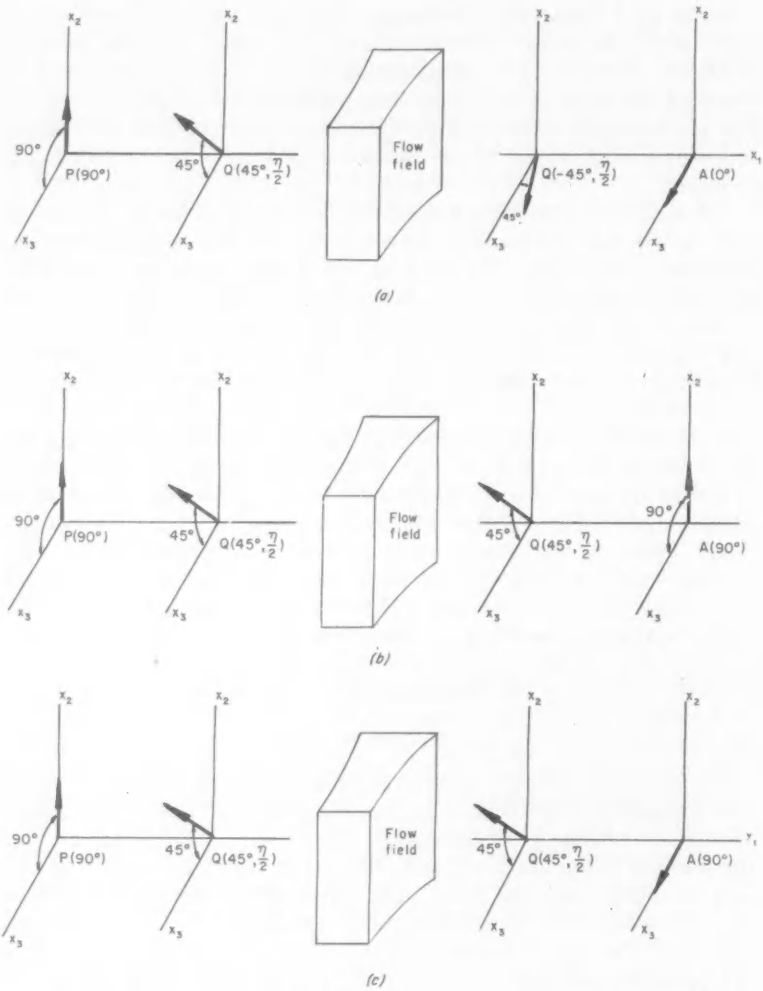

Fig. 2. Types of circular polariscopes: (*a*) crossed; (*b*) parallel; (*c*) mixed.

axes is an integral multiple of the wavelength of light used (called *isochromatics*) and (*b*) in which the plane of polarization of the incoming light is parallel to either of the isoclinic directions (called *isoclinics*). If the polarizer and analyzer are rotated together, coupled in the crossed position, the isochromatic pattern will remain fixed, while the isoclinic will, in general, vary. A series of isoclinic maps can be taken by systematic rotation of the polarizer-analyzer combination.

Although the isochromatics can be obtained from the configuration just discussed, they are more usually obtained by passing circularly polarized

light through the test region. This is obtained by introducing a quarter wave plate just after the polarizer, with axes at 45° to the plane of polarization. A second quarter wave plate follows the test region. If its fast axis is parallel to the slow axis of the first $\lambda/4$ plate and the polarizer is crossed with respect to the analyzer we have the *crossed circular polariscope* (Fig. 2*a*). If the fast axes of the $\lambda/4$ plates are parallel and the polarizer and analyzer are parallel, we have the *parallel circular polariscope* (Fig. 2*b*). In either of these cases extinction will occur wherever the retardation is an integral number of wavelengths. If the quarter wave plates remain parallel, but the analyzer is crossed with respect to the polarizer, we have the *mixed circular polariscope* (Fig. 2*c*). In this case extinction occurs when the retardation is an odd number of half wavelengths.

These methods, using monochromatic light, are primarily useful when the maximum retardation in the field is several wavelengths so that several fringes are available to use in analyzing details of the flow pattern. Fractional fringes can be more easily studied if white light is used, but the

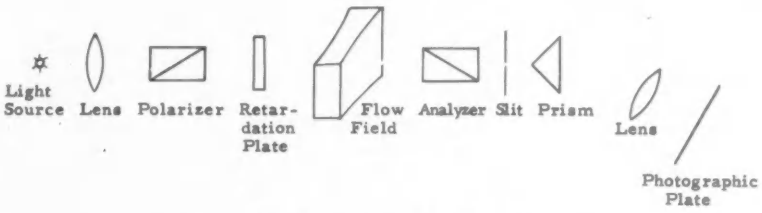

Fig. 3. Sadron's spectographic flow polarimeter.

circular polariscope loses some of its quantitative character since a quarter wave plate can give strictly circularly polarized light at only one wavelength.

Sadron[3] developed a spectroscopic technique to permit analysis of small differences of retardation. He was dealing with a system (plane Poiseuille flow in sesame oil) in which the isoclinics were at 45° to the streamlines. A beam of plane polarized light with the plane of polarization parallel to the streamlines was passed through a full wave retardation plate, cut to give one wavelength retardation at 5800 A., with optic axes at 45° to the plane of polarization (Fig. 3). The analyzer was crossed with respect to the polarizer. The light from the analyzer was photographed through a spectroscope. With no flow, extinction would occur at $\lambda_0 = 5800$ A. across the field. A retardation introduced by the flow would shift the extinction position, and the amount of retardation was correlated with position across the flow. This method can be made extremely sensitive, but requires knowledge of the isoclinic directions. Except for the early work of Sadron[3] and Alcock and Sadron,[4] this method does not seem to have been exploited.

2. *Point by Point Measurements*

Point by point scanning of the flow field is particularly desirable when the amount of birefringence is small. This has been developed by Wayland[18] and Sutera and Wayland[19] to permit obtaining optical data to within 0.1 mm. of a wall. To obtain a narrow pencil of light the optical arrangement of Björnståhl[20] is the most suitable. The pinhole nearest the light source (Fig. 4) is imaged at the lower window of the flow channel and the second pinhole is imaged at the upper window of the flow channel. The diameter of the pinholes can be so chosen that their images have equal diameters. It has proved possible to work with images such that the diameter of the first dark diffraction zone is 0.2 mm. Since monochromatic light is used, only a simple lens is necessary. The beam can be translated parallel to itself by means of a plane parallel sheet of glass (the deflector plate in Fig. 4) which can be rotated about an axis perpendicular to the axis of the light beam. The thickness and index of

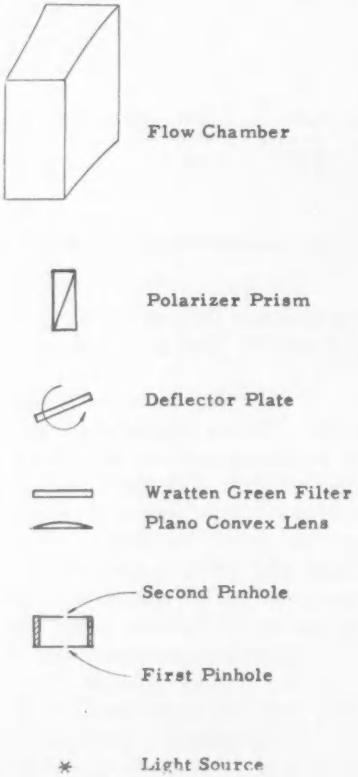

Fig. 4. Optical system for point-by-point scanning

refraction of the glass can be chosen to give the required amount of translation, although the system is practical only if the total translation is limited to a few millimeters.

Various methods are available to analyze the effect of the birefringent medium on this polarized pencil of light. Since this point by point method seems particularly suitable for the study of systems with small retardation, a brief resume will be given of some useful methods for this case. The most difficult measurement is that of the angle of isocline. With crossed polarizer and analyzer the intensity of light passing the analyzer for a retardation δ when one of the axes of the birefringent medium makes an angle of β with plane of polarization (see Fig. 5*a*) is

$$I \approx \sin^2 2\beta(1 - \cos \delta) \tag{1}$$

If the retardation is small, and β is approaching the extinction angle, we have

$$I \approx \beta^2\delta^2 \tag{2}$$

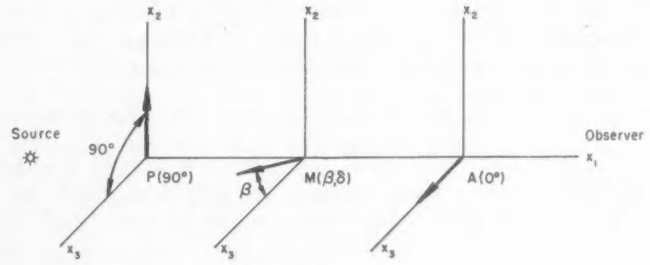

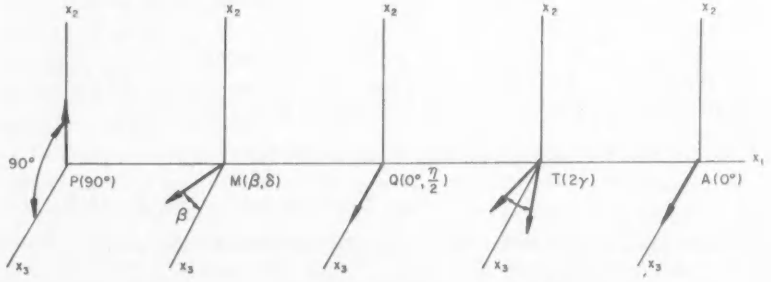

Fig. 5. Arrangements for locating the angle of isocline: (*a*) location with crossed polarizer and analyzer; (*b*) location with modulated optical rotation.

It is seen that in this case the null is proportional to the square of both the angular position and the amount of birefringence. A variety of techniques has been developed to increase the sensitivity of location of the angle of isocline. Of these, only the method using a modulated optical rotation will be discussed in detail. Certain visual half-shadow methods give linear dependence of intensity with angular position and amount of birefringence, but lack the advantage of ac photoelectric detection. The relationship of these methods to the modulated methods is discussed by Wayland and Badoz.[21]

Referring to Figure 5*b*, monochromatic light polarized parallel to the x_2 axis passes through the birefringent medium M of retardation δ with one optic axis at the angle β to the x_3 axis. The light then passes through a quarter wave plate Q oriented as shown, and then through an optical rotator T which rotates the plane of polarization sinusoidally through $\pm\gamma$. This modulation can readily be accomplished by passing the light through a Faraday cell in which the magnetic field is actuated by an alternating current. The light then passes through the analyzer A, crossed with respect to the polarizer. If the light falling on the polarizer is of unit intensity, the intensity of light passing the analyzer will be given by the expression (when the rotator gives the fixed rotation γ)

$$I = {}^1/_4\,[\,1 - \cos 2\gamma(\cos^2 2\beta + \sin^2 2\beta \cos\delta) - \sin 2\gamma \sin 2\beta \sin\delta\,] \quad (3)$$

If $\gamma = \gamma_0 \sin \omega t$ and γ_0 is small, this expression consists of a continuous term, a term at the driving frequency and a term at double the driving frequency. If the amplifying system on the photomultiplier current is tuned to amplify the fundamental and to reject dc and the second harmonic, the detected signal will be given by the expression

$$S = {}^1/_4 \sin 2\gamma \sin 2\beta \sin\delta \approx \delta\beta\gamma_0 \sin \omega t \quad (4)$$

which is linear in both the retardation δ and the angular displacement from the null point β.

To determine the amount of birefringence with this arrangement, the entire assembly of polarizer, quarter-wave plate and analyzer is rotated through 45° from the isocline β of the medium. If the analyzer is now uncoupled from the system it can be rotated independently to seek a new null position. If it is rotated an angle α from being crossed with respect to the polarizer, the intensity of light transmitted by the analyzer is

$$I = {}^1/_4\,[1 - \cos 2\alpha(\cos 2\gamma \cos\delta - \sin 2\gamma \sin\delta) - \sin 2\alpha(\sin 2\gamma \cos\delta + \cos 2\gamma \sin\delta)\,] \quad (5)$$

Modulating the rotation and detecting only the fundamental we get

$$I \approx \gamma_0 \sin \omega t[\cos 2\alpha \sin\delta - \sin 2\alpha \cos\delta] = \gamma_0 \sin \omega t \sin(\delta - 2\alpha) \quad (6)$$

This vanishes when $\alpha = (\delta/2)$ and the change in signal is linear in angular unbalance when near the null point.

In practical application the angle of isocline can readily be determined to 1° for a relative retardation of 5×10^{-9} cm. using the mercury green line. The least count of the measurement of retardation in the apparatus constructed at the California Institute of Technology was 0.3 A. For extremely small birefringences the precision was increased by measuring the retardation as a function of angular position over about 200° of rotation and obtaining both the amount of birefringence and the isoclinic positions from a smooth curve drawn through these data points. This limitation was not due to the lack of sensitivity and stability of the detecting system, but to limitations in measuring the angular position of the analyzer ($\pm 0.01°$) and in extraneous birefringence in the windows. A detailed discussion of the experimental arrangements and the correction of errors will be found in the doctoral thesis of Intaglietta,[22] and will be published in detail elsewhere.

III. Pure Newtonian Liquids

Certain oils and organic liquids show SBR well within the range of Newtonian viscosity behavior. As early as 1928 Raman and Krishnan[23] developed a theory of SBR for pure liquids. This was based upon two experimental facts: (*1*) an extensive series of measurements on organic liquids by Vorländer and Walter[24] appeared to show that all liquids showing measurable SBR possessed highly asymmetric molecules, and (*2*) measurements in simple shear flow showed that for these pure liquids the optic axes were at 45° to the streamlines, i.e., were parallel to both the principal stress and strain rate axes (since these are coincident for a Newtonian fluid). Raman and Krishnan assumed that such asymmetric molecules would tend to be oriented by the stresses in the fluid in such a manner that the long axis of the molecule would be along the axis of principal tension. Thermal agitation would give rise to Brownian motion, tending to disorient the molecules. Classical statistical mechanics was applied to calculate the resulting equilibrium distribution for a given flow condition, giving the relationship between the local stress field and the resulting birefringence.

Sadron[25] later threw considerable doubt on the validity of the Raman-Krishnan theory, and the Vorländer-Walter data were proved to be virtually useless since many of the measurements were made in non-laminar flow which Jerrard[26] and Wayland[18] have shown can lead to completely misleading results.

Peterlin and Stuart[27] have developed a theory of SBR of pure liquids in which the flow orientation of the asymmetric molecules is included as well as certain internal field corrections due to molecular interactions. This predicts that the angle of isocline will deviate from coincidence with the principal strain rate axes for high enough velocity gradients, but for most organic liquids with essentially Newtonian viscosity this requires such high gradients that thermal effects make measurements extremely difficult. The definitive experiment distinguishing between these two theories

is reported by Tolstoi.[28] The birefringence induced in purified transformer oil by a combination of shear flow and an electrostatic field was compared with theoretical treatments based on the statistical mechanical theory and the flow orientation theory. The results gave strong support to the flow orientation theory of Peterlin and Stuart.

Both theories predict that at moderate shear rates in simple shear flow the optic axes will remain parallel to the principal stress and strain rate axes. At very high shear rates the Peterlin-Stuart theory predicts a departure from coincidence of the optic and strain rate axes, but in the pure liquids studied to date this departure does not show up until the shear rate exceeds 10^4 sec.$^{-1}$. No critical work has been done on the relationship of the SBR to the stress or strain rate in flow other than of the Couette type. Since the relaxation time for the angular rotation of the molecules of these liquids is very short, it is reasonable to expect that the optic axes will coincide with the principal stress and strain rate axes. This means that if the liquid is calibrated in Couette flow, a measurement of the direction of the isoclinic axes and the amount of birefringence at a network of points in the flow will permit a determination of the principal stresses and strain rates from the optical measurements. From these data the flow field can be reconstructed if it is known along some boundary or streamline, as will be discussed in Section IV.

The earliest reported attempt at quantitative flow measurements by SBR was made with a Newtonian liquid, sesame oil. This was the work of Sadron[3] and Alcock and Sadron[4] using the spectroscopic method discussed in Section II.1. Their measurements on flow between parallel plates agreed with the calculated flow within about 4%, with most of the error occurring close to the walls where strains in the windows near the clamped edge may be large and spurious birefringence due to reflections can introduce significant errors. These latter errors can be reduced by care in maintaining the parallel nature of the light beam (now possible with a laser light source) and by covering the wall with a dielectric of index of refraction less than that of the flowing liquid so that light reflected from the walls at grazing incidence will be totally reflected.[29] In the case of diverging flow the agreement was not so good. Their published data are not sufficiently detailed to ascertain whether this lack of agreement is due to extraneous birefringence, failure to take into account the variation in the isoclinic direction as the flow is traversed, or something more fundamental. Critical experiments are still needed to clarify the validity of the assumptions concerning the relationship between the SBR of these Newtonian liquids and the stress and strain rate fields in converging and diverging flow situations. The specific birefringence of such liquids is generally quite small—ethyl cinnamate, one of the more active substances, has a specific birefringence of 5.04×10^{-3} (A./cm.) sec. A careful set of experiments in a complicated, but calculable, flow using point by point measurements would be helpful in clarifying the potential role of using the SBR of pure Newtonian liquids as a flow visualization tool.

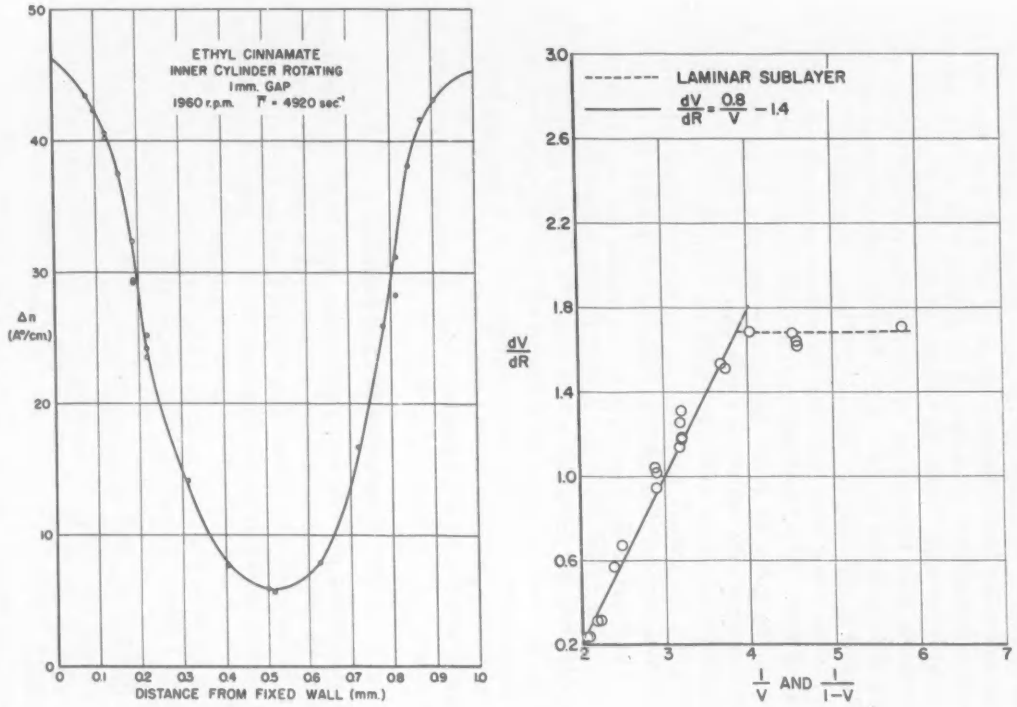

(*a*) (*b*)

Fig 6. Point-by-point SBR measurements in turbulent couette flow: (*a*) retardation as a function of position; (*b*) velocity gradient versus reciprocal velocity.

Point by point studies have been made with ethyl cinnamate in cylindrical Couette flow above the Taylor transition velocity.[18] Experimentally it was found that the isoclinics remained at 45° to the mean streamline direction even in the turbulent portion of the flow. Assuming that the amount of birefringence was proportional to the mean velocity gradient, and using the calibration made in laminar flow, the velocity profile was reconstructed by numerical integration from the zero velocity at the fixed outer wall. With the velocity of the moving wall 168 cm./sec. integration gave 180 cm./sec. or 7% high; for the wall at 252 cm./sec. integration gave 249 cm./sec. or 3% low; and for the wall at 492 cm./sec., integration gave 476 cm./sec. or 3% low. This result is, at best, empirical, since there is no adequate theoretical treatment for SBR in a turbulent flow. It is, however, an excellent illustration of the possibilities in the point by point method for studying boundary layers. The measurements were made in a 1 mm. gap, and the basic data for the highest rotative speed are shown in Figure 6*a*. Squire[30] compared these data with his theoretical treatment of turbulent cylindrical Couette flow. Introducing the dimensionless velocity V, related to the linear velocity of the wall of the inner cylinder, he plotted the velocity gradient deduced from the birefringence data against the reciprocal of the dimensionless velocity from the fixed wall to the center of the gap and against $1/(1-V)$ from the moving wall to the center of the gap (Fig. 6*b*). The horizontal dotted portion of the curve corresponds to a laminar sublayer (constant velocity gradient) near the walls, and the sloping linear portion is consistent with the behavior predicted from his theoretical treatment in turbulent flow.

IV. Suspensions of Rigid Particles

Most engineering work on flow visualization with SBR has been done with colloidal solutions. Although a considerable body of theory is available on which to base flow interpretation from the optical data, all of this theory applies only to situations in which interactions among particles are neglected. There is a great temptation to increase particle concentration to such a point as to give large optical effects, but in every case which I have reviewed in which the particle concentration exceeds a few tenths of a per cent there is evidence that the medium no longer follows the laws used in interpreting the data. The theoretical treatment on which flow interpretations are based will be summarized and the current state of the experimental art will be discussed in terms of this background.

Peterlin and Stuart[31] laid the basis for a quantitative theory of the SBR of a dilute solution of rigid ellipsoids in Couette flow, which Wayland[32] has extended to general two-dimensional laminar flow. These treatments are based on the following assumptions:

(*1*) The particles are rigid ellipsoids of revolution.

(*2*) There are no hydrodynamic, chemical, or electrical interactions

(3) The number of particles along the length of the light beam is large.

(4) There is a finite number of discrete particle sizes (although the extension to a continuous distribution is straightforward).

(5) The unperturbed flow field throughout distances comparable to the largest particle dimension can be calculated from a knowledge of the velocity and the velocity gradient at any point, i.e., second and higher space derivatives of the velocity can be neglected over one particle length.

(6) The linearized Navier-Stokes equations can be used in describing the motion of the individual particles between Brownian fluctuations, hence inertial terms can be neglected in describing the rotation of the particles.

(7) The particles are subject to Brownian motion, and the diffusion law is valid.

(8) The relaxation time for rotation of the individual particles is short enough that the particles can be assumed to be in equilibrium with the flow at every point.

(9) The particles are short with respect to the wavelength of light used.

On the basis of these assumptions the position of the isoclinic χ from the first principal strain rate axis, and the amount of birefringence, Δn, for a monodisperse system will be given by

$$\chi = -\frac{E \sin 2\Lambda_0}{6D}\left[1 - \frac{E^2}{27D^2}\left(\sin^2 2\Lambda_0 + \frac{24b^2}{35}\right) + O\left(\frac{E^4}{D^4}\right)\right]$$

$$= -\frac{\gamma_s}{12D}\left[1 - \frac{1}{27D^2}\left(\frac{\gamma_s^2}{4} + \frac{24b^2}{35}E^2\right) + \ldots\right] \tag{7}$$

$$\Delta n = \left(\frac{4\pi}{15}\right)\left(\frac{Gcb}{\hat{n}}\right)\left(\frac{E}{D}\right)\left[1 - \frac{E^2}{18D^2}\left(\sin^2 2\Lambda_0 + \frac{6b^2}{35}\right) + O\left(\frac{E^4}{D^4}\right)\right]$$

$$= \left(\frac{4\pi}{15}\right)\left(\frac{Gcb}{\hat{n}}\right)\left[\left(\frac{E}{D}\right)\left(1 - \frac{1}{18D^2}\frac{\gamma_s^2}{4} + \frac{6b^2}{35}E^2\right) + \ldots\right] \tag{8}$$

where E is the magnitude of the principal strain rate; Λ_0 is the angle between the principal strain rate axis and the streamline; $b = (a_1^2 - a_2^2)/(a_1^2 + a_2^2)$ with a_1 = major axis and a_2 = minor axis of ellipsoid of revolution; $\gamma_s = 2E \sin 2\Lambda_0$, the shear rate along the streamline; D is the rotary diffusion coefficient for the ellipsoid, c is the volume concentration; $G = g_1 - g_2$, the optical anisotropy for the particle; and $\hat{n}$ is the mean index of refraction for the solution.

In Couette flow $\Lambda_0 = 45°$, hence $2E = \gamma_s$. Down the centerline of a symmetric converging or diverging channel flow, $\Lambda_0 = 0$, hence $\chi = 0$ and the quadratic term in Δn is considerably different from that for Couette flow. In the case of sufficiently elongated particles, $b = 1$, and we have the following expression for Δn:

Couette flow

$$\Delta n = A\left(\frac{E}{D}\right)\left[1 - 0.260\left(\frac{E}{D}\right)^2\right] \tag{9}$$

On the centerline of converging or diverging channel flow

$$\Delta n = A\left(\frac{E}{D}\right)\left[1 - 0.038\left(\frac{E}{D}\right)^2\right] \tag{10}$$

If there is a sufficiently strong shear component that $\Lambda_0 \approx 45°$ one can interrelate E to Δn as measured in Couette flow even outside the range in which Δn is linear with shear rate. For more general flows, however, this correlation cannot be made without a knowledge of the angle of isocline and of the axial ratio parameter b. In the case of a polydisperse system, the expressions are considerably more complicated and, to work in the nonlinear range, would require an elaborate calibration.

It seems probable that no work on flow visualization using colloidal solutions has met all of the assumptions listed above. Tobacco mosaic virus in the concentrations used by Sutera and Wayland[19] probably comes the closest to meeting all of these conditions, but in their concentrations (less than 0.3%) the effects are very small. Furthermore, the particles are not short compared to the wavelength of light used (particle length 3000 A., λ = 5460 A.). By increasing the viscosity approximately 80 fold by addition of glycerine, it was possible to increase the relaxation time so that the birefringence measured at a point reflected the previous flow history rather than giving information on the flow field at this point.

Bentonite, one of the most popular materials, probably does not consist of rigid particles, and shows only a small specific birefringence at concentrations low enough that interaction effects are not significant as shown by Lindgren.[13]

The substance most recently to achieve popularity for flow birefringence work is the dye milling yellow. As yet I have seen no accurate characterization of its size and shape but the phenomenological data reported in the literature lead me to raise the following questions concerning interpretation of flow data from SBR of milling yellow in the concentrations used in the experiments so far reported ($1^1/_4$–$1^1/_2$%). In the first place, the amount of birefringence shows a far from linear dependence on concentration, which suggests strong interaction phenomena, and immediately vitiates application of the theory for rigid, isolated particles. Another indication of interaction effects is the viscometric data reported by Honeycutt and Peebles[33] which shows a rather strong shear dependence of viscosity, stronger than seems explicable on the basis of orientation effects alone, and sufficient to question the use of a constant viscosity in calculating the flow fields studied to date.

Even assuming that the milling yellow solutions obey the laws for a monodisperse, non-interacting colloidal solution of rigid ellipsoids, it is

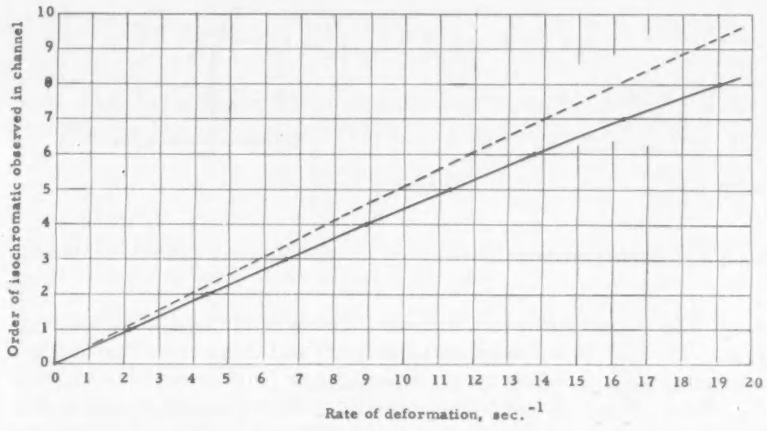

Fig. 7. Data of Prados and Peebles for milling yellow solution T-7: (——) data in Couette flow; (- - -) calculated data for centerline of converging flow.

interesting to look at the effect of the observed nonlinearity of the Δn versus velocity gradient curve on the possible interpretation of the local value of E. The curve of Prados and Peebles[34] for their solution T-7 at 25.20°C. is given as a solid line in Figure 7. Since this was taken in Couette flow, the coefficients in eq. (9) were empirically determined to match this curve. On the centerline of converging channel flow, where $\Lambda_0 = 0$, the quadratic dependence is reduced by a factor of 6.85, giving the dotted curve in Figure 7. It is true that the total strain rate is not apt to be large on the centerline of converging channel flow, but certainly caution must be exercised when working outside the region in which Δn is linear with strain rate.

I feel that we can honestly raise the question as to whether the discrepancies reported by Bogue and Peebles[35] between optically derived velocity profiles and the theoretical profiles for channel flow are due to entrance conditions, as they suggest, or to something more fundamental, such as non-Newtonian character of the milling yellow solution, or the need to take the nonlinear behavior of Δn with strain rate into consideration. An even more fundamental difficulty may arise: the basic relationship between Δn and strain rate may not even be of the form of eq. (8), and hence Δn may depend on E in a somewhat different fashion when the flow is not Couette flow. This should not be surprising: the interactions which lead to an amount of SBR considerably larger than that expected from orientation of individual particles may introduce a mechanism somewhat akin to network deformation such as appears to be responsible for the SBR of certain polymer solutions (to be discussed in the next section) superposed on a flow orientation component. In this case the SBR would be related to a complicated combination of stress and

Fig. 8. Coordinate systems for flow analysis: (*a*) local Cartesian coordinates; (*b*) local streamline coordinates.

strain rate—an area in which little satisfactory theoretical work has been done. The fact that Prados and Peebles,[34] and Bogue and Peebles[35] get reasonably good agreement with expected flow profiles seems to indicate that these effects are not extremely large in the situations studied, but they may well represent a fundamental limitation on the use of milling yellow, or any other colloidal suspension, in sufficient concentrations for photographic techniques to be applicable.

If one is working in the range of validity of eqs. (7) and (8) it is possible to reconstruct the flow field from a knowledge of the birefringence field and a knowledge of the flow along some streamline—usually an application of the no-slip condition to a boundary. Prados and Peebles[34] give step by step procedures for various flow situations based on an assumed relationship between the SBR and the flow parameters. The following treatment[19] is more directly based on the theory of SBR in generalized two-dimensional flow. If we are in the linear range, eqs. (7) and (8) reduce to

$$\chi = c_1 E \sin 2\Lambda_0 \tag{11}$$

$$\Delta n = c_2 E \tag{12}$$

From a knowledge of Δn at each point in the flow we can obtain E provided we obtain c_2 by calibration in Couette flow. Suppose we start from a point on a fixed boundary where we know the streamline direction and have measured Δn and the directions of the isoclinics. From Δn we calculate E from the Couette calibration and the deviation of the isoclinics from the principal axes, $\chi_c = c_1 E$. We know that one of the optic axes in the unknown flow will make an angle of $\Lambda_0 - \chi$ with the streamline, and this we know from the position of the isoclinics. Consequently we solve for Λ_0 from the transcendental equation

$$(\Lambda_0 - \chi) = \Lambda_0 - \chi_c \sin 2\Lambda_0 \tag{13}$$

If we take a local set of Cartesian coordinates with the x-axis in the positive streamline direction (Fig. 8*a*) we have the following relationship for an incompressible fluid

$$\dot{e}_{xx} = \frac{\partial u}{\partial x} = -\dot{e}_{yy} = -\frac{\partial v}{\partial y} = E \cos 2\Lambda_0 \tag{14}$$

$$\dot{e}_{xy} = \dot{e}_{yx} = \frac{1}{2}\left[\frac{\partial u}{\partial y} + \frac{\partial v}{\partial x}\right] = E \sin 2\Lambda_0 \tag{15}$$

Since x has been chosen to be tangent to the streamline, $(\partial v/\partial x) = 0$ at that point and eq. (15) can be rewritten

$$\frac{\partial u}{\partial y} = 2E \sin 2\Lambda_0 \tag{16}$$

From eqs. (14 and 16) we compute the velocity increment to a neighboring point $(0, \Delta y)$ obtaining

$$\begin{aligned} u(0, \Delta y) &= u_0 + (2E \sin 2\Lambda_0)\Delta y \\ v(0, \Delta y) &= -(E \cos 2\Lambda_0)\Delta y \end{aligned} \tag{17}$$

This gives enough information to determine the total velocity and the streamline direction at the new point, from which the procedure can be continued. Starting from a series of points on the known streamline, the streamline pattern can be developed.

In the case of a monodisperse population in which b is known it is possible to set up an iterative procedure for determining the principal strain rate directions from the optical data in the quadratic region, but preliminary attempts make it seem doubtful if it is worth the effort. For polydisperse systems a look at the equations[32] is enough to discourage working outside the linear range except in the case in which the shear component dominates. If we are dealing with a flow in which the maximum deviation of $\sin 2\Lambda_0$ from unity can be neglected, the analysis of the flow is considerably simplified. If we need a knowledge of the angle of isocline, as required in the above method, we must limit the analysis to the case in which $\Lambda_0 \approx 45°$. The application of the above method is readily extended to this case, obtaining the appropriate value of E from the plot of Δn against E for Couette flow, even if not linear. The application to pure liquids, where Δn is proportional to E and the angle of isocline is always coincident with the principal strain rate axis is obvious.

Since variation in Λ_0 has considerably less influence on Δn than on χ, the method of Bogue and Prados[35] using only Δn appears very attractive. In their published example of converging channel flow, they use cylindrical coordinates which are streamline coordinates for their case. They also introduce a stream function, but it does not appear to be fundamental to their method, and the physical picture is clearer without it. Let us first introduce general two-dimensional orthogonal curvilinear coordinates α, β (Fig. 8*b*) with the line element of the form

$$ds^2 = h_\alpha^2\, d\alpha^2 + h_\beta^2\, d\beta^2 \tag{18}$$

The strain rates will be

$$\dot{e}_{\alpha\alpha} = \frac{1}{h_\alpha}\frac{\partial u_\alpha}{\partial \alpha} + \frac{u_\beta}{h_\alpha h_\beta}\frac{\partial h_\alpha}{\partial \beta}$$

$$\dot{e}_{\beta\beta} = \frac{1}{h_\beta}\frac{\partial u_\beta}{\partial \beta} + \frac{u_\alpha}{h_\alpha h_\beta}\frac{\partial h_\beta}{\partial \alpha} \tag{19}$$

$$\dot{e}_{\alpha\beta} = \frac{1}{2}\left[\frac{h_\beta}{h_\alpha}\frac{\partial}{\partial \alpha}\frac{u_\beta}{h_\beta} + \frac{h_\alpha}{h_\beta}\frac{\partial}{\partial \beta}\frac{u_\alpha}{h_\alpha}\right]$$

If we now take the curves β = const. to be the streamlines of the flow and α = const. their orthogonal trajectories we will have $u_\beta = 0$ and $u_\alpha = V$. Keeping in mind that

$$\frac{1}{h_\alpha h_\beta}\frac{\partial h_\alpha}{\partial \beta} = \frac{1}{r}; \quad \frac{1}{h_\alpha h_\beta}\frac{\partial h_\beta}{\partial \alpha} = \frac{1}{r'} \tag{20}$$

where r is the radius of curvature of the streamline and r' that of its orthogonal trajectory, we write

$$\dot{e}_{\alpha\alpha} = -\frac{V}{r'} = -\dot{e}_{\beta\beta}$$

$$\dot{e}_{\alpha\beta} = \dot{e}_{\beta\alpha} = \frac{1}{2}\left[\frac{\partial V}{\partial n} - \frac{V}{r}\right] \tag{21}$$

The expression for E becomes

$$E^2 = \frac{1}{4}\left[\left(\frac{\partial V}{\partial n}\right)^2 - \frac{2V}{r}\frac{\partial V}{\partial n} + \left(\frac{1}{r^2} + \frac{1}{r'^2}\right)V^2\right] \tag{22}$$

A network of values of E is available from the optical measurements. Starting from a wall, which we know to be a streamline, and along which $V = 0$ from the no-slip condition we can calculate $(\partial V)/(\partial n)$ from eq. (22). (We know r from the geometry of the wall, and must estimate r'.) With a value for $(\partial V)/(\partial n)$ we can calculate the velocity increment along the orthogonal to the streamline, and hence carry the velocity field on into the flow. An iterative process can be used to improve the estimation of r' as the streamline pattern is developed and the orthogonal trajectories can be more precisely drawn. In cases in which the general comportment of the streamlines can be estimated in advance the calculations will be less difficult.

V. Solutions of Polymers

There is a considerable body of experimental data, much of it due to Philippoff and his coworkers, on various polymeric systems which follow a stress-optical law, at least in the simple flow situations so far reported, of the type used so effectively in photoelastic studies. Caution must be used, however, in concluding that all polymer solutions have these same properties. A brief discussion of some of the theoretical background will help keep perspective on the use of SBR for flow visualization studies in polymeric systems.

Philippoff[36] has given a rather extensive treatment of the interrelationship to be expected between elastic stresses and the optical properties of viscoelastic liquids if it is assumed that there is a simple correlation between the elastic deformation tensor and the optical tensor. Lodge[37] appears to be the first to develop a rational theoretical model explaining such relationships. He pointed out that, in certain flowing liquids one might expect the same mechanism, such as network deformation, to give rise both to birefringence and stress. If these two phenomena arise from the same source, it is reasonable to suppose that the optic and stress ellipsoids will be coaxial, and the differences of the principal axes of either ellipsoid will be proportional to the differences of the corresponding axes of the other ellipsoid. He developed a model compatible with this hypothesis based on the method of Green and Tobolsky in their theory of rubberlike elasticity. The molecular interactions between the molecules of the polymer are assumed to be sufficiently localized and long-lived to be treated as junctions in a deforming network, and he considers that the stress, apart from an additive isotropic component, arises entirely from entropy changes consequent on the deformation of the network. Some parts of the network will be older than others and will be more deformed, but it is assumed that a network element of a given age gives its own contribution to the total stress, independent of the rest of the network, of an amount given by the statistical theory of rubberlike elasticity. The total stress is the sum of the contributions. The birefringence is assumed to be due to orientation by network deformation of optically anisotropic chain links. Hydrodynamic flow forces are neglected, as are contributions from orientation of free chains by solvent flow and from double refraction of entire macromolecules. The flow gradient is also taken to be so small as not to affect the mean lifetime of junction points. On this model he concludes that, for laminar flow in the x_1 direction, with a gradient Γ in the x_2 direction, the angle of isocline will be given by

$$\tan 2\chi = \frac{2s_{21}}{s_{11}-s_{22}} \tag{23}$$

i.e., the isoclinic axes coincide with the principal stress axes; and that

$$\frac{\Delta n \sin 2\chi}{\bar{n}} = \left(\frac{4\pi}{5}\right)\left[\frac{\bar{n}^2+2}{3\bar{n}}\right]^2\left(\frac{(\alpha_1-\alpha_2)}{kT}\right)(\eta-\eta_0)\Gamma \tag{24}$$

where $\bar{n}$ is the mean index of refraction; α_1, α_2 are principal polarizabilities of a chain; η is the viscosity of solution; and η_0 is the viscosity of solvent. With this model he also finds

$$\eta = \frac{s_{21}}{\Gamma} = \text{const.} \tag{25}$$

This lack of dependence of η on Γ is due to his assumption of a quasitatic process: it is assumed that a chain, on leaving the network, is ables

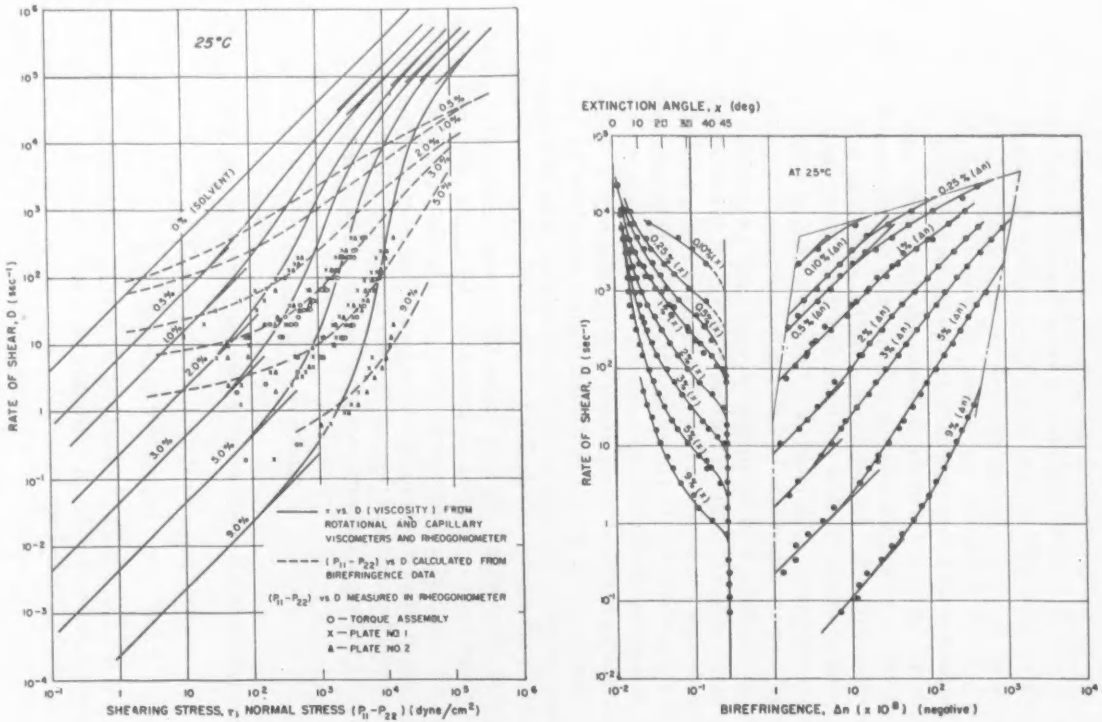

Fig. 9. Stress and birefringence data for polyisobutylene in Decalin: (*a*) shearing stress and normal stress as functions of shear rate; (*b*) birefringence Δn and extinction angle χ versus shear rate.

to retract fully before joining the network again. The concentration and shear rate range are, therefore, limited. In particular, the solution must be sufficiently concentrated to possess network structure. The upper limit of concentration is also influenced by the assumption that the mean distance between successive chains is large enough for a Gaussian approximation to be valid.

Philippoff and his coworkers[38,39] have studied the relation of birefringence and shear stress for solutions of polyisobutylene (PIB) in decalin from concentrations of 0.1–9% as well as 100% PIB over a shear range from 10^{-1} to 10^{4} sec.$^{-1}$. His results for the various solutions are shown in Figure 9*a*. Using viscosity data obtained with various types of viscometers, depending on the range, these are replotted in Figure 9*b* in which Δn, the amount of birefringence, is plotted against half the difference of principal stresses $\tau/\sin 2\chi$. This plot uses the whole shearing stress (i.e., the viscosity of the solvent has not been subtracted out as suggested by Lodge). Subtracting out the solvent viscosity would pull the points for the lowest concentrations to the left just about to the limit of scatter of the data, and would have less and less influence at the higher concentration. The linearity of the data as plotted may be an argument for using the viscosity of the solution, as suggested by Philippoff, or, if the corrected data must be used, may represent a departure of the behavior of the solution from the Lodge theory. There is some real doubt if the Lodge theory should be expected to be valid at the lower concentrations, since Janeschitz-Kriegl[40] has shown that form birefringence becomes important in such cases: but if this is true, the stress-optical law will not be valid, either.

Philippoff has also made direct normal stress measurements using a modified Weissenberg rheogoniometer. These data are plotted in Figure 10. The dotted lines represent the same data as deduced from the birefringence measurements, correlating with the total shear stress and not correcting for the viscosity of the solvent. We see that the fit is pretty good, but far from perfect, especially considering the logarithmic scale. Unfortunately there are no direct mechanical measurements at the lower concentrations.

From these results it appears that, for PIB in decalin, the stress-optical law is well enough demonstrated to be usefully applicable over a wide range of stresses and a wide range of concentrations. For the higher concentrations, it is not particularly important whether the SBR depends on $(\eta - \eta_0)$ or on η. The optical measurements are, in general, more sensitive than mechanical measurements for normal stresses provided we can be sure that the deviation of the angle of isocline from the principal strain rate direction is due to stress effects and not to orientation effects. The fact that the data for 100% PIB also fell in line with the solution data raises further theoretical questions since Lodge's theory definitely should not hold for this case.

Concentrated polymer solutions have been considered by Janeschitz-Kriegl[40] in another quasi-static model. He concludes that the amount of

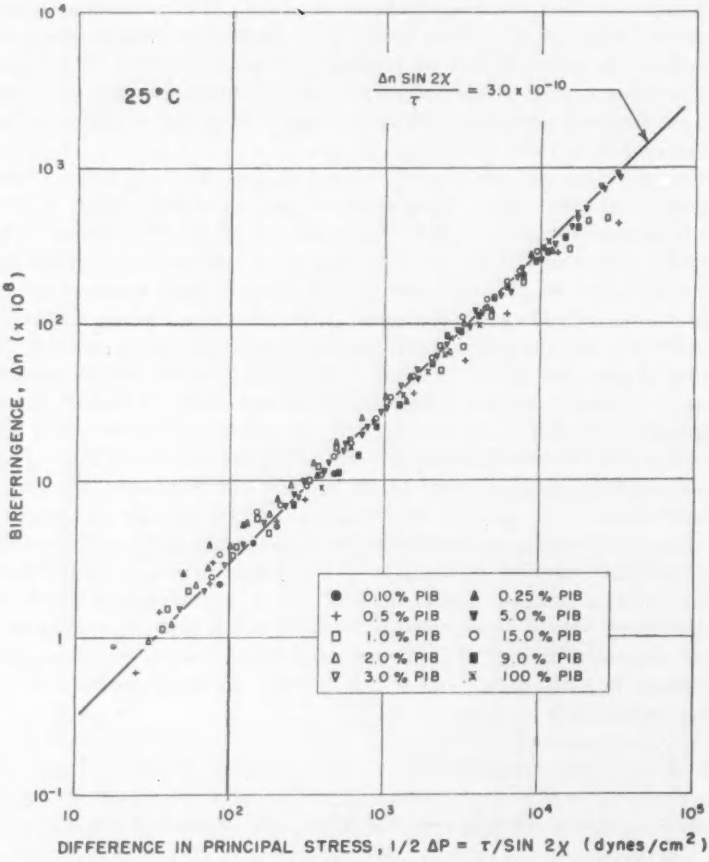

Fig. 10. Birefringence as a function of difference in principal stress for polyisobutylene in Decalin.

birefringence depends on $\Gamma(\eta - \eta_0)$ provided the velocity gradient is sufficiently small. He also calculates the amount of form birefringence for isolated polymer molecules in dilute solutions when the index of refraction of the polymer and that of the solvent are different, and finds a distinct and measurable effect. Cerf[41] has looked at the case of dilute solutions of deformable molecules and has shown that for very low velocity gradients they should behave like rigid particles, for very high gradients like deformable systems, with all intermediates in between. This type of behavior has been experimentally observed by Leray.[42]

We can summarize the theoretical findings by saying that, if we can describe the mechanism producing SBR by a quasi-static statistical process in which form birefringence is small and overall orientation of asymmetric

macromolecules is not important, the stress-optical law will be valid. If, on the other hand, the form of the flow field is varying too rapidly from point to point for equilibrium to be approximated, we should not expect to have a simple stress optical law. The question naturally arises: how fast is too fast? This will depend on the relaxation time spectrum of the elements giving rise to the SBR. Just because we appear to get a simple stress optical law for a substantially stagnant flow such as Couette flow does not mean *a priori*, that the stress optical law will still be valid in a more general situation: the rate of change of hydrodynamic "history" must be slow enough that the molecular arrangement reflects the local conditions. If we must take the prior history into account we have a rather cumbersome tool, at best. For the systems, such as polyisobutylene, for which a stress-optical law is valid in Couette and capillary flow there still seems to be too little evidence to judge how rapidly the optical properties will follow a change in flow conditions, either for transient changes or complicated steady flow patterns.

Assuming we have a fluid which strictly follows the stress-optical law, what of a quantitative nature can we deduce from the optical measurements? First we must confine our flow studies to two-dimensional situations. If we measure both the angle of isocline and the amount of birefringence we can deduce the direction of the two axes of the deviatoric stress ellipsoid lying in the plane of the flow, and the difference of the principal stresses, and no more. For two-dimensional incompressible flow we have two equations of motion, the equation of continuity and the constitutive equation with which to work. We have six unknown quantities in the plane: s_{11}, s_{12}, s_{22}, u, v, and p. We know s_{12} and $s_{11} - s_{22}$, so presumably we have enough information to reconstruct the flow. Practically this is not simple. We probably do not know enough about the system to use the constitutive equation effectively, and the equations of motion are, in general, nonlinear. The reconstruction of the deviatoric stress field can be carried along lines equivalent to those used for flow analysis of colloidal solutions given in Section IV, with the simplification that the optic axes are coaxial with the principal stress axes. Bogue and Peebles[35] suggest using the Airy stress function as a means of constructing the stress pattern from the SBR data, similar to the method of reconstructing the flow pattern in Newtonian systems from the stream function. This will require a measurement of the stress distribution (including the normal stresses) over the boundaries. The stress distribution will, however, not give the flow pattern unless we know the relationship between the stress tensor and the strain-rate tensor for the polymer being studied.

One of the most ingenious and important applications of the stress-optical law has been to check the Weissenberg hypothesis concerning the equality of s_{22} and s_{33} in shear flow. If the magnitude of the SBR is, indeed, proportional to the difference of the principal stresses, then if observations are made along the streamlines in shear flow no birefringence should be detected. Philippoff[43] made observations along the axis of a

capillary in a variety of solutions of polyisobutylene, rubber, polysiloxane and nitrocellulose, finding no birefringence, hence deducing that the Weissenberg hypothesis is valid for these systems. Systems of rigid particles, such as vanadium pentoxide and tobacco mosaic virus showed marked birefringence, as would be expected for orientable systems. It would be interesting to extend this type of experiment to the type of system discussed by Cerf[41] in which orientation effects should predominate at low shear and deformation effects at high shear.

VI. Summary and Conclusions

1. Qualitative Studies

The use of streaming birefringence for qualitative observation of the character of flow separation, onset of turbulence, existence of secondary flows, etc., has already proved extremely effective. Great care must be exercised, however, that the rheological properties of the birefringent liquid used are fully understood, and, indeed are those of the system of interest. Even small departures from Newtonian behavior may introduce marked qualitative differences in the nature of the flow. SBR should be particularly valuable in qualitative studies of the flow of viscoelastic systems to detect the existence or absence of secondary flows.

2. Quantitative Studies

(a) **Pure Newtonian Liquids.** Pure liquids with Newtonian viscosity behavior can probably be used for quantitative analysis of complex two-dimensional flows using SBR if the measuring techniques are sufficiently sensitive. The case in which the fluid elements change hydrodynamic environment with great rapidity has not been checked experimentally although the short relaxation time for the small molecules of these substances will probably insure that the optical properties are reflecting the local flow situation rather than the past history.

(b) **Colloidal Solutions.** Flow analysis from the SBR data for colloidal solutions can be made with assurance only if all portions of the flow are within the range in which both the retardation Δn and the variation of the angle of isocline χ are linear with velocity gradient in Couette flow, the change in birefringence with concentration is linear, and the relaxation time of the colloidal particles is short enough that one can be sure that the local optical effect is due to the local flow field and does not depend on the upstream history of the particles. This is, indeed, a very stringent limitation. For many engineering purposes one can work considerably outside this range to obtain "adequately" quantitative data but one must recognize that the discrepancies with theoretically predicted results are probably due to systematic errors and not to random errors.

(c) **Polymeric Solutions.** Certain polymeric solutions, particularly polyisobutylene in decalin have been sufficiently studied to assure that a stress

optical law is valid and the Weissenberg hypothesis is also valid. For a study of the stress patterns in flow of such viscoelastic systems, SBR should be most useful. Care must be taken that time-history effects are not important (unless it is these one wants to study). If a new polymeric system is to be used, it would be essential to ascertain that the stress-optical law is valid; that the Weissenberg hypothesis is valid; and that the relaxation time is short enough that the optical properties correctly reflect the local stress situation.

The construction of the flow pattern for these systems will require measurements other than with SBR, or the knowledge of the constitutive equation of the system.

3. Instrumental

Photographic techniques are the easiest to use if the amount of retardation is sufficient to give adequate resolution. It seems probable that even boundary layer studies might be possible by using a light beam which has virtually no converging or diverging rays, as can be obtained with a laser. This should be particularly valuable with polymer solutions, where large effects are often available. It seems questionable if any colloidal system will show enough birefringence for the photographic method to be applicable for quantitative investigation, or even for qualitative investigations unless non-Newtonian effects are being studied.

Point-by-point measuring techniques can be used for spatial resolution of the order of 0.1 mm. and can be made extremely sensitive and relatively easy to use with photoelectric detection.

References

1. Maxwell, J. C., *Proc. Roy. Soc.*, **148,** 46 (1873).
2. Humphrey, R. H., *Proc. Phys. Soc. (London)*, **35,** 217 (1923).
3. Sadron, Ch., *Compt. Rend. Acad. Sci.*, **197,** 1293 (1933).
4. Alcock, E. D., and Ch. Sadron, *Physics*, **6,** 92 (1935).
5. Hauser, E. A., and D. R. Dewey, II, *Ind. Eng. Chem.*, **31,** 786 (Letter) (1939).
6. Hauser, E. A., and D. R. Dewey, II, *J. Phys. Chem.*, **46,** 212 (1942).
7. Dewey, D. R., II, *Visual Studies of Fluid Flow Patterns Resulting from Streaming, Double Refraction*, Doctoral Dissertation, Massachusetts Institute of Technology (1941).
8. Knapp, R. T., V. A. Vanoni, and J. W. Daily, *The High Speed Water Tunnel at the California Institute of Technology*, Hydrodynamic Laboratory Report ND1 (May 29, 1942).
9. Knapp, R. T., J. Levy, J. P. O'Neill, and F. B. Brown, *Trans. ASME*, **70,** 437 (1948).
10. Leaf, W., *Mech. Eng.*, **67,** 586 (1945).
11. Binnie, A. M., *Proc. Phys. Soc.*, **57,** 390 (1945).
12. Binnie, A. M., and J. S. Fowler, *Proc. Roy. Soc.*, **192,** 32 (1947).
13. Lindgren, E. R., *Arkiv. Fysik*, **7,** 293 (1953); *Appl. Sci. Res.*, **4(A),** 313 (1954); *Arkiv. Fysik*, **12,** 1 (1957); *ibid.*, **15,** 97, 503 (1959); *ibid.*, **16,** 101 (1959); *ibid.*, **18,** 449, 533 (1960).
14. Ericksen, J. L., *Quart. Appl. Math.*, **14,** 319 (1956).

15. Criminale, W. O., Jr., J. L. Ericksen, and G. L. Filbey, Jr., *Arch. Rational Mech. Anal.*, **1**, 410 (1957).
16. Jerrard, H. G., *Chem. Revs.*, **59**, 345 (1959).
17. Frocht, M. M., *Photoelasticity*, Vol. I, Wiley, New York, 1941.
18. Wayland, H., *J. Appl. Phys.*, **26**, 1197 (1955).
19. Sutera, S. P., and H. Wayland, *J. Appl. Phys.*, **32**, 721 (1961).
20. Björnståhl, Y., *J. Opt. Soc. Am.*, **29**, 201 (1939).
21. Wayland, H., and J. Badoz, *Compt. rend. acad. sci.*, **250**, 688 (1960).
22. Intaglietta, M., *Streaming Birefringence Study of the Interactions of Submicroscopic Particles*, Doctoral Dissertation, California Institute of Technology (1963).
23. Raman, C. V., and K. S. Krishnan, *Phil. Mag.*, **5**, 769 (1928).
24. Vorländer, D., and R. Walter, *Z. Phys. Chem.*, **118**, 1 (1925).
25. Sadron, Ch., *J. Phys. Radium* (7), **7**, 263 (1936).
26. Jerrard, H. G., *J. Appl. Phys.*, **21**, 1007 (1950).
27. Peterlin, A., and H. A. Stuart, *Z. Phys.*, **113**, 663 (1939).
28. Tolstoi, N. A., *Dok. Akad. Nauk, SSSR*, **59**, 1563 (1948).
29. Wayland, H., *J. Phys. Radium*, **16**, 278 (1955).
30. Squire, W., *App. Sci. Res. A (Netherlands)*, **10**, 439 (1961).
31. Peterlin, A., and H. A. Stuart, *Z. Physik*, **12**, 1 129 (1939); *Hand- und Jahrbuch der Chemischen Physik*, Becker u. Erler, Leipzig, **8, Abt. 1B** (1943).
32. Wayland, H., *J. Chem. Phys*, **33**, 769 (1960).
33. Honeycut, E. H., Jr., and F. N. Peebles, *Rheological Properties of Aqueous Solutions of Milling Yellow Dye*, Progress Report 3 (Contract Nonr-811(04) Univ. of Tennessee, Knoxville 1955.
34. Prados, J. W., and F. N. Peebles, *A. I. Ch. E. J.*, **5**, 225 (1959).
35. Bogue, D. C., and F. N. Peebles, *Trans. Soc. Rheol.*, **6**, 317 (1962).
36. Philippoff, W., *Trans. Soc. Rheol.*, **5**, 163 (1961); *Ind. Eng. Chem.*, **51**, 323 (1959).
37. Lodge, A. S., *Nature*, **176**, 838 (1955); *Trans. Faraday Soc.*, **52**, 120 (1956).
38. Philippoff, W.. *Trans. Soc. Rheol.*, **1**, 95 (1957).
39. Brodnyan, J. G.. F. H. Gaskins, and W. Philippoff, *Trans. Soc. Rheol.*, **1**, 109 (1957).
40. Janeschitz-Kriegl, H., *Makromol. Chem.*, **33**, 55 (1959); *ibid.*, **40**, 140 (1960).
41. Cerf, R., *J. Phys. Radium*, **19**, 122 (1958).
42. Leray, J., *J. Chim. Phys.*, **57**, 323 (1960).
43. Philippoff, W., *Rheol. Acta*, **1**, 37 (1961).

Résumé

Cet article rassemble les données théoriques et expérimentales généralament valables pour établir des critères permettant à l'expérimentateur qui le désire d'utiliser la biréfringence d'écoulement comme un instrument pour l'étude de l'écoulement fluide. On y décrit et on discute les techniques expérimentales et les possibilités pour rendre visible l'écoulement qualitatif et quantitatif par la biréfringence d'écoulement dans les liquides Newtoniens puis les suspensions colloïdales et des solutions polymériques diluées ou concentrées. On signale des méthodes de reconstruction de la vitesse et des champs de tension à partir des données de biréfringence.

Zusammenfassung

In der vorliegenden Mitteilung werden die gegenwärtig vorhandenen theoretischen und experimentellen Unterlagen zur Aufstellung von Kriterien, die dem Experimentator bei der Benützung der Strömungsdoppelbrechung als Werkzeug zur Untersuchung des Flüssigkeitsfliessens behilflich sein können, besprochen. Ein Überblick über die Versuchmethodik wird gegeben und die Möglichkeit für eine qualitative und quantitative Darstellung des Fliessens durch Strömungsdoppelbrechung in rein Newton'schen Flüssigkeiten, killoiden Suspensionen sowie verdünnten und konzentrierten Polymerlösungen wird diskutiert. Methoden zur Rekonstruktion des Geschwindigkeits- und Spannungsfeldes aus Doppelbrechungsdaten werden angegeben.

JOURNAL OF POLYMER SCIENCE: PART C NO. 5, PP. 37-53

Birefringent and Rheologic Properties of Milling Yellow Suspensions

F. N. PEEBLES, J. W. PRADOS, and E. H. HONEYCUTT, JR.,
The University of Tennessee, Knoxville, Tennessee

Synopsis

Aqueous suspensions of Milling Yellow dye have been found to be useful for engineering flow studies by employing established birefringent techniques. In the present work, the basic birefringent and rheologic properties of Milling Yellow suspensions were measured for a range of deformation rates important to the engineering applications. A concentric-cylinder polariscope was used to measure the amount of birefringence and the angle of extinction for ten Milling Yellow suspensions at 25°C. varying in concentration from 1.25 to 1.46% dye by weight. The optical properties exhibited by these suspensions are similar to those of a number of colloidal suspensions as reported by past investigators. Rheologic data for Milling Yellow suspensions in the same concentration range were measured at 25°C. for deformation rates of 50–10^4 sec.$^{-1}$ by means of a capillary viscometer. Over the complete range of deformation rates the rheologic data are accurately described with the Powell-Eyring relationship for pseudo-plastic materials.

Introduction

The engineering application of optical techniques based on flow birefringence for determination of velocity profiles and stress distribution in laminar flow, detection of regions of flow separation and boundary layer reattachment, and onset of turbulence is well-known and employed widely. In 1953, some of the possibilities for visualization of flow phenomena with aqueous suspensions of Milling Yellow dye were discussed,[10] and since then it has been shown that quantitative measurements of velocity and stress distributions can be made for two-dimensional laminar flows.[2,9,13] Other work with Milling Yellow dye suspensions includes the dynamic birefringence studies of Thurston,[14] the work on laminar-turbulent transition by Gilbrech,[5] and a large number of flow studies not reported in the literature.

It is the purpose of this paper to present experimental data on the basic birefringent and rheologic properties of Milling Yellow suspensions. Such data were obtained at 25°C. for a range of dye concentrations of interest for flow studies. Birefringence and extinction angle measurements were made with a concentric cylinder polariscope using well-established techniques.[3] The rheologic measurements were made with a capillary viscometer. Viscosity data were obtained from the pseudo-shear diagrams by standard methods.[7]

Optical Theory

The use of plane polarized light to measure the amount of birefringence produced by liquid motion is well-known, and the quantitative features of the phenomenon have been described by many writers.[4,6] In summary, if a plane-polarized light wave moves through a birefringent liquid and then through a second polarizer, the vibration of the transmitted light wave can be represented by

$$u = a \sin 2\phi \sin \frac{\pi\delta}{\lambda} \cos (ct - x - \delta/2) \tag{1}$$

where u is the displacement of the vibration from the axis at time t; a is the amplitude of the vibration; λ is the wavelength of the light vibration; x is the arbitrary phase retardation indicating the displacement is not necessarily zero at $t = 0$; δ is the relative retardation due to passage through the birefringent liquid; and ϕ is the angle between optic axis and plane of vibration of the incident wave.

Since the intensity of transmitted light is proportional to the square of its amplitude of vibration, eq. (1) indicates that zero intensity results when

$$\phi = N(\pi/2) \text{ and } \delta = N\lambda \tag{2}$$

where N is the fringe order ($= 0, 1, 2, 3, \ldots$).

These are the well-known conditions for the extinction angle and the isochromatic fringes, respectively.

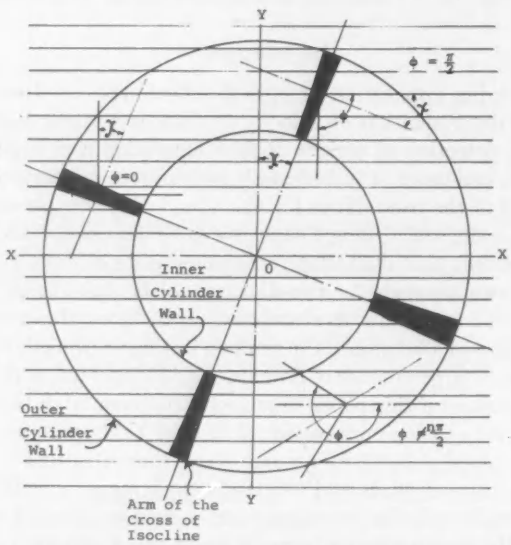

Fig. 1. Top view of annulus of the concentric cylinder polariscope showing the cross of isocline and the optical orientation of the birefringent liquid. Parallel lines indicate plane of vibration of light leaving the polarizer (direction OX in Fig. 1).

The extinction angle X is defined by Edsall[3] as the angle made by the optic axis of the birefringent liquid with the streamlines. In the concentric cylinder polariscope used in this work, four dark areas, forming the well-known cross-of-isocline, appear in the annulus of the flow cell at the points where $\phi = 0, \pi/2, \pi$, and $3(\pi/2)$, as indicated by eq. (2). This is shown pictorially in Figure 1. The small angle made by the arms of this cross with the axes of polarization OX and OY is the extinction angle, χ.

The isochromatic fringes which are indicative of the amount of birefringence appear as dark bands concentric with the axis of the flow cell. These bands move outward across the annulus and the higher order fringes move into the annular field in succession as the speed of the outer cylinder is increased. The amount of birefringence can be measured by counting the isochromatic fringes as the speed of the rotating cylinder is increased from zero, thereby determining N. ($N = 0$ corresponds to the zero retardation occurring when the liquid is at rest.) The amount of birefringence expressed as the difference in the indices of refraction for the extraordinary and the ordinary rays passing through the test liquid contained in the flow cell can be calculated from

$$|n_e - n_0| = \frac{N\lambda}{S} \tag{3}$$

where $|n_e - n_0|$ is the amount of birefringence and S is the length of light path in the liquid.

Equation (3) makes use of the condition for the existence of the isochromatic fringes as given by eq. (2) and the calculation of the relative retardation of the two light waves as determined by the length of light path and light speed for the two rays.

Experimental

Test liquids were prepared from commercial Milling Yellow NGS dye (National Aniline and Dye Co.) by mixing the powder with distilled water to give about 1% dye by weight. The mixture was then heated to the boiling point to dissolve the dye, and evaporated to the desired concentration. For the test liquids investigated the dye concentration was determined by carefully evaporating a weighed sample of the liquid to dryness at 100°C., and then weighing the residue. Determinations of the dye concentration by this means could be reproduced within $\pm 0.002\%$ dye by weight.

Birefringent and rheological properties of Milling Yellow dye suspensions in the concentration range of 1.25–1.45% by weight were determined at 25.0°C. Following is a brief description of the concentric cylinder polariscope, capillary viscometer, and experimental procedures employed in the measurements.

Concentric Cylinder Polariscope

The measurements of extinction angle and amount of birefringence for the Milling Yellow dye suspensions were carried out in a concentric cylinder

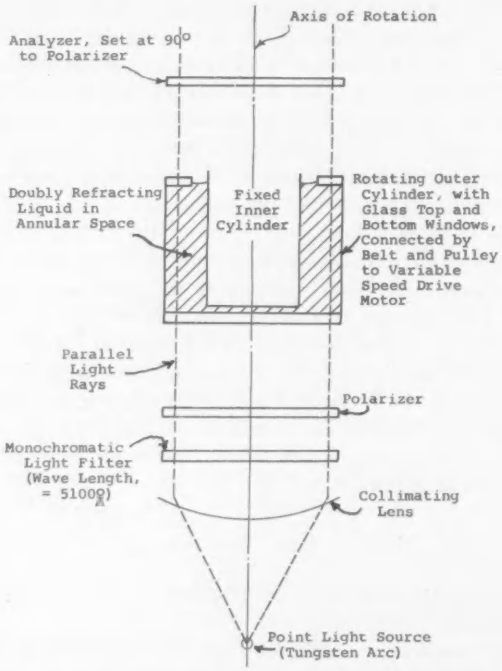
Axis of Rotation
Analyzer, Set at 90° to Polarizer
Doubly Refracting Liquid in Annular Space
Fixed Inner Cylinder
Rotating Outer Cylinder, with Glass Top and Bottom Windows, Connected by Belt and Pulley to Variable Speed Drive Motor
Parallel Light Rays
Polarizer
Monochromatic Light Filter (Wave Length, = 5100 Å)
Collimating Lens
Point Light Source (Tungsten Arc)

Fig. 2. Schematic diagram showing the components of the concentric cylinder polariscope.

polariscope manufactured by the Rao Instrument Company, New York. An instrument almost identical in every respect with the one used in the present work was described by Edsall,[3] and their article may be consulted for any details not given here. The assembly of major components of this unit is indicated schematically in Figure 2. All components except the monochromatic filter are attached to an optical bench for rigid, precise alignment.

The light source is a tungsten arc lamp (Sylvania type C-25) which gives an intense light, emanating from a small area, thereby approximating a point source. It is mounted at the focal point of a collimating lens, which focuses parallel rays of light upward through the bottom of the flow cell. A monochromatic light filter (green, wavelength 5100 A.) is placed above the lens for measurements of the birefringence, but is removed for extinction angle determinations. The polarizer is located below the flow cell in a friction mounting, which allows it to be adjusted and removed for cleaning. The analyzer is mounted above, on a support which may be removed completely from the optical bench to allow the flow cell to be filled conveniently. The analyzer support assembly also contains a quarter wave plate which may be positioned below the analyzer for use as a compensator.

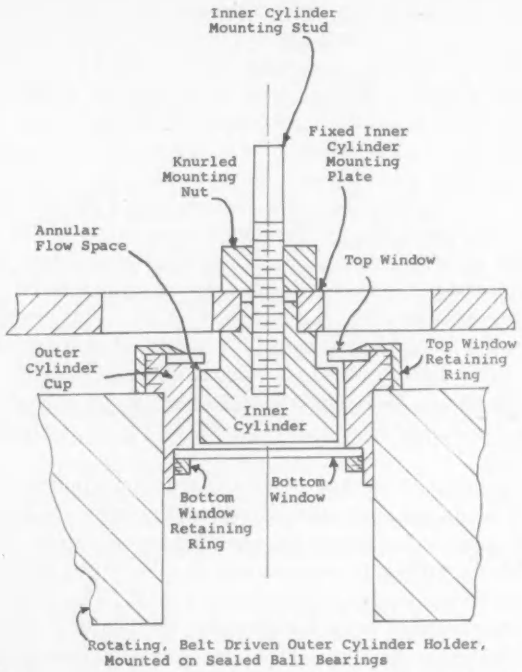

Fig. 3. Cross sectional assembly drawing of concentric cylinder flow cell.

Its utilization would enable one to measure amounts of double refraction corresponding to a retardation of less than one wavelength of light. However, the Milling Yellow suspensions employed in the present investigation produced relatively large retardation at low rates of shear, and the compensator was not needed. Not indicated in Figure 2 is a set of movable 90° cross hairs, mounted between the polarizer and the bottom of the flow cell. These were used to measure the extinction angle.

A drawing of the flow cell is shown in Figure 3. The annular flow region is formed by the space between the fixed inner cylinder and the rotating outer cylinder. The inner cylinder is mounted from above by a supporting plate, which holds it free from the outer cylinder and assures that its position is concentric to that of the outher cylinder. The outer cylinder assembly is made up of two elements; a rotor, mounted on sealed ball bearings and equipped with a drive pulley, and a cup which fits in the rotor and forms the outer surface of the flow cell. The bottom of the cup is of glass, and a glass top window prevents the formation of a meniscus in the liquid, which would act as a lens and distort the parallel light rays. Except for the glass top and bottom windows, all cylinder parts are of stainless steel. Each glass piece is mounted between two neoprene washers, and is held in place by a threaded fitting. The annular dimensions can be varied

by interchanging the three inner cylinders provided. This permits measurements to be made over a wide range of shear rates, with the same range of instrument rotation speeds. The radial dimensions of the cylinders are as follows: outer cylinder, 0.500 in.; large inner cylinder, 0.480 in.; medium inner cylinder, 0.460 in.; small inner cylinder, 0.349 in.

The liquid depth in the cell is determined by the distance from glass bottom to top glass ring of the outer cylinder cup. For the cylinders furnished by the manufacturer, this distance was 1.768 in. However, in order to increase the clarity of the interference bands in the liquid, four new cylinders were fabricated, one outer, and three inner, with radical dimensions identical to those of the original cylinders but shorter in length, so as to provide a liquid depth of 0.570 in. This modification was made to improve fringe definition at high orders. For fringe orders above nine to ten, the observed optical phenomena in the polariscope become indistinct. This results from overlapping of light waves of slightly different wavelengths, because of incomplete filtering action by the monochromatic light filter.

The outer cylinder of the flow cell is connected by a pulley and an elastic belt to the drive motor. The drive unit itself consists of a variable-speed, direct current operated motor and a regulated power supply. The motor is provided with six pulleys, three operating on a low speed shaft driven by a gear train, and three directly on the armature shaft. This arrangement provides a continuous speed range for the outer cylinder of the flow cell, from approximately 0.8 to 4000 rpm. This range was more than adequate for all the measurements made in this investigation.

The speed of rotation of the cell was measured by counting revolutions of the outer cylinder for timed intervals, up to about 120 rpm. At higher speeds, a flashing stroboscope (Type BL-631 Strobotac, manufactured by the General Radio Corporation) was used.

Birefringence and Extinction Angle Measurements

The techniques used in the measurement of the extinction angle and the birefringence, while simply in principle, required considerable practice and refinement before reproducible results were obtained. Two factors, in particular, worked to disrupt the accuracy of the results: (*a*) temperature variations and (*b*) evaporation of water from the solution in the flow cell. Since the birefringent properties of Milling Yellow suspensions are highly dependent on temperature and dye concentration, both of these sources of error were important. A temperature rise of 0.2–0.3°C. was sufficient to lower noticeably the amount of birefringence at a given rate of shear. Therefore, it was necessary to empty the cell and allow it to cool at frequent intervals. The effect was most marked in tests on the more viscous solutions, and even with the dilute solutions at high rates of shear. The effects of evaporation were noticeable if the fluid was left in the cell for longer than fifteen or twenty minutes. This was manifested in an increased amount of birefringence (due to increased dye concentration) for a given rate

of shear. By making measurements rapidly and refilling the cell at frequent intervals, it was possible to keep the effects of evaporation to a minimum.

To prepare the concentric cylinder polariscope for measurements, first the optical system was adjusted. The collimating lens was set to give parallel rays of light by placing the inner and outer cylinders in position, and projecting the image of the annulus on a piece of white cardboard, held about a foot above the cell, in a darkened room. The lens was moved until a clear sharp image of the annulus, without halos, appeared on the cardboard. The plane of polarization of the polarizer was oriented with the cross hair scale by use of a 3° bifield polarizer. A 3° bifield polarizer is a plate of polarizing material really consisting of two polarizers whose planes of polarization are 3° apart. A line scribed on the plate bisects these planes. To adjust the instrument polarizer, the bifield was set so that this line was perpendicular to the desired plane of polarization (aligned with a cross-hair at the 90° position). Then the instrument polarizer was turned until both halves of the bifield appeared equally dark. A very accurate adjustment could be made in this manner. The analyzer support assembly was mounted on the optical bench, and the analyzer turned until it produced maximum extinction of the light coming from the polarizer. These adjustments for the polarizer and analyzer were checked at intervals, but rarely needed correction.

When the optical system had been adjusted, the inner and outer cylinders were assembled as shown in Figure 3, and were slowly filled with a long-needled syringe. Care was taken to prevent the entrapment of air bubbles in the cell. Once the cell had been filled, the optical measurements were begun.

The measurements of the amount of birefringence were carried out as follows. The motor was started and its speed slowly increased until a dark band was observed to move outward across the annulus. When the band was at the center of the annulus (this could be estimated accurately by eye, since the annular gap was quite narrow) the speed of rotation of the outer cylinder was measured. This was done by timing a number of revolutions with a stopwatch at low speeds (less than 120 rpm) or with the Strobotac at higher speeds. The speed of the cylinder was increased and recorded as each band moved into the center of the annulus. At intervals, the cylinder was slowed down so that previously observed bands appeared, and second speed measurements were made. This served as a check as to whether or not the liquid was being heated up enough to change its birefringent properties. If a point could not be reproduced, the motor was stopped; the cylinder was cleaned and allowed to cool, then refilled with fresh liquid and the irreproducible portion of the run repeated. The cylinder was never run for more than fifteen or twenty minutes at a time without refilling, in order to prevent the evaporation effects from becoming noticeable.

Much trial and error indicated that better results could be obtained by making separate runs to measure the extinction angle, rather than trying to

measure it along with the amount of birefringence. Attempts to measure the two simultaneously, slowed down the run to such an extent that only a few measurements could be made before it became necessary to refill the cell to prevent evaporation effects. The extinction angle measurements were made by aligning one of the instrument cross-hairs to coincide with an arm of the cross of isocline, as viewed through the analyzer. Four such measurements were made at a given speed of rotation, one for each arm of the cross, and the arithmetic average of the readings was taken. This provided somewhat greater accuracy in the extinction angle values, which were difficult to determine, even at low speeds of rotation, to much closer than $\pm 0.5°$. At high speeds, variation in rate of shear across the annulus, due to non-Newtonian flow behavior, caused the cross to spread out and become quite diffuse. This reduced the accuracy of the extinction angle readings to about $\pm 2.0°$. Since the extinction angle values were less accurate and did not seem to be as sensitive to changes in temperature and concentration as for the amount of birefringence, it was not necessary to empty and refill the cell as frequently during the extinction angle measurements as it was during measurements of the birefringence.

The amount of birefringence was calculated from the observed fringe order means of eq. (3).

The shear rate at the center of the annular space of the flow cell was calculated from

$$G = \frac{8\Omega r_1^2 r_2^2}{(r_1 + r_2)^2(r_2^2 - r_1^2)} \tag{4}$$

where G is the shear rate; Ω is the speed of rotation of outer cylinder; r_1 is the radius of inner cylinder; and r_2 is the radius of outer cylinder.

Capillary Viscometer and Procedure

The capillary viscometer used for rheologic measurements is a simple modification of the Ostwald-type. The important features are illustrated in Figure 4. The capillary section is approximately 0.04 cm. i.d. by 20 cm. long, and the sample bulbs are nominally 5 cc. internal volume. The dimensions of the capillary and the volumes of the sample bulbs were determined from very careful physical measurements and viscometric measurements with standard oils. In general it was found the viscosity of standard oils determined from the dimensions of the capillary agreed with the National Bureau of Standards' values within 0.1%.

Figure 5 shows schematically the viscometer with the necessary auxiliary equipment for pressure drop measurement and temperature control. Runs were made by timing with a stopwatch the interval for the volume of test liquid in the sample bulb to flow through the capillary. Data for a wide range of shear rates were obtained by using a range of drive-fluid pressures from a few millimeters to about 100 cm. of mercury.

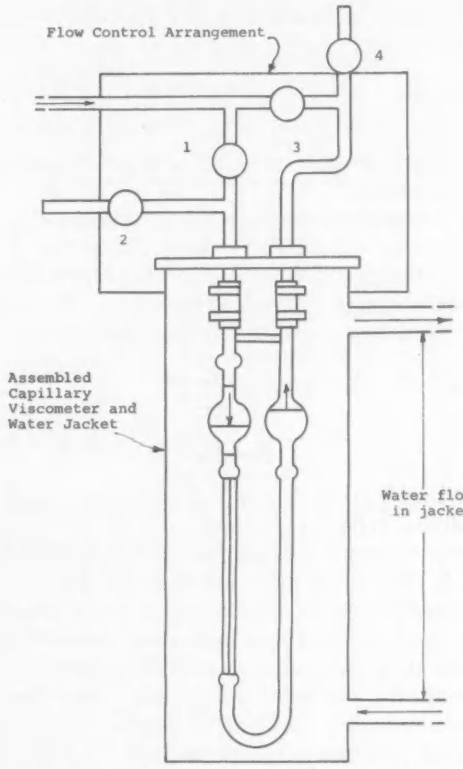

Fig. 4. Assembled capillary and flow control unit.

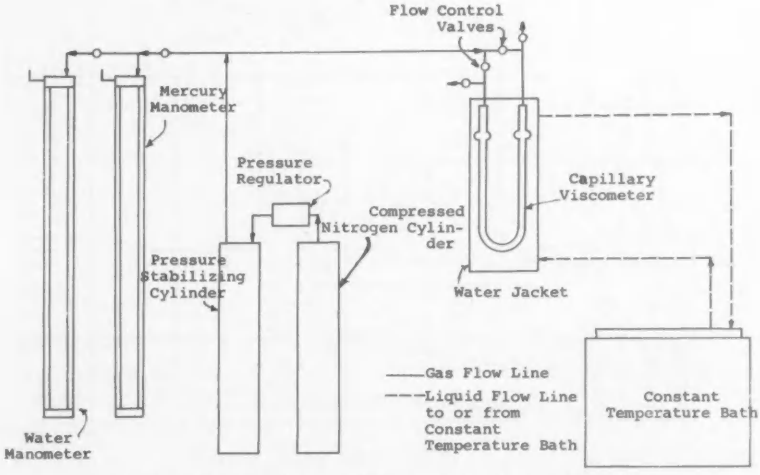

Fig. 5. Schematic diagram of the capillary viscometer facility.

Viscosity values were calculated from the apparent values by means of the relationship

$$\frac{1}{\mu} = \frac{1}{\mu_a} + \frac{\tau_w}{4} \frac{d(1/\mu_a)}{d\tau_w} \tag{5}$$

where μ is the viscosity at shear stress, τ_w; μ_a is the apparent viscosity; and γ_w is the wall shear stress.

The apparent viscosity was calculated from the Hagen-Poiseville equation for steady laminar flow in a capillary. Values for the derivative in eq. (5) were obtained by numerical differentiation of the experimental relationship between apparent viscosity and wall shear stress. The shear rate corresponding to the viscosity was calculated from the equation,

$$G = \frac{\tau_w}{\mu} \tag{6}$$

Results

Experimental results for the amount of birefringence and the extinction angle for nine Milling Yellow suspensions are given in Figures 6 through 10. The amount of birefringence is shown plotted as a function of shear rate in Figures 6 and 7. For the liquids tested it can be noted that at low shear rates the birefringence is proportional to shear rate as suggested by the theoretical work of Boeder,[1] Peterlin and Stuart,[11] and Wayland.[15] In the case of increasing shear rates the relation between $|n_e - n_0|$ and shear rate becomes nonlinear, and for very high shear rates the data suggest a second range of linearity. The results clearly reveal the marked dependence on dye concentration in the range of 1.2–1.5% dye by weight.

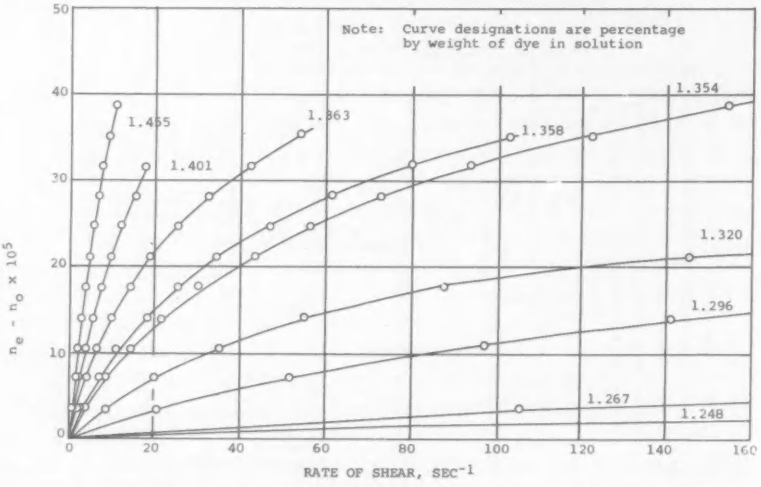

Fig. 6. Birefringence as a function of rate of shear for liquids tested.

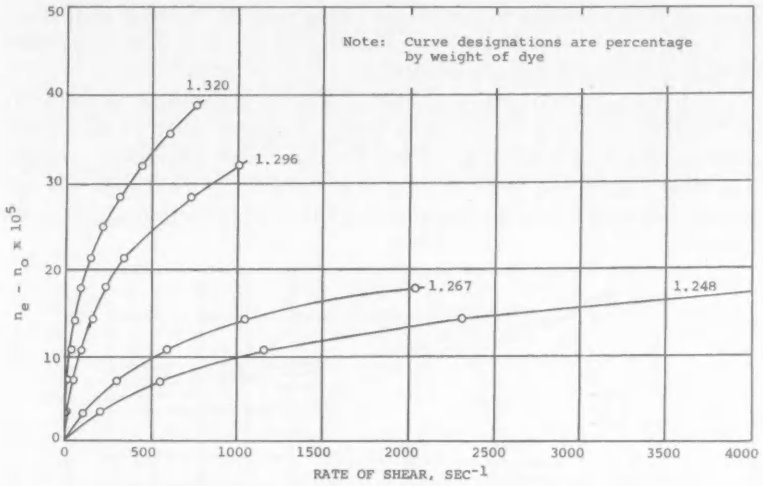

Fig. 7. Birefringence as a function of rate of shear for dilute solutions (high speed range).

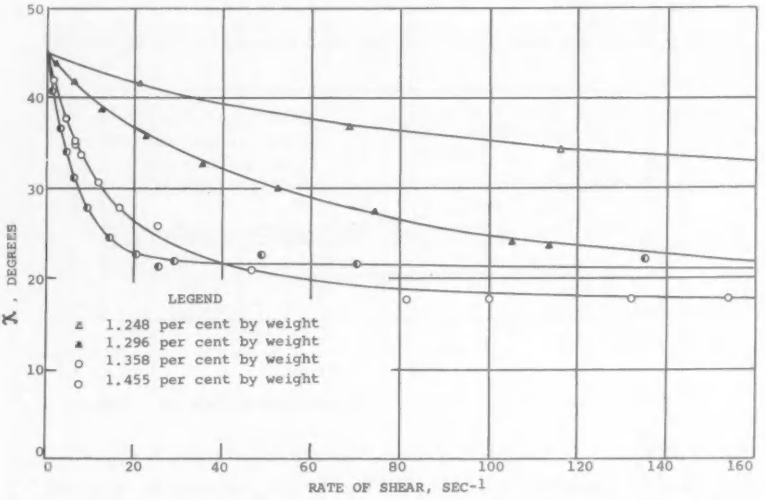

Fig. 8. Extinction angle as a function of rate of shear for four representative solutions in a moderate shear range.

Below about 1.2% dye the Milling Yellow suspensions do not exhibit birefringence, and at the higher concentrations where intense birefringent behavior is found, the dye suspensions are gels and show birefringence even in the absence of flow.

Values of the extinction angle are plotted in Figures 8, 9, and 10, a function of shear rate. In all instances, the extinction angle is 45° at zero shear

rate and then decreases to saturation values near 20° at very high shear rates. The shear rate range for saturation extinction angles decreases with increasing Milling Yellow concentration.

The birefringent properties of Milling Yellow suspensions, as reflected by the high values of birefringence (10^{-4} compared to 10^{-12} for liquids showing molecular birefringence) and the shear rate dependence, suggest that these liquids can be considered as suspensions of rigid rods. If one accepts this model then the experimental values of extinction angle can be

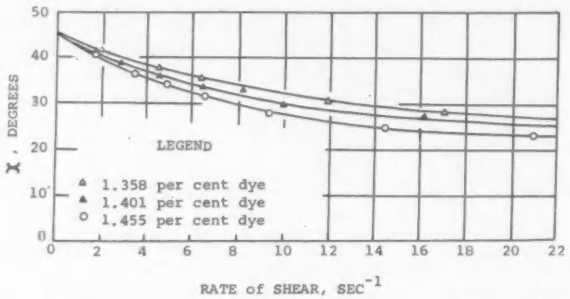

Fig. 9. Extinction angle of three concentrated solutions at low rates of shear.

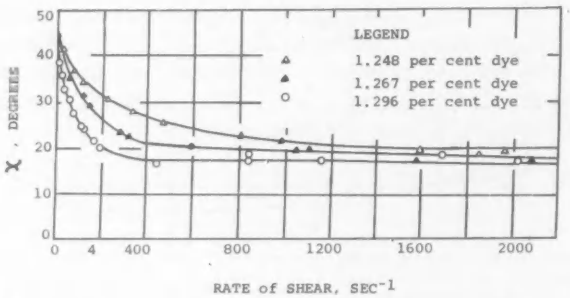

Fig. 10. Extinction angle of three dilute solutions at high rates of shear.

used with theoretical results on particle orientation[1] to show that the effective particle diameter is in the Milling Yellow suspensions about 0.5 μ. Details of these calculations are given.[12]

In general, Milling Yellow suspensions exhibit non-Newtonian flow characteristics. Figures 11 and 12 show typical rheologic curves plotted as shear diagrams. The data for liquids in the range of concentrations from about 1.2 to 1.5% dye by weight show linearity at low and high shear rates, and as in the case of the optical data show a marked dependence on dye concentration. Viscosity values range from near 1.5 cp at shear rates approaching 10^4 reciprocal sec.–400 cp at very low shear rates, depending on the dye concentration.

As cited in the previous section, the shear rates were obtained by calculation from the apparent viscosity values. The basis of this established method of calculation is that the shear stress is a unique function of shear rate. One test of the validity of this assumption is that the apparent viscosity of a given liquid is a function of wall shear stress and independent of capillary diameter. Figure 13 shows data on the apparent viscosity of a Milling Yellow suspension containing 1.442% dye as measured in three

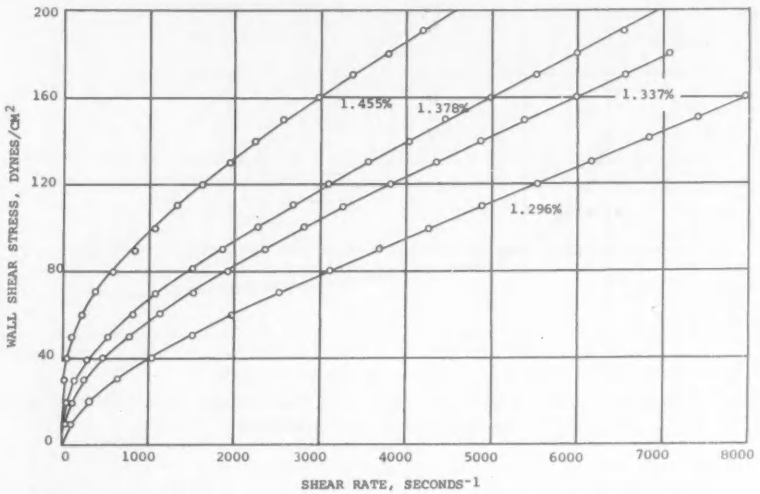

Fig. 11. Wall shear stress as a function of shear rate for the solutions tested.

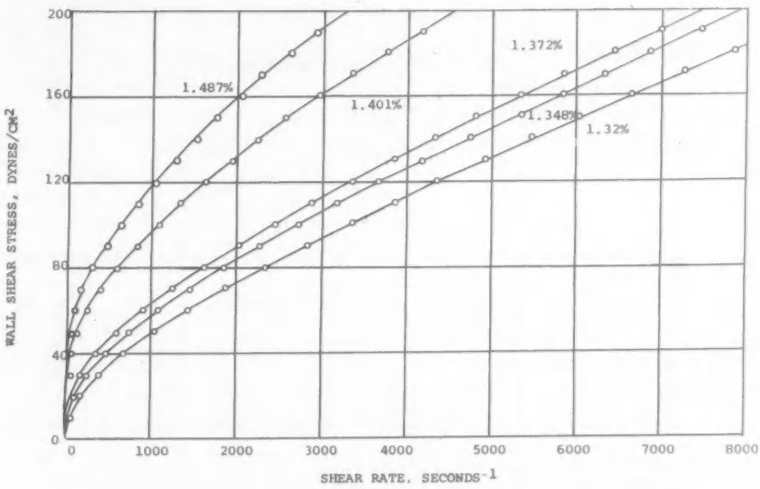

Fig. 12. Wall shear stress as a function of shear rate for the solutions tested.

capillaries. The narrow band of dispersion of data points about the mean curve drawn through the data suggest the validity of the assumption regarding uniqueness of the shear stress–shear rate relationship.

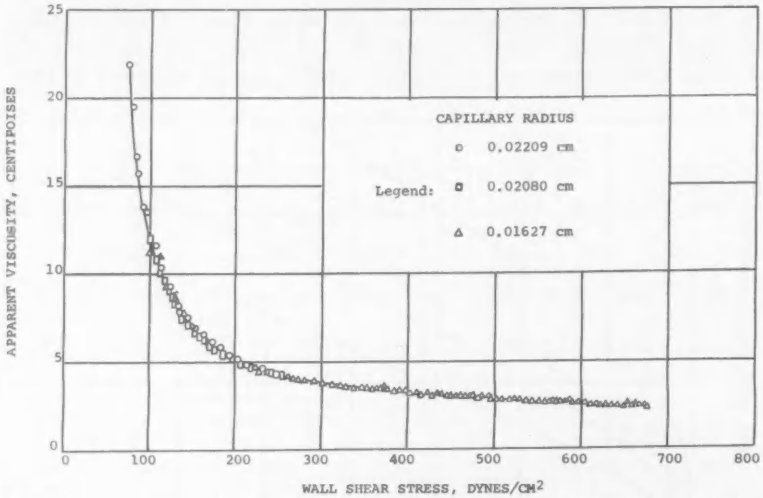

Fig. 13. Apparent viscosity as a function of wall shear stress for the 1.442% solution using three different capillaries.

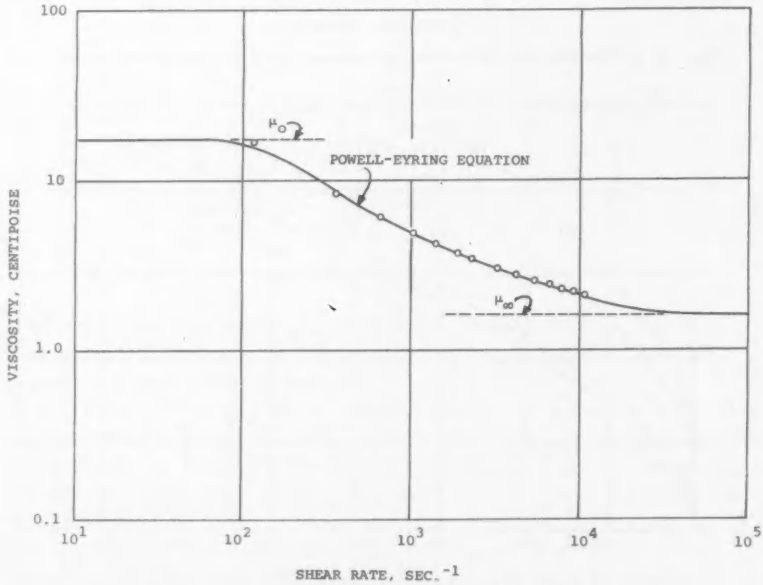

Fig. 14. Viscosity data for 1.32% Milling Yellow suspension.

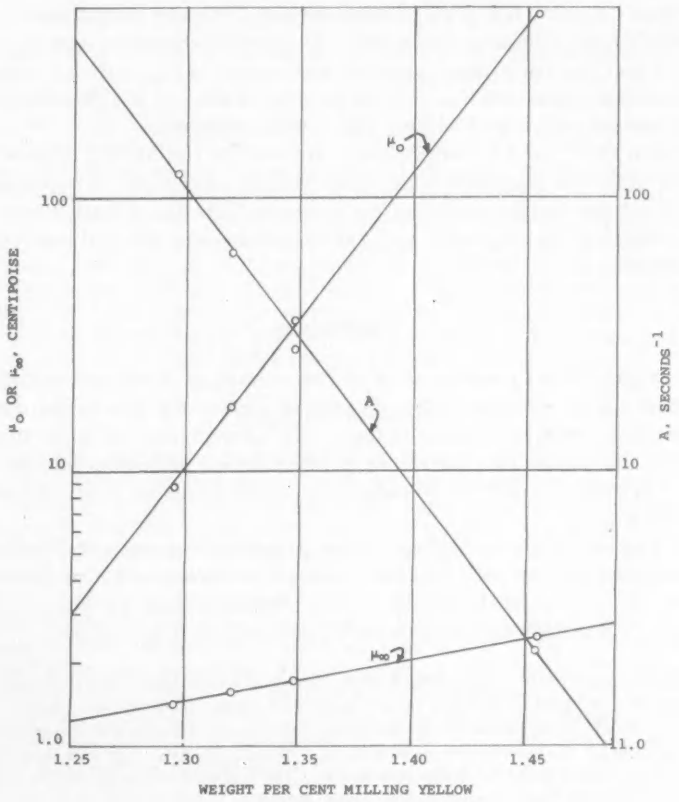

Fig. 15. Powell-Eyring parameters for Milling Yellow suspensions.

The viscosity data for the Milling Yellow suspensions are well represented by the Powell-Eyring equation for pseudo-plastic materials, expressed as

$$\mu = \mu_\infty + \frac{A(\mu_0 - \mu_\infty)\sinh^{-1}(G/A)}{G} \tag{7}$$

where μ_0, μ_∞ are viscosity at zero and infinite shear rates; A is a constant; and G is the shear rate ($= -(du/dr)$ for tube flow).

The constants of eq. (7) were obtained from experimental data for a given test liquid by the familiar method-of-averages,[8] i.e., the constants were calculated from the requirement that

$$\sum_{i=0}^{M} \left\{ \mu_i - \left[\mu_\infty + \frac{A(\mu - \mu_\infty \sinh^{-1}(G_i/A)}{G_i} \right] \right\} = 0 \tag{8}$$

Figure 14 shows a typical plot of viscosity data and comparison to the Powell-Eyring equation. In general, the agreement between experimental points and the correlation equation was within $\pm 1\%$, with an average deviation of about $\pm 0.5\%$. Figure 15 shows values of the Powell-Eyring parameters for a range of Milling Yellow concentrations.

Use of the Powell-Eyring equation to describe the Milling Yellow viscosity data does not imply that other viscosity models are not applicable. Work is under way to examine other representations that will allow a unified treatment of the rheologic and birefringence data for Milling Yellow suspensions.

Conclusions

1. Experimental measurements of the amount of birefringence and extinction angle for Milling Yellow dye suspensions over a wide range of shear rates show a behavior similar to that observed with other colloidal suspensions. The shear rate dependence of these optical properties suggest that the suspensions may be considered as suspensions of rigid, ellipsoidal particles.

2. Viscosity data for Milling Yellow suspensions reveal non-Newtonian behavior in general, with Newtonian ranges at the low and high shear rate extremes. Accurate description of the rheologic data for the complete range of shear rates can be made with the Powell-Eyring equation.

The authors wish to acknowledge indebtedness to the late Robert Marsh Boarts, late Professor and Head of the Chemical Engineering Department at the University of Tennessee, who suggested to the senior author that flow birefringence techniques should be valuable for fluid mechanics investigations. Stanley H. Jury suggested that Milling Yellow dye was a useful birefringent material. The research was supported by a grant from the Office of Naval Research, Mechanics Branch.

References

1. Boeder, P., *Z. Physik*, **75**, 258 (1932).
2. Bogue, D. C., and F. N. Peebles, *Trans. Soc. Rheol.*, **6**, 317 (1962).
3. Edsall, J. T., et al., *Rev. Sci. Inst.*, **23**, 695 (1952).
4. Frocht, M. M., *Photoelasticity*, Wiley, New York, 1941.
5. Gilbrech, D. A., and G. D. Combs, *Devel. Theo. Appl. Mech.*, **1**, 292 (1963).
6. Jessop, H. T., and F. C. Harris, *Photoelasticity, Principles and Methods*, Dover, New York, 1950.
7. Kreiger, I. M., and S. H. Maron, *J. Appl. Phys.*, **23**, 147 (1952).
8. Lipka, J., *Graphical and Mechanical Computation*, Wiley, New York, 1918.
9. Liu, Keh-Chang, and F. N. Peebles, *Trans. Soc. Rheol.*, **7**, 42 (1963).
10. Peebles, F. N., H. J. Garber, and S. H. Jury, *Proc. Third Midwest Fluid Mech.*, Vol 441 (1953).
11. Peterlin, A., and H. A. Stuart, *Z. Physik*, **112**, 1 (1939).
12. Prados, J. W., M. S. Thesis, University of Tennessee, 1954.
13. Prados, J. W., and F. N. Peebles, *Am. Inst. Chem. Engrs. J.*, **5**, 225 (1959).
14. Thurston, G. B., and J. L. Schrag, *Trans. Soc. Rheol.*, **6**, 325 (1962).
15. Wayland, J. H., *J. Appl. Phys.*, **32**, 721 (1961).

Résumé

Des suspensions aqueuses de colorant Milling Yellow ont été trouvées utiles pour des études d'écoulement en employant des techniques bien établies de biréfringence. Dans le présent travail, les propriétés de birefringence fondamentales et les propriétés rhéologiques de suspensions de Milling Yellow ont été mesurées dans un domaine de vitesses de déformation importante pour les applications industrielles. Un polariscope à cylindre concentrique a été utilisé pour mesurer le degré de biréfringence et l'angle d'extinction pour dix suspensions de Milling Yellow à 25°C, en variant le concentration de 1.25 à 1.46% de colorant en poids. Les propriétés optiques de ces suspensions sont semblables à celles d'un nombre de suspensions colloïdales comme cela a été raporté par des études précédentes. Les données rhéologiques pour des suspensions de Milling Yellow dans le même domaine de concentration ont été mesurées à 25°C pour des vitesses de déformation de 50–10^4 $sec.^{-1}$ au moyen d'un viscomètre capillaire. Dans le domaine complet des vitesses de déformation, les données rhéologiques sont décrites parfaitement au moyen de la relation de Powell-Eyring pour des matériaux pseudoplastiques.

Zusammenfassung

Wässrige Suspension en des Farbstoffes Milling Yellow erwiesen sich für technische Fliessuntersuchungen mit bekannten Doppelbrechungsmethoden als brauchbar. In der vorliegenden Arbeit wurden die grundlegenden Doppelbrechungs- und Fliesseigenschaften von Milling-Yellow-Suspension in dem für die technische Anwendung wichtigen Bereich an Deformationsgeschwindigkeiten emessen. Zur Messung des Betrages der Doppelbrechung und des Auslöschungswinkels an zehn Milling-Yellow-Suspension bei 25°C im Konzentrationsbereich von 1,25 bis 1,46 Gewichtsprozent Farbstoff wurde ein Konzentrisch-Zylinder-Polariskop verwendet. Die optischen Eigenschaften dieser Suspensionen weisen eine Ähnlichkeit mit den von früheren Autoren für eine Anzahl von kolloiden Suspensionen mitgeteilten auf. Rheologische Daten wurden für Milling-Yellow-Suspensionen bei 25°C und Deformationsgeschwindigkeiten von 50–10 sec^{-1} in einem Kapillarviskosimeter bestimmt. Im ganzen Bereich an Deformationsgeschwindigkeiten können die rheologischen Daten durch die Powell-Eyring-Beziehung für pseudoplastische Stoffe genau wiedergegeben werden.

JOURNAL OF POLYMER SCIENCE: PART C NO. 5, PP. 55–66

Particle Size Distribution in Dilute Liquid/ Liquid Dispersions by Light Scattering

E. E. LINDSEY, *University of Massachusetts*, D. C. CHAPPELEAR, *Monsanto Chemical Company*, D. M. SULLIVAN, *Shawinigan Resins Corporation*, V. A. AUGSTKALNS,* *University of Massachusetts, Amherst, Massachusetts*

Summary

1. Equal energy per unit mass (or volume) proved to be a valid scaling criterion for particle size distribution as well as mean particle size for geometrically similar vessels with a volume range of 4 to 1.

2. Binodal particle size distributions were observed. Although the coarse fraction varied as the $-6/5$ power of the agitation rate, the fine size was relatively independent of agitation rate.

3. The system with the greater drop viscosity gave a smaller fine-fraction and a larger coarse-fraction than the other system (IB/W).

4. Both systems approached equilibrium size slowly (many minutes). Equilibrium was approached more rapidly at high agitation rates. Differences were small between different tank sizes at equal energy dissipation rates per unit mass.

5. The average size of the fine fraction remains about the same through the run (although the amount increases). The size of the coarse fraction decreases with time. More experiments are necessary to elucidate the mechanism behind this.

Introduction

We became interested in this problem because of practical considerations in emulsion and suspension polymerization. Often it is important for the product to have the right particle size or distribution of sizes. Yet the mechanism of breakup and the factors affecting size are little understood. Very little is known about the affect of physical properties, e.g., viscosity, interfacial tension, density, etc. Even less is known about the cause of variation from one piece of apparatus to another.

This is essentially a progress report of two phases of our work:

1. Equilibrium dispersions in which agitation is carried on long enough so that the particle sizes have reached some distribution which does not vary further with time. These dispersions were produced in geometrically simi-

* Now in service, U. S. Army.

lar tanks but of different agitator speeds selected to give equal power input per unit mass.

2. Transient dispersions in which the agitation was started with the stratified phases, and the change in particle size distribution with time was observed. The same apparatus was used.

Particle Size Measurement

The use of light scattering seemed to be the most advantageous method of measuring drop sizes and size distributions of unstabilized dispersions having drop radii of the order of 0.2–50 μ. The technique has been described by Sloan, Wortz, and Arrington.[3]

There is a relationship between the intensity of light I scattered at any angle, θ from the incident beam and the size of the particle that scatters it. Sloan has defined conditions under which a plot of $I\theta^2$ versus θ can be used

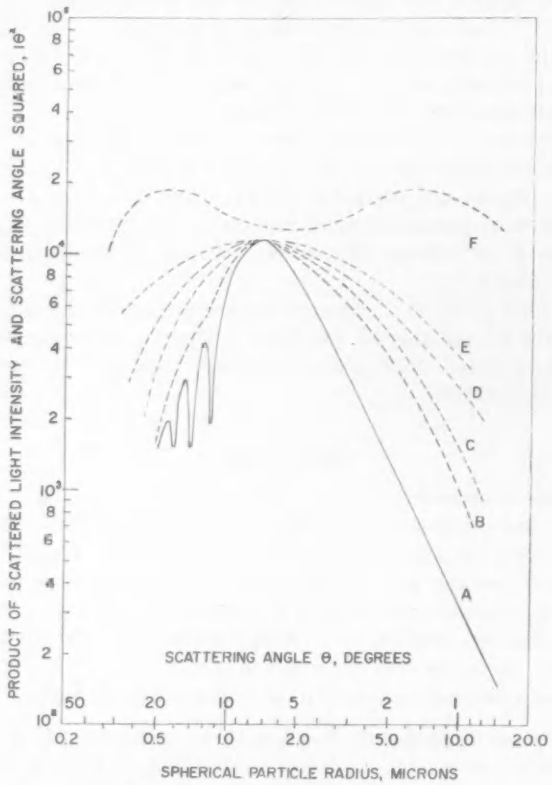

Fig. 1. Theoretical light-scattering curves: (*A*) monodisperse; (*B, C, D, E*) polydisperse; (*F*) binodal dispersions (*8*).

to obtain information about the average particle size and the distribution of particle sizes.

The method requires that certain conditions be met: (*1*) There is no angular dependent absorption of the incident light; (*2*) Secondary scattering is not significant; (*3*) The particle radius is in the region of 0.1–100 μ; (*4*) The ratio of refractive indices of continuous and drop phases should be not too far from unity.

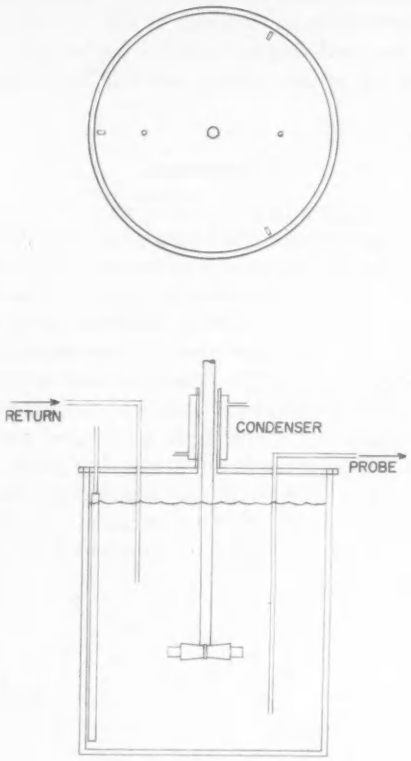

Fig. 2. Agitation tank.

Sloan has defined conditions under which a plot of $I\theta^2$ versus logarithm θ for a monodisperse system has the appearance of curve A in Figure 1. The location of the peak of the curve along the abscissa is related to the diameter d by the relation $d\theta = I$, where K = a constant, which according to Arrington should be 19.4 for the conditions of this work and for spherical particles. Curves B, C, D, and E indicate the progressive change of the light scattering curves as the dispersion becomes more polydisperse. A change in the average size would be accompanied by a shift of the peak of the curve along the abscissa. The occurrence of two peaks in a single

curve, as in F, would indicate that the dispersion contained two maxima of rather narrow particle size in its distribution curve.

The Sloan method of plotting gives, then, curves which change in a manner similar to distribution curves, but they are not true size distribution curves. The location of the peaks gives a reliable indication of average size. The flatness of the curves gives only semiquantitative indication of the distribution of sizes, but such information was adequate for this work.

To obtain a more adequate idea of what was happening in the transient system, the Wortz differential analysis of the I versus θ curve was performed. Wortz has used this method to examine five distributions previously examined by sedimentation methods and obtained very good agreement.

Apparatus

The experimental apparatus consisted of an agitation system, a continuous circulating sample system, and a light-scattering apparatus.

Three sizes of geometrically similar agitation vessels of the conventional design often used in industry were used to observe a small range of scale-up effects. The tanks were of the baffled cylindrical type with diameters of 7.5, 9.0, and 12 in. The agitators were turbines consisting of six vertical, flat, rectangular blades. (Fig. 2.) The drive mechanism for the agitators had a variable-speed transmission and was mounted so that reaction torque could be measured. Power input to the fluid could be determined.

The circulation system consisted of a sampling probe, tubes, flowmeter, and return tube. A bellows pump was used downstream from the cell in the equilibrium tests. In an effort to get still lower shear, a peristaltic-action rubber-tube pump was used in the transient studies.

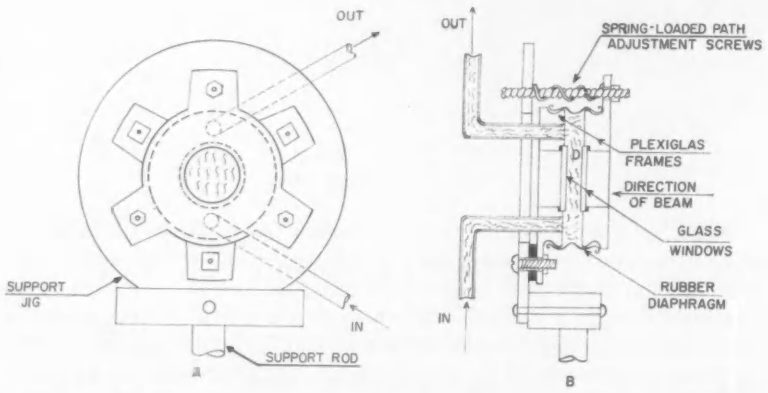

Fig. 3. Projected and partially cut-a-way views of light scattering cell: (A) along light beam (B) horizontally across light beam; (D) exaggerated length of wet length path.

The light scattering apparatus used in the equilibrium tests was from Monsanto Chemical Company[4] and that in the transient tests was a commercial Scattermaster. Figure 3 shows the details of construction of the scattering cell. The length of the light path through the cell was adjustable. Both apparatus gave essentially the same diameter on a latex of known size

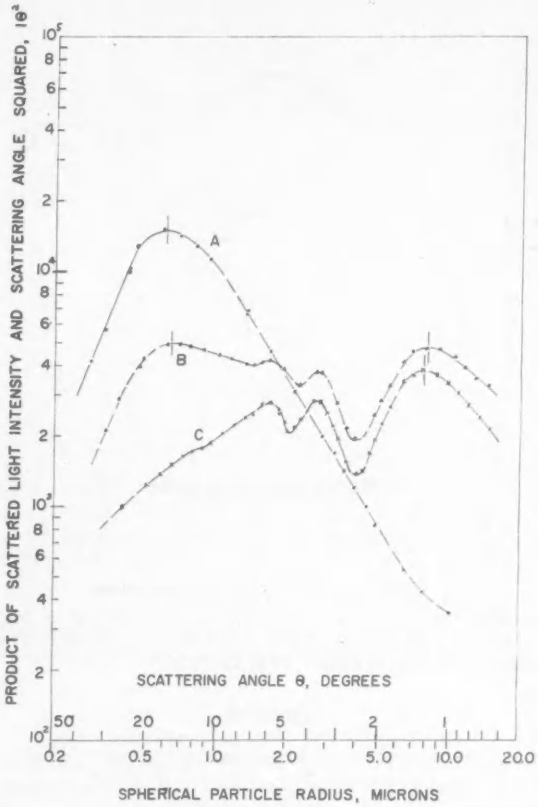

Fig. 4. Light-scattering curves: (*A*) polystyrene latex (radius 0.6 μ); (*B*) mulberry pollen (radius 6.5 μ); (*C*) mixture.

(1.171 $\pm$ 0.013 μ) curve *A*, Figure 4 and a mulberry pollen (15 μ) curve *B*, Figure 4. Curve *C* is for a mixture.

The sample transit time between tank and cell is about twelve seconds. It was concluded from several kinds of tests that the sample in the cell is identical with that in the tank. Some of the larger drop sizes in the cell are broken up in recirculating pump before going back to the tank, but that this bias is uniform and small.

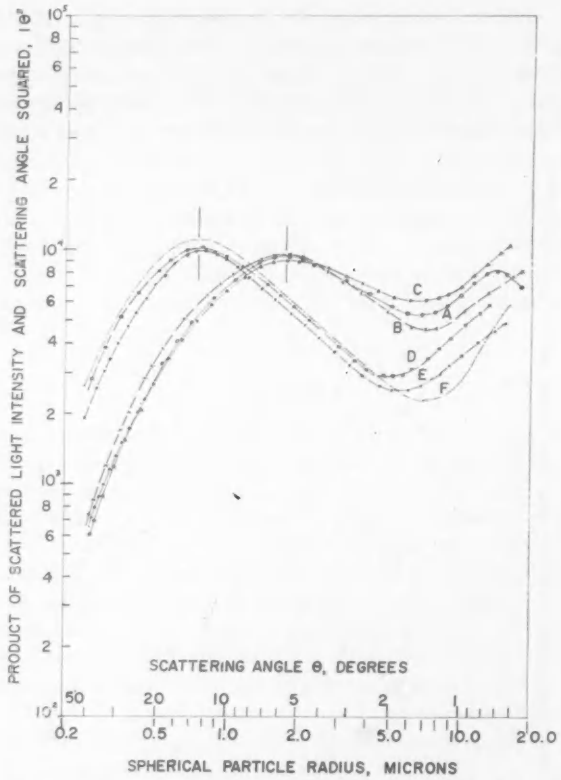

Fig. 5. Light-scattering curves at low speeds: (*A*) IB/W, 7.5 in. tank I.D.; (*B*) IB/W, 9.0 in. tank I.D.; (*C*) IB/W, 12.0 in. tank I.D.; (*D*) CH/W, 7.5 in. tank I.D.; (*E*) CH/W, 9.0 in. tank I.D.; (*F*) CH/W, 12 in. tank I.D.

Materials

Two different immiscible liquid systems were used. The first (IB/W) consisted of 2-butanol and water. The second (CH/W) consisted of cyclohexanol and water. These are both partly miscible and were selected to minimize interfacial tensions and phase density differences. This was considered to be helpful in minimizing drop coalescence in the circulating system.

In both systems, the organic-rich phase was the dispersed phase (2.5% volume in equilibrium study and 0.5% in transient study) and the water-rich was the continuous phase.

Equilibrium Dispersion Results

With the IB/W system in the smallest tank, a low agitation speed was selected which was slightly above the minimum necessary to maintain

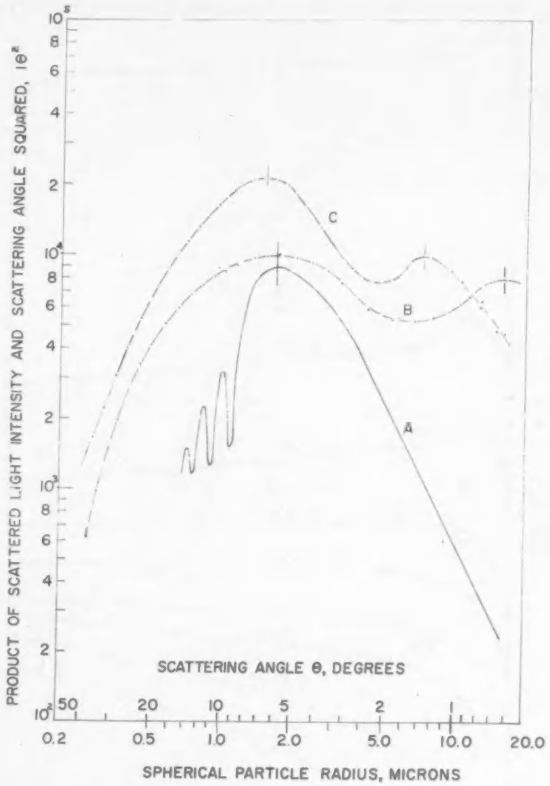

Fig. 6. Light-scattering curves for IB/W system (tank 7.5 in. I.D.); (*A*) theoretical monodisperse system with same average size as (*B*); (*B*) low agitator speed; (*C*) high agitator speed.

dispersion. When the dispersion had equilibrated at this speed, light-scattering data were obtained. The agitator speed was then doubled and, after re-equilibration, a new light scattering curve was obtained. For the two other tanks, the high and low speeds were selected to give the same energy dissipation rates per unit mass. These same experiments were repeated with the IB/W system using the same agitator speeds.

For illustration, results obtained with the three tanks at a single energy dissipation rate are compared in Figure 5. Similar results were obtained at the higher rates. A typical difference between high and low energy dissipation rates is illustrated in Figure 6. Most curves show two maxima corresponding to a coarse and a fine size range. For comparison, a Sloan curve for a monodisperse system is shown.

A relationship reported by Vermeulen[5] and others[2] indicates that the diameters of sufficiently large drops vary as the $-6/5$ power of the agitator

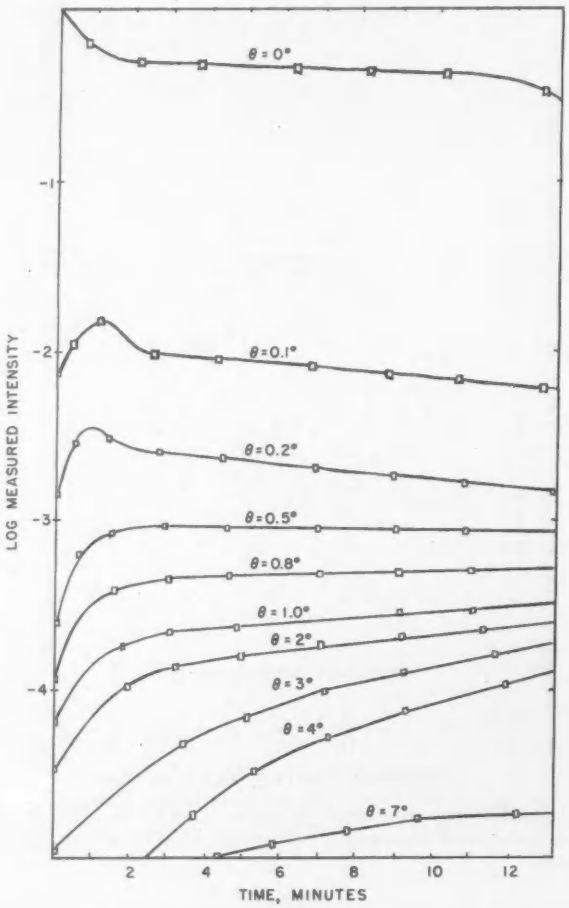

Fig. 7. Typical light-scattering data during transient period.

speed. Consequently, doubling the speed should decrease the diameter 56.5%. The largest decrease in the mean diameter of the fine fraction was only from 3.64 to 2.86 μ or only about 21%. In IB/W system where the coarse maxima are clearly evident, the corresponding shift of the coarse fraction is from about 33 to 15 μ or 54%, which is certainly better agreement.

The microscale of turbulence η varied from 30 to 70 μ in these experiments.* The $-6/5$ power should hold for drop diameters greater than the

* The microscale of turbulence is a measure of the size below which viscous forces become greater than inertial forces. It is calculated from the kinematic viscosity ν and the energy dissipation rate per unit mass ϵ according to the equation: $\eta = 4\sqrt{\nu^3/\epsilon}$.

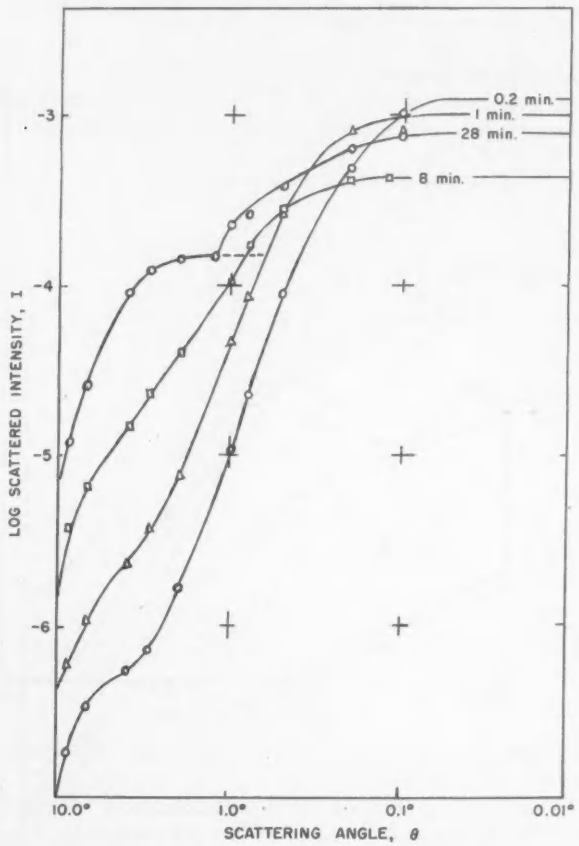

Fig. 8. Cross plot of scattering data of constant time. (IB/W) 12″ tank. Intermediate agitation.

microscale of turbulence. Since this is far from the case with the fine fraction, this may explain the difference in behavior.

Transient Results

The period before the attainment of equilibrium particle size was studied not only for its practical value but also to provide, hopefully, some insight into the mechanism of drop breakup and coalescence.

Runs were made with the IB/W system at three energy dissipation rates per unit mass: about 1.0, 3.2, and 7.2 ft.^{2}/sec.^{3} (1 ft.^{2}/sec.^{3} = 0.929 × 10^3 ergs/g. sec.). Runs were also made with the CH/W system at the lowest and highest energy rates in the two larger tanks. Reynolds numbers varied between 23,000 and 82,000, and the microscale of turbulence varied

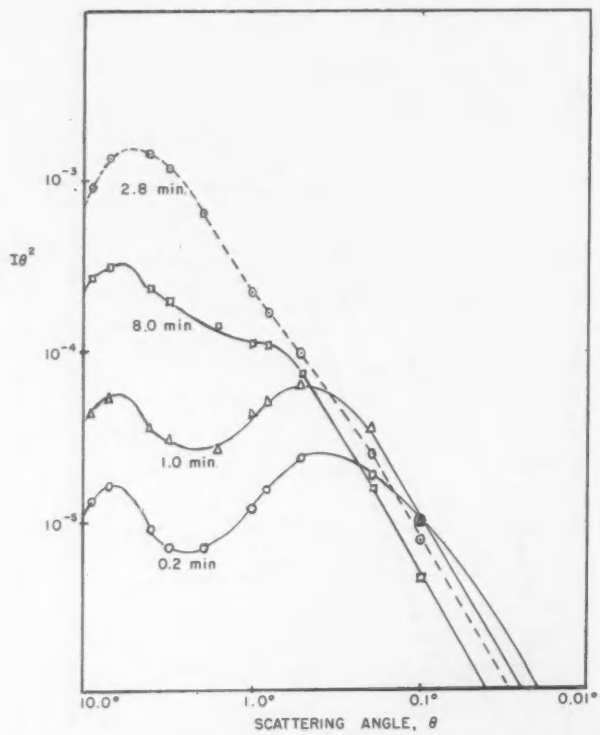

Fig. 9. $I\theta^2$ versus θ curve for IB/W system in 12″ tank. Intermediate agitation.

between 37 and 70 μ. It would seem that conditions were favorable for turbulence which was locally isotropic[2] but not necessarily homogeneous.

Since large changes occurred in the first minutes, rapid and accurate scanning was required. The intensity was read at only certain critical angles, so that a scan could be made in about two minutes. A plot of time against corrected intensity was made for each angle (Fig. 7) and then cross plotted to give curves of intensity versus scattering angle at specific times (Fig. 8). This plot then formed the basis for the Sloan and Wortz analyses (Figs. 9 and 10).

Figure 11 shows a typical Wortz analysis of the data. Drop size as ordinate is plotted against time from the beginning of the dispersion processing, with the cumulative per cent below a given size as a parameter. For example, after four minutes, 90% by weight of the dispersed phase had a drop size of 28 μ or less.

The data when interpreted by the Sloan method reveal two peaks indicating a binodal size distribution (Fig. 9). Unfortunately, the coarse peak is more difficult to identify in the later stages of a run because it tends to be obscured by scattering from increasing amounts of fine material.

However, the plot indicates that the average size of the fine material remains about constant while that of the coarse decreases.

Comparison of the CH/W with the IB/W system indicates that the effect of increased drop-phase viscosity (CH/W) is to decrease the average drop size of the fine fraction and increase the average size of the coarse fraction

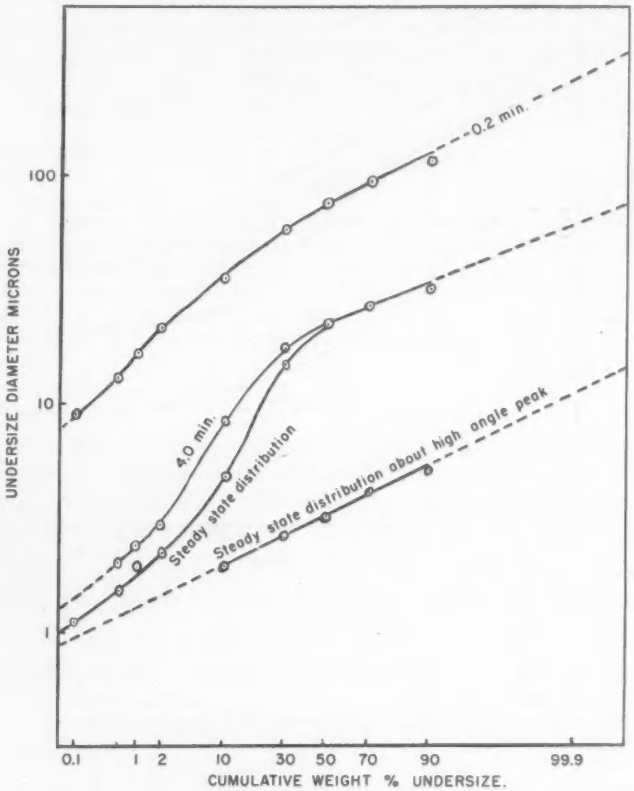

Fig. 10. Size distribution during agitation. Log-probability plot. 12″ tank. Intermediate agitation.

at equilibrium. The viscosities of the aqueous continuous phases were approximately the same in both systems. Differences in interfacial tensions and densities were relatively smaller than the drop viscosity difference, (25.5 cycles/sec. for CH/W versus 2.39 cycles/sec. for IB/W).

Comparison of results in one tank at different speeds indicates that time to reach equilibrium size decreases as speed increases and that the total energy required to produce a given distribution may be constant and independent of speed.

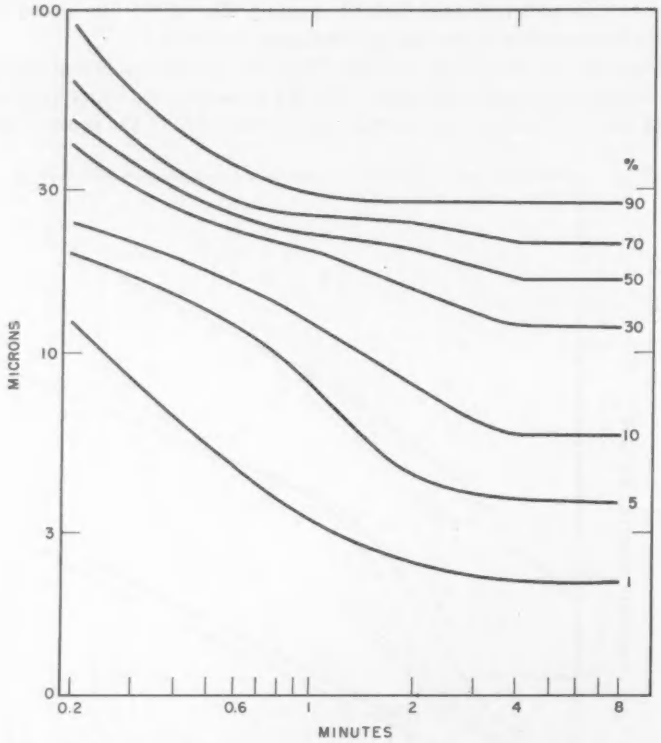

Fig. 11. Change in cumulative undersize distribution during agitation. IB/W. 12″ tank. High agitation.

We are grateful to the National Science Foundation, DuPont, Monsanto, and Shawinigan Resins for their support.

We wish to thank *Industrial and Engineering Chemistry Fundamentals* for permission to reproduce Figures 1–6.

References

1. Rodger, W. S., V. G. Trice, Jr., and J. H. Rushton, *Chem. Engr. Prog.*, **52**, 515 (1956).

2. Shinnar, R., J. M. Church, *Ind. Eng. Chem.*, **52**, 253 (1960).

3. Sloan, C. K., C. G. Wortz, and C. H. Arrington, Jr., *Angular-Dependence Light Scattering, Sections I-V.* Experimental Station. E. I. du Pont de Nemours & Co., Inc., Wilmington, Delaware.

4. Sullivan, D. M., and E. E. Lindsey, *Ind. Eng. Chem., Fundamentals*, **1**, 87 (1962).

5. Vermeulen, T., G. M. Williams, and G. E. Langlois, *Chem. Engr. Prog.*, **51**, 85F (1955).

JOURNAL OF POLYMER SCIENCE: PART C NO. 5, PP. 67–74

On Phenomenological Rheo-Optic Constitutive Relations

ELLIS HAROLD DILL, *Department of Aeronautics and Astronautics, University of Washington, Seattle, Washington*

Synopsis

The birefringence exhibited by high polymers can be explained by considering light as an electromagnetic wave propagating through an anisotropic dielectric. The observed dependence of the birefringence on the deformation state is described by expressing the dielectric tensor as a functional of the strain history. For small strains, the functional can be approximated by an integral so that the birefringence and strain are related by a law of the Boltzmann superposition integral form.

Introduction

The birefringence exhibited by high polymers can be explained by considering light as an electromagnetic wave propagating through an ideal anisotropic dielectric. The nature of the wave is determined by the relation* between the free charge potential (electric displacement) **D** and the electric field **E**. For a material at rest

$$D_i = \epsilon_0 K_{ij} E_j \tag{1}$$

Here ϵ_0 is the dielectric coefficient in free space and K_{ij} will be called the dielectric tensor.

Suppose that the z_3-axis is everywhere a principal axis of the dielectric tensor. The electromagnetic field equations show[1] that a plane wave propagated along the z_3 axis is divided into two linearly polarized waves. The direction of vibration of each wave coincides with one of the remaining principal axes of the dielectric tensor and has a refractive index equal to the square root of the corresponding principal value of the dielectric tensor.

This suggests the introduction of a new tensor N_{ij} which has the same principal axis as the dielectric tensor but which has principal values N_i equal to the square root of the principal values of the dielectric tensor:

$$N_{ij} = K_{ij}^{1/2} \tag{2}$$

The birefringence of a wave propagated along the z_3 axis is

$$\Delta = N_1 - N_2 \tag{3}$$

* All quantities are referred to a fixed rectangular cartesian system z_i. All indices have the range 1, 2, 3 and a repeated index indicates summation over this range.

The N_{ij} will be called the refraction tensor since the principal values of N_{ij} are the refractive indices of the propagated wave. The refraction tensor is regarded, here, as the fundamental optical quantity in the formulation of constitutive relations. Other tensors which have been used in the formulation of constitutive relations are the velocity tensor.[2]

$$V_{ij} = cK_{ij}^{-1/2} \tag{4}$$

and the Fresnel tensor[3]

$$n_{ij} = K_{ij}^{-1} \tag{5}$$

The birefringence has also been used directly[4] in the formulation of constitutive relations but, since the birefringence is not a tensor quantity, this procedure is unsatisfactory for a general treatment.

Constitutive Relations

The birefringence of high polymers is observed to depend upon the history of mechanical states. Since the refraction tensor N_{ij} completely determines the birefringence, one might express this dependence mathematically by a relation between N_{ij} and the history of mechanical states.

Consider an isothermal process at temperature θ_0. Let t denote the present time and τ denote a past instant. The history of deformation is completely described[5] by the strain tensor $e_{ij}(\tau)$, $0 \leqq \tau \leqq t$. If $N_{ij}(t)$ is uniquely determined by the history of deformation, then $N_{ij}(t)$ must be a functional of $e_{ij}(\tau)$ and a function of $e_{ij}(t)$:

$$N_{ij}(t) = F_{ij}[\underset{\tau = 0}{e_{ij}^{t}(\tau)};\ e_{ij}(t)] \tag{6}$$

The functional may be expanded in a power series:[6,13]

$$\begin{aligned} F_{ij}[\underset{\tau=0}{\mathbf{e}^{t}(\tau)};\ \mathbf{e}(t)] &= f_{ij}(\mathbf{e}(t)) + \int_0^t g_{ijrs}(\mathbf{e}(t),\ t,\ \tau)e_{rs}(\tau)d\tau \\ &+ \int_0^t\int_0^t h_{ijrsmn}(\mathbf{e}(t),\ t,\ \tau,\ \eta,)e_{rs}(\tau)e_{mn}(\eta)d\tau d\eta \\ &+ \text{---} \end{aligned} \tag{7}$$

The functions may also be expanded in a power series:

$$f_{ij}(e) = N_{ij}^{0} + a_{ijrs}e_{rs} + b_{ijrsmn}e_{rs}e_{mn} + \text{---} \tag{8}$$

etc.

If only small strains are considered, then all series can be truncated so that eq. (6) becomes linear in the strains:

$$N_{ij}(t) = N_{ij}^{0} + a_{ijrs}e_{rs}(t) + \int_0^t A_{ijrs}(t,\tau)e_{rs}(\tau)d\tau \tag{9}$$

Since the constitutive relation should be invariant with respect to a shift of the time origin, the functions A_{ijkr} must be of the form $A_{ijkr}(t - \tau)$.

Therefore, the constitutive relation for a anisotropic material experiencing small, isothermal deformations is

$$N_{ij}(t) = N_{ij}^{0} + \int_0^t B_{ijkr}(t - \tau)(d/d\tau)e_{kr}(\tau)d\tau \tag{10}$$

where

$$B_{ijkr}(0) = a_{ijkr}$$
$$(d/dt)B_{ijkr}(t) = A_{ijkr}(t)$$

Since **E** is symmetric, there is no loss in generality if **B** is symmetric in the last two indices. Assume that N_{ij} is symmetric then **B** is also symmetric in the first two indices.

The material will be called isotropic if **B** is an isotropic tensor:[7]

$$B_{ijkr} = A\delta_{ij}\delta_{kr} + B(\delta_{ik}\delta_{jr} + \delta_{ir}\delta_{jr}) \tag{11}$$

where δ_{ij} is the Kronecker data. Since $N_{ij} = N^{0}\delta_{ij}$, the constitutive relation for an isotropic material experiencing small, isothermal deformations is

$$N_{ij} = N^{0}\delta_{ij} + \int_0^t \{A(t - \tau)\delta_{ij}(d/d\tau)[e_{rr}(\tau)] + B(t - \tau)2(d/d\tau)[e_{ij}(\tau)]\}d\tau \tag{12}$$

Equation (12) has the usual form of the convolution integral. All of the well-known results which have been of use in viscoelasticity[8] can be immediately applied. In particular, the functions $A(t)$ and $B(t)$ can be represented in terms of their spectrum. In the case of a discrete spectrum, the constitutive relation can be related to a "spring-dash pot" model.

Denote the deviatoric part of the refraction tensor by

$$R_{ij} = N_{ij} - \frac{1}{3}N_{rr}\delta_{ij} \tag{13}$$

and the deviatoric part of the strain tensor by

$$\epsilon_{ij} = e_{ij} - \frac{1}{3}e_{rr}\delta_{ij}$$

Then eq. (12) yields

$$R_{ij}(t) = \int_0^t 2B(t - \tau)(d/d\tau)[\epsilon_{ij}(\tau)]d\tau \tag{14}$$

A relaxation process is defined as the response to a step change in strain. If ϵ_{ij} has the step change ϵ_{ij}^{0} at $t = 0$, then eq. (14) gives

$$R_{ij}(t) = 2B(t)\epsilon_{ij}^{0} \tag{15}$$

Therefore $B(t)$ will be called the optical relaxation function.

Suppose that it is found experimentally that (dB/dt) varies monotonically and that $B(t)$ approaches a limit B_∞ when $t \to \infty$. Then define a function $\phi(t)$ such that

$$B(t) = B_0 + (B_\infty - B_0)\phi(t) \tag{16}$$

Then $\phi(t)$ increases from zero to unity with monotonic slope (Fig. 1) and will be called the reduced relaxation function.

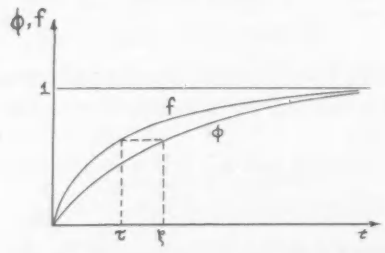

Fig. 1. Reduced relaxation function.

Consider isothermal relaxation at a different temperature θ. Denote the optical relaxation function by $F(t)$ and define a reduced relaxation function $f(t)$ analogous to eq. (16). Then there exists a function $\xi(\tau)$, which may be called the reduced time (Fig. 1), such that

$$f(\tau) = \phi(\xi(\tau)) \tag{17}$$

In the case of stress relaxation of a linear viscoelastic material, it is found that

$$\xi(\tau) = a(\theta)\tau \tag{18}$$

The function $a(\theta)$ is termed the temperature shift factor and depends upon the choice of reference temperature θ_0. Assume that eq. (18) also holds for isothermal optical relaxation but perhaps with a shift factor different from the mechanical case.

Consider now relaxation at varying temperature $\theta(t)$. Again denote the optical relaxation by $F(t)$ and introduce a function $f(t)$ defined analogous to eq. (16). Then again there exists a reduced time $\xi(t)$ such that eq. (17) holds. Therefore

$$(df/dt) = (d\xi/dt)(d\phi/d\xi) \tag{19}$$

In the isothermal case

$$(df/dt) = a(\theta)(d\phi/d\xi)$$

This suggests the hypothesis

$$(d\xi/dt) = a(\theta(t)) \tag{20}$$

and

$$\xi(t) = \int_0^t a(\theta(\tau))d\tau \tag{21}$$

in the case of varying temperature.

Now suppose that the temperature varies in the same way, $\theta(t)$, but the strain increment occurs at time τ. Denote the resulting creep function by $F(t,\tau)$. In this case the fundamental constitutive relation, eq. (14), must be written

$$R_{ij} = \int_0^t 2\,F(t,\tau)(d/d\tau)[\epsilon_{ij}(\tau)]d\tau \tag{22}$$

that is the kernel can not be expressed as a function of the difference $t - \tau$.

Analogous to the isothermal case, let $F(t,\tau) = F_0$ and assume that $[\partial F(t,\tau)]/(\partial t)$ varies monotonically with t while $F(t,\tau) \to F_\infty$ as $t \to \infty$. Then the function $f(t,\tau)$ may again be defined as in eq. (16):

$$F(t,\tau) = F_0 + (F_\infty - F_0)f(t,\tau) \tag{23}$$

In this case there exists a reduced time $\rho(t,\tau)$ such that

$$f(t,\tau) = \phi(\rho(t,\tau)) \tag{24}$$

and

$$(\partial f/\partial t) = (\partial \rho/\partial t)(\partial \phi/\partial \rho) \tag{25}$$

The similarity to eq. (19) suggests that

$$(\partial \rho/\partial t) = a(\theta(t)) \tag{26}$$

Since $f(t,\tau) = \phi(0) = 0$, $\rho(t,\tau) = 0$. Therefore

$$\rho(t,\tau) = \int_\tau^t a(\theta(\eta))d\eta \tag{27}$$

$$= \xi(t) - \xi(\tau)$$

Therefore the creep function at varying temperature has the form

$$F(t,\tau) = F_0 + (F_\infty - F_0)\phi(\xi(t) - \xi(\tau)) \tag{28}$$

If F_0 and F_∞ are independent of temperature, then

$$F(t,\tau) = B(\xi(t) - \xi(\tau)) \tag{29}$$

In this latter case, the fundamental constitutive relation for varying temperature, eq. (22), takes the form

$$R_{ij}^*(\xi) = \int_0^\xi 2B(\xi - \eta)(d/d\eta)[\epsilon_{ij}^*(\eta)]d\eta \tag{30}$$

where

$$R_{ij}^*(\xi(t)) = R_{ij}(t)$$

$$\epsilon_{ij}^*(\xi(t) = \epsilon_{ij}(t))$$

Similar reasoning may be applied to the trace of N_{ij}.

The eqs. (10), (12), and (30) are the fundamental constitutive equations in the various special instances. Similar results can be derived if one prefers to relate the birefringence to stress. Moreover, since the stress and strain histories are uniquely related for most materials, the fundamental equations here can usually be transformed into stress-birefringence relations.

Linear Viscoelasticity

The constitutive equations for materials such that the stress depends on the deformation history may also be expressed in terms of functionals.[9,10] For small isothermal deformations,[8]

$$\sigma_{ij}(t) = \int_0^t 2G(t - \tau)(d/d\tau)[\epsilon_{ij}(\tau)]d\tau \tag{31}$$

where $\mathfrak{d}$ is the deviatoric part of the stress tensor. A similar expression[8] can be derived for the mean stress.

Equations (14) and (31) imply

$$R_{ij} = \int_0^t C(t - \tau)(d/d\tau)[\sigma_{ij}(\tau)]d\tau \tag{32}$$

Therefore a unique relation between birefringence and strain history implies a unique relation between birefringence and stress history in the case of linear viscoelastic materials.

In the case of varying temperature, hypotheses analogous to those used above concerning the temperature shift factor and the reduced time can be used[11] to derive a constitutive relation for stress. In the notation of eq. (30),

$$\sigma^*_{ij}(\xi) = \int_0^{\xi} 2G(\xi - \eta)(d/d\eta)[\epsilon_{ij}^*(\eta)]d\eta \tag{33}$$

If the mechanical shift factor is the same as the optical shift factor, as supposed here, then eq. (30) and eq. (33) yield

$$R_{ij}^*(\xi) = \int_0^{\xi} C(\xi - \eta)(d/d\eta)[\sigma_{ij}^*(\eta)]d\eta \tag{34}$$

Plane Polariscope

Now consider an idealization of the situation in a plane polariscope. A slice of the dielectric is bounded by the planes $z_3 = 0,h$. The z_3-axis is everywhere a principal axis of K_{ij} and therefore of N_{ij}. By means of a

polarizer, a linearly polarized plane electromagnetic wave propagating along the z_3-axis is obtained. Every such wave can be divided into the sum of monochromatic waves and each monochromatic wave can be decomposed into components such that the direction of vibration coincides with one of the principal axis of N_{ij}.

Consider one such wave. When this wave is incident on the dielectric it is partly reflected and partly transmitted. A similar reflection and transmission occurs at the exit surface. By applying the jump conditions of the electromagnetic field equations the amplitude of the exited wave can be related to the amplitude of the incident wave. If the exited wave is now viewed through a polarizer which has its axis at right angles to that of the first polarizer, the amplitude of the transmitted light is approximately[12] proportional to the factor

$$I = \sin 2\alpha \sin 2n\pi \tag{35}$$

where $\alpha(t)$ is the angle between the axis of the polarizer and the first principal axis of N_{ij}, and

$$n = (h\omega/2\pi c)\Delta \tag{36}$$

is the fringe order. Here, h is the model thickness, ω is the circular frequency, and c is the velocity of light in free space.

Thus, if the model is subjected to a non-homogeneous deformation field, there will appear lines of zero light intensity (isoclinics) connecting the points where $\alpha(t) = 0, (\pi/2)$. There will appear lines of relative minimum intensity where the fringe order is an integer. Therefore by observing the isoclinic and isochromatic pattern, the functions $\alpha(t)$ and $\Delta(t)$ can be determined.

Using the inverse of eq. (32),

$$\sigma_{ij}(t) = \frac{1}{2}\int_0^t \psi(t - \tau)(d/d\tau)[R_{ij}(\tau)]d\tau \tag{37}$$

it follows that

$$\begin{aligned}\sigma_{11}(t) - \sigma_{22}(t) &= \frac{1}{2}\int_0^t \psi(t - \tau)(d/d\tau)[\Delta(\tau)\cos 2\alpha(\tau)]d\tau \\ \sigma_{12}(t) &= \frac{1}{2}\int_0^t \psi(t - \tau)(d/d\tau)[\Delta(\tau)\sin 2\alpha(\tau)]d\tau\end{aligned} \tag{38}$$

The principal axes of stress and the difference in principal stresses can then be calculated. Similar results apply to the strain tensor.

References

1. Landau, L. D., and E. M. Lifshitz, *Electrodynamics of Continuous Media*, Addison Wesley, 1960, pp. 315–317.
2. Read, W. T., *J. Appl. Phys.*, **21**, 671 (1950).
3. Mindlin, R. D., *J. Appl. Phys.*, **20**, 206 (1949).
4. Stein, R. S., S. Onogi, and D. A. Keedy, *J. Polymer Sci.*, **57**, 801 (1962).
5. Truesdell, C., and R. Toupin, *Encyclopedia of Physics, 3, Part 1*, Springer-Verlag, Berlin, 1960.
6. Volterra, V., *Theory of Functions*, Blackie and Sons, London, 1931, p. 21.
7. Thomas, T. Y., *Tensor Analysis and Differential Geometry*, Academic Press, London, 1961, p. 68.
8. Staverman, A. J., and F. Schwarzl, *Die Physik der Hochpolymeren, Vol. IV* (H. A. Stuart, ed.), Springer-Verlag, Berlin, 1956, Chap. 1.
9. Green, A. E., and R. S. Rivlin, *Arch. Rat. Mech. Anal.*, **1**, 1 (1957).
10. Noll, W., *Arch. Rat. Mech. Anal.*, **2**, 197 (1958).
11. Morland, L. W., and E. H. Lee, *Trans. Soc. Rheol.*, **4**, 223 (1960).
12. Dill, E. H., "A Theory for Photoviscoelasticity," in *Proceedings of the Fourth International Congress on Rheology*, Interscience, New York, 1964.
13. Coleman, B. D., and W. Noll, *Rev. Mod. Phys.*, **33**, 239 (1961).

Résumé

La biréfringence présentée par les hauts polymères peut s'expliquer en considérant la lumière comme une onde électromagnétique se propageant à travers un diélectrique anisotrope. La dépendance de la biréfringence vis-à-vis de l'état de déformation est décrite en exprimant le tenseur diélectrique en fonction de l'évolution de la tension interne. Pour de faibles tensions, on peut décrire approximativement la fonction par une intégrale de telle sorte que la biréfringence et la tension sont reliées par une loi du type intégrale de superposition de Boltzmann.

Zusammenfassung

Die Doppelbrechung von Hochpolymeren kann durch Betrachtung des Lichtes als eine elektromagnetische, sich in einem anisotropen Dielektrikum ausbreitende Welle verstanden werden. Die beobachtete Abhängigkeit der Doppelbrechung vom Deformierungszustand wird durch Darstellung des dielektrischen Tensors als ein Funktional der Verformungsvorgeschichte beschrieben. Für geringe Verformung kann das Funktional durch ein Integral angenähert werden, sodass Doppelbrechung und Verformung durch ein Gesetzt von der Form des Boltzmannschen Superpositionsintegrals verbunden sind.

JOURNAL OF POLYMER SCIENCE: PART C NO. 5, PP. 75–86

Stress-Strain-Time-Birefringence Relations in Photoelastic Plastics with Creep

CHINTAKINDI L. AMBA-RAO, *School of Aeronautical and Engineering Sciences, Purdue University, West Lafayette, Indiana*

Synopsis

The above is an exploratory study started in September 1961 with a view to solving the time dependent stress and strain distributions in structural problems through optical model analysis. The present analysis, however, is restricted to monotonically increasing uniaxial loading. Finally, "optical creep parallels mechanical creep" is the basis on which this analysis is built.

Introduction

Purpose

The aim of the author in deriving the stress-strain-optic law for plastics in the presence of creep is to extend the conventional photoelastic method of stress analysis to the solutions of static structural problems in the presence of creep. Earlier attempts made in this area are similar in nature; although the problems are different, they are closely allied. There is a classical paper by Mindlin[1] and a recent paper by Theocaris and Mylonas;[2] the title of the former is rather misleading. Both papers deal with "the conditions under which models or birefringent coatings made of viscoelastic materials may be employed to solve boundary value problems in the linear theory of elasticity" through photoelastic principles.

Various Methods of Specifying Viscoelastic Properties

According to Alfrey,[3] there are no less than seven distinct (but all mathematically equivalent) methods of specifying the properties of linear viscoelastic materials, divided into two classes.

Class I

(*A*) The Voigt model, consisting of a set of Voigt elements in series.

(*B*) The Maxwell model, consisting of a set of Maxwell elements in parallel.

(*C*) The operator equation, $P(\sigma) = Q(\epsilon)$ where P and Q are linear differential operators.

(*D*) The mechanical impedance function $Z(\omega)$.

Class II

(*E*) The creep curve—strain as a function of time at constant stress.

(*F*) The relaxation curve—stress as a function of time at constant strain.

(*G*) The dynamic modulus curve—elastic modulus as a function of frequency.

The class II methods are ideally suited for the development of an analysis which basically rests upon experimental observations, while class I methods are suitable for obtaining solutions of theoretical problems; and each method has its own limitations.

Since birefringence is a consequence of the material being stressed (or strained), the author is inclined to believe that optical anisotropy is a consequence of mechanical anisotropy. Hence, the approach to the field of optical viscoelasticity may be made on lines similar to those of mechanical viscoelasticity.

Survey of Literature

The following lines from the doctoral dissertation (University of Illinois, 1957) of Dr. Daniel Post* seem to be appropriate at this stage.

"The stress optic law is well established but even today, the validity of the law rests largely upon experimental verification.[4] There has been no completely satisfactory explanation of the stress-optical phenomenon as exhibited by amorphous solids in terms of the electromagnetic character of light and the electric and magnetic properties of the stressed solid."[5,6]

The author's approach to the present problem is largely based on experimentally observed facts in an engineering laboratory. He is of the opinion that there is no unique way in which the stress-strain-time-birefringence relation can be derived in the presence of creep as can be seen from the published work. Besides, statistical mechanics applied to the optical properties of the whole network on the lines of Kuhn and Grün[7] and work on the plastics at the transition temperature may also yield fruitful results.

The Optic Law in Elasticity

The optic law in classical photoelasticity takes the following simple form:

$$\begin{aligned}(n/d) &= c_\sigma(\sigma_1 - \sigma_2) \\ &= c_\epsilon(\epsilon_1 - \epsilon_2)\end{aligned} \tag{1}$$

where

$$c_\epsilon = c_\sigma E/1 + v \tag{2}$$

* Dr. Post is a noted authority on optics applied to photoelasticity and is widely known for his fringe sharpening and fringe multiplication techniques.

and where n = relative retardation, d = thickness of specimen, c_σ = stress optical coefficient, c_ϵ = strain-optical coefficient, $\sigma_1 - \sigma_2$ = principal stress difference, $\epsilon_1 - \epsilon_2$ = principal strain difference, E = Young's modulus, and v = Poisson's ratio.

Within the elastic range, the stress is proportional to strain; hence, it is immaterial whether one considers the optical birefringence as being due to principal stress difference or strain difference. However, when the medium creeps (call it viscoelastic), the optic law takes a much more complicated form.

The Optic Law for a Medium Which Creeps

A historical review of the work includes the following:

$$(n/d) = c_\sigma(\sigma_1 - \sigma_2) + c_\epsilon(\epsilon_1 - \epsilon_2) \tag{3}$$

Coker and Filon.[8] c_σ varied from 5.4 to 9.6 Brewsters. c_ϵ varied from 0.4 to 1.58 Brewsters.

$$(n/d) = c_\sigma(t)(\sigma_1 - \sigma_2) \tag{4}$$

Durelli and Lake.[9]

$$(n/d) = c_\sigma(t)(\sigma_1 - \sigma_2) \tag{5}$$

Theocaris and Mylonas.[2]

$$K_t = \frac{1}{c_\sigma} = K_\sigma + at + b \log t \tag{6}$$

where k_t, k_σ, a, b are empirical constants.

$$(n/d) = c_{(p)}(\sigma_1 - \sigma_2)_{(p)} + c_{(e)}(\sigma_1 - \sigma_2)_{(e)} \tag{7}$$

Where $c_{(p)}$ and $c_{(e)}$ refer to the optical coefficients of the plastic phase and the elastic phase (Kuske[10]). "Though chemists question the multiphase nature of plastics," Kuske experimentally verified his law on many materials.

Recently, Dill[11] has put forward a hypothesis based on electromagnetic theory and Boltzmann's superposition principle. Although it has some very interesting characteristics, it has a restrictive assumption that in the form presented it is valid only for linear viscoelastic materials. Professor Drucker of Brown University in a general lecture at the Fourth U. S. National Congress of Applied Mechanics pointed out that linear viscoelastic problems are far from reality. It is known that most of the metals at high temperature and plastics at high stress or strain levels do not behave as linear viscoelastic materials. Crystallizable polymers and incompletely polymerized resins change their properties during creep and do not satisfy the superposition principle. This is an observation made by the author, following the work of Leaderman[12] on Boltzmann Principle

The Analysis

Theoretical Foundation

Guided by the existing knowledge, the present analysis is based strictly on experimentally observed facts. In the present analysis, the author concentrated on class II methods suggested by Alfrey. Relaxation and creep tests are suitable for viscoelastic studies in the time scale of 1 to 10^5 sec., while dynamic modulus measurements are suitable for the time scale of 1 to 10^{-5} sec. Since the author's main interests lie in static problems, the latter approach is ruled out. Main concentration is made on creep tests as no Instron Testers are available to perform relaxation tests.

Creep Tests under Constant Load

Creep tests under constant load are assumed to be the same as the creep tests under constant stress as there is negligible change in the cross-sectional area. The following analysis lays a theoretical foundation for the study of some model materials. A series of assumptions are made to start with, and the ultimate justification for the assumptions depends upon the final results.

Let it be assumed that

$$\begin{aligned} \epsilon_c(t) &= f_1(\sigma,t) = A(\sigma)g(t) \\ &= \sigma^p g(t) \end{aligned} \tag{8}$$

$p = 1$, if it has linear mechanical creep.

$$\epsilon_c(t) = \epsilon(t) - \epsilon_e \text{ and } \dot{\epsilon}_c(t) = \dot{\epsilon}$$

Dot denotes differentiation with respect to time. Similarly

$$n_c(t) = n(t) - n_e$$

and

$$\dot{n}_c(t) = \dot{n}$$

and

$$n_c(t) = f_2(\sigma,\epsilon,t) \tag{9}$$

where subscripts c and e refer to creep and elastic components. In the absence of any specific information whether birefringence is due to stress or strain, it is reasonable to assume that birefringence is a function of both stress and strain.

Substituting eq. (8) in eq. (9), one obtains

$$\begin{aligned} n_c &= f_3(\sigma,t) = B(\sigma)f(t) \\ &= \sigma^q f(t) \end{aligned} \tag{10}$$

$q = 1$, if it has linear optical creep.

It has been experimentally verified that $g(t)$ and $f(t)$ are similar in nature for many model materials. Equation (8) is valid for many materials for the primary and secondary creep stages of the creep curve. Rabotnov, a well-known authority on creep says in a recent paper,[13] "when we take into account the great discrepancies in experimental data on creep, we see that it is *rather pointless* to strive for precision in such predictions. Therefore, improvements in the equations of creep are often held to be meaningless, and it is frequently suggested that *one apply the simplest theories.*" (The emphasis is made by the author.)

The author fully concurs with Rabotnov's remarks and believes in simple expressions for creep curves.

Optical Creep Parallels Mechanical Creep

Experiments by Maxwell[14] indicate that the relationship between change of index of refraction and stresses is the same as that between strain and stresses for an elastic medium.

$$\begin{aligned} n_1 - N_0 &= c_1\sigma_1 + c_2(\sigma_2 + \sigma_3) \\ n_2 - N_0 &= c_1\sigma_2 + c_2(\sigma_3 + \sigma_1) \\ n_3 - N_0 &= c_1\sigma_3 + c_2(\sigma_1 + \sigma_2) \end{aligned} \tag{11}$$

where n_1, n_2, n_3 are the three principal indices of refraction along the 1, 2, 3, directions and N_0 is the radius of the index sphere before stress is applied.

$$\begin{aligned} \epsilon_1 &= \frac{1}{E}\sigma_1 - \frac{v}{E}(\sigma_2 + \sigma_3) \\ \epsilon_2 &= \frac{1}{E}\sigma_2 - \frac{v}{E}(\sigma_3 + \sigma_1) \\ \epsilon_3 &= \frac{1}{E}\sigma_3 - \frac{v}{E}(\sigma_1 + \sigma_2) \end{aligned} \tag{12}$$

The creep behavior is considered to be a small perturbation from the elastic behavior at $t = 0$. Hence, it is reasonable to assume that the mechanical creep strain parallels the optical creep birefringence.[3] This is the idea underlying the analysis developed in this report. From the literature one could collect the following evidences.

On Catalin, up to 10 min. after loading, Mylonas[15] obtained the relations:

$$n(t) = \sigma(A + Bt^{1/3}) \tag{13}$$

$$\epsilon(t) = \sigma(A' + B't^{1/3}) \tag{14}$$

where A, B, A', B' are constants.

Coker and Filon[8] fitted the following equation (up to an hour after loading) for xylonite (celluloid):

$$n_c(t) = pt^{1/3} + vt \tag{15}$$

$$\epsilon_c(t) = at^{1/3} + bt \tag{16}$$

where a and p are proportional to σ^2 approximately; and b and q "are *very* small quantities not accurately determined." (The emphasis is made by the author.)

For Xylonite, eqs. (15) and (16) approximately reduce to

$$n_c(t) = K_1\sigma^2 t^{1/2} \qquad (15a)$$

$$t \geq 0$$

$$\epsilon_c(t) = K_2\sigma^2 t^{1/2} \qquad (16a)$$

For CR-39, the author found that

$$n(t) = \sigma t^{0.0308} \qquad (17)$$

$$t > 0$$

$$\epsilon(t) = \sigma t^{0.0356} \qquad (18)$$

Photoviscoelastic Law

Choose a model material which creeps. Prepare optical and mechanical creep curves in uniaxial tension. In order to enable master curves to be prepared, eqs. (8) and (10) may be written as follows:

$$[\epsilon_c(t)/A(\sigma)] = g(t) \qquad (19)$$

$$[n_c(t)/B(\sigma)] = f(t) \qquad (20)$$

Linear viscoelastic model material is a particular case, where

$$A(\sigma) = B(\sigma) = \sigma$$

One can easily see from eqs. (19) and (20) that, in the most general case,

$$\left(\frac{n_c(t)}{B(\sigma)}\right) = f_n\left(\frac{\epsilon_c(t)}{A(\sigma)}\right) + \text{Constant} \qquad (21)$$

The justification for eq. (21) is the fact that for Xylonite and Catalin, investigated upon and reported in the literature, and, from the experimental observations of the author on other materials,[16] "the curve between the optical creep strain per unit stress and time is of the same (or similar) type as

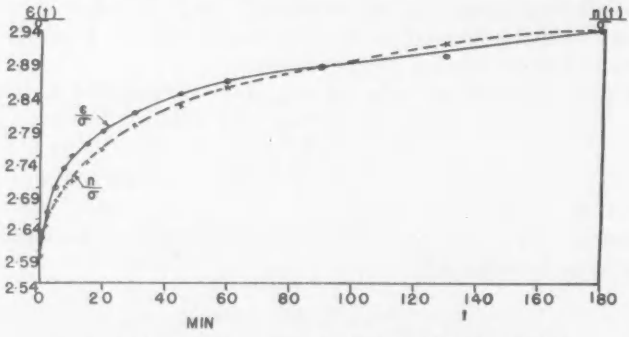

Fig. 1. $\epsilon(t)/\sigma$ and $n(t)\sigma$ versus time for Araldite 502 at 74°F.

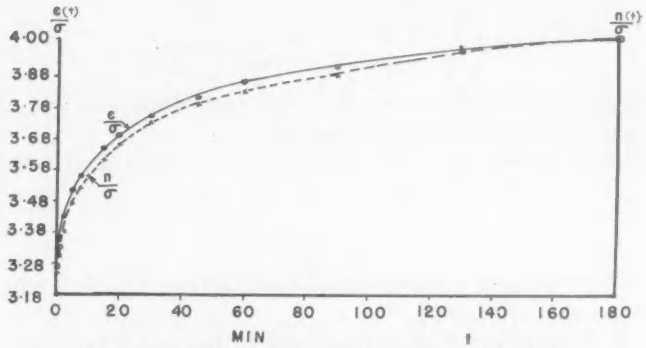

Fig. 2. $\epsilon(t)/\sigma$ and $n(t)/\sigma$ versus time for CR-39 at 72°F.

the curve between the mechanical creep strain per unit stress and time." This can be seen from the expressions for the optical and mechanical creep curves and the experimental results plotted in Figures 1 and 2. In Figures 1 and 2, $(n(t)/\sigma)$ and $(\epsilon(t)/\sigma)$ are plotted against t for CR-39 and Araldite 502. They are found to be coincident within $\pm 3.5\%$ from the mean, basing the deviation on the creep components only. Similar coincidence has been obtained even for cases in which the stress is arbitrary, but uniaxial.

Effect of Rate of Loading and Rate of Straining

Experiments were also conducted to find the dependence of mechanical and optical creep curves on different rates of loading. The effect of strain rate on stress-strain and stress-birefringence curves was also studied. The conclusions are as follows: For CR-39, the maximum difference in birefringence and strain between a constant load creep test and a variable load creep test under the worst conditions investigated is about 12%.

Strain rate has an effect on stress-birefringence and stress-strain curves. This is in line with the behavior of viscoelastic materials. Strain rate was varied from about 6 to 600 μin./in./min. and the maximum variations in stress-birefringence and stress-strain curves at 1600 psi stress level are 20% on birefringence and 27% on strain. Therefore,

$$n_c = f_n(\dot{\sigma},\dot{\epsilon})$$

$$\epsilon_c = f_n(\dot{\sigma},\dot{\epsilon})$$

Experimental Observations

In the above analysis, if one makes $p = v = 1$ in eqs. (8) and (10) and combines them with the quantities in the elastic state, one gets the linear viscoelastic law.

If $(n(t)/\sigma)$ plotted against $(\epsilon(t)/\sigma)$ is a straight line, then

$$\frac{n(t)}{\sigma} = \frac{n_e + n_c(t)}{\sigma} = A\,\frac{\epsilon_e + \epsilon_c(t)}{\sigma} + B$$

That is,

$$n_e + n_c(t) \approx A[\epsilon_e + \epsilon_c(t)] + B\sigma \tag{22}$$

It may be mentioned that A and B are constants while, $n_c(t)$ and $\epsilon_c(t)$ depend upon the history and rate of loading.

The above relation, eq. (22) is valid for the following ranges investigated:

$$0 < t < 180 \text{ min.}$$

$$0 < \sigma < 2{,}000 \text{ psi.}$$

Equation (22) is valid as a stress-strain-time-birefringence relation for some model materials which creep.

On the basis of experiments conducted by the author on Araldite 502

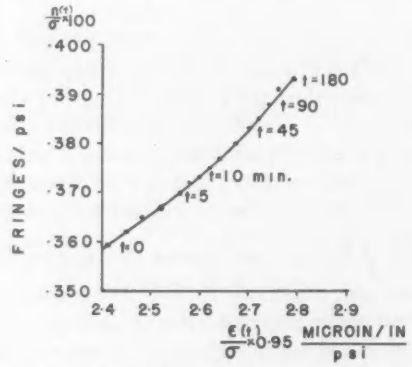

Fig. 3. $n(t)/\sigma$ versus $\epsilon(t)/\sigma$ for Araldite 502 at 74°F.

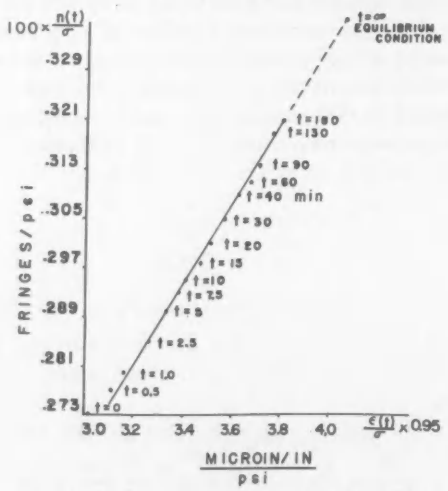

Fig. 4. $n(t)/\sigma$ versus $\epsilon(t)/\sigma$ for CR-39 at 72°F.

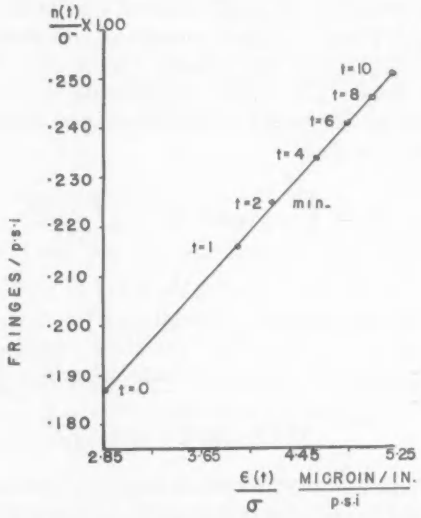

Fig. 5. $n(t)/\sigma$ versus $\epsilon(t)/\sigma$ for Catalin 800 at 19.5°C.[15]

with 9% hardener HN 951, it is found that the relation between $(n(t)/\sigma)$ versus $(\epsilon(t)/\sigma)$ is slightly nonlinear while, on the basis of experiments on CR-39, the author found the relation between $(n(t)/\sigma)$ versus $(\epsilon(t)/\sigma)$as linear. Both the model materials are found to behave as linearly viscoelastic in the range tested. The details of the experiments for CR-39 are given in earlier publications;[17,18] and, Figures 3 and 4 indicate the relationships for both the model materials. In Figure 3 and 4, 0.95 ϵ takes into consideration the stiffening effect of the strain gages in measuring the strains.

For Catalin 800, the author has taken the experimental values from the literature[15] and obtained

$$n(t) = A[\epsilon_1(t) - \epsilon_2(t)] + B\sigma \tag{23}$$

for $0 < t < 10$ min. and $261.7 < \sigma < 963.4$ psi (see Fig. 5).

The above laws, eqs. (22) and (23) derived by the author for photoviscoelasticity agree in principle with the earlier work of Bayoumi and Frankl[19] on photoplasticity. The present work is done independently by the author and some of the results were presented as an IAS (Institute of Aerospace Sciences) student paper in April 1962. A recent paper of Javornicky[20] from Czechoslovakia has results which confirm the main observations reported in this paper.

The Optical Boltzmann Principle

It is well known that the Boltzmann Principle holds good for linear mechanical viscoelastic materials, under certain conditions; and it was

proved earlier in some typical model material that optical creep parallels mechanical creep. There is a great amount of literature on mechanical linear viscoelasticity; and, if one replaces ϵ by n, one obtains the linear photoviscoelastic laws. The author experimentally verified the photoviscoelastic law in the following form for CR-39 and Araldite 502 for arbitrary uniaxial tensile loading

$$n(t) = \int_0^t [c_\sigma \text{ creep}]\ (t - \tau)\ \frac{d\sigma(\tau)}{d\tau}\ d\tau \tag{24}$$

where $[C_\sigma$ creep$]$ is the birefringence variation in time following a unit stress input, generally termed as the optical creep function. The percentage error was found to be less than 2%. The above experiments confirm the hypothesis proposed by Dill[11] on the basis of electromagnetic theory.

The Model Materials

The prime purpose in using CR-39 and fully polymerized Araldite 502 as the model materials for the present analysis is the fact that their mechanical and optical properties are stable as contrasted to the plasticized, incompletely cured epoxies, prepared in the laboratory, whose properties vary substantially with time.[21] CR-39, like most other model material, including fully polymerized epoxies, does not flow while, some incompletely (and/or plasticized) polymerized epoxies do flow. The great disadvantage with the latter is the fact that their properties vary from day to day and one is likely to get non-repeatable results. Creep properties are very sensitive to the composition and the curing of the specimen and the author found discrepancies as high as 10% even between two identical specimens from the same sheet. Hence, one is forced to use the same specimen for all the tests. This is not possible with a model material which flows, as some residual creep strain is left over after every test. Annealing, if resorted to, besides removing the residual strain, also changes the composition of the material. These are basically the difficulties which the research group at New York University[22] has run into.

CR-39, Columbia Resin, was a very popular model material for photoelasticity all over the world, until the discovery of Epoxy resins in 1951, in spite of the fact that it creeps. It is linearly viscoelastic up to about 2,000 psi stress level.

The other model material with which the author worked is Araldite 502 (also known as Araldite D) with 9% of hardener HN 951. The monomer belongs to the family of epoxy resins manufactured and marketed by Ciba, Inc. The author is one of the earliest to investigate the suitability of this resin for photoelastic investigations[16] in 1956. For the present investigation, the author used a complicated heating and annealing cycle to stabilize the optical and mechanical properties as follows: Make the casting at room temperature; and, after fifteen days, subject it to annealing at

100°C. for five days, and store the specimen at room temperature for nine months.

Conclusions and Possible Extensions

In conclusion, the present analysis may be extended to the following cases:

(*a*) Nonlinear creep problems.
(*b*) Large (finite) deformation.
(*c*) $A(\sigma) \neq B(\sigma)$ (see eqs. (19) and (20)).
(*d*) $f(t) \neq g(t)$ (see eqs. (19) and (20)).

Work is in progress to extend the present analysis to biaxial stress states and arbitrary loadings.

The above analysis is applied to predict the time-dependent stress and strain distributions in a rectangular beam in pure bending. The results will be published somewhere else.

The author is grateful to Professor Ervin O. Stitz for serving as his thesis advisor during the course of this investigation. The author is indebted to the reviewer for valuable suggestions.

References

1. Mindlin, R. D., *J. Appl. Phys.*, **20**, 206 (1949).
2. Theocaris, P. S., and C. Mylonas, *J. Appl. Mech.*, **28**, 601 (1961).
3. Alfrey, T., *Mechanical Behavior of High Polymers*, Interscience, New York, 1948, p. 223.
4. Frocht, M. M., *Photoelasticity, Vol. II*, Wiley, New York, 1948, chap. 10.
5. Toupin, R. A., *J. Rat. Mech. Anal.*, **5**, 849 (1956).
6. Stuart, H. A., *Koll. Z.*, **120**, 57 (1951).
7. Kuhn, W., and F. Grün, *Kolloid- Z.*, **101**, 248 (1942).
8. Coker, E. G., and L. N. G. Filon, *A Treatise on Photoelasticity*, Cambridge Univ. Press, Cambridge, 1937, p. 272.
9. Durelli, A. J., and R. L. Lake, *Proc. Soc. Exptl. Stress Anal.*, **9**, 97 (1957).
10. Kuske, A., *Exptl. Mech.*, **2**, 278 (1962).
11. Dill, E. H., The Trend in Engineering, 14–16, College of Engineering, Univ. of Washington, (1962).
12. Leaderman, H., *Elastic and Creep of Filamentous Materials, and other High Polymers*, The Textile Foundation, Washington D. C. (1943).
13. Rabotnov, Y. N., *Proc. Soc. Nav. Mech. Conf.*, 338 (1960).
14. Maxwell, J. C., *Trans. Roy. Soc. Edinburgh*, **20**, 87 (1849–1850).
15. Mylonas, C., *Proc. Cong. Appl. Mech. 8th*, 165 (1948), London.
16. Amba-Rao, C. L., *Brit. J. Appl. Phys.*, **7**, 229 (1956).
17. Amba-Rao, C. L., Minta Martin First Award Student Papers, Inst. Aerospace Sciences, 1962, p. 5.
18. Clark, A. B. J., *Proc. Soc. Exptl. Stress Anal.*, **14**, 195 (1957).
19. Bayoumi, S. E. A., and E. K. Frankl, *Brit. J. Appl. Phys.*, **4**, 306 (1953).
20. Javornickỹ, J., *Exptl. Mech.*, **3**, 175 (1963).
21. Amba-Rao, C. L., *J. Appl. Mech.*, **29**, 598 (1962).
22. Becker, H. and A. W. Zachar, College of Engineering, New York Univ., TRSM 62-12 (1962).

Résumé

Ce travail constitue une étude préliminaire commencée en septembre 1961 en vue d'expliquer la dépendance du temps des distributions de tension et d'élongation dans le problème de structure par une analyse de modèles optiques. La présente analyse se limite cependant à l'étude de systèmes si la charge augmente de manière monotone. Enfin, la mise en parallèle du fluage optique et du fluage mécanique est la base qui a servi à l'élaboration de cette étude.

Zusammenfassung

Die vorliegende orientierende Untersuchung wurde im September 1961 mit der Absicht begonnen, die zeitabhängige Spannungs- und Verformungsverteilung bei Strukturproblemen durch eine optische Modellanalyse zu klären. Diese Analyse ist aber auf monoton wachsende einachsige Belastung beschränkt. Schliesslich ist "Optisches Kriechen geht parallel zu Mechanischem Kriechen" die Grundlage, auf der diese Analyse aufgebaut ist.

JOURNAL OF POLYMER SCIENCE: PART C NO. 5, PP. 87–100

Dynamic Birefringence of Amorphous Polymers

B. E. READ, *Basic Physics Division, National Physical Laboratory, Teddington, Middlesex, England*

Synopsis

The principles underlying the dynamic birefringence method are outlined, giving particular emphasis to the use of this technique in investigating the molecular mechanism of relaxation in amorphous polymers. Data are presented for amorphous polyacetaldehyde ([—CH(CH$_3$)—O—]$_n$) in the frequency range 1–20 cycles/sec. and temperature range 0 to −25°C. The results are discussed and compared briefly with dielectric data for polyacetaldehyde and also with earlier dynamic birefringence data obtained for polymethylacrylate.

Introduction

The dynamic birefringence technique has recently emerged as a valuable new tool for investigating the molecular mechanism of mechanical relaxation in polymers. In this method the real and imaginary components of both the complex strain-optical coefficient and the complex stress-optical coefficient are determined as a function of frequency. Such data may be compared with the corresponding frequency dependence of the components of the complex modulus or compliance. Furthermore the strain-optical and stress-optical relaxation spectra may be evaluated and compared with the mechanical relaxation and retardation spectra. Since birefringence provides a measure of molecular orientation, such comparisons may yield information concerning the molecular orientational rearrangements responsible for the mechanical relaxation behavior.

In this laboratory dynamic birefringence studies have initially been made upon amorphous polymers in the relaxation region associated with their rubberglass transformation. The behavior in this region is generally attributed to the segmental motions of the polymer chain backbone. Our experimental method has been described in some detail[1] and results have been reported for polymethylacrylate (PMA).[2] In this paper data are presented for amorphous polyacetaldehyde ([—CH(CH$_3$)—O—]$_n$). This polymer was chosen for investigation because the —CH$_3$ side groups were expected to have less influence on the relaxation of birefringence than the —COOCH$_3$ side groups in the PMA chain. Further-

more, comparable dielectric results have also been obtained for polyacetaldehyde in this laboratory. Owing to the presence of the dipole moment *within* the chain backbone, the dielectric relaxation of this polymer also arises from main chain motions.

Theory

Phenomenological

For a polymer sample subjected to a sinusoidally varying tensile strain ϵ we arbitrarily assume that the stress f and birefringence Δn cycles lead the prescribed strain cycle by phase angles δ and δ', respectively. Hence we have (in complex notation),

$$\begin{aligned} \epsilon^* &= \epsilon_0 \exp\{i\omega t\} \\ f^* &= f_0 \exp\{i(\omega t + \delta)\} \\ \Delta n^* &= \Delta n_0 \exp\{i(\omega t + \delta')\} \end{aligned} \tag{1}$$

where ϵ_0, f_0, and Δn_0 are the strain, stress, and birefringence amplitudes, respectively, ω the experimental frequency in radians/sec. and t is the time in seconds. In the present experiment ϵ_0, f_0, Δn_0, δ and δ' are each measured as a function of frequency and temperature. From these measurements we obtain the real and imaginary components of (*a*) the complex modulus ($E^* = f^*/\epsilon^* = E' + iE''$), (*b*) the complex compliance ($D^* = \epsilon^*/f^* = D' - iD''$), (*c*) the complex strain-optical coefficient ($K^* = \Delta n^*/\epsilon^* = K' + iK''$) and (*d*) the complex stress-optical coefficient ($C^* = \Delta n^*/f^* = C' - iC''$), where for example,

$$\begin{aligned} K' &= |K| \cos\delta', & K'' &= |K| \sin \delta' \\ C' &= |C| \cos(\delta - \delta'), & C'' &= |C| \sin (\delta - \delta') \end{aligned} \tag{2}$$

where $|K| = \Delta n_0/\epsilon_0$ and $|C| = \Delta n_0/f_0$.

According to the phenomenological theories, the dependence of E' and E'' on frequency may be expressed generally in terms of well-known expressions involving the mechanical relaxation spectrum $\phi_E(\ln \tau)$. Also the frequency dependence of D' and D'' can be written in terms of the *retardation* spectrum $\phi_D(\ln \tau)$. We have similarly defined a strain-optical relaxation spectrum, $\phi_K(\ln \tau)$, and also a stress-optical relaxation spectrum, $\phi_C(\ln \tau)$, which relate the components of K^* and C^*, respectively, to frequency. For example,

$$K' = \int_{-\infty}^{+\infty} \phi_K(\ln \tau) \frac{\omega^2\tau^2}{1 + \omega^2\tau^2} d \ln \tau \tag{3}$$

and

$$K'' = \int_{-\infty}^{+\infty} \phi_K(\ln \tau) \frac{\omega\tau}{1 + \omega^2\tau^2} d \ln \tau$$

where $\phi_K(\ln \tau)$ represents the contribution to $K'_\infty - K'_0$ from processes having strain-optical relaxation times between $\ln \tau$ and $\ln \tau + d \ln \tau$. K'_∞

and K'_0 are the limiting values of K' at infinite and zero frequency, respectively. An analogous definition has been given[2] for $\phi_c(\ln \tau)$. To a first order approximation, each of the above distribution functions may be calculated from the experimental data according to equations given.[2] It is to be emphasized that whereas $\phi_E(\ln \tau)$ and $\phi_D(\ln \tau)$ are always positive, $\phi_K(\ln \tau)$ may be either positive or negative in different region of τ depending on whether the mechanism with relaxation time τ contributes a positive or negative amount to $K'_\infty - K'_0$. Hence it is possible for K' to either increase or decrease with frequency in a particular frequency range depending on whether $\phi_K(\ln \tau)$ is positive or negative for the appropriate relaxation mechanisms.

The above phenomenological discussion refers to the dynamic mechanical and optical behavior of a polymer over a wide frequency range at constant temperature. Since our present measurements are limited to about 1.5 decades of frequency, a method of reduced variables has been tentatively proposed for effectively extending this frequency range. This procedure involves an initial reduction of both the mechanical and optical data to a standard temperature T_0 as described.[2] Subsequently the reduced experimental plots are shifted along the log (frequency) axis until they superpose. Master curves are thus obtained of E'_{T_0}, E''_{T_0}, D'_{T_0}, D''_{T_0}, K'_{T_0}, K''_{T_0}, C'_{T_0}, and C''_{T_0} against log $a_T f$ where f is the frequency in c/s, and log a_T is the horizontal shift factor. Since greater precision has so far been attained with the mechanical data than with the optical data the log a_T values are usually determined from the mechanical plots and then used to construct the optical master curves.

Molecular

According to the proposed molecular theory,[3] the mechanical and optical relaxation arises from the diffusion of chain molecules toward a new set of most probable configurations subsequent to a deformation of the sample. Each real molecular chain is replaced by an idealized chain comprising a large number of freely jointed, optically anisotropic, links. The configurational rearrangements therefore lead to a positive entropy change but zero change in internal energy. The molecules are each subdivided into ν submolecules each of which contains sufficient links so that its end-to-end distance conforms to the Gaussian distribution. The configuration of an entire chain is specified initially in terms of the Cartesian coordinates of one end of each submolecule relative to the other end as origin.

A basic postulate underlying the theory is that when the specimen undergoes an instantaneous deformation, the components of the vectors joining the ends of each submolecule *initially* undergo a change in the same ratio as the change in dimensions of the bulk specimen (i.e., an affine deformation). If the sample is held at constant external strain the submolecules return to less extended configurations during the subsequent relaxation process. After transforming the original Cartesian coordinates to a system of normal coordinates, the variation of the birefringence and

stress with time (at constant strain) are calculated in terms of the time dependence of each normal coordinate. Under dynamic conditions the above configurational changes are superimposed onto the configurational changes due to the prescribed sinusoidal strain. The following results are obtained,

$$E' = 3NkT \sum_{p=1}^{p} \frac{\omega^2\tau_p^2}{1 + \omega^2\tau_p^2}, \qquad E'' = 3NkT \sum_{p=1}^{p} \frac{\omega\tau_p}{1 + \omega^2\tau_p^2} \tag{4}$$

and

$$K' = K \sum_{p=1}^{p} \frac{\omega^2\tau_p^2}{1 + \omega^2\tau_p^2}, \qquad K'' = K \sum_{p=1}^{p} \frac{\omega\tau_p}{1 + \omega^2\tau_p^2} \tag{5}$$

where τ_p is the relaxation time characterizing motions of the p'th normal mode, N is the number of molecules per unit volume, k is Boltzmann's constant, and T the absolute temperature. K is an optical constant proportional to N and $\alpha_\parallel - \alpha_\perp$, the polarizability anisotropy of the statistical link. To a good approximation the above summations may be replaced by integrals if the three longest relaxation times ($\tau_1 \rightarrow \tau_3$) are not involved. The theory then predicts that $\phi_E(\ln \tau)$ and $\phi_K(\ln \tau)$ should be proportional to $\tau^{-1/2}$.

The theory also predicts that the birefringence should be in phase with the stress ($\delta - \delta' = 0$) and that $|C|$ should be independent of frequency. It follows that C' should also be independent of frequency and that C'' and $\phi_C(\ln \tau)$ should be zero at all frequencies or relaxation times. These predictions arise from the fact that at any instant both the birefringence and the stress are determined by the internal configurational states of the molecules. The stress is related to these configurations via the configurational entropy.

From eqs. (4) and (5) the limiting high frequency values of E' and K' are given by $E'_\infty = 3\nu NkT$ and $K'_\infty = K\nu$, respectively. However, there is an upper frequency limit at which the theory is valid since configurational changes *within* the submolecules are ignored. Furthermore, at very high frequencies (or low temperatures) the elastic deformation mechanism will involve the distortion of valence angles and separation of chains against their forces or attraction. These local distortions will result in an internal energy change rather than the entropy change assumed in the above orientational mechanism. The release of these distortions should also contribute to the relaxation of birefringence, although at present no molecular theory has been developed for this mechanism. However the dynamic birefringence technique should provide information concerning the frequency ranges in which the orientational and distortional mechanisms, respectively, predominate.

Experimental

Our experimental method for measuring Δn_0, f_0, ϵ_0, δ, and δ' over a range of frequency and temperature has been described previously.[1] In the

present work measurements have been made upon amorphous polyacetaldehyde in the frequency range 1–20 cycles/sec. and temperature range 0 to −25°C. The polymer was prepared from acetaldehyde monomer at −75°C., using silica gel as catalyst, as described by Weissermel and Schmieder.[4] The crude polymer was twice precipitated from acetone solution with water, dried under vacuum, dissolved in dry benzene containing a little Nonox antioxidant, and then freeze-dried. The molecular weight of the polymer, determined from intrinsic viscosity measurements in methyl ethyl ketone, was about 1.5×10^5. The glass transition temperature of the polymer, determined dilatometrically, was -30.4 ± 1°C. For the dynamic birefringence measurements strips of the polymer, approximately $2.5'' \times 0.5'' \times 0.1''$, were molded at 50°C.

Results

Mechanical

The variation of E', E'', and tan δ with frequency is shown in Figure 1. The different temperatures studied are indicated by different symbols as illustrated on the E' plots. This same system of symbols is used in all later diagrams. The data shown in Figure 1 were obtained on three different samples each from the same preparation. In the temperature range 0 to − 7.2°C. a ±0.75% dynamic strain superimposed on a 16% static strain was employed. At lower temperatures a combination of ±0.17% dynamic strain and 22% static strain was used. E' is seen to increase with increasing frequency at each temperature, while E'' exhibits a maximum at about 3–4 cycles/sec. at −21.5°C. A maximum in the tan δ curves is observed within the experimental frequency range at −10.8, −13.1, and −15°C.

Reduced master plots of log E'_{T_0}, log E''_{T_0}, tan δ, log D'_{T_0}, and log D''_{T_0} against log $a_T f$ are shown in Figure 2. The reference temperature T_0 was conveniently chosen as 0°C., the highest temperature of measurement. At −18.7°C., and lower temperatures, the shift factors (log a_T) derived from the formation of the modulus and compliance master curves are somewhat larger than those required for the tan δ master plot. This discrepancy has probably arisen from errors in determining the stress magnitudes, since both the sample and proof ring were changed at this

TABLE I

Temperature, °C.	Log a_T	Temperature, °C.	Log a_T
0.0	0.0	−16.6	3.09
−3.0	0.49	−18.7	3.45
−7.2	1.22	−20.0	4.01
−10.8	1.91	−21.5	4.36
−13.1	2.37	−25.0	5.56
−15.0	2.74		

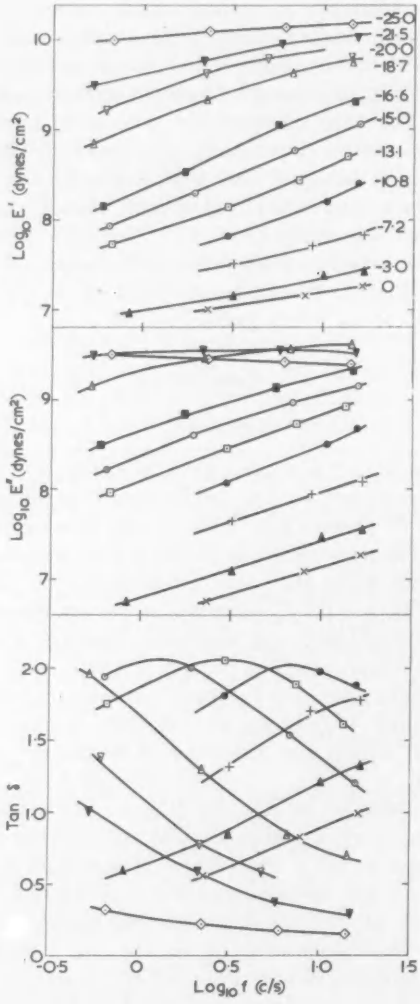

Fig. 1. The variation of E', E'', and tan δ with frequency for polyacetaldehyde. The different temperatures studied are indicated by different point symbols as shown on the E' plots.

temperature. Since the tan δ values are independent of the stress magnitude, the shift factors obtained from the tan δ plots are probably more accurate and furthermore they yield a smoother log a_T versus temperature curve. Hence the log a_T values quoted in Table I are those derived from the tan δ results.

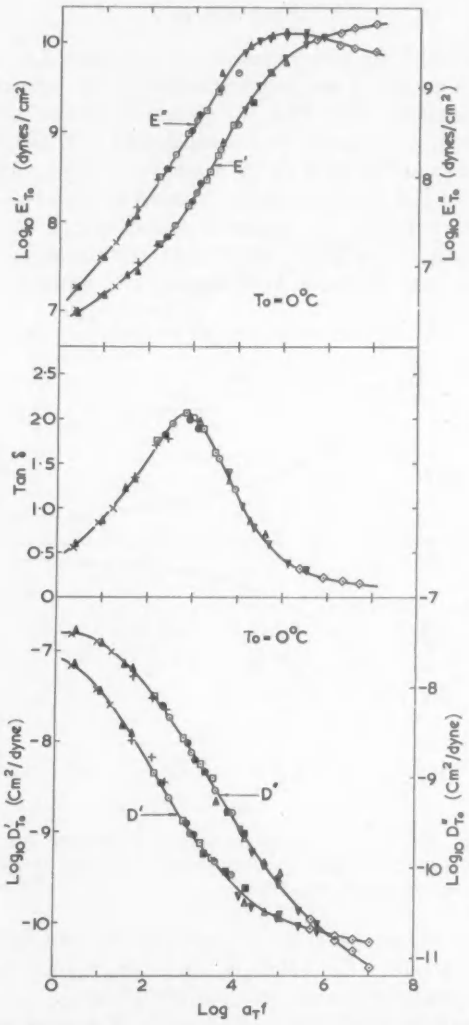

Fig. 2. Reduced master curves of E'_{T_0}, E''_{T_0}, tan δ, D'_{T_0} and D''_{T_0} against log $a_T f$. The reference temperature $T_0 = 0°C$. Point symbols as in Figure 1.

The master curves given in Figure 2 are typical of those observed for the rubberglass relaxation of amorphous polymers. The maximum in the E'' master curve occurs at a higher reduced frequency than the tan δ maximum and corresponds to the region where E' is approaching its limiting glassy value. A maximum in D'' is not observed within the range of reduced frequency investigated, but it is estimated to occur at about 1 cycles/sec. at 0°C.

Birefringence

Figure 3 illustrates the determination of the factors $\Delta n_{T_0}/\Delta n_T$ which are required in the proposed method for reducing the optical data to the reference temperature T_0. The top diagram shows the variation of birefringence with temperature (in the range 0 to −30°C.) for a polyacetaldehyde sample maintained at 19.7% extension. The sample was initially stretched at 0°C. and the birefringence allowed to relax to a steady value. The agreement between the results obtained during the cooling and subsequent heating experiment shows that the measurements were reversible. The small increase in birefringence with decreasing temperature

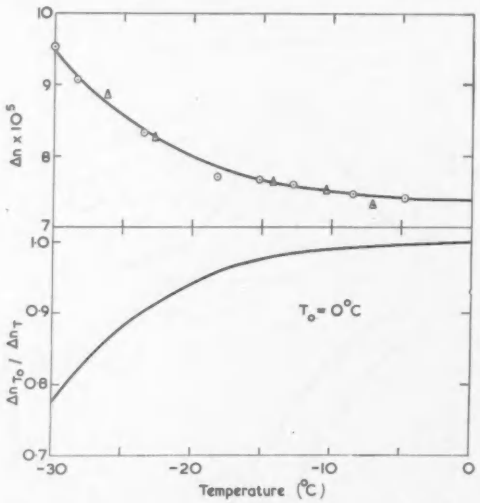

Fig. 3. (Upper), plot of the birefringence against temperature for polyacetaldehyde at 19.7% extension during cooling (⊙) and reheating (△); (lower), the variation of $\Delta n_{0°C.}/\Delta n_T$ with temperature for polyacetaldehyde.

is attributed to an increase in $\alpha_\parallel - \alpha_\perp$, the equilibrium optical anisotropy of the statistical link. The values of $\Delta n_{0°C.}/\Delta n_T$ shown in the lower diagram are averages determined from two separate runs.

The master plots of $|K|_{T_0}$, $|C|_{T_0}$, δ', and $\delta - \delta'$ against log $a_T f$ are given in Figure 4. At a reduced frequency of about 10^4 cycles/sec. $|K|_{T_0}$ exhibits a maximum and the birefringence and strain are in phase ($\delta' = 0$). At lower frequencies $|K|_{T_0}$ increases with frequency and the birefringence cycle leads the strain cycle (δ' positive), whereas at higher frequencies the reverse situation exists. $|C|_{T_0}$ is seen to increase as the frequency decreases but tends toward the static value of 1.1×10^{-10} cm.^{2}/dyne at the lowest reduced frequencies. This static stress-optical coefficient, indicated by the point of the ordinate, was measured for a (rubberlike) specimen at room temperature after hanging known weights onto its end. The stress

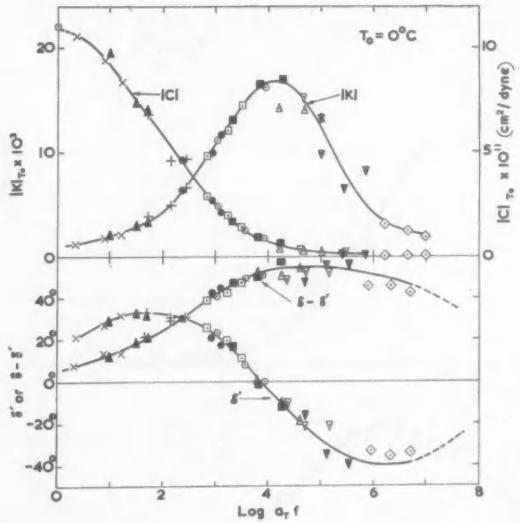

Fig. 4. Master curves of $|K|_{T_0}$, $|C|_{T_0}$, δ', and $\delta - \delta'$. Point symbols as in Figure 1.

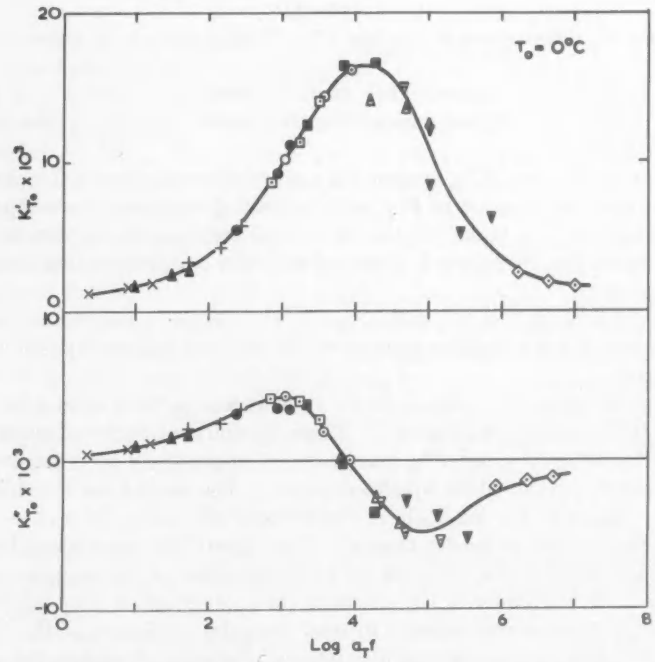

Fig. 5. Master curves of K'_{T_0} and K''_{T_0}. Point symbols as in Figure 1.

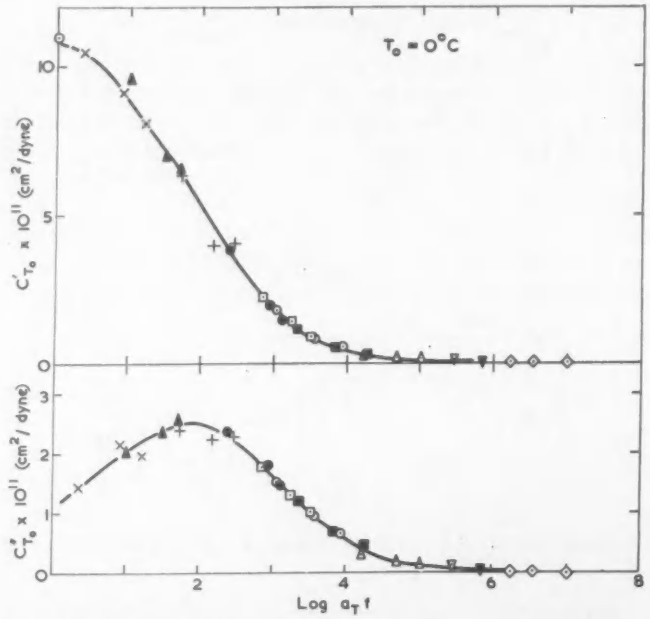

Fig. 6. Master curves of C'_{T_0} and C''_{T_0}. Point symbols as in Figure 1.

cycle leads the birefringence cycle at all reduced frequencies ($\delta - \delta'$ positive), and the $\delta - \delta'$ plot passes through a broad maximum in the region of 10^5 cycles/sec.

Plots of K'_{T_0} and K''_{T_0} against log $a_T f$ are shown in Figure 5. At low frequencies the increase in K'_{T_0} with increasing frequency is accompanied by a positive K''_{T_0} peak. In the high frequency region a decrease in K'_{T_0} with increasing frequency is observed and also a corresponding negative K''_{T_0} peak.

Figure 6 shows the C'_{T_0} and C''_{T_0} curves. The C''_{T_0} curve has a single maximum which correlates approximately with the inflection point in the C'_{T_0} plot.

Plots of log $\phi_E(\ln \tau)$, log $\phi_D(\ln \tau)$, $\phi_K(\ln \tau)$ and $\phi_C(\ln \tau)$ against log τ at $T_0 = 0°C$. are shown in Figure 7. These distributions were evaluated from the E''_{T_0}, D''_{T_0}, K''_{T_0} and C''_{T_0} master curves respectively according to the first-order approximation equations given.[2] The dashed line shown in the long τ region of the log $\phi_E(\ln \tau)$ versus log τ plot has a slope of $-1/2$ as predicted by the molecular theory. The slope of the experimental curve generally differs from $-1/2$ but tends to this value at the longest τ investigated. A maximum in the ϕ_E spectrum is observed at $\tau \approx 10^{-5.8}$ sec. while the ϕ_D spectrum appears to tend toward a maximum in the long τ region. The ϕ_K spectrum divides into two regions. Processes for which $\tau < 10^{-4.7}$ sec. contribute a net *negative* amount to $K'_\infty - K'_0$ and ϕ_K

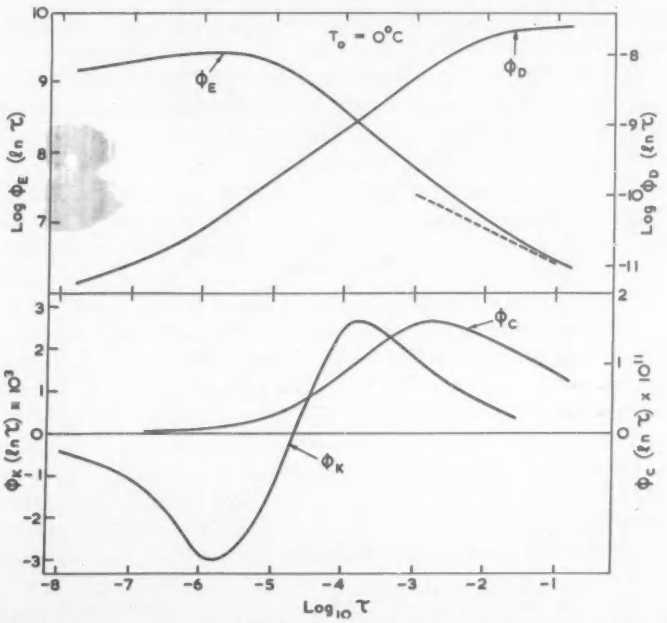

Fig. 7. Plots of log $\phi_E(\ln \tau)$, log $\phi_D(\ln \tau)$, $\phi_K(\ln \tau)$, and $\phi_C(\ln \tau)$ against log τ at 0°C. The dashed line shown with the ϕ_E spectrum has the theoretical slope of $-1/2$.

exhibits a minimum at $\tau \approx 10^{-5.8}$ sec. which correlates with the mechanical ϕ_E maximum. For $\tau > 10^{-4.7}$ sec. the relaxation processes contribute a net *positive* amount to $K'_\infty - K'_0$ and ϕ_K shows a maximum at $\tau \approx 10^{-3.8}$ sec. The ϕ_C spectrum has a single maximum at $\tau \approx 10^{-2.7}$ sec.

The apparent frequencies of the E'', K'', and C'' maxima and the K'' minimum are plotted against $1/T$ in Figure 8. Points are included on the diagram for which a maximum was directly observed within the experimental frequency range. Other points were subsequently derived from the log a_T values given in Table I. The dashed curve illustrates the estimated frequency-temperature location of the D'' maximum assuming that at 0°C. the peak occurs at 1 cycle/sec. Also plotted in Figure 8 are points corresponding to the maximum in the dielectric loss factor ϵ''.[5] These points lie fairly close to those corresponding to the K'' maximum.

Discussion

The observed frequency dependence of the mechanical and optical properties probably arises from the motions of segments *within* the main polymer chain and corresponds to the transformation from the rubberlike to glasslike state of polyacetaldehyde.

The high modulus observed on the high frequency side of the reduced modulus curve is typical of values found for polymers in the glassy state

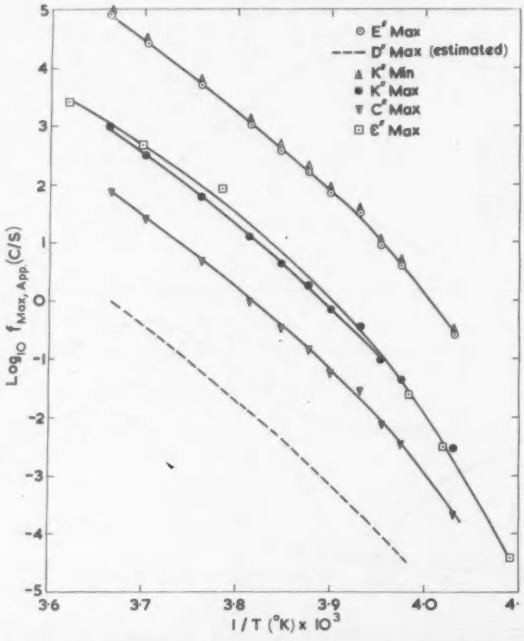

Fig. 8. Variation of the apparent frequencies of the (⊙) E''; (●) K''; and (▽) C''_{Max}; and (△) the K''_{Min} with reciprocal absolute temperature. Also shown are the locations of the (⊡) dielectric ϵ''_{Max}; and (- - -) the estimated D''_{Max}.

and may be attributed to the distortion of local groups within the structure. The corresponding distortional birefringence in this region leads to relatively small positive values for K'_{T_0} and C'_{T_0}. The initial increase in K'_{T_0} with decreasing frequency indicates that motions arising from the release of these local distortions produce an increase in the average orientation of chain links. Such a mechanism would be responsible for the negative peak in the K''_{T_0} master plot and the maximum in the E''_{T_0} curve and also the associated peaks in the ϕ_K and ϕ_E spectra at $\tau \approx 10^{-5.8}$ sec. at 0°C.

After passing through a maximum, the subsequent decrease in K'_{T_0} with decreasing frequency suggests that an additional relaxation mechanism predominates in the low frequency region. It is probable that this mechanism involves the motions of relatively long flexible chain segments such that at constant strain the chains tend to more coiled-up configurations as the frequency decreases. This process, which forms the basis of the molecular theory outlined earlier, leads to the positive peaks in the K''_{T_0} and C''_{T_0} plots and the corresponding maxima in the ϕ_K and ϕ_C spectra. However the theoretical predictions are not obeyed since the slope of the log $\phi_E(\ln \tau)$ versus log τ plot differs from $-1/2$, C'_{T_0} is not independent

of frequency, and $\delta - \delta'$, C''_{T_0} and ϕ_C are not zero. A probable explanation for the failure of these predictions is that the "distortional" mechanisms, which predominate in the high frequency region, overlap the orientational processes which predominate at low frequencies. In order to resolve satisfactorily the two proposed mechanisms a molecular theory appropriate to the high frequency range is required. The correlation noted above between the frequency-temperature location of the K'' maximum and the dielectric ϵ'' peak indicates perhaps that the dielectric relaxation in polyacetaldehyde is determined largely by the longer range chain rearrangements.

In the case of PMA it was also concluded that overlapping distortional and orientational mechanisms were involved in the relaxation region associated with the rubber-glass transformation. However in this case chain orientation produces a *negative* birefringence, possibly owing to the orientation of $—COOCH_3$ groups perpendicular to the stretching direction. Consequently a *positive* K'' peak was observed at high frequencies and a *negative* K'' peak in the low-frequency range. Also, for PMA a close correlation was found between the locations of the high frequency K'' maximum and the ϵ'' maximum. Hence, unlike polyacetaldehyde, the dielectric relaxation of PMA probably results from the short-range distortional rearrangements which could perhaps induce, or modify, rotations of the dipolar side groups.

The author thanks Mrs. J. Hawkins for preparing the polyacetaldehyde and for general assistance. The work described above has been carried out as part of the research program of the National Physical Laboratory and this paper is published by permission of the Director of the Laboratory.

References

1. Read, B. E., *Techniques of Polymer Science*, S.C.I. Monograph No. 17, *Soc. Chem. Ind.*, London, 1963, p. 198.
2. Read, B. E., *Polymer*, to be published.
3. Read, B. E., *Polymer*, **3**, 143 (1962).
4. Weissermel, K. and W. Schmieder, *Makromol. Chem.*, **51**, 39 (1962).
5. Williams, G., *Trans. Faraday Soc.*, **59**, 1397 (1963).

Résumé

On souligne les principes à la base de la méthode de biréfringence dynamique en attribuant une emphase particulière à l'usage de cette technique dans la recherche de mécanismes moléculaires de relaxation dans les polymères amorphes. Les résultats sont donnés pour le polyacétaldéhyde amorphe ($[—CH(CH_3)—O—]_n$) pour des fréquences de l'ordre de 1 à 20 cycles/seconde et des températures de l'order de 0°C à −25°C. Ces résultats sont discutés et comparés brièvement avec les données de biréfringence dynamique obtenues précédemment pour le polyméthacrylate de méthyle.

Zusammenfassung

Die Prinzipien für die Methode der dynamischen Doppelbrechung werden unter besonderer Betonung der Verwendung dieser Methode zur Untersuchung des molekularen Relaxationsmechanismus bei amorphen Polymeren dargelegt. Daten für amorphen Polyacetaldehyd ($[-CH(CH_3)-O-]_n$) werden im Frequenzbereich von 1–20 Hertz und im Temperaturbereich von 0 aus $-25\,^{\circ}C$ angegeben. Die Ergebnisse werden diskutiert und kurz mit dielektrischen Daten für Polyacetaldehyd und auch mit früheren dynamischen Doppelbrechungsdaten für Polymethylacrylat verglichen.

JOURNAL OF POLYMER SCIENCE: PART C NO. 5, PP. 101–112

Temperature Dependence of Orientation Birefringence of Polymers in the Glassy and Rubbery States

R. D. ANDREWS* and T. J. HAMMACK,* *Materials Research Laboratory, Department of Civil Engineering, Massachusetts Institute of Technology, Cambridge, Massachusetts*

Synopsis

The temperature dependence of orientation birefringence has been measured for several different polymers, by producing samples with a fixed degree of orientation by mechanical stretching, and varying the temperature. The following three polymers were studied: polystyrene, poly(methyl acrylate), and poly(methyl methacrylate)—the last in both atactic and stereospecific forms. These all have negative orientation birefringence at room temperature. Measurements were carried out in a range of temperatures below the glass transition temperature, except for poly(methyl acrylate) which was crosslinked. The curves obtained for the different polymers showed considerable differences in form; they were reversible in regard to temperature cycling, and showed no appreciable time effects. Polystyrene showed little change in its orientation birefringence with temperature. The other polymers showed appreciable changes with temperature, and an actual change of sign of the birefringence from negative to positive with increasing temperature. The crossover temperature was near the glass transition temperature for the various stereo forms of PMMA, and measurement of this crossover temperature might therefore provide a fairly accurate method for determining the stereo composition of a PMMA sample. However, the crossover temperature is considerably above T_g in the case of PMA. We believe that these curves reflect thermal motions of the molecular groups with polarizability anisotropy (such as the phenyl and ester side groups) whose orientation gives rise to the birefringence. The small change in the case of polystyrene is undoubtedly a consequence of the rigidity of the phenyl ring and the steric hindrance of its immediate environment. These results may also reflect chain backbone motions, and other effects, in an indirect way. The theory and experimental data for a complete interpretation of these results is not yet available. However, some of the evident consequences of the present findings are discussed.

Birefringence studies of solid polymers have generally involved measurements of the stress-optical coefficient, the strain-optical coefficient, or orientation birefringence at some standard temperature (usually room temperature) as an index of the degree of orientation. In the present paper we describe some preliminary results from a somewhat different type of experiment, in which samples with a fixed degree of orientation are produced, and the effect of temperature alone on the orientation birefringence is measured. This study of the temperature variable has provided results of unusual interest.

* Present address: Textile Division, Department of Mechanical Engineering, M.I.T.

The polymers examined in the present study were:

(*1*) Polystyrene—linear
atactic
(*2*) Poly(methyl acrylate)—crosslinked
atactic
(*3*) Poly(methyl methacrylate)—linear
atactic
isotactic
syndiotactic
stereo-block

These polymers were amorphous in all cases; the stereospecific PMMA samples were quenched into the amorphous glassy state in the original compression molding process. The three atactic materials were polymerized in place as cast sheets. All of these polymers have negative orientation birefringence at room temperature.

Samples and Experimental Procedure

The original polymer sheets were $^1/_{16}$–$^1/_8$ in. thick and a few inches square; small strips were cut from these (by machining, or with a razor blade in the case of PMA) which were perhaps $^5/_8$ in. wide and 3 in. long. These strips of the glassy polymers were suspended in a temperature box under moderate load, and the temperature was slowly raised to a point slightly above the glass transition temperature. The sample was allowed to creep to a suitable extent, to give the degree of orientation desired, and the box was then opened and the sample quickly cooled by circulation of room-temperature air, while remaining under load. The sample could then be removed if desired. The procedure was slightly different for the poly(methyl acrylate), which was in the rubbery state at room temperature and apparently crosslinked; in this case the sample was loaded and allowed to reach elastic equilibrium in the rubbery state, and this fixed load was then kept on the sample at all times as the temperature was varied.

Temperature changes involved the use of two different air thermostats, one operating above room temperature with electric heating coils of the conventional sort, and the other operating below room temperature, down to liquid nitrogen temperature, in which liquid nitrogen was added to a double-cylinder brass cooling jacket surrounding the sample. The construction of the latter thermostat will be described elsewhere. The uncrosslinked polymers could not be heated above the glass transition temperature in the oriented state, since this would have led to significant disorientation. Birefringence was measured by use of a Sénarmont compensator, which has been described in a previous publication.[1] Birefringence was not calculated as such; the data are presented simply as compensator extinction angle values (which are proportional to the birefringence) as a function of temperature. The aim in the present measurements was

merely to establish the general form of the curves obtained in this type of experiment.

Experimental Results

Polystyrene

The results obtained for a sample of cast polystyrene sheet are shown in Figure 1. The temperature was varied between liquid nitrogen temperature (−196°C.) and +50°C., and the curve is essentially flat, showing an almost complete lack of temperature dependence of the orientation birefringence. Actually there appears to be a slight minimum in the curve, at about 0°C., which might justify some further investigation.

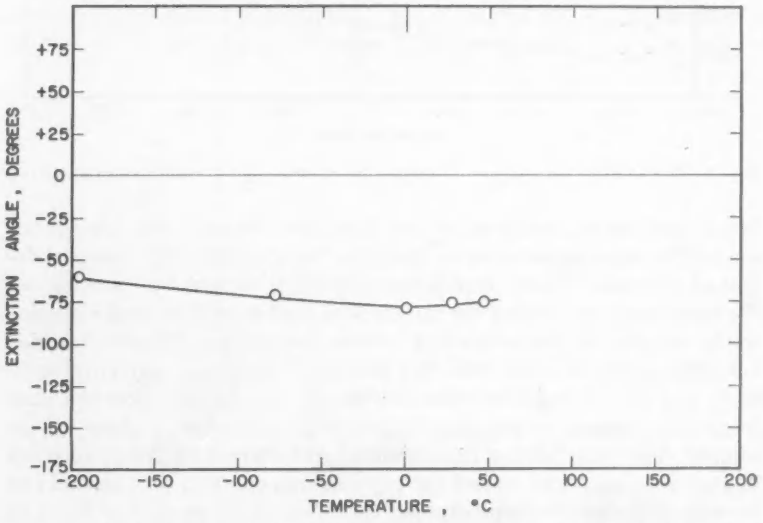

Fig. 1. Temperature dependence of orientation birefringence: polystyrene cast sheet.

Poly(methyl acrylate)

An analogous curve for poly(methyl acrylate) is shown in Figure 2. This sample appeared to have been crosslinked (presumably by chain transfer) during the polymerization, and therefore the temperature range covered could be extended into the rubbery as well as the glassy state, and the curve shown extends from liquid nitrogen up to about +115°C., approximately 110° above the glass transition temperature of +4°C. As noted previously, these measurements were carried out by hanging a dead load on the sample in the rubbery state and changing temperature under this constant load. The experiment therefore corresponded strictly neither to constant length nor constant elongation, because of combined effects of thermal expansion and the temperature dependence of modulus in the rub-

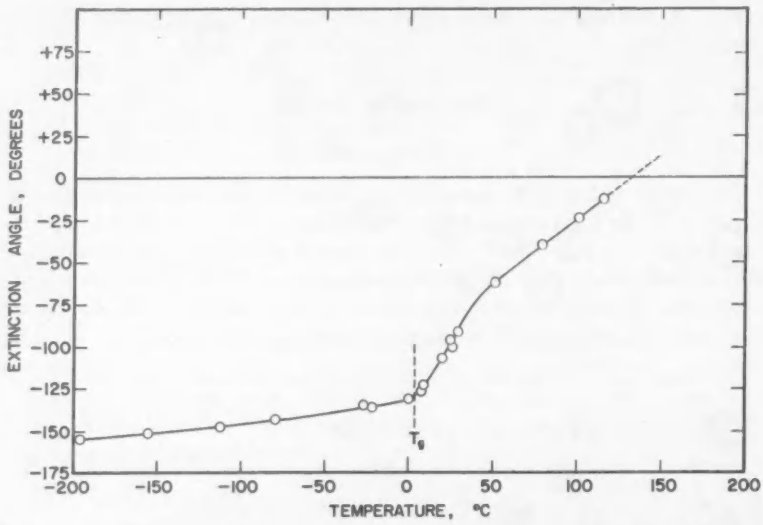

Fig. 2. Temperature dependence of orientation birefringence: poly(methyl acrylate).

bery state (kinetic theory of rubber elasticity); however, the experiment can still be regarded as being carried out at an approximately constant degree of orientation, since these perturbing effects are small. Carrying out the experiment by holding the sample at a fixed length by rigid clamping would actually be less satisfactory: Stein, Krimm, and Tobolsky[2] carried out a measurement in this way on a sample of crosslinked poly(ethyl acrylate), and they found that when the sample was cooled below the glass transition, thermal contraction introduced a distortional stress in the sample; this introduced a corresponding distortional birefringence effect of opposite sign, which caused the experimental curve to turn around and increase at the lowest temperatures.

As seen from the figure, there is a relatively small change of orientation birefringence with temperature in the glassy state, although the effect is larger than was observed with polystyrene: the negative orientation birefringence decreases in magnitude with increasing temperature, at a slightly increasing rate as the glass transition is approached. As temperature increases above T_g (which is indicated in the figure by a vertical dashed line) there is an abrupt rise in the curve, followed by a change in slope in the neighborhood of +40°, leading to a perfectly linear region of the curve. An extrapolation of the final linear region suggests that the birefringence will cross the zero axis at approximately +130°C. and become positive in sign. The sample unfortunately broke before this temperature could be reached. It is of interest that Stein, Krimm, and Tobolsky observe no abrupt change around the glass transition in their birefringence-temperature curve for crosslinked poly(ethyl acrylate).

Poly(methyl methacrylate)

Somewhat more detailed measurements were made on PMMA, including investigation of the effects of stereospecific structure. Although the type of experiment which we are carrying out here seems to be a relatively new one, some fragmentary data of this sort on PMMA have previously been reported. Kolsky and Shearman,[3] for example, have published a curve showing the effects of temperature cycling on the birefringence of a sample of oriented PMMA, in the glassy state. A birefringence-temperature curve has also been published by Trapeznikova and Zhurina[4] which is reproduced as Figure 3. They made their measurements on an oriented sample prepared from a solvent-cast film (presumably atactic polymer), and they report their data in the same manner as our own—i.e., as Sénarmont compensator extinction angle vs. temperature. This curve is not in very good agreement with our own curves for PMMA, as will be pointed out later. Other data on Plexiglas II commercial cast sheet have been

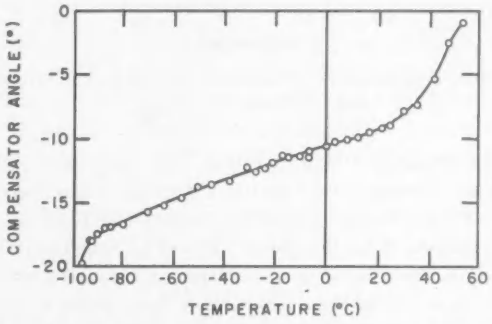

Fig. 3. Temperature dependence of orientation birefringence: poly(methyl methacrylate) data of Trapeznikova and Zhurina.[4]

reported in a thesis by McLoughlin.[5] He oriented strip samples by loading at temperatures above the glass transition (T_g = 100°C., roughly), followed by cooling through the glass transition region under dead load. He observed a positive birefringence on initial loading, and the curves of birefringence vs. temperature passed smoothly through zero to increasingly negative values as the temperature progressively decreased. His data covered only a limited temperature range, however.

Data of our own on PMMA are shown in Figure 4, which allow a comparison of curves for atactic, isotactic and syndiotactic polymers. These different polymers all give curves of the same general form. The curves show an appreciable change of orientation birefringence with temperature in the glassy state, and even at liquid nitrogen temperature the curves have not flattened to a final constant value. This argues for the existence of a significant degree of molecular motion in the glassy state, in contrast to the concept of a glassy polymer as a totally frozen structure; this will be dis-

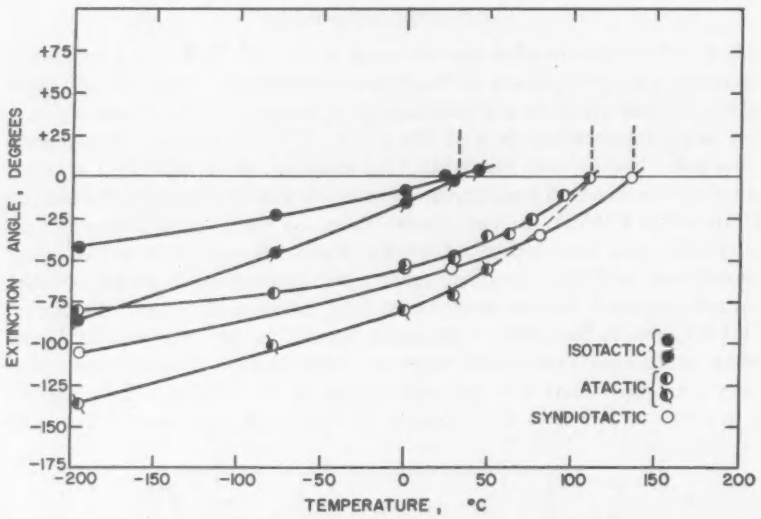

Fig. 4. Temperature dependence of orientation birefringence: poly(methyl methacrylate), different stereo forms.

cussed in more detail in a later section. As temperature increases, the curves rise at an increasing rate and finally cross the zero axis, where the birefringence shows a change of sign from negative to positive, in agreement with the observations of McLoughlin. It will be noted that Trapeznikova and Zhurina draw their curve so as to approach the zero axis asymptotically as temperature increases, although their data points would equally well allow the curve to be drawn through the zero axis into the positive region. If the curve were drawn in this way, their crossover point would be about +50°C., which would be considerably below that (+110°) which we observe for our own atactic sample; this is probably due to residual solvent in their film which would lower the glass transition temperature of their polymer. Finally, we see no evidence in our own curves of the abrupt drop which they show at the low-temperature end of their curve, at about −100°C.; this must be some artifact in their measurements.

The crossover points (or temperatures) for the different stereo forms are indicated in Figure 4 by vertical dashed lines above the zero axis; these values seem to correspond roughly with the glass transition temperatures determined for these same polymers from volume-temperature measurements, as follows:

Polymer	Crossover temp. (°C.)	T_g (°C.)
Isotactic	+31	+48
Atactic	+110	+100
Syndiotactic	+135	+110

However, there is no reason to think that the crossover temperature and glass transition temperature should coincide, and the lack of generality of any such principle, even for acrylic polymers, is evident from the curve for PMA in Figure 2, where the crossover point lies more than 100° above T_g. Two curves are shown for both the isotactic and atactic polymers in Figure 4; these were obtained from samples with different degrees of orientation, and they show that such curves differ essentially only by a vertical scale factor, and seem to have the same crossover point (cf. particularly the isotactic curves). This suggests that the crossover temperature, which can be easily measured, may provide a convenient method of determining the average stereo composition of a polymer such as PMMA with good accuracy. It is interesting that the crossover temperature for our atactic polymer (which is believed from other measurements to contain about 75% syndiotactic structure) lies about 75% of the way between the values for the isotactic and syndiotactic polymers; this would suggest that the relation between crossover temperature and stereo composition might be almost linear.

The birefringence vs. temperature curve for a stereo-block PMMA (which is a block copolymer of isotactic and syndiotactic sequences, having a dilatometric T_g value of +82°C.) is shown in Figure 5. This curve is similar in form to the other PMMA samples, and appears to have a crossover temperature of about +97°C. However, the curve seems to show a peculiar

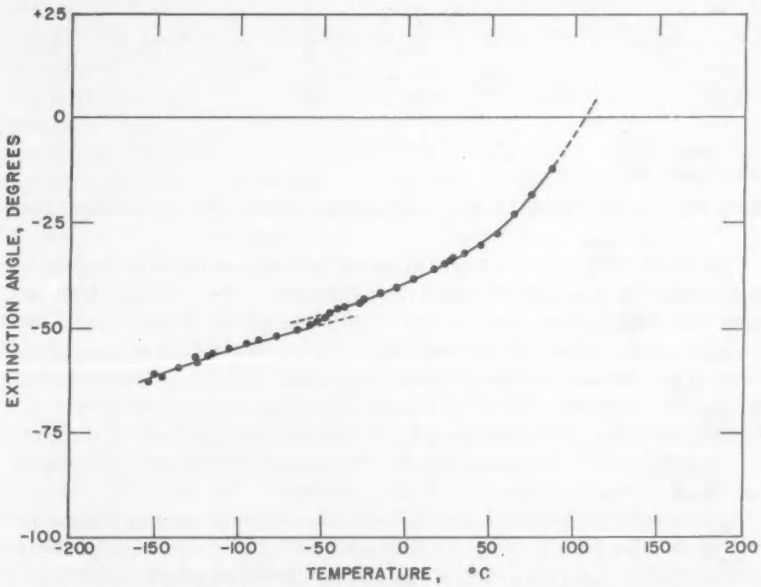

Fig. 5. Temperature dependence of orientation birefringence: poly(methyl methacrylate), stereo-block.

inflection at about −50°C. which was not seen in any of the curves in Figure 4; this requires further verification, but is presented here as being of general interest, and because it may have some relation to the stereoblock structure.

Experiments with temperature cycling indicated that the curves obtained in all these experiments were reversible: the same curve was obtained with both increasing and decreasing temperature. Also, no time-delay effects were observed: birefringence changes followed temperature changes instantly, as nearly as could be determined.

Discussion

In interpreting these results, as in all cases of birefringence phenomena in polymers, we may postulate the following general principle: *Birefringence arises from the orientation of molecular groups having polarizability anisotropy.* Some degree of polarizability anisotropy is associated with the hydrocarbon backbone chain of the polymers investigated here. However, the anisotropy is predominantly associated with the phenyl and ester side groups. This is illustrated in a schematic way in Figure 6, where longer and shorter arrows have been drawn beside these groups to indicate the approximate magnitudes and directions of their principal polarizabilities.

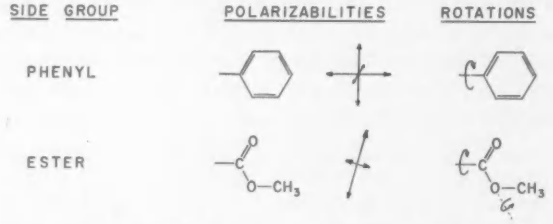

Fig. 6. Principal polarizabilities and rotational motions for phenyl and ester side groups.

The reversibility of the birefringence-temperature curves in regard to temperature cycling, and the effectively instantaneous change of birefringence with temperature change (no time-delay effects being observable) strongly suggests that the birefringence values which we are observing are thermal equilibrium values, which are associated with the thermal energy level of the material. More specifically, it would appear that we are observing the effects of thermal agitation (vibration and rotation) on the state of orientation of the side groups which were produced by extending the chain backbone during the original orientation process.

In the case of polystyrene, the polarizability of the phenyl ring is approximately twice as great in the plane of the ring as in the direction perpendicular to the plane, and the ring is a rigid, planar structure which has no internal degrees of freedom of motion; the only motion possible is a rotation around the bond connecting it to the chain backbone, as illustrated in Fig-

ure 6. The lack of temperature dependence of the birefringence in oriented polystyrene seems to illustrate not only the rigidity of the ring, which is unaffected by temperature change, but also a lack of rotation of the ring about the connecting bond to the chain. This suggests that rotational motion of the ring must be highly hindered sterically; and previous investigations of the stress-optical effect in glassy polystyrene[6] have indicated that this is indeed the case. Signer[7] has also pointed out that for polystyrene to have a negative orientation birefringence, the plane of the phenyl ring must lie not in the plane defined by the oriented chain backbone (which would produce an approximately zero birefringence contribution), but in a plane roughly perpendicular to it.

The greater temperature dependence of the orientation birefringence in the acrylic polymers seems to reflect the greater mobility of the nonrigid ester side group. The rotation of the end methyl group around the adjacent C—O bond axis (see Fig. 6) can have an effect not only on the anisotropy of the ester group, but may also facilitate rotation of the ester group as a whole around the bond connecting it to the chain backbone. In analogy with the behavior of the phenyl ring, the —COO— part of the ester group is a rigid planar structure, and if this plane were to lie in the plane of the oriented chain backbone, the birefringence effect would be positive; this would become negative as the plane rotated into a position perpendicular to the backbone plane. It would therefore be possible to explain the decrease of negative birefringence with temperature, and even the transition to positive values, on the basis of thermal motions of the ester group alone. This is essentially the explanation offered by Kolsky and Shearman[3] to explain their own data, and we are in agreement with this interpretation. Tsvetkov and Verkhotina[8] have estimated, using chain models and bond polarizabilities, that to obtain a positive birefringence for oriented PMMA requires a practically free rotation of the ester group. A somewhat different explanation is offered by Trapeznikova and Zhurina.[4] They propose that the observed birefringence in PMMA is a summation of two contributions—a negative contribution from the ester group, and a positive contribution from the alpha-methyl group on the chain. They interpret the positive birefringence observed at high temperatures as resulting from the disorientation of the negative component; they note that the positive birefringence could not be "frozen in" even with very rapid cooling. Peukert[9] also was surprised to find that it was not possible to freeze in the positive birefringence first produced when PMMA was hot-stretched. He gives a slightly different version of the two-contribution theory, in which he postulates a positive component due to molecular orientation and a negative component due to stress.

Assigning a significant positive contribution to the alpha-methyl group seems unreasonable, since the polarizability anisotropy of this group is almost zero; its major effect is probably simply as a source of steric hindrance to motion of the ester group. The effect of the chain backbone requires more extended comment. The polymers studied here have the

major part of their polarizability anisotropy concentrated in the side groups, and although the oriented chain backbone should contribute a small positive effect, this is less important than the effect of the side groups. It would be interesting to carry out this same type of measurement on polymers (such as natural rubber and silicone) where the predominant contribution comes from the chain backbone. In addition, it should be noted that backbone motions will of course affect the orientation of side groups indirectly, and this may be making a contribution to the form of our present curves. The abrupt change in birefringence observed in PMA just above the glass transition (Fig. 2) might be explainable as resulting from the suddenly increased freedom of motion of the chain backbone.

Such effects as a change in equilibrium chain configuration with temperature (due to a change in statistical distribution between trans and gauche forms) would also be expected to show up in measurements of this sort, though this type of effect should be observable particularly in the rubbery state above T_g, rather than in the glassy state. Stein, Krimm, and Tobolsky[2] interpret the change in birefringence with temperature which they observe in crosslinked poly(ethyl acrylate) simply as a change in size of the "statistical segment" with temperature. This would be one way of looking at the effects of chain configurational energy.

Data of the present type clearly have important implications in connection with the interpretation of the variation of stress-optical and strain-optical coefficients with temperature. And in a broader sense, if birefringence behavior is studied as a function of both temperature and time (or frequency), in a way analogous to static and dynamic rheological or viscoelastic properties of polymers (as has been recommended in another publication[10]), it seems evident that time-temperature superposition procedures, for example, cannot be successfully carried out for birefringence data without an explicit allowance being made for this intrinsic temperature dependence of birefringence, in addition to the effect of temperature on the rates of the rheo-optical processes.

The interpretation of these curves as reflecting thermally activated molecular motions suggests that it would be valuable to compare data of this sort with other types of physical data which also give indications of molecular motions, such as that from dynamic mechanical, dielectric, and nuclear magnetic resonance measurements. An interesting and also slightly puzzling point, for example, is that the birefringence-temperature curves for PMMA show no evidence of the β-peak or dispersion region below the glass transition which is seen clearly in dynamic mechanical and dielectric data, and is interpreted in these latter cases as resulting from the rotation of the ester side group.

Still another valuable use for data of this type would be in providing a clearer understanding of the glass transition phenomenon. The glass transition is interpreted as a change in the state of motion of the molecules, and these orientation birefringence curves measured through the glass transition region, when properly interpreted, should provide consid-

erable information on the exact nature of the changes in molecular motions which take place.

In conclusion, it is clear that these birefringence-temperature curves show a great deal of individual character in the case of different polymers, and it therefore seems likely that considerable information of value could be deduced from them. Unfortunately, the theory needed for this purpose is not available at the present time, and must be developed. It is planned to obtain additional data of this type covering a wider range of polymers and experimental conditions, to provide clearer indications of the general nature of the theory which is needed, and thus facilitate its rapid and successful development.

The authors would like to express their thanks to the American Society for Testing and Materials (A.S.T.M.) for a Grant-in-Aid in support of this work, and also to the National Science Foundation for their financial aid through an M.I.T. Institutional Grant. They are indebted to Mrs. N. S. Steck of the Rohm and Haas Co. (Bristol, Pa.) for specially preparing the acrylate and methacrylate polymers used, and for furnishing data on their properties.

References

1. Gurnee, E. F., L. T. Patterson, and R. D. Andrews, *J. Appl. Phys.*, **26**, 1106 (1955).

2. Stein, R. S., S. Krimm, and A. V. Tobolsky, *Textile Res. J.*, **19**, 8 (1949).

3. Kolsky, H., and A. C. Shearman, *Proc. Phys. Soc.*, **55**, 383 (1943).

4. Trapeznikova, O. N., and M. N. Zhurina, *J. Phys. Chem. (USSR)*, **24**, 1471 (1950). An English translation of this paper, by Mrs. V. Tolkmith and J. F. Rudd of the Dow Chemical Co., Midland, Mich., is available through the Crerar Library, Chicago.

5. McLoughlin, J. R., Ph.D. Thesis, Dept. of Chemistry, Princeton Univ. (April, 1951).

6. Rudd, J. F., and R. D. Andrews, *J. Appl. Phys.*, **31**, 818 (1960).

7. Signer, R., *Trans. Faraday Soc.*, **32**, 296 (1936).

8. Tsvetkov, V. N., and L. N. Verkhotina, *J. Tech. Phys. (USSR)*, **28**, 97 (1958); English translation in: *Sov. Phys.-Tech. Phys.*, **3**, 87 (1958).

9. Peukert, H., *Kunststoffe*, **41**, 154 (1951).

10. Andrews, R. D., Jr., "The Photoelastic Study of Polymers," M.C.A.-M.I.T. Plastics Research Project Progress Report, Department of Civil Engineering, M.I.T. (July 15, 1959). Note: Unfortunately, supplies of this report are exhausted, and copies are no longer available.

Résumé

La dépendance vis-à-vis de la température de la biréfringence d'orientation a été mesurée pour différents polymères, en faisant des échantillons possédant un degré d'orientation déterminé par étirage mécanique et variation de la température. On a étudié les trois polymères suivants: le polystyrène, le polyacrylate de méthyle, et le polyméthacrylate de méthyle—ce dernier dans ses formes atactiques et stériospécifiques. Tous ces polymères ont une biréfrirgence d'orientation négative à température ambiante. Des mesures ont été effectuées dans un domaine de température en dessous de la température de transition vitreuse, excepté pour le polyacrylate de méthyle, qui était ponté. Les courbes obtenues pour les différents polymères montrent des différences considérables de forme: elles sont réversibles quant à la variation cyclique de la température et ne montrent pas d'effets de durée appréciables. Le polystyrène montre un léger changement de biréfringence d'orientation avec la température. Les autres polymères mon-

trent des changements appréciables avec la températures et un changement de signe de la biréfringence, du négatif au positif par une augmentation de la température. La température de changement de signe est proche de la température de transition vitreuse pour les différentes stéréoformes du PMMA, et la mesure de cette température de changement de signe peut donc constituer une méthode excellente pour déterminer la composition stéréo des échantillons de PMMA. Néanmoins la température de changement de signe est considérablement plus élevée que T_g dans le cas du PMMA. Nous croyons que ces courbes reflètent les mouvements thermiques des groupements moléculaires dus à l'anisotropie de polarisabilité (comme les groupes latéraux phényles et esters), et dont l'orientation engendre une augmentation de la biréfringence. Le faible changement dans le cas du polystyrène, est indubitablement la conséquence de la rigidité du cycle phényle, et de l'empêchement stérique de son environnement immédiat. Ces résultats peuvent ainsi refléter des mouvements de la chaîne principale et d'autres effets, d'une façon indirecte. La théorie et les données expérimentales ne permettent pas encore de donner une interpretation complète. Néanmoins certaines conséquences évidentes des résultats actuels sont discutés.

Zusammenfassung

Die Temperaturabhängigkeit der Orientierungsdoppelbrechung wurde für verschiedene Polymere durch Herstellung von Proben mit einem fixen Orientierungsgrad durch mechenische Dehnung und Variierung der Temperatur bestimmt. Folgende drei Polymere wurden untersucht: Polystyrol, Polymethylacrylat und Polymethylmethacrylat—letzteres sowohl in ataktischer als auch stereospezifischer Form. Alle Proben zeigen bei Raumtemperatur negative Orientierungsdoppelbrechung. Die Messungen wurden in einem Temperaturbereich unterhalb der Glasumwandlungstemperatur aus geführt, ausgenommen Polymethylacrylat, das vernetzt war. Die für die verschiedenen Polymeren erhaltenen Kurven zeigen beträchtliche Formunterschiede. sie waren in bezug auf den Temperaturzyklus umkehrbar und zeigten keine merkliche Zeitabhängigkeit. Polystyrol zeigte kaum eine Änderung seiner Orientierungsdoppelbrechung mit der Temperatur. Die anderen Polymeren zeigten merkliche Änderungen mit der Temperatur, und sogar einen Vorzeichenwechsel der Doppelbrechung von negativ zu positiv mit zunehmender Temperatur. Die Übergangstemperatur lag für die verschiedenen Stereoformen von PMMA in der Nähe der Glasumwandlungstemperatur; Messungen dieser Übergangstemperatur könnten daher eine ziemlich genaue Methode zur Bestimmung der Stereozusammensetzung einer PMMA-Probe bilden. Bei PMA liegt jedoch die Übergangstemperatur beträchtlich über T_g. Wir glauben, dass diese Kurven die thermische Bewegung der Molekülgruppen mit Polarisationsanisotropie (wie die Phenyl- und Esterseitengruppen) wiedergeben, deren Orientierung die Doppelbrechung verursacht. Die kleine Änderung bei Polystyrol ist zweifellos eine Folge der Starrheit des Phenylringes und der sterischen Hinderung seiner unmittelbaren Umgebung. Diese Ergebnisse könnten indirekt auch die Bewegung der Hauptkette und andere Effekte erkennen lassen. Die Theorie und die experimentellen Daten für ein vollständige Erklärung dieser Ergebnisse sind zwar noch nicht greifbar, einige offensichtliche Folgerungen aus den vorliegenden Ergebnissen können aber diskutiert werden.

JOURNAL OF POLYMER SCIENCE: PART C NO. 5, PP. 113–122

Application of Equivalent Model Method to Dynamic Rheo-Optical Properties of Crystalline Polymer

MOTOWO TAKAYANAGI, SHINSAKU UEMURA, and SHUNSUKE MINAMI, *Department of Applied Chemistry, Faculty of Engineering, Kyushu University, Fukuoka, Japan*

Synopsis

Assuming that the crystalline polymer consists of the crystalline and the non-crystalline phase, a mechanical model for the crystalline polymer is constructed. We introduced into this model such complicated circumstances as some parts of the crystalline phase will be largely deformed under a stress concentration and other parts not so much. The temperature dependence of complex moduli of the crystalline polymers with various degrees of crystallinity is illustrated by using the model. On the basis of the model, we have derived an equation for calculating the strain-optical coefficient of the crystalline polymer from those of the crystalline and the non-crystalline phase. The equation gives a relation among the rheo-optical quantities, the viscoelastic quantities and the parameters representing the fine structure and the crystallinity of the polymer. It is concluded from this equation that the strain optical coefficients cannot be expressed by such a simple additive relation as usually employed.

1. Introduction

One method of description of the rheo-optical properties of polymers has been recently presented by Stein, Onogi, and Keedy.[1] They introduced two distribution functions $A(\tau)$ and $B(\tau)$ to express the birefringence of polymers in the similar way as in the viscoelasticity. The two distribution functions for amorphous polymers have a possibility to be interpreted by the molecular theory. It is, however, difficult to interpret the distribution functions for the crystalline polymers by the molecular theory, because there exists a heterogeneity of molecular aggregation in the crystalline textures. As a result of this circumstance, some parts in the crystalline region will be largely deformed under a stress concentration and other parts not so much.

In this report, a model method developed by us to interpret the viscoelastic properties of the crystalline polymers and the polymer blends is applied to express the relationship among the rheo-optical properties, the viscoelastic properties and the texture of the crystallized polymer. In this case, the texture of the crystalline polymer is simplified to be expressed by the degree of crystallinity and one parameter representing the mixing state.

2. Equivalent Model Method for Viscoelastic Properties of Two-phase System

The left side of Figure 1 is a schematic representation of the two-phase system, in which the particles 2 (as phase 2) are dispersed in the medium 1 (as phase 1). The phase 1 and the phase 2 are perfectly bonded to each other.

When such a sample as the left side of Figure 1 is subjected to tension, some of the lines of force in the sample pass only through the phase 1 and the others through both the phases in series.

Taking the above circumstance into consideration, the sample may be symbolized in the simplest case as shown in the right-hand side. λ and φ in the figure are parameters relating to the mixing state and the composition

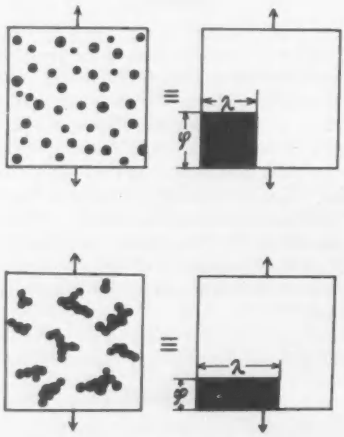

Fig. 1. Schematic representations of the mixing state of the two-phase system (the left side) and their equivalent models (the right side). The upper figure shows a homogeneously dispersed system and the lower figure a heterogeneously dispersed system.

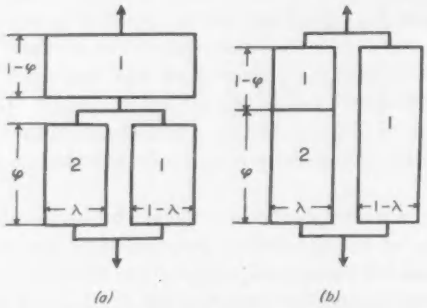

Fig. 2. Two mechanical models for calculating the modulus of the equivalent model in Figure 1. Model (*a*) is adopted in our method.

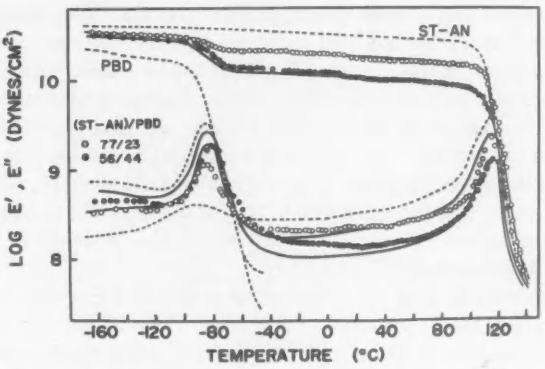

Fig. 3. E' and E'' versus temperature for the interpolymer of polybutadiene (PBD) with styrene (ST) and acrylonitrile (AN) monomer at 138 cycles/sec.: (○) observed values for the volume fraction of PBD, $V_2 = 0.23$; (●) observed values for the volume fraction of PBD, $V_2 = 0.44$; solid lines for white circles are calculated based upon the equivalent model with $\lambda = 0.600$, $\varphi = 0.380$, and $V_2 = 0.23$; solid lines for black circles are calculated based upon the equivalent model with $\lambda = 0.775$, $\varphi = 0.568$, and $V_2 = 0.44$; dotted lines are the observed ones for the component polymers.

of the sample. When these simplifications are allowed for the actual two-phase system, the models on the right-hand side of Figure 1 can be said to be the equivalent models for them. Two simple mechanical models are considered for calculating the modulus of the equivalent model in the right hand side. Figure 2 shows these two models. In the model (*a*) in Figure 2, the strain of the element of the phase 2 is the same as that of the right-element neighboring it. In the model (*b*), the strain of the phase 2 is different from those of the other elements. It has been proved by the model experiments that the model (*a*) is more suitable to calculate the modulus of the equivalent model.[2] Therefore, the model (*a*) will be adopted for calculating the modulus of the actual system.

The gross complex modulus E^* of the system, in which the particles 2 are dispersed in the medium 1, is expressed by use of its equivalent model of Figure 1 as follows:

$$E^* = \left[\frac{\varphi}{(1-\lambda)E_1^* + \lambda E_2^*} + \frac{1-\varphi}{E_2^*}\right]^{-1} \tag{1}$$

where E_1^* and E_2^* are the complex moduli of the medium and the dispersed particles respectively, λ and φ are the parameters representing the mixing state, and they are in the relation that $\lambda\varphi$ is equal to the volume fraction of the particles. When the particles are spheres, λ and φ depend on the volume fraction of phase 2, V_2, as follows:

$$\lambda = (2 + 3V_2)/5 \tag{2}$$

$$\varphi = 5V_2/(2 + 3V_2) \tag{3}$$

These equations have been derived from the condition that Kerner's equation[3] and eq. (1) should hold at the same time. Kerner's equation relates the modulus of the two-phase system to the elastic constants of the continuous phase and the dispersed phase, assuming that the dispersed phase is in the shape of spherical particles and that there is perfect adhesion between the two phases. The equation is derived on the basis of the elastic theory. If the dispersed phase 2 takes a more extended shape, such as sheet or rod, the value of λ increases and that of φ decreases in comparison with the predicted values by eq. (2) or (3), that is, the tendency of the series-connection is intensified.

Figure 3 shows E' and E'' versus temperature at 138 cycles/sec. for the system in which the polybutadiene particles (phase 2) are dispersed in the styrene-acrylonitrile copolymer phase (phase 1), being graft-polymerized in their intersurface. The full lines in the figure are calculated by using the values listed in Table I for the parameters of the equivalent model of Figure 1. Satisfactory agreement between the observed and the calculated curves will be seen, except a slight deviation on the dispersion region. This tendency is duly ascribed to the uncontrollable factors in polymerization. The simple equivalent model contains only one parameter representing a mixing state, if the composition of the system is given. If necessary, eq. (1) can be extended to the generalized form to express a more complex behavior.[2,4]

TABLE I

Volume ratio of (ST-AN)/PBD	V_2(PBD)	λ	φ	Curves
77/23 (white circle)	0.23	0.600 (0.54)[a]	0.380	Full line
56/44 (black circle)	0.44	0.775 (0.66)[a]	0.568	Full line

[a] Values when the phase 2 is assumed to be dispersed in the spherical shape.

3. Application of Equivalent Model Method to Crystalline Polymer

It is assumed that the texture of the crystalline polymer is composed of the crystalline and the non-crystalline region. The non-crystalline region concerned with the primary dispersion is considered to exist separately from the lamella phase, being squeezed out from the lamella phase, as illustrated schematically in Figure 4. After the model of Figure 4, the lamella phase has a strong tendency to form a continuous crystalline phase, the support of which is also obtained from the mechanism of crystal growth. The left side of Figure 5 is a schematic representation of the crystalline texture, corresponding to the local structure given in Figure 4. Owing to these circumstances of the crystalline texture, the actual crystalline polymer will be reasonably represented by the simplified mechanical model, in which the

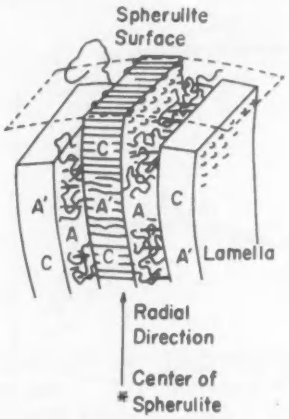

Fig. 4. Model of the local structure of spherulite. Region A is the non-crystalline region, region A' is the defective region, and region C is the crystalline region with perfect regularity

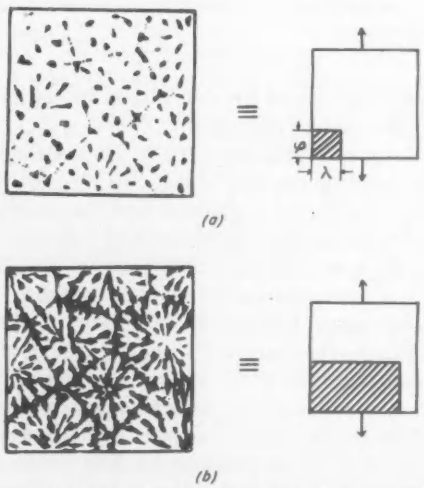

Fig. 5. Schematic representations of the texture of the crystalline polymers with crystallinities of (*a*) about 90% and (*b*) about 50%, and their equivalent models. Black area expresses the non-crystalline region.

non-crystalline region is dispersed in the crystalline phase as shown in the right hand side of Figure 5. In the same way as in the section 2, setting the non-crystalline region as phase 2 and the crystalline region as phase 1, the mechanical model can be constructed as shown in the left hand side of Figure 2.

It should be noted that the viscoelastic behavior of the crystalline polymer cannot be interpreted unless the properties of the non-crystalline re-

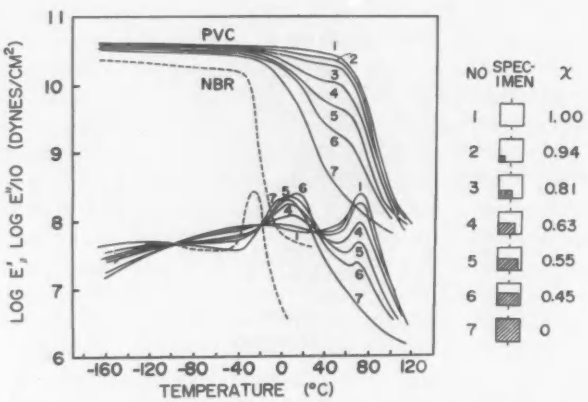

Fig. 6. E' and E'' versus temperature for the model specimens constructed from a PVC film (curve 1) as the substitute for the crystalline phase and a PVC/NBR = 42/58 film (curve 7) as that of the amorphous phase. The models used for calculating the complex moduli are indicated in the figure. χ is the volume fraction of PVC and corresponds to the crystallinity. PVC and NBR are the abbreviations of polyvinyl chloride and nitrile–butadiene rubber, respectively.

gion can be clarified. Because of the difficulty of its clarification, we have inevitably adopted the model experiment.

Figure 6 shows the viscoelastic behaviors of the model specimens, which are constructed by bonding together a polyvinylchloride (abbreviated as PVC) film as phase 1 to a film of the homogeneously mixed system of polyvinylchloride and nitrile-butadiene rubber (NBR) as phase 2. The constructions of the model specimens are shown in the figure. The PVC/NBR film is a molecularly mixed system of both polymers with its volume ratio of 42/58, and gives a transparent film, showing a very broad shape of dispersion. Curve 1 in Figure 6 corresponds to the dispersion curve of the PVC film, and curve 7 to that of the PVC/NBR film. The value of χ cited in Figure 6 is the volume fraction of the phase 1 and corresponds to the degree of crystallinity, when this model specimen is considered to represent the crystalline polymer. In case of χ taking 80–90% (curves 2 and 3), the crystalline dispersion becomes remarkable and this tendency accords with characteristics of linear polyethylene. In cases of χ = 50–60% (curves 4 and 5), the increase of intensity of the non-crystalline dispersion is seen in contrast with the decrease of the crystalline dispersion. These features are actually seen in the dispersion curves of polypropylene or branched polyethylene. Polyester, polyamide, and others with crystallinity of about 50% correspond to curve 6. Equivalent models employed here are selected not only to satisfy the composition of the system but also to satisfy the *S*-shape law,[5] which holds generally in the relation of log modulus vs. composition for the two-phase system. Figure 7 represents this relation. This relation comes from the fact that the dispersed phase and the medium

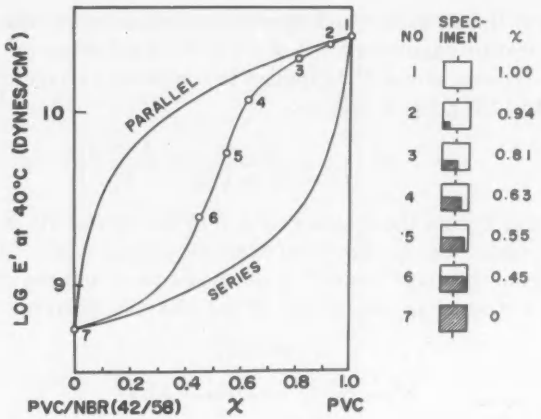

Fig. 7. Dependence of dynamic modulus at 40°C. upon the composition for the two-phase model specimen constructed by a PVC/NBR = 42/58 film and a PVC film in the form such as indicated in the right side of the figure. Model number corresponds to those in Figure 6.

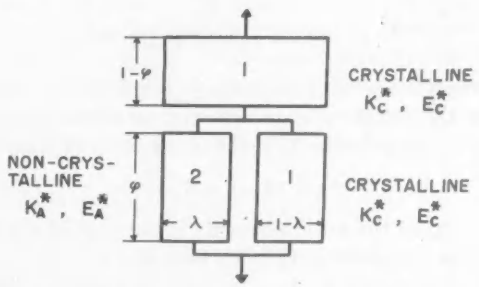

Fig. 8. Model for calculating the strain-optical coefficient of the crystalline polymer.

phase change their roles inversely in the intermediate compositions. The parallel and the series relation correspond to this limiting relation, respectively. From the results mentioned above, it may be said that the mechanical model in the left side of Figure 2 is the most simple mechanical model of crystalline polymer in which the fine structure of crystalline polymer is taken into consideration.

4. Application of Equivalent Mechanical Model to Dynamic Rheo-Optical Properties of Crystalline Polymer

The viscoelastic properties of the crystalline polymers have a possibility to be interpreted by the equivalent model method, as mentioned before. The similar model method may be applied to the rheo-optical properties of polymers. In this case, the complex strain-optical coefficient of the crystalline polymer will be expressed in terms of the complex strain-optical

coefficients of the crystalline and the non-crystalline region, the crystallinity and the texture parameter λ or φ of the crystallized polymer.

When a dynamic stress S^* is applied to the model in Figure 8, the dynamic strain γ^* is given as follows:

$$\gamma^* = S^* \left\{ \frac{\varphi}{(1-\lambda) + \lambda E_A^*} + \frac{1-\varphi}{E_C^*} \right\} \tag{4}$$

where E_C^* and E_A^* are the complex moduli of the crystalline and the non-crystalline region, λ and φ are parameters mentioned above. Let the dynamic strain of the upper element in the model be γ_1^* and the strain of the two lower elements γ_2^*, the stress S* satisfies the following equations.

$$S^* = \gamma_1^* E_C^* \tag{5}$$

$$S^* = \gamma_2^* \{(1-\lambda)E_C^* + \lambda E_A^*\} \tag{6}$$

From eqs. (4), (5), and (6), we obtain

$$\gamma_1^* = \gamma^* \frac{(1-\lambda)E_C^* + \lambda E_A^*}{(1-\lambda+\lambda\varphi)E_C^* + \lambda(1-\varphi)E_A^*} \tag{7}$$

$$\gamma_2^* = \gamma^* \frac{E_C^*}{(1-\lambda+\lambda\varphi)E_C^* + \lambda(1-\varphi)E_A^*} \tag{8}$$

Since the retardation of an element is proportional to the strain of the element and to the strain-optical coefficient corrected by the magnitude of the element, the retardation Δ_1^* of the upper element is given by

$$\Delta_1^* = (1-\varphi)K_C^*\gamma_1^* \tag{9}$$

The retardation Δ_2^* of the lower elements is the sum of the quantities of both the elements connected in parallel, that is

$$\Delta_2^* = (1-\lambda)\varphi K_C^*\gamma_2^* + \lambda\varphi K_A^*\gamma_2^* \tag{10}$$

In eqs. (9) and (10), K_C^* and K_A^* are the strain-optical coefficients of the crystalline and the non-crystalline region. The first term of the right side of eq. (10) corresponds to the lower left element of Figure 8 and the second corresponds to the right element. The total retardation Δ^* of the model is assumed to be the sum of the retardations of all elements.

$$\Delta^* = \Delta_1^* + \Delta_2^* \tag{11}$$

From eqs. (9) and (10), the total retardation Δ^* is

$$\Delta^* = (1-\varphi)K_C^*\gamma_1^* + \{(1-\lambda)\varphi K_C^* + \lambda\varphi K_A^*\}\gamma_2^* \tag{12}$$

Since the magnitude of the model is a unity, the retardation of the model is its birefringence. The strain-optical coefficient K^* of the model is defined as the birefringence divided by the strain.

$$K^* = \Delta^*/\gamma^* \tag{13}$$

From eqs. (7), (8), (12), and (13), we obtain the following expression for the strain-optical coefficient K^*,

$$K^* = K_C^* + \frac{\lambda\varphi E_C^*}{(1 - \lambda + \lambda\varphi)E_C^* + \lambda(1 - \varphi)E_A^*}(K_A^* - K_C^*) \quad (14)$$

By rearranging this equation, we obtain

$$R^* \equiv \frac{K_C^* - K^*}{K_C^* - K_A^*} = \frac{\lambda\varphi E_C^*}{(1 - \lambda + \lambda\varphi)E_C^* + \lambda(1 - \varphi)E_A^*} \quad (15)$$

or

$$R^* = \frac{V_A E^*}{(1 - \lambda)E_C^* + \lambda E_A^*} \quad (16)$$

where $V_A = \lambda\varphi$ and R^* is the non-dimensional complex number defined by eq. (15).

Equation (15) represents the relationship between the viscoelastic properties and the rheo-optical properties of the crystalline polymers. If the viscoelastic and the rheo-optical properties of the crystalline and the non-crystalline region of the real system are given respectively, the rheo-optical properties of the real system will be determined by these equations.

It is noteworthy that the non-dimensional complex number R^* is not equal to the volume fraction V_A, but it depends on the moduli, the volume fraction of the non-crystalline region and the mixing state parameter. Strictly speaking, the frequently used eq. (17) is not correct. Instead of V_A in eq. (17), R^* must be used as expressed in eq. (18), which is derived from eq. (15).

$$K^* = K_C^*(1 - V_A) + V_A K_A^* \quad (17)$$

$$K^* = K_C^*(1 - R^*) + R^* K_A^* \quad (18)$$

Characteristic properties of the crystalline region has a possibility to be evaluated by the direct measurement on a single crystal sample.[6] If the properties of the non-crystalline region could be separated from those of the crystalline texture by use of an appropriately oriented material, the relationship among the crystalline texture, the viscoelastic properties and the rheo-optical properties of the bulk crystallized polymer will be described by this method.

References

1. Stein, R. S., S. Onogi, and D. A. Keedy, *J. Polymer Sci.*, **57**, 801 (1962).

2. Takayanagi, M., H. Harima, and Y. Iwata, *J. Soc. Mat. Sci. (Japan)*, **12**, 389 (1963); *Mem. Fac. Eng. Kyushu Univ.*, **23**, 1 (1963).

3. Kerner, D. H., *Proc. Phys. Soc.*, **B69**, 808 (1956).

4. Takayanagi, M., and H. Harima, Symposium of Plastics Chemistry, 144th Annual Meeting American Chemical Society, New York, September, 1963.

5. Takayanagi, M., *Plastics (Japan)*, **13**, 1 (1962).

6. Takayanagi, M., *Proceedings of the Fourth International Congress on Rheology 1963*, Wiley, New York, 1964.

Résumé

On a construit un modèle mécanique pour un polymère cristallin en admettant qu'il se compose d'une phase cristalline et d'une phase non-cristalline. Nous avons introduit dans ce modèle des conditions compliquées au point que certaines parties de la phase cristalline seront fortement déformées par des tensions de concentration et d'autres ne le seront pas. En utilisant le modèle, on illustre la dépendance de la température vis-à-vis des modules complexes des polymères cristallins pour différents degrés de cristallinité. Sur la base du modèle nous avons dérivé une équation permettant de calculer le coefficient optique de tension du polymère cristallin a départ de ceux de la phase cristalline et non-cristalline. Cette équation fournit une relation entre les grandeurs rhéo-optiques, viscoélastiques et les paramètres représentant la structure fine ainsi que la cristallinité du polymère. De cette équation il est conclu que les coefficients optiques de tension ne peuvent être exprimés par une relation additive simple comme cela est fait habituellement.

Zusammenfassung

Unter der Annahme eines Aufbaus des kristallinen Polymeren aus der kristallinen und der nicht-kristallinen Phase wird ein mechanisches Modell für das kristalline Polymere konstruiert. In das Modell wurden so komplexe Verhältnisse eingebaut, dass z. B. gewisee Teile der kristallinen Phase bei einer Spannungskonzentration weitgehend deformiert wurden und andere Teile nicht. Die Temperaturabhängigkeit des komplexen Moduls von kristallinen Polymeren mit verschiedenem Kristallinitätsgrad wird anhand des Modells erläutert. Auf der Grundlage des Modells wurde eine Gleichung zur Berechnung des spannungs-optischen Koeffizienten des kristallinen Polymeren aus denjenigen der kristallinen und nicht-kristallinen Phase abgeleitet. Die Gleichung liefert eine Beziehung zwischen den rheo-optischen Grössen, den visco-elastischen Grössen und den Feinstruktur- und Kristallinitätsparametern des Polymeren. Die Gleichung führt zu dem Schulss, dass die spannungs-optischen Koeffizienten night durch die üblicherweise verwendete, einfache additive Beziehung dargestellt werden können.

JOURNAL OF POLYMER SCIENCE: PART C NO. 5, PP. 123–137

Dynamic Birefringence of Several High Polymers

R. YAMADA and C. HAYASHI, *Research Laboratory of Nippon Rayon Co., Ltd., Uji-City, Kyoto Prefecture, Japan*, and S. ONOGI and M. HORIO, *Department of Polymer Chemistry, Faculty of Engineering, Kyoto University, Kyoto, Japan*

Synopsis

The complex strain-optical coefficient, complex stress-optical coefficient, complex modulus of elasticity and the corresponding loss tangent of phase angles between the stress, strain and birefringence have been measured for several high polymers in the frequency range from 0.001 to 10 cycles/sec. Frequency and temperature dependences of the dynamic optical properties of vulcanized Hevea rubber are very similar to those of the dynamic mechanical properties. On the other hand, the dynamic optical properties of polyethylene and polypropylene show remarkable dispersions in the above frequency range. The dynamic optical behavior of these three materials are very typical and are quite different from each other. The differences have been explained by considering different frequency dependences of three kinds of deformation mechanism, namely, orientation of molecules in amorphous region, deformation of spherulites, and orientation of crystals.

Introduction

Introduction of dynamic birefringence into the high polymer study has recently been achieved by Stein, Onogi, and Keedy,[1–3] and the experiments performed with several high polymers based upon the theoretical foundation developed by them have revealed a sequence of novel information. One of the most important results obtained by them would be that the strain-optical coefficient, that is—the birefringence per unit strain, is dependent upon the frequency. This suggests that the dispersion as observed in dynamic modulus might be found with respect to the strain-optical coefficient. The effect of dispersion of modulus is verified by the measurement of the imaginary part of modulus, loss tangent or the phase difference between stress and strain by any means. However, the measurement of such quantity with respect to birefringence has not so far been achieved yet.

The main purpose of this study is to measure the phase difference between birefringence and strain, as well as the phase difference between birefringence and stress, and thereby to enrich our knowledge on the dispersion effect, which has been confined to the conception of viscoelastic system.

In analogy to the complex modulus in the viscoelastic system, which is given by

$$E^* = \frac{S}{\gamma} = E' + iE''$$

we define the following complex quantities with respect to the strain-optical and stress-optical coefficient as follows:

$$K^* = \frac{\Delta}{\gamma} = K' + iK''$$

and

$$M^* = \frac{\Delta}{S} = M' - iM''$$

where S is the stress, γ the strain, Δ the birefringence, and the star denotes the complex quantity.

Like the loss tangent in the viscoelastic system, that is

$$\frac{E''}{E'} = \tan \delta$$

we define the following quantities with respect to the strain-optical and stress-optical coefficient, respectively,

$$\frac{K''}{K'} = \tan \alpha$$

and

$$\frac{M''}{M'} = \tan \beta$$

As δ is the phase angle between stress and strain, so is α the phase angle between birefringence and strain, and β the phase angle between birefringence and stress. As can be deduced from the expression of S/γ, the stress is always ahead of the strain in the phase by δ, but the birefringence can be ahead of or behind the strain in phase, according as K'' is positive or negative.

The experiment was performed with the specimens of crosslinked rubber, polyethylene, polypropylene, nylon 6, and polyethylene terephthalate. E', E'', K', K'', M', M'', $\tan \delta$, $\tan \alpha$ and $\tan \beta$ of these specimens were measured at a certain frequency (1.50 cycles/sec.), and it was displayed that there are several different types of dynamic birefringence in reference to the relation among the vectors of stress, strain, and birefringence. Further, the frequency dependence of these quantities was measured within the frequency range from 10^{-2} to 10. Some of the materials manifested the distinct dispersion or indication of dispersion of dynamic birefringence in this frequency range. The change in birefringence would arise from the line-up of the molecules in the amorphous domains, orientation of crystallites (spherulites) and deformation of crystallites (spherulites). The result of the experiment was discussed in this light.

Apparatus

The phase difference was measured by the hysteresis loop method with the aid of a cathode ray oscilloscope, as well as by the direct method with the aid of an electromagnetic oscillograph. The construction of the apparatus and the block diagram are sketched in Figures 1 and 2. The periodical extension of the sample was effected by the sinusoidal movement of the lower

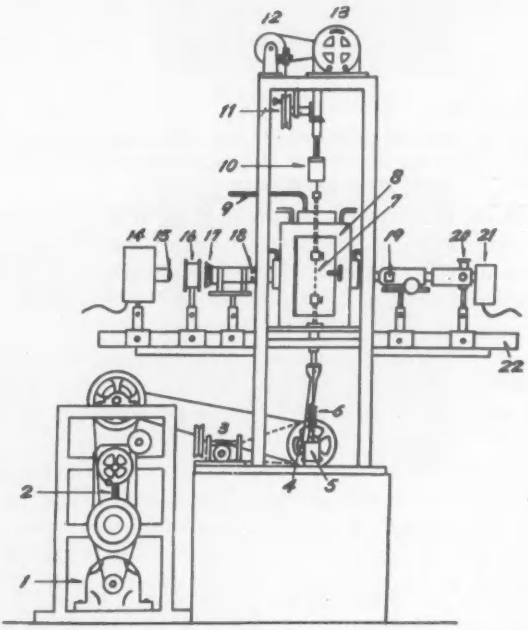

Fig. 1. Sketch of apparatus: (*1*) motor; (*2*) PIV; (*3*) worm gear; (*4*) cam; (*5*) strain gage, (*6*) spring; (*7*) sample; (*8*) sample chamber; (*9*) thermometer; (*10*) strain gage; (*11*) extension device; (*12*) worm gear; (*13*) motor; (*14*) lamp house; (*15*) lens and iris; (*16*) filter; (*17*) polarizer; (*18*) compensator; (*19*) analyzer; (*20*) viewer; (*21*) photomultiplier and, (*22*) optical bench.

clamp which is connected to an eccentric cam device rotating with a constant speed. The upper clamp is connected with a strain gage, by means of which the stress is changed into an electric signal. The movement of the lower clamp is also changed into an electric signal by means of another strain gage. The phase difference which is occasionally produced by the electric circuit itself was compensated by a compensating circuit.

The optical system for the measurement of birefringence consists principally of a light source (a high pressure mercury vapor lamp), filter, lens system, polarizer and analyzer which are crossed and placed before and behind the sample chamber, respectively, and a photomultiplier tube. The plane

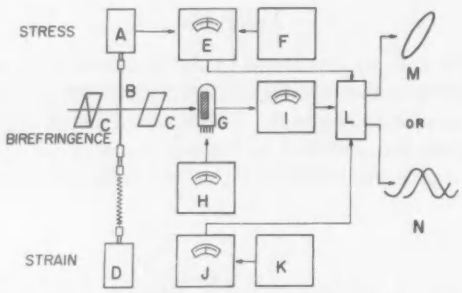

Fig. 2. Block diagram: (*A*) strain gage; (*B*) sample; (*C*) cross nicols; (*D*) strain gage; (*E*) strain meter; (*F*) electric source; (*G*) photomultiplier tube; (*H*) high voltage source; (*I*) ammeter; (*J*) strain meter; (*K*) electric source; (*L*) phase compensator; (*M*) cathode ray oscilloscope; and (*N*) electromagnetic oscillograph.

of polarization of the polarizer and analyzer is tilted 45° to the direction of stretching. A compensator is supplemented so that the measurement can be performed in the region where the relation between retardation and the current generated by the photomultiplier tube is practically linear. The monochromatic light of $\lambda = 546$ mμ was used.

The sample chamber is furnished with two windows on the opposite sides to permit the light to pass through the sample. The chamber is sufficiently insulated, and the temperature in the chamber can be controlled between $-40°$ and 200°C.

Every time before starting the experiments, an elastic spring is employed in place of the sample, and the circuit is so adjusted that the linear Lissajous' figure is obtained. Similar test was done also before starting the measurement of birefringence. In this case the area of the slit was changed sinusoidally in the same phase as that of the displacement of the lower clamp.

Figures 3 and 4 show the Lissajous' figure after phase-matching. Figure 3 refers to the same phase vibration of force and deformation, and Figure 4 to the same phase vibration of light intensity and deformation.

The sample was put between the upper and lower clamps, and being slightly stretched, and left in the chamber for a certain period of time to permit the sample to relax sufficiently before starting the measurement.

The amplitude of vibration was from 1 to 5% of the length of sample. The lengths of samples were from 6 to 8 cm. The frequency of vibration can be changed from 1/200 to 10 cycles/sec.

Specimens

(*1*) Rubber. Three parts of crosslinking agent (tertiary butyl-perbenzoate) and 0.5 part of antioxidant (2.6-ditertiary butylcresol) were mixed thoroughly with 100 parts of pale crepe, and the blend was heated at 140°C. for 30 min. The product was formed into a sheet having a thickness of 0.45 mm.

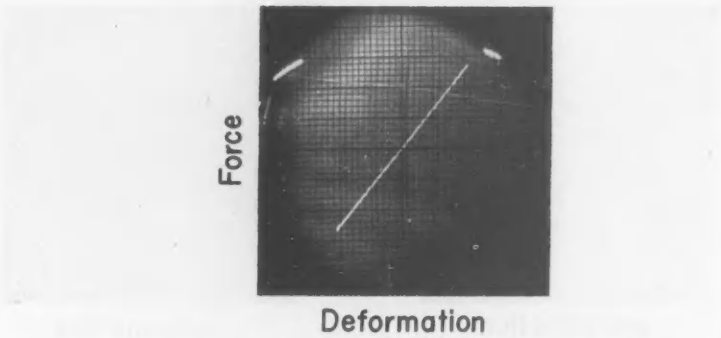

Fig. 3. Lissajous' figure of the same phase vibration of force and deformation.

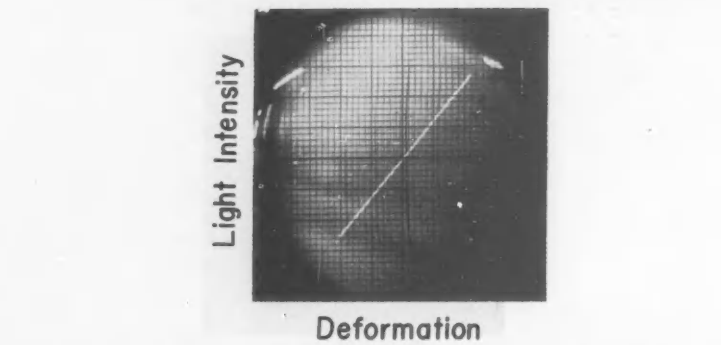

Fig. 4. Lissajous' figure of the same phase vibration of light intensity and deformation.

(*2*) Low-density polyethylene. Commercial pellets (Sumikathene F204) were cast into a sheet having a thickness of 0.2 mm. by the inflation method.

(*3*) Polypropylene. Commercial pellets of isotactic polypropylene (Avisan 1041) were extruded from a linear slit and formed into a sheet having a thickness of 0.35 mm.

(*4*) Nylon 6. Commercial pellets were cast into a sheet in the same manner as before. The thickness of the sheet was 0.073 mm.

(*5*) Polyester. Polyethylene terephthalate was cast into a sheet having a thickness of 0.073 mm. in the same manner as the above.

Results

A. Rubber

The Lissajous' figures of stress-strain, birefringence-strain and birefringence-stress at a frequency of 1.50 cycles/sec. at 30°C. are given in Figures 5*a*, 5*b*, and 5*c*, respectively. As can be deduced from the direction

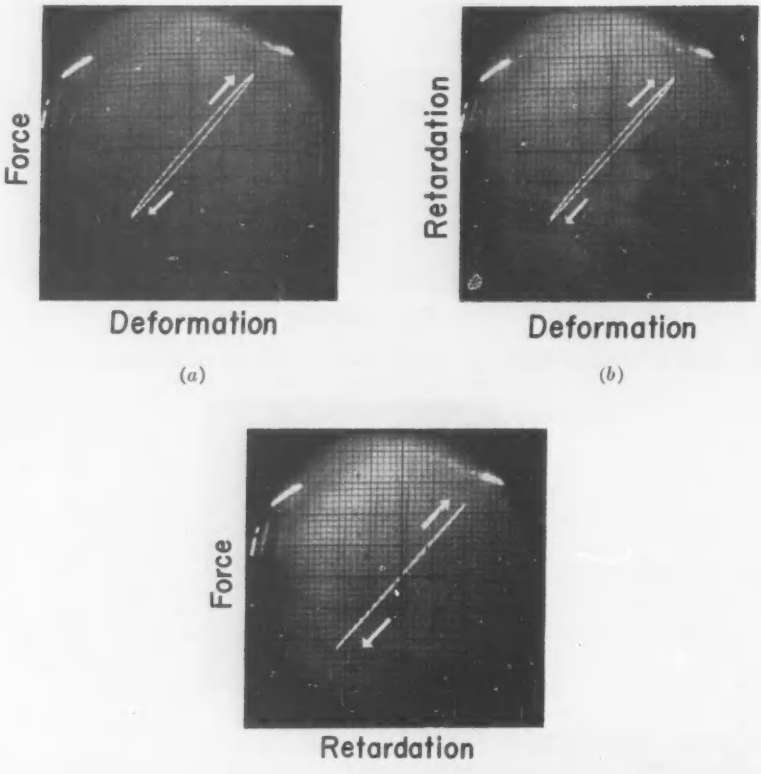

Fig. 5. Lissajous' figures of (*a*) stress-strain; (*b*) birefringence-strain; and (*c*) stress-birefringence of rubber. Arrows indicate the direction of scanning.

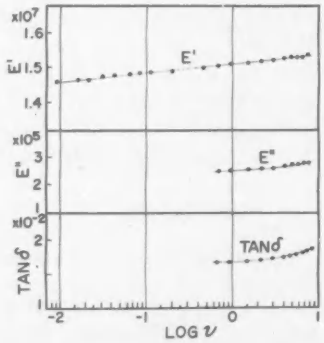

Fig. 6. E', E'', and tan δ versus log ν curves of rubber.

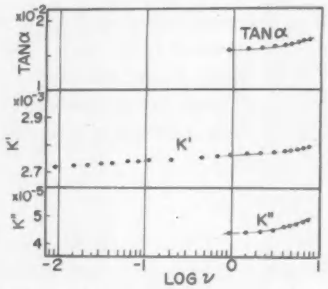

Fig. 7. K', E'' and tan α versus log ν curves of rubber.

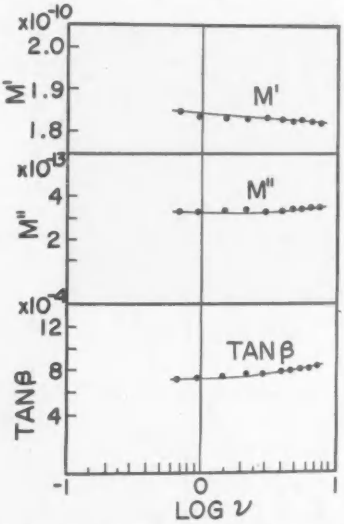

Fig. 8. M', M'', and tan β versus log ν curves of rubber.

of scanning shown in Figure 5*a*, the phase of stress is ahead of the phase of strain. Similarly, Figure 5*b* leads to the conclusion that the strain is behind the birefringence. On the other hand, the phase difference between stress and birefringence is very small, as shown in Figure 5*c*, but careful observation reveals that the stress is ahead of the birefringence.

Subsequently to the measurements at a constant frequency, the dependence of birefringence upon frequency will be treated below. Figure 6 shows the values of E', E'', and tan δ of rubber at 30°C. as a function of frequency. Within the region of frequencies covered by the experiment these quantities at 30°C. have only slight tendencies to increases with increasing frequency, but on the whole the curves are monotonous. Similar results are obtained for K', K'', and tan α as well as for M', M'', and tan β, as shown in Figures 7 and 8.

The analogy between modulus and strain-optical coefficient is seen also in the temperature dependence of these quantities. At temperatures below −20°C., the glass transition takes place, and the indication of dispersion comes in sight, that is—E', E'', and tan δ measured at a frequency of 1.5 cycles/sec. increases rapidly with decreasing temperature, as displayed in

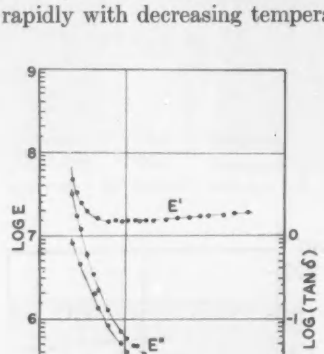

Fig. 9. Log E', log E'', and log tan δ of rubber as a function of temperature. Frequency is 1.5 cycles/sec.

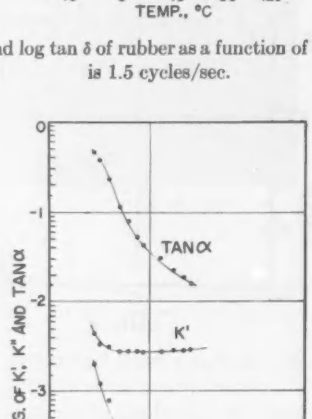

Fig. 10. Log K', log K'', and log tan α of rubber as a function of temperature. Frequency is 1.5 cycles/sec.

Figure 9. The same thing happens for strain-optical coefficient, K', K'', and tan α, as shown in Figure 10. In a word, the dynamic birefringence of rubber as a function of frequency and temperature is quite similar to the dynamic modulus as a function of frequency and temperature.

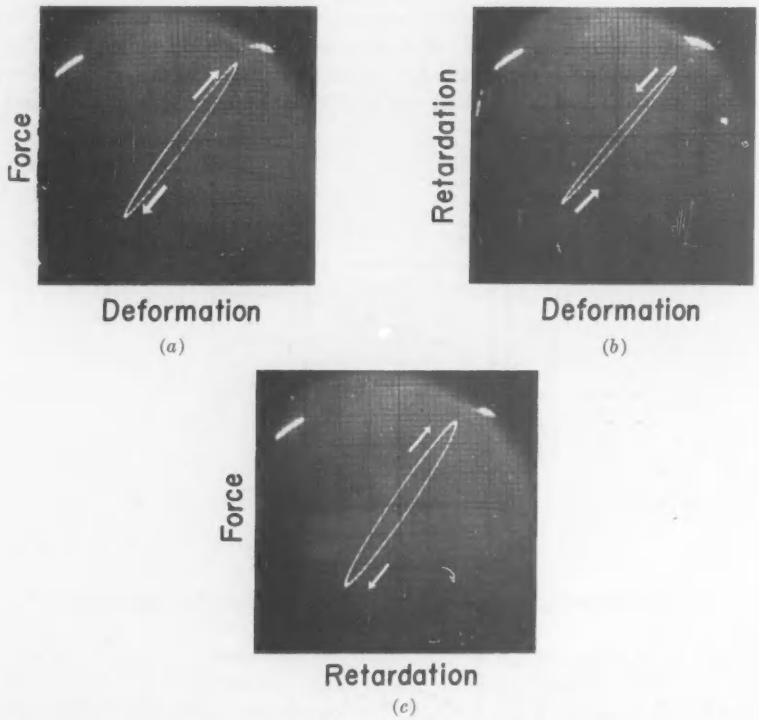

Fig. 11. Lissajous' figure of (*a*) stress-strain; (*b*) birefringence-strain; and (*c*) stress-birefringence of low-density polyethylene. Arrows indicate the direction of scanning.

B. Low-Density Polyethylene

Considerably different results have been obtained with the specimen of low-density polyethylene. The Lissajous' figures of stress-strain, birefringence-strain, and birefringence-stress at a frequency of 1.50 cycles/sec. at 30°C. are given in Figures 11*a*, 11*b*, and 11*c*. As can be expected, the stress is ahead of the strain (Fig. 11*a*), but, contrary to the case of rubber, the retardation is behind the strain (Fig. 11*b*). In the case of rubber, the stress and birefringence were almost in the same phase, but in the case of polyethylene the stress is far ahead of the birefringence, as can be seen in Figure 11*c*. In other words, β is the greatest and α is the smallest.

With respect to the frequency dependence also remarkable difference from that of rubber is observed. The E', E'', and tan δ versus frequency curves are shown in Figure 12. The tan δ versus frequency curve seems to have a flat peak around the frequency of 0.1 cycles/sec. The relaxation spectrum measured by Faucher[4] with the low-density polyethylene also shows a flat peak at the time scale of 10 sec. This may be regarded wishfully in the same light with the peak of tan δ curve. The dynamic measurements of bire-

fringence offer the curves having more distinct character as can be seen in Figure 13, which shows K', K'' and tan α as a function of frequency. The most important point is that the K'' versus frequency and tan α versus frequency curve have a distinct peak at about 0.1 cycles/sec. Stein, Onogi, and

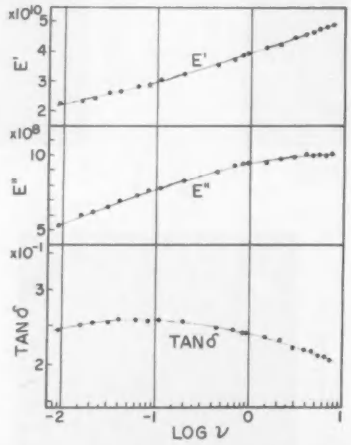

Fig. 12. E', E'', and tan δ versus log ν curves of low-density polyethylene.

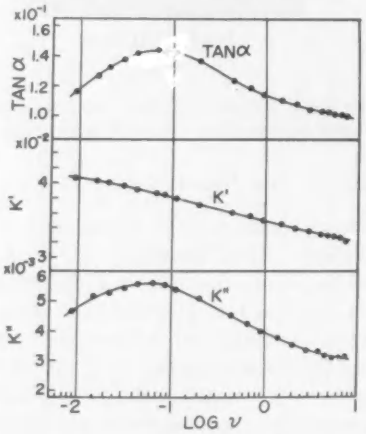

Fig. 13. K', K'', and tan α versus log ν curves of low-density polyethylene.

Keedy[2,3] suggested preliminarily by their measurement of K' that the dispersion might happen at this frequency, but the measurement of K'' and tan α as a function of frequency as shown in Figure 13 seems to authenticate their opinion. The tan β versus frequency curve shown in Figure 14 also suggests the dispersion as happening at the frequency of about 0.1 cycles/sec.

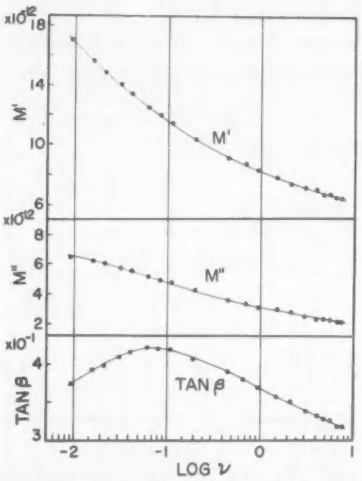

Fig. 14. M', M'', and tan β versus log ν curves of low-density polyethylene.

C. Polypropylene

The strain-optical coefficient of polypropylene is characteristic in the point that it is negative-signed within the region of small strain, as is the case in the present experiment. The observation of Lissajous' figures shows that δ is the greatest and β is the smallest. In this meaning, the relation is the same as that of rubber, but β is not so small as in the case of rubber.

In Figure 15 the relation between δ, α, and β is displayed schematically together with the vectors of stress, strain, and birefringence, and the values of tan δ, tan α, and tan β are given for the reference.

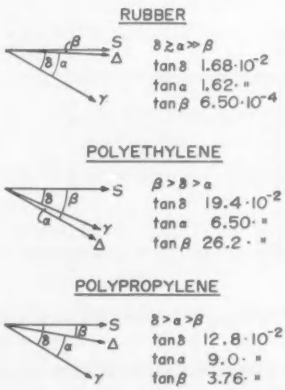

Fig. 15. Vectors of stress, strain, and birefringence, and the relation between angles of phase difference, δ, α, and β. The values of loss tangents are given.

The frequency dependence of E', E'' and tan δ is shown in Figure 16. The tan δ versus frequency curve displays a tendency to increase both towards the higher frequencies and towards the lower frequencies. This

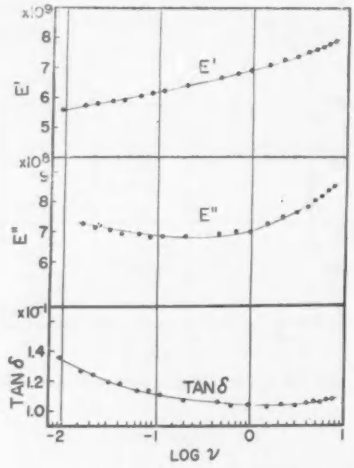

Fig. 16. E', E'', and tan δ versus log ν curves of polypropylene.

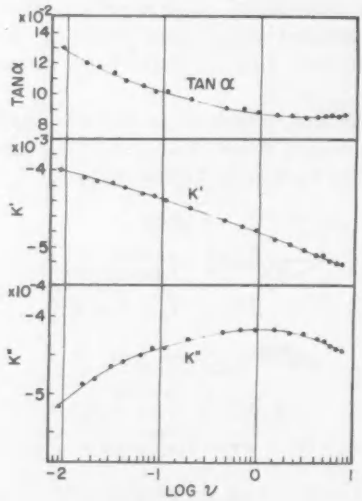

Fig. 17. K', K'', and tan β versus log ν curves of polypropylene.

seems to imply that the dispersions would take place in the regions of both the higher and lower frequencies than those covered by this figure. Figure 17 presents the K', K'', and tan α versus frequency curves. K' and K''

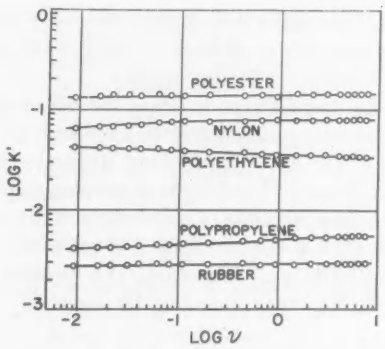

Fig. 18. Log K' versus log ν curves of nylon 6, polyethylene terephthalate, rubber, polyethylene, and polypropylene.

have negative values. The shape of the curve of tan α versus frequency is very similar to that of the tan δ versus frequency curve.

D. Nylon 6 and Polyester

Figure 18 presents the plots of log K' versus log ν of nylon 6 and polyethylene terephthalate, together with those of rubber, polyethylene, and polypropylene. In each case the dependence of K' upon frequency is not noticeable in the region of frequencies covered by this experiment. This is the case also with the frequency dependence of E'.

Discussion

With reference to the frequency dependence of birefringence and loss tangent three types of response of high polymers to vibration are distinguished.

(*1*) As can be seen with rubber, K' is positive and dependent only little upon the frequency. The stress and birefringence are almost the same in phase, and tan β is extremely small.

(*2*) A distinct dispersion is observed within the limit of frequencies covered by this experiment. Both the tan α versus frequency curve and tan β versus frequency curve show a peak almost at the same frequency. The birefringence is far behind the strain. This is the case with low-density polyethylene.

(*3*) As represented by polypropylene K' is negative, and the absolute value increases with the increase in frequency. The phase of strain is behind those of stress and birefringence.

The first type of response is characteristic of the rubber state. The specimen of rubber employed in this study behaves as a material having the ideal rubber elasticity at the ordinary temperatures, and birefringence arises mainly from the orientation of molecules to the direction of stretching, and should be almost independent of the frequency at lower frequencies covered

by this experiment. Since the deformation is mostly elastic, not only the phase difference between stress and strain, but also the phase difference between stress and birefringence is very small.

The response of the second type involves the deformation characterized by the relaxation time comparable with the time scale of the present experiment; that is 10^{-1} to 10^{2} sec. The distinct dispersion which was revealed very clearly by the dynamic birefringence measurement is related to this mechanism. The relaxation time of orientation of crystallites is naturally shorter by far than that of the orientation of molecules, and is postulated to be the order of 10–100 sec. Therefore, the dispersion as found in this study with polyethylene may possibly be ascribed to the rotation of spherulites.

The value of K' decreases with increasing frequency, and this happens the more distinctly, the greater is the crystallinity and the greater the size of crystallites. The rotation of the spherulites can take place only slowly and, therefore, when the frequency increases, the motion of spherulites can not follow the rapid vibration, and consequently K' decreases. In a word, the orientation of molecules and orientation of spherulites are the response of polyethylene to the external force.

The interpretation of the third type of response as is found in polypropylene is very difficult at present. According to Sasaguri, Hoshino, and Stein,[5] the birefringence which would arise from the deformation of spherulites is negative-signed. Since the relaxation time of the deformation of spherulites is assumed to be longer by far than the time scale of this experiment, the birefringence should be influenced only little by the change in frequency. The K' versus frequency curve of polypropylene would be the arithmetic sum of the negative contribution due to the crystal deformation and the positive contribution arising from the orientation of molecules and that of crystallites.

We postulate that K' is composed of three types of contribution, that is

$$K' = K'_A + K'_D + K'_0$$

where K'_A is the contribution from the orientation of molecules in amorphous domains, K'_D the contribution from the deformation of spherulites and K_0' the contribution from the orientation of crystallites.

In the first type of response (rubber) K' is almost equal to K'_A. In the second type of response (polyethylene), three terms of the right-hand side of the equation have significance, but in the region of frequencies covered by the experiment K'_A and K'_0 are predominant, and in the region of lower frequencies K'_0 would surpass the K'_A. In the third type of response (polypropylene), all the three terms are significant. However, the fact that K' is negative suggests the K_D to be most predominant.

References

1. Onogi, S., D. A. Keedy, and R. S. Stein, *J. Polymer Sci.*, **50**, S15 (1961).
2. Stein, R. S., S. Onogi, and D. A. Keedy, *J. Polymer Sci.*, **57**, 801 (1962).

3. Stein, R. S., S. Onogi, K. Sasaguri, and D. A. Keedy, *J. Appl. Phys.*, **34**, 80 (1963).
4. Faucher, J. A., *Trans. Soc. Rheol.*, **3**, 81 (1959).
5. Sasaguri, K., S. Hoshino, and R. S. Stein, paper presented at the March Meeting at St. Louis of the American Physical Society (1963).

Résumé

Le coefficient optique complexé de déformation, le coefficient optique complexe de tension, le module complexe d'élasticité, la tangente correspondante a l'angle de déphasage entre la tension et l'élongation, et la biréfringence ont été étudiés pour plusieurs hauts polymères a des fréquences variant de 0.001 à 10 cycles/seconde. La dépendance des propriétés optiques dynamiques de la fréquence et de la température sont trés semblables à celles des propriétés mécaniques dynamiques. D'autre part, les propriétés optiques optiques dynamiques montrent des dispersions remarquables dans le domaine de fréquence rapporté. Le comportement optique dynamique de ces trois matériaux est trés caractérisé et tout à fait différent l'un de l'autre. On explique ces différences en considérant que la dépendance de la fréquence varie pour chacun des trois mécanismes de déformation envisagés a savoir l'orientation des molécules dans la région amorphe, la déformation des sphérulites et l'orientation des cristaux.

Zusammenfassung

An einigen Hochpolymeren wurden im Frequenzbereich von 0,001 bis 10 Hertz der komplexe dehnungs-optische Koeffizient, der komplexe spannungs-optische Koeffizient, der komplexe Elastizitätsmodul sowie der entsprechende Verlusttangens des Phasenwinkels zwischen Dehnung, Spannung und Doppelbrechung gemessen. Frequenz- und Temperaturabhängigkeit der dynamisch-optischen Eigenschaften von vulkanisiertem Heveakautschuk sind derjenigen der dynamisch-mechanischen Eigenschaften sehr ähnlich. Andrerseits zeigen die dynamisch-optischen Eigenschaften von Polyäthylen und Polypropylen im obigen Frequenzbereich eine bemerkenswerte Dispersion. Das dynamisch-optische Verhalten dieser drei Stoffe ist recht typisch und in jedem Fall ganz verschiedenartig. Die Unterschiede wurden durch Annahme einer verschiedenen Frequenzabhängigkeit der drei Arten von Deformationsmechanismen, nämlich Molekülorientierung im amorphen Bereich, Sphärolithdeformation und Kristallorientierung, erklärt.

JOURNAL OF POLYMER SCIENCE: PART C NO. 5, PP. 139–152

Dynamic Birefringence of Polyolefins*

K. SASAGURI† and R. S. STEIN, *Polymer Research Institute, University of Massachusetts, Amherst, Massachusetts*

Synopsis

The use of the dynamic birefringence method was extended to the study of the relationship between structural changes and mechanical properties for polyethylene, atactic and isotactic polypropylene, and polybutene-1. The phase angle between birefringence and strain was measured which permitted the resolution of the strain-optical coefficient into real and imaginary parts. The real and imaginary parts of the dynamic relaxation modulus were also measured and compared with the optical data. Results for the crystalline polymers were interpreted in terms of the two-stage mechanism of deformation, involving spherulite deformation followed by internal crystalline reorientation. For the atactic polymer, the viscoelastic flow of amorphous regions contributes to the birefringence. The temperature dependence of birefringence and stress is similar for this mechanism but not for the crystalline contribution.

Introduction

In previous papers, a linear phenomenological theory for time-dependent birefringence was presented and dynamic birefringence data for several polymers were reported.[1–5] The birefringence values for polyethylene, polypropylene, and polybutene-1 were found to be time-dependent, both in experiments in relaxation at constant length, at constant strain rate, and dynamic experiments where the sample is subjected to vibrational strain at varying frequency. All of these experiments were shown to be interrelated through a strain-optical coefficient relaxation spectrum. This spectrum characterizes the distribution of optical response mechanisms of the crystalline polymers which is dependent upon the structure and morphology of the polymer as affected by thermal and mechanical treatment and by the temperature of the experiment. The response has been shown to vary with aging of polypropylene and polybutene-1 samples as influenced by secondary crystallization and crystal structure transitions. This time-dependence of birefringence was related to the characteristic time required for crystal orientation following deformation of the polymer.

A theory of crystal orientation involving spherulite deformation followed by rearrangement of crystals and recrystallization within the deformed

* Supported by grants from the Air Force Office of Scientific Research, the Army Research Office (Durham) and the Petroleum Research Fund, and by a contract with the Office of Naval Research.

† On leave from the Ashai Chemical Company, Japan.

spherulites has been proposed.[4,6,7] Direct microscopic observation of the spherulite deformation has been made and related to changes in the low-angle light scattering pattern.[7] A measurement of the rate of this spherulite deformation process by the laser light scattering technique has been reported.[8] An attempt has been made to relate the predictions of this theory to changes in crystal orientation functions measured by x-ray diffraction.[9] It is useful to interpret the dynamic birefringence in terms of this mechanism.

In this paper, further experiments on the dynamic birefringence of polyolefins in periodic strain, relaxation at constant length, and constant rate of strain experiments are reported. Dynamic mechanical properties are studied simultaneously in periodic strain experiments and their relationship to optical properties is discussed. Phase relationships between stress and strain and birefringence have been measured and are in agreement with predictions of the theory and experimental measurements reported by Yamada, Hayashi, Onogi, and Horio.[10]

Polyethylene Dynamic Birefringence

The time dependent birefringence of polyethylene films was studied at room temperature in vibrational experiments. Strain-optical coefficient for low density quenched, low density annealed, and high density quenched films of polyethylene are shown as a function of frequency in Figure 1. Structural properties of these polymers are listed in Table I, where density was measured by density gradient column, crystallinity by x-ray diffraction, applying Hermanns' method[12,13] and crystallite size from half-width of (110) diffraction.

TABLE I

	Density	Crystallinity, %	Cryst. size, A.
Low density quenched polyethylene	0.911	44.4	78
Low density annealed polyethylene	0.919	47.4	89
High density quenched polyethylene	0.946	66.9	118

The strain-optical coefficient decreases with increasing frequency. This is related to the time dependence of crystal reorientation within the deformed polyethylene spherulites. The spherulite deformation theory indicates that the birefringence change produced by affinely deforming a polyethylene spherulite without any internal crystalline rearrangement would be negative. The fact that a positive birefringence is always observed would indicate that there is sufficient internal crystal mobility within these polyethylene spherulites to allow sufficient change in the crystal orientation with deformation from a *b*-axis radial to a *c*-axis radial state to always produce positive birefringence. That is, if the parameter γ of the spherulite deformation theory which characterizes internal mobility of crystals[4,6] is

sufficiently great, the predicted birefringence-elongation curve will always be positive. This high mobility of polyethylene crystals is associated with the probable ease with which the crystals may deform by means of dislocation migration mechanisms. There has been experimental indication for this in the electron microscopic studies of Geil, demonstrating deformation of polyethylene single crystals.[11]

With increase in degree of crystallinity, crystal size, and density, the crystal dispersion is shifted to lower frequencies indicating a greater relaxation time for the crystal motion. There is also a greater decrease in birefringence with increasing frequency under these conditions.

By measurement of the phase angle between strain and birefringence, it was possible to resolve the dynamic strain-optical coefficient into its real and imaginary parts, K' and K''. This was accomplished for the larger

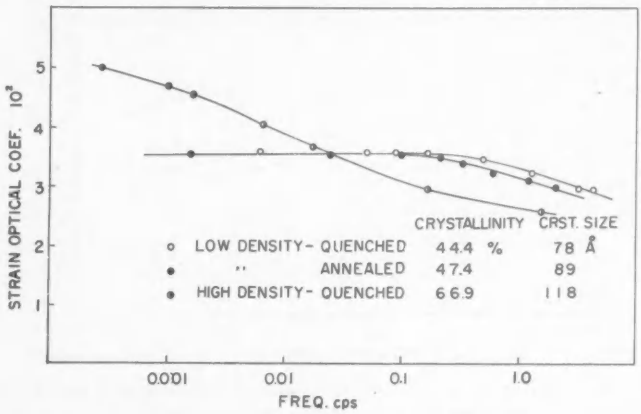

Fig. 1. The variation of the dynamic strain-optical coefficient for 3 types of polyethylene with frequency.

phase differences (with $\tan \alpha > 0.2$), by directly comparing the tracings of strain and birefringence obtained with the two channel Sanborn recorder of the apparatus which has been described.[2] For smaller phase differences, a Lissajous' figure technique was used similar to that employed by Yamada, et al.[10] The strain signal, amplified by the D.C. amplifier of a Ballantine Model 643 VTVM, and the birefringence signal, amplified by a General Radio Model D.C. Electrometer Amplifier, were placed on the X and Y deflecting plates of a Tektronix Model 502 Oscilloscope. With no phase difference, a 45° straight line trace is obtained, while with a finite phase difference, an elliptical figure results. The phase balancing of the two circuits was checked by vibrating a quartz wedge in the optical path where a birefringence signal certain to be in phase with the strain is obtained. This gave the expected 45° straight line.

The phase angle α between birefringence and strain was determined in the conventional fashion from the Lissajous' figure by the equation

$$\sin \alpha = \pm (A^*/A_0) \tag{1}$$

where A_0 is the maximum amplitude of the oscilloscope trace in a particular direction (say the x direction) and A^* is the intercept of the Lissajous' figure with the coordinate axis in this direction.

The real and imaginary parts of the complex strain-optical coefficient K^* (ratio of maximum birefringence to maximum strain) may be obtained by

$$K' = K^* \cos \alpha \tag{2}$$

and

$$K'' = K^* \sin \alpha \tag{3}$$

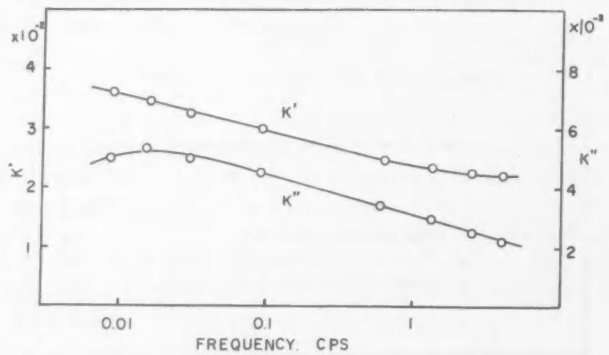

Fig. 2. The variation of the dynamic strain-optical coefficient of a medium density quenched polyethylene with frequency at 20°C.

A plot of the variation of the real and imaginary parts of the strain-optical coefficient with frequency is given in Figure 2 for a quenched medium-density polyethylene film at 20°C. It is seen that the imaginary component exhibits a maximum in the region where the real component is decreasing with frequency as predicted by the phenomenological theory.

For comparison, the real and imaginary components of the complex dynamic modulus were determined on the same sample with the same apparatus over the same frequency range. A stress measuring device consisting of a Schaevitz TDC-4M miniature dynamometer is placed in series with the upper clamp. This was excited by a 10 K.C. carrier signal which was amplified by a Ballantine Model 643 amplifier demodulated with a solid state diode circuit and compared with the strain signal using the Lissajous' figure technique on the oscilloscope. Phase balance was checked by determining whether a 0° phase difference was obtained when a spring was connected between the clamps. The real and imaginary modulus was

calculated from the ratio of the magnitude of the stress and strain and the phase difference was obtained by conventional techniques.

The real and imaginary moduli are plotted in Figure 3 for the same sample as in Figure 2. A maximum is seen in E'' at about the same frequency as for K'' but the E'' maximum is lower. It is suggested that the K'' maximum is associated with the time for crystal orientation change within the spherulite involving both the motion of crystals within the amorphous matrix as well as changes within the crystals themselves involving plastic flow, defect migration, and recrystallization. These changes apparently affect the birefringence more then they do the stress, resulting in the higher K'' maximum.

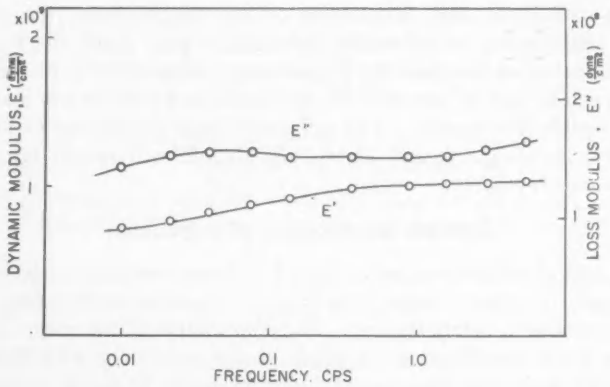

Fig. 3. Dynamic modulus and loss modulus-frequency plots for low density polyethylene quenched film at 20°C.

It is also seen that while K'' falls off at higher frequencies, E'' does not and appears to be increasing toward a second high frequency maximum. This second maximum is likely to be associated with motion in amorphous or disordered regions. The strain-optical coefficient for amorphous regions is known to be less than that associated with crystal orientation.

These experiments may be interpreted in terms of the phenomenological theory of dynamic birefringence[2,3] in terms of which

$$K' = \int_{-\infty}^{\infty} \frac{A_0(\ln \tau)\omega^2\tau^2 + B_0 (\ln \tau)}{1 + \omega^2\tau^2} d \ln \tau \tag{4}$$

$$K'' = \int_{-\infty}^{\infty} \frac{[A_0(\ln \tau) - B_0 (\ln \tau)]\omega\tau}{1 + \omega^2\tau^2} d \ln \tau \tag{5}$$

$$K^* = K' + iK'' \tag{6}$$

$$K(\omega) = |K^*| = [(K')^2 + (K'')^2]^{1/2} \tag{7}$$

$$\tan \alpha = K''/K' \tag{8}$$

The determination of the variation of $B_0(\ln \tau) - A_9(\ln \tau)$ with $\ln \tau$ has been discussed. This may be approximated by

$$A_0(\ln \tau) - B_0(\ln \tau) = \left(\frac{\partial[K(\omega) \cos \alpha]}{\partial \ln \omega}\right)_{\omega=1/\tau} \tag{9}$$

By this technique, it was shown that for polyethylene, $B_0(\ln \tau) > A_0(\ln \tau)$ over the entire range of measurements. A_0 $(\ln \tau)$ is the strain-optical coefficient associated with the elastic response while $B_0(\ln \tau)$ is that associated with viscous processes. In the case of polyethylene, it was concluded that the positive viscous birefringence contributed by the *c*-axis orientation of crystals upon stretching is greater than the elastic contribution arising from amorphous chain orientation and spherulite deformation. It is conceivable that at sufficiently high frequencies or low temperatures, the negative elastic contribution for spherulite deformation may dominate, but there is no indication of this over the present range of measurements. Since $B_0 \gg A_0$, both K' and K'' are positive, giving rise to a positive tan α and over the accessible frequencies. If at sufficiently high frequencies or low temperatures, A_0 is negative and $A_0\omega^2\tau^2 > B_0$, then K' will reverse sign and tan α will become negative.

Dynamic Birefringence of Polybutene

The optical behavior of polybutene-1 was reported previously.[4,14] The birefringence of polybutene-1 film becomes negative on stretching due to *b*-axis orientation before necking. The deformation of the spherulites containing stable modification-I crystals occurs elastically with little reorganization leading to negative total birefringence. Dynamic birefringence of polybutene-1 has been shown to be independent of frequency over the range of 0.01–10 cycles/sec. and is negative.[4]

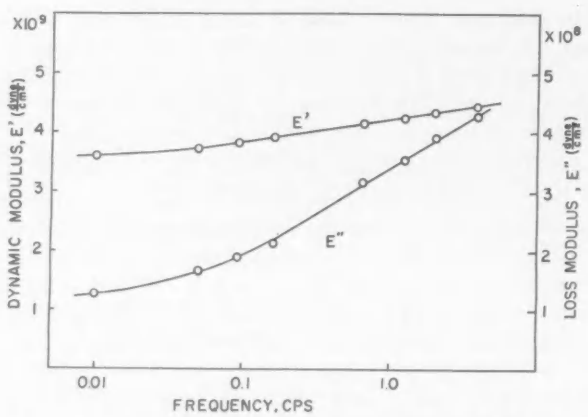

Fig. 4. The variation of dynamic modulus and loss modulus of polybutene-1 with frequency at 20°C.

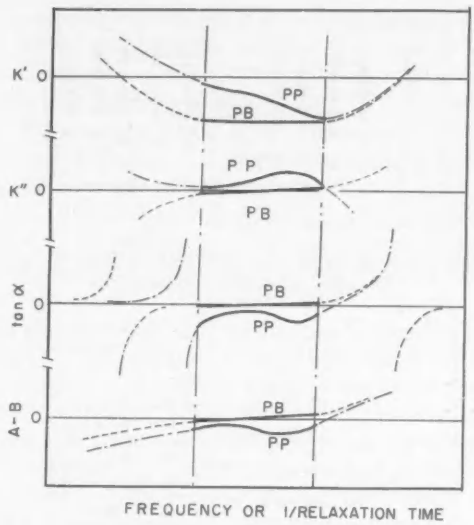

Fig. 5. A postulated variation of $(A_0 - B_0)$ with linear τ and of K', K'', and tan α with log $(1/\omega)$ for aged isotactic polybutene-1 and polypropylene.

In Figure 4 dynamic modulus E' and loss modulus E'' for polybutene-1 measured at 20°C. are plotted against frequency. Increases in both the dynamic modulus and the loss modulus with frequency are observed. These changes may be related to the so-called β-transition which is located in the neighborhood of -10°C.[15] and associated with motion of amorphous regions. The mechanical loss occurring in these regions of negligible change in dynamic birefringence indicates again that the amorphous transitions affect modulus much more than birefringence.

For this polymer there are no mechanisms having an appreciable strain-optical coefficient for which there is a relaxation time corresponding to $(1/\omega)$ over the range of frequencies of the measurement. The measured negative strain-optical coefficient is for the elastic mechanism of spherulite deformation which has a relaxation time $\tau_a < 0.01$ sec. for aged polybutene-1. The relaxation time for internal crystal rearrangement, $\tau_a > 10^4$ sec.: Consequently, the spectrum of $(B_0 - A_0)$ might appear as in Figure 5 together with the accompanying values of K', K'', and tan α. This figure will also be referred to in discussing the optical properties of the other polymers.

Dynamic Birefringence of Isotactic Polypropylene

The variation of birefringence of isotactic polypropylene during extension, relaxation at constant length, retraction, and during vibrational experiments has been reported.[4] These results are consistent with a two-stage deformation process involving first, the elastic deformation of the spherulites contributing a negative birefringence, followed by a viscoelastic

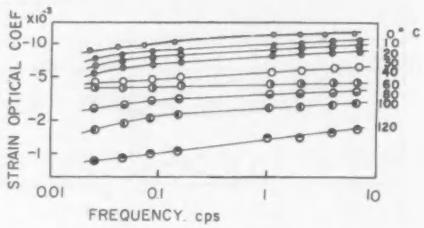

Fig. 6. The variation of strain-optical coefficient or isotactic polypropylene with frequency at various temperatures.

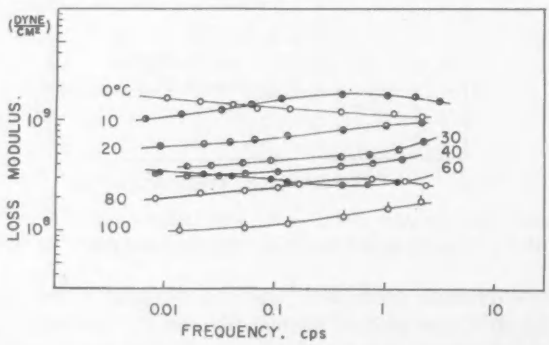

Fig. 7. Frequency dependency of loss modulus of isotactic polypropylene at various temperatures.

rearrangement of the crystals within the spherulites making a positive birefringence contribution. Relaxation at constant length involves an increase in birefringence with time which has been associated with an increasing positive contribution resulting from the viscoelastic intra-spherulitic rearrangement. The birefringence initially increases on retraction as a result of the decreasing negative elastic contribution, and then decreases as a result of the decreasing positive contribution from internal crystal orientation. The strain-optical coefficient in vibrational experiments is negative since the negative elastic deformation contribution predominates at the small strains involved. It becomes less negative with decreasing frequency, however, because of the increasing positive contribution from the intraspherulitic rearrangement which is only seen at longer times. This frequency dependence was found to be greater for aged samples and at lower temperatures where the internal mobility of the crystals is less.

This temperature dependence is seen in the strain-optical coefficient data in Figure 6 where the strain-optical coefficient of an aged isotactic polypropylene sample is plotted against frequency at a number of temperatures. The coefficient is seen to be negative at all temperatures and is more temperature dependent at the lower temperatures. The curves are not super-

posable. The temperature dependence is not uniform but is greater in the interval of 20°–40°C. indicating the presence of an optical loss maximum in this region. This is also seen in the room temperature measurements of Yamada, et al.[10] which exhibit a negative K' which decreases with increasing frequency and a K'' maximum at about 1 cycle/sec. The strain-optical coefficient appears to be again changing greatly with temperature at temperatures in the region of 100–120°C. or greater.

The mechanical dynamic loss modulus E'' for this polymer is plotted in Figure 7 for this range of temperature. The loss maxima shift toward higher frequencies with increasing temperature. Loss maxima are seen in the region of 1 cycle/sec. at 10°C. and at about 90°C. The lower temperature maximum has been associated with the onset of micro-Brownian motion of amorphous chains,[14–16] and has been shown to decrease in intensity with decreasing atactic content.[15] It is likely that the contribution of crystal orientation to the strain-optical coefficient is much greater than that of amorphous orientation in this region, so that the effect of this amorphous transition on the optical properties is believed to take place through the effect of these amorphous regions on the ability of the crystals to orient. That is, the effective viscosity of the amorphous regions for crystal orientational motion is changing in this region.

The optical behavior of isotactic polypropylene may be understood in terms of Figure 5. The relaxation time for crystal rearrangement is shorter for isotactic polypropylene than for polybutene-1 so that the frequency at which the optical dispersion for this process occurs is within the range of normal measurements. Consequently, the increase in negative K' with increasing frequency arises from this higher relaxation time mechanism and leads to a negative tan α. It is conceivable that at larger relaxation times and higher temperatures, K' will reverse in sign and become positive and tan α will go to $-\infty$ and then reverse to $+\infty$ as α goes through 90° as will be seen for atactic polypropylene. Thus far this has not been observed for isotactic polypropylene.

The higher-temperature mechanical loss maximum is associated with the onset of motion within crystals[16,17] and is found to increase in intensity with decreasing atactic content.[15] It seems possible that such motion enables crystal orientation to occur through plastic deformation involving motion of chains within the crystal with respect to each other.

Dynamic Birefringence of Atactic Polypropylene

Atactic polypropylene samples obtained by elution fractionation were used, which were considered to contain 3–5% soluble low molecular weight crystalline species. If this atactic film is stretched and held at constant length, birefringence decays rapidly to a positive value at a low temperature and to a negative value at a higher temperature as shown in Figure 8. At a much higher temperature, birefringence is initially negative and decays to a much more negative value.

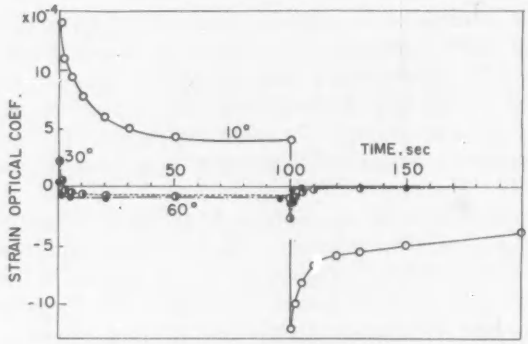

Fig. 8. Birefringence relaxation and recovery curves for atactic polypropylene.

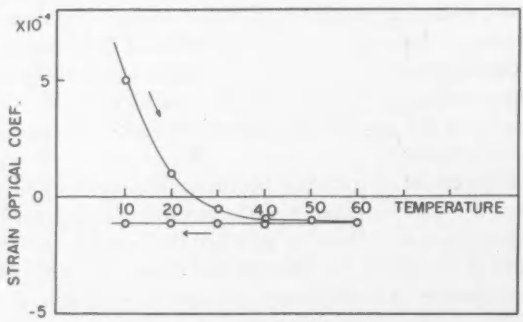

Fig. 9. Temperature dependency of equilibrium birefringence of atactic polypropylene.

If the load is removed after the birefringence has leveled off, the birefringence decreases instantaneously to a negative value and then increases rapidly towards zero. Similar results were observed by Tsvetkov and his coworkers for atactic polypropylene fraction.[18] He attributed this negative birefringence to a small amount of isotactic species in the atactic polypropylene, which cannot be revealed by x-ray. This might be reasonable also in our case because small amounts of isotactic polypropylene in atactic polypropylene can be detected by infrared spectra.[19]

Thus the initial positive birefringence is caused by amorphous chain orientation, and birefringence decays with the relaxation of amorphous chains with time. In addition to this amorphous relaxation, orientation of microcrystallites formed by small amounts of isotactic polypropylene species probably leads to negative equilibrium birefringence.

This equilibrium birefringence was studied further by heating and cooling the sample at a constant length and measuring birefringence changes. This equilibrium birefringence is decreased to a negative value by heating the sample at constant length to 60°C. On cooling, birefringence of the sample is observed to be constant (Fig. 9). This result indicates that this

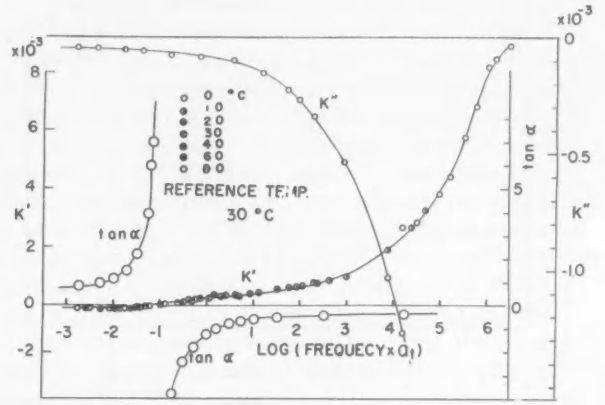

Fig. 10. Master curves of dynamic birefringence K', K'', and tan α of atactic polypropylene plotted against frequency.

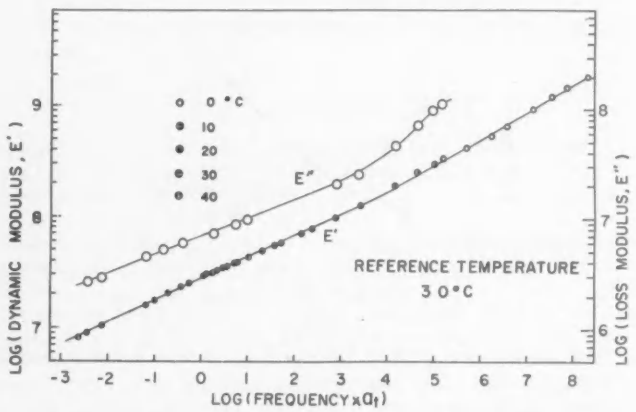

Fig. 11. Master curves of dynamic modulus and loss modulus plotted against frequency

negative birefringence arises from an irreversible process and may be due to microcrystallite orientation in the amorphous medium.

The dynamic birefringence of atactic polypropylene was studied at various temperatures with simultaneous measurements of dynamic stress. The curves obtained were superposed by shifting along the ln τ axis by adding factors ln a_T at each temperature to obtain the master curves which are shown in Figures 10 and 11.

In Figure 10 the dynamic-optical coefficients K' and K'' and the tangent of the phase angle α are plotted against reduced frequency, where the reference temperature is 30°. The imaginary part of the dynamic-optical coefficient K'' is always negative and decreases with increasing frequency. The real part of the dynamic-optical coefficient K' is initially negative at

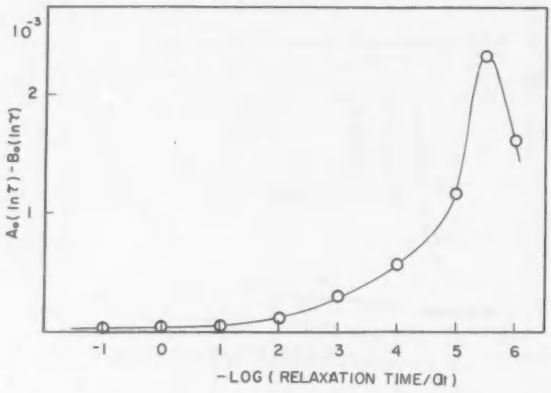

Fig. 12. The calculated reduced strain-optical spectrum for mostly atactic polypropylene. Reference temperature 30°C.

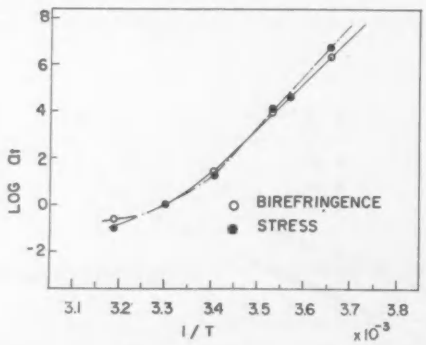

Fig. 13. Shift factors versus $(1/T)$ for birefringence and stress of atactic polypropylene.

low frequency or at high temperature and increases rapidly with frequency. The birefringence is observed to change sign at a frequency which is referred to as the critical frequency.

The relaxation curve at 0°C. shows one optical dispersion which may be the glass transition of the amorphous chains. The tangent of the phase angle α is initially negative at low frequency or at high temperature and increases to infinity at the critical frequency. Above this critical frequency, tan α changes sign and increases from negative infinity. This behavior may be understood in terms of the optical relaxation time distribution for this polymer shown in Figure 12 which has been calculated from the experimental data. The broad optical relaxation time distribution is that associated with the viscoelastic flow of the amorphous chains and is similar to the mechanical relaxation spectrum for linear amorphous polymers.[20] It has been shown[21] that the birefringence and stress should be proportioned in the

rubbery region for such viscoelastic flow. The strain-optical coefficient is positive for this orientation of amorphous polypropylene chains.

The reversal in sign of birefringence at long times or low frequencies is a consequence of a long relaxation time mechanism with a negative strain-optical coefficient which, as indicated before, is associated with the negative orientation of microcrystalline structure contributing negatively to B_0 but not appreciably to A_0. When the real part of the strain-optical coefficient changes sign and goes through zero, it is apparent from eq. (5) that tan α will pass through infinity. This "maximum" in tan α does not signify any molecular loss mechanism at this frequency but is merely an accident of the difference in sign of birefringence of competing mechanisms.

The temperature dependence of both the birefringence and the stress of atactic polypropylene may be expressed in terms of the variation of the shift factors a_T required to produce superposition in Figures 10 and 11 with temperature. A plot of log a_T against $(1/T)$ is given in Figure 13 for stress and for birefringence. The variation is similar for both indicating that the same molecular mechanism is responsible for the temperature dependence of both phenomena. This is the approach to a glass transition at the higher frequencies and lower temperatures associated with the loss of motion of the main chains.

References

1. Onogi, S., D. A. Keedy, and R. S. Stein, *J. Polymer Sci.*, **50**, 153 (1961).
2. Stein, R. S., S. Onogi, and D. A. Keedy, *J. Polymer Sci.*, **57**, 301 (1962).
3. Stein, R. S., S. Onogi, K. Sasaguri, and D. A. Keedy, *J. Appl. Phys.*, **34**, 80 (1963).
4. Sasaguri, K., S. Hoshino, and R. S. Stein, Papers presented at American Chemical Society Meeting, Los Angeles, Calif., April, 1963, and at American Physical Soc. Meeting, St. Louis, Mo., March, 1963; *J. Appl. Phys.*, in press.
5. LeGrand, D., and P. Erhardt, *Trans. Soc. Rheol.*, **6**, 301 (1962).
6. Stein, R. S., and K. Sasaguri, ONR Technical Report No. 54, Project: NR 356–378, Contract Nonr 3357(01) Univ. of Mass., Amherst, Mass.
7. Sasaguri, K., M. B. Rhodes, and R. S. Stein, ONR Technical Report No. 62, Project: NR356–378, Contract Nonr 3357(01); *J. Polymer Sci.*, **B1**, 571 (1963).
8. Erhardt, Peter, K. Sasaguri, and R. S. Stein, ONR Technical Report No. 60, Project: NR 356-378 Contract Nonr 3357(01) (1963); *J. Polymer Sci.*, **C5**, 179 (1964).
9. Fugino, K., H. Kawai, T. Oda, and H. Maeda, presented before 4th International Congress on Rheology, Providence, R. I., Aug., 1963, Meeting Abstract, p. 202.
10. Yamada, R., C. Hayashi, S. Onogi, and M. Horio, *J. Polymer Sci.*, **C5**, 123 (1964).
11. Geil, P. H., preprints No. 16, 17, and 18, Research Triangle Institute, Camille Dreyfus Lab., Durham, N. C., July 1963; Submitted for publication to *J. Polymer Sci.*
12. Hermans, P. H., and A. Weidinger, *Makromol. Chem.*, **24**, 44 (1961).
13. Hoshino, S. and K. Sasaguri, ONR Technical Report No. 50 Project: NR 356-378, Contract Nonr 3357(01) (1962).
14. Sasaguri, K., S. Hoshino, and R. S. Stein, ONR Report No. 55, Project NR 356-378, Contract Nonr 3357(01) (1962).
15. Takayanagi, M., *Mem. Fac. Eng. Kyushu Univ.*, **23**, 41 (1963).
16. Sauer, J. A., R. A. Wall, N. Fuschillo, and A. E. Woodward, *J. Appl. Phys.*, **29**, 1355 (1958).

17. Muus, L. T., N. G. McCrumm, and F. C. McGrew, *SPE J.*, **15**, 368 (1958).
18. Tsvetkov, V. N., *J. Polymer Sci.*, **57**, 727 (1962).
19. LeGrand, D. G., private communication.
20. Ferry, J. D., *Viscoelastic Properties of Polymers*, Wiley, New York, 1961.
21. Read, B. E., *Polymer*, **3**, 143 (1962).

Résumé

L'usage de la méthode de biréfringence dynamique a été étendu à l'étude de la relation entre les changements de structure et les propriétés mécaniques pour le polyéthylène, le polypropylène atactique et isotactique et le polybutène-1. L'angle de phase entre la biréfringence et l'élongation est mesuré, ce qui permet la résolution du coefficient optique de l'élongation en parties réelles et imaginaires. Les parties réelles et imaginaires du module de relaxation dynamique ont été mesurées et comparées avec les données optiques. Les résultats pour les polymères cristallins sont interprêtés en termes d'un mécanisme de déformation en deux étapes, comprenant une déformation du sphérulite suivi d'une réorientation cristalline interne. Pour le polymère atactique l'écoulement viscoélastique des régions amorphes contribue à la birèiringence. La dépendance vis-à-vis de la température de la biréfringence et de la tension est semblable pour ce mécanisme, mais pas en ce qui concerne la contribution cristalline.

Zusammenfassung

Die Verwendung der dynamischen Doppelbrechungsmethode wurde auf die Untersuchung der Beziehung zwischen Strukturänderungen und mechanischen Eigenschaften für Polyäthylen, ataktisches und isotaktisches Polypropylen und Polybuten-1 ausgedehut. Der Phasenwinkel zwischen Doppelbrechung und Verformung, der die Trennung des spannungs-optischen Koeffizienten in Real- und Imaginärteil gestattet wurde gemessen. Auch der Real- und Imaginärteil des dynamischen Relaxationsmoduls wurde bestimmt und mit den optischen Daten verglichen. Die Ergebnisse für die kristallinen Polymeren wurden auf Grundlage des Zweistufenmechanismus der Deformation mit Sphärolithdeformation und nachfolgender innerer kristalliner Reorientierung gedeutet. Beim ataktischen Polymeren trägt das viscoelastische Fliessen der amorphen Bereiche zur Doppelbrechung bei. Die Temperaturabhängigkeit der Doppelbrechung und Spannung ist bei diesen Mechanismen ähnlich, nicht aber beim kristallinen Anteil.

JOURNAL OF POLYMER SCIENCE: PART C NO. 5, PP. 153–161

Rheo-Optical Properties of Polymers. X. Relaxation

D. G. LEGRAND and W. R. HAAF, *General Electric Research Laboratory, Schenectady, New York*

Synopsis

Light scattering relaxation in thin strained polyethylene films has been determined. Results for swollen and unswollen films are presented. Concurrent studies of stress relaxation indicate that the mechanism by which relaxation takes place is associated with changes in the average fluctuation in refractive index of the material. The ratio of the change in the fluctuation in refractive index to stress appears to be independent of time.

INTRODUCTION

In previous papers, we have presented data on time dependent studies of light scattering from thin polymer films of polyethylene.[1,2] Due to the necessity of working at large deformations, the results were difficult to interpret. Due to many modifications in the original experimental apparatus, as well as the use of samples prepared under very carefully controlled conditions, which will be described in detail elsewhere,[3] we have been able to obtain more reproducible data which can be discussed in terms of current theories and which elucidates some of the mechanisms by which relaxation takes place in polyethylene.

Experimental

In order to perform relaxation experiments, we use the straining system shown in Figure 1. The sample S is clamped on two blocks D and E, which are caused to move apart via a screw A, which has a left-handed thread at one end and a right-handed one at the other. A Heller thyratron DC motor is connected to the screw A. By connecting the motor control to a timed circuit, the motor can be turned on and off for any period of time between 1 msec. to 10 min. This unit can be placed in the light scattering apparatus either with the stretching axis vertical or horizontal to the scattering plane. A displacement transducer measures the rate of separation of the clamps. Since the sample is deformed from both ends, the center of the sample stays in the same position at all times. The rate of separation of the clamps was measured by the displacement transducer T.

Prior to usage, each sample was examined for microscopic defects and orientation in a polariscope. In order to eliminate surface scattering, a drop of silicone oil was placed on each surface; thin glass microscope cover

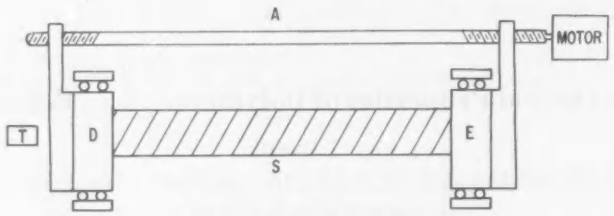

Fig. 1. Straining system.

slides were then placed on top of the silicone oil. With a judicious application of silicone oil, it was found that the presence of the cover slides did not affect the results since reruns on the same samples showed very little change in observed intensity. For samples swollen in various solvents the same procedure was used.

Results and Discussion

For thin polymer films, most of the scattering occurs due to orientation and density fluctuations. Stein and Wilson have considered this in detail for static scattering from unstrained samples, and using the assumption of random orientation fluctuations, arrive at the following expression for vertically polarized incident and scattered light

$$V_v = K\left\{\overline{\eta^2}\int\gamma(r)\frac{\sin hr}{hr}r^2dr + \frac{4}{45}\overline{\delta^2}\int f(r)\left[\frac{\overline{\eta^2}}{\alpha^2}\gamma(r)+1\right]\frac{\sin hr}{hr}r^2dr\right\} \quad (1)$$

where K is an angular independent proportionality constant, α is the mean polarizability per unit volume of the medium, $\overline{\eta^2}$ is the mean-squared difference between the principal polarizabilities of the volume elements (assuming cylindrical symmetry), $h = (4\pi/\lambda)\sin(\theta/2)$, λ is the wavelength of the light in the medium, θ is the scattering angle, and $\gamma(r)$ is a correlation function for fluctuations in the density.[4] For the horizontal component of scattered light using vertically polarized incident, they obtain

$$H_v = K\left\{\overline{\delta^2}\int f(r)\left[\frac{\overline{\eta^2}}{\alpha^2}\gamma(r)+1\right]\frac{\sin hr}{hr}r^2dr\right\} \quad (2)$$

In order to justify the use of the random orientation fluctuation approximation, we show the change in scattering at $\theta' = 6.6°$ and $10°$ as a function of rotation of crossed polars for an unstrained sample in Figure 2. The angle ξ characterized the angle between the polarizer and scattering plane. For a system where this approximation is not valid, a large variation between $0°$ and $45°$ should be seen. The data indicates about a 10% change. Data on other types of polyethylene show changes of approximately 60%.

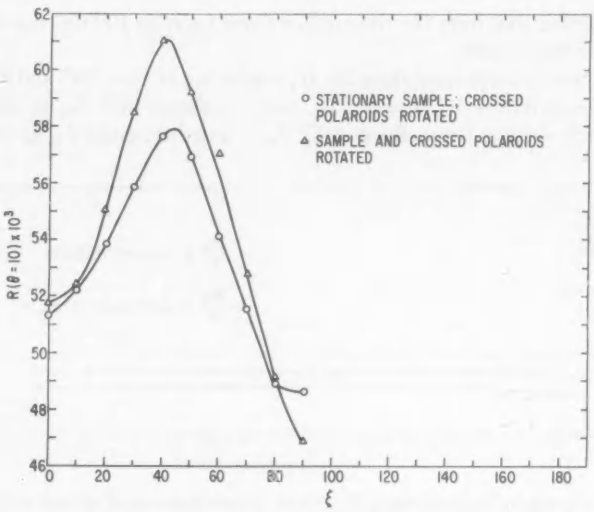

Fig. 2. Change in Rayleigh ratio (H_V) at $\theta = 10°$ as a function of angle ξ.

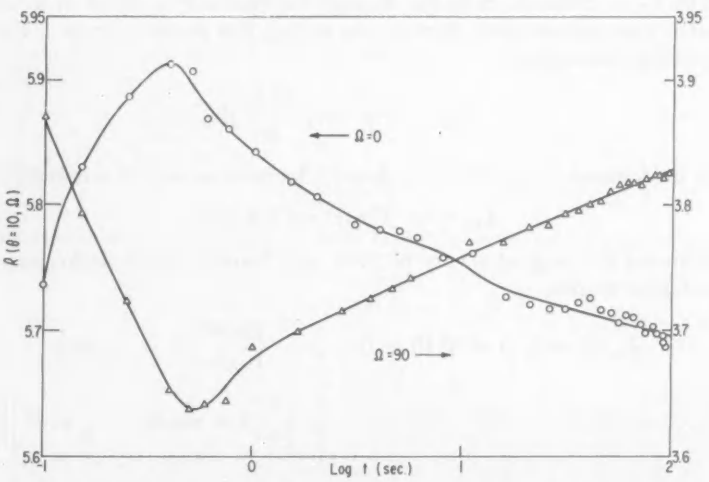

Fig. 3. Change in Rayleigh ratio (V_V) of $\theta = 10°$ as a function of log time at $\Omega = 0$ and $\Omega = 90°$.

Stein has proposed an extension of parts of this theory to explain time dependent phenomena.[5] However, he limits his treatment to only the terms pertaining to orientational fluctuations.

In Figure 3 we present data for the change in the Rayleigh ratio as a function of log time at $\theta = 10°$ for V_v scattering at $\Omega = 0$ (stretching axis perpendicular to scattering plane) and $\Omega = 90°$ (parallel to scattering plane).

It is observed that over the time period from 1 sec. to 100 sec. considerable relaxation takes place.

In Figure 4, we present data for H_v scattering at $\Omega = 90°$ and $\theta = 10°$. The obvious difference between I_{V_v} and I_{H_v} shows that I_{H_v} is associated with much shorter time effects than I_{V_v}. Further, since I_{V_v} is changing

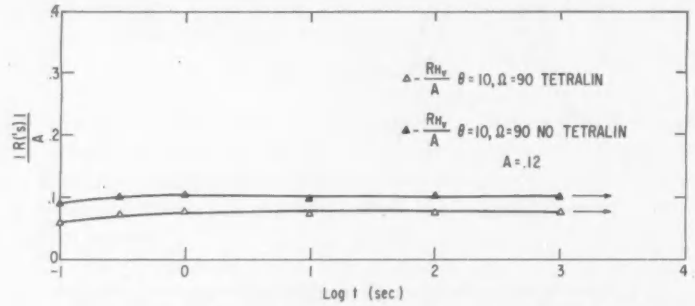

Fig. 4. Change in Rayleigh ratio (H_V) of $\theta = 10°$ as a function of log time at $\Omega = 90°$.

while I_{H_v} is constant, then the changes are primarily a result of density rather than orientational fluctuations during this period of time. Using eq. (1), we then have

$$I_{V_v} = \overline{\eta^2} \int \gamma(r) \frac{\sin hr}{hr} dr \tag{3}$$

For an oriented sample with only density fluctuations, eq. (3) is rewritten as

$$I_{V_v} = \overline{\eta^2} \int \gamma(\mathbf{r}) \cos k(\mathbf{r}\cdot\mathbf{s}) d\mathbf{r} \tag{4}$$

Following the original theory of Stein and Norris,[6] this equation can be evaluated to give

$$I_{V_v}(\Omega = 0, \theta) = \overline{\eta^2}(\Omega = 0) \exp - \left\{\frac{2a^2\pi^2}{\lambda^2}(1 - \cos\theta)\right\} \tag{5}$$

$$I_{V_v}(\Omega = 90, \theta) = \overline{\eta^2}(\Omega = 90) \exp - \left\{\pi^2\left[\frac{a^2}{\lambda^2}(1 - \cos\theta)^2 + \frac{c^2}{\lambda^2}\sin^2\theta\right]\right\} \tag{6}$$

where $\gamma(\mathbf{r})$ has been replaced by an empirical Gaussian function proposed by Stein and Norris

$$\gamma(\mathbf{r}) = \exp - \left\{\left(\frac{x^2}{a^2} + \frac{y^2}{b^2} + \frac{z^2}{c^2}\right)\right\} \tag{7}$$

and Ω is the angle characterizing the relative orientation between the stretching and scattering direction. The parameters a and c specify characteristic correlation distances in the sample perpendicular and parallel to the

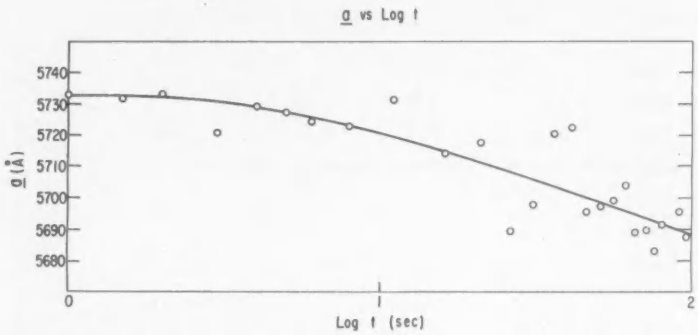

Fig. 5. Change in correlation distance a during relaxation at constant strain as a function of log time.

stretching direction. In order to evaluate a, I_{V_v} data is compared at two θ's for $\Omega = 0$, and a is given by

$$a = \frac{\lambda}{\pi\sqrt{2}}\left[\frac{\ln \dfrac{I_{V_v}(\Omega = 0, \theta_1)}{I_{V_v}(\Omega = 0, \theta_2)}}{\cos\theta_2 - \cos\theta_1}\right]^{1/2} \tag{8}$$

To evaluate c, $I_{V_v}(\Omega = 90)$ at different θ's are used simultaneously with the data from a,

$$c = \left[\frac{\dfrac{\lambda^2}{\pi^2}\ln\dfrac{I_{V_v}(\Omega = 90, \theta_1)}{I_{V_v}(\Omega = 90, \theta_2)} + a^2[(1 - \cos\theta_1)^2 - (1 - \cos\theta_2)^2]}{\sin^2\theta_1 - \sin^2\theta_2}\right]^{1/2} \tag{9}$$

Finally, in order to evaluate $\overline{\eta^2}(\Omega = 0)$ and $\overline{\eta^2}(\Omega = 90)$ use is made of eqs. (5) and (6),

$$\overline{\eta^2}(\Omega = 0) = \frac{R(\theta', \Omega = 0)\,\lambda_0^4}{\pi^2 F_{V_v}(\Omega = 0)} \tag{10}$$

$$\overline{\eta^2}(\Omega = 90) = \frac{R(\theta', \Omega = 90)\,\lambda_0^4}{\pi^2 F_{V_v}(\Omega = 90)} \tag{11}$$

Equations (8–11) were used to evaluate the changes in a, c, and $\overline{\eta^2}$ as a function of time in our experiments. Using data taken from several runs, the change in these parameters is shown in Figures 5–7 as a function of log time. It is of interest to show all the results from the start of an experiment to the end. This is shown in Figure 8 on a linear time basis. These results were obtained at a strain rate of ~55%/sec. and at the strain .03. The following conclusions can be drawn. During the straining a decreases while $\overline{\eta^2}(\Omega = 0)$ increases and simultaneously c increases while $\overline{\eta^2}(\Omega = 90)$ decreases, thus accounting for the behavior of the Rayleigh ratio. However, during the subsequent relaxation, a continues to decrease while $\overline{\eta^2}$

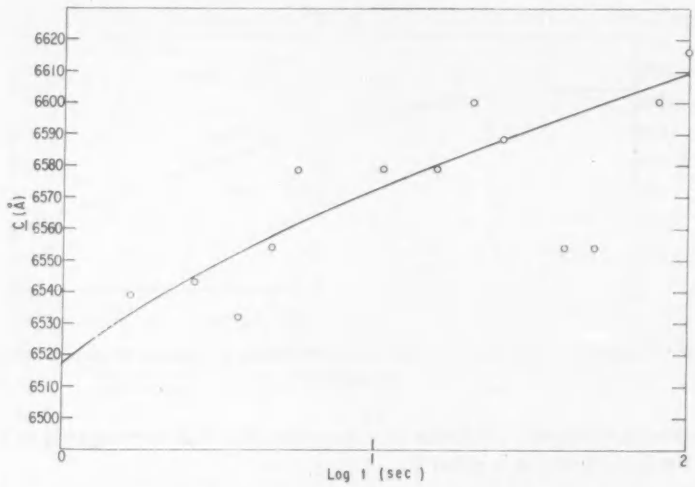

Fig. 6. Change in correlation distance c during relaxation at constant strain as a function of log time.

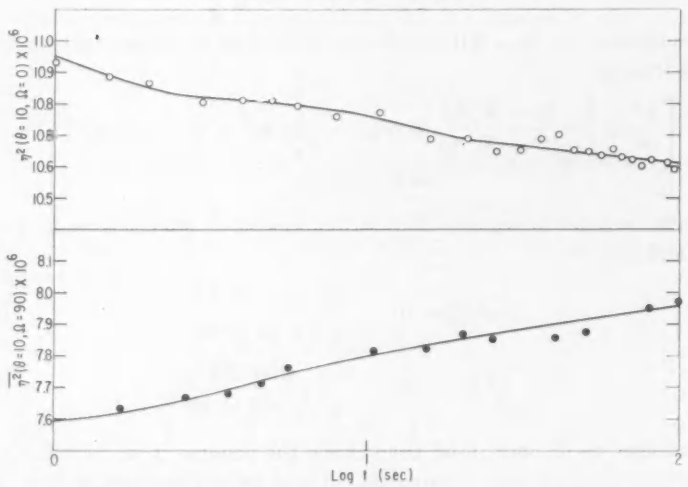

Fig. 7. Change in $\overline{\eta^2}$ at $\Omega = 0$ and $\Omega = 90$ during relaxation at constant strain as a function of log time.

($\Omega = 0$) decreases and similarly c increases while $\overline{\eta^2}$ increases. It would thus appear that the major cause for the change during a relaxation experiment is connected with the $\overline{\eta^2}$ term in eqs. (8) and (9). Also the final state of the sample after relaxation gives approximately the same results as noted by Stein and Norris, i.e., a general decrease in the scattering level for

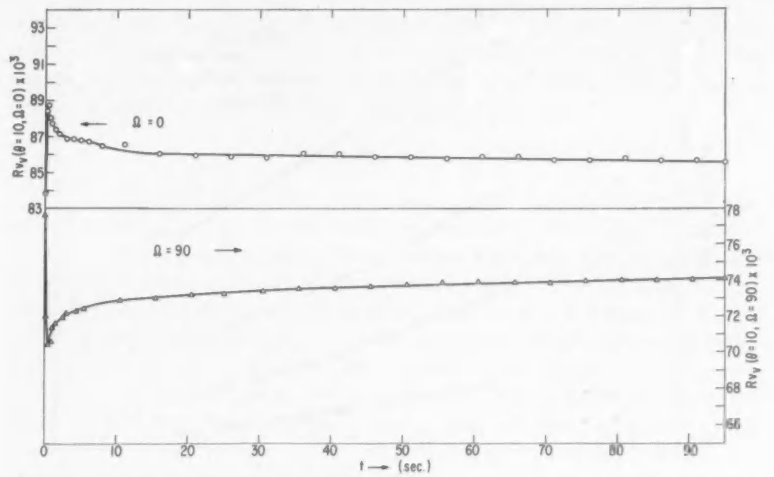

Fig. 8. Change in Rayleigh ratio (V_V) at $\Omega = 0$ and $\Omega = 90$ from beginning to end of experiment on linear time scale.

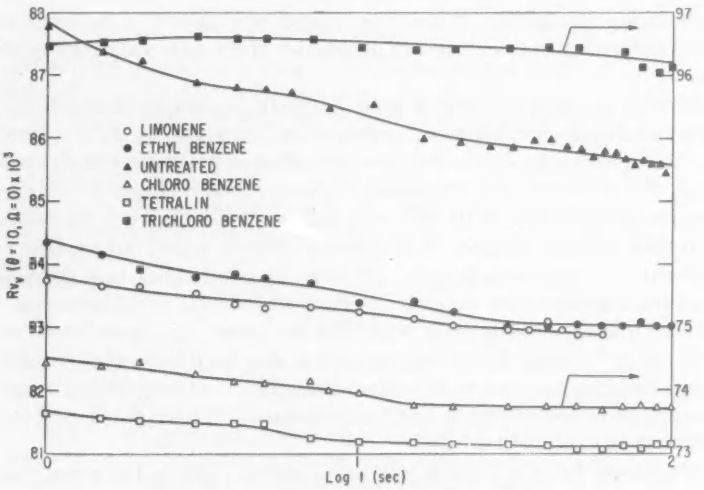

Fig. 9. Effect of swelling with various solvents on Rayleigh ratios during relaxation experiments.

I_{V_0} at $\Omega = 0$, $\Omega = 90$.[6] The magnitudes of the changes are also in accord with the findings of Stein and Norris.[6] Several explanations can be put forth to explain the change in $\overline{\eta^2}$, which we have found.

It may be due to: (*1*) voids in the sample; (*2*) fluctuations in refractive index between crystalline and amorphous material; (*3*) melting of crystalline material during stretching with recrystallization and orientation taking

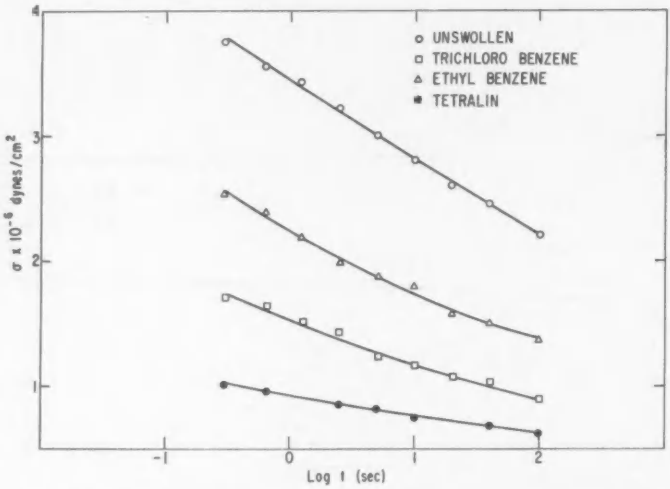

Fig. 10. Stress relaxation curves for swollen and unswollen samples.

place during relaxation; (*4*) rearrangement of crystals within the spherulite; or (*5*) differences in orientation of aggregates of crystals within the spherulite.

In order to eliminate some of these possibilities, samples were swollen in various solvents varying in refractive index from 1.46 to 1.56. Since it has been previously shown that the solvent does not enter the crystalline areas, the swelling must take place in the amorphous material.[7] A general decrease in scattering of 10–20% was observed. In Figure 9, we compare relaxation data for samples at the same scattering angle, but swollen with different solvents (as indicated). It must be pointed out that depending upon the angular region which is observed, the effect of swelling varies. It is found that as noted by Stein et al., that the lower angles are affected more by swelling.[7] Thus, in the angular region discussed here, the correlation size parameter appears to decrease on swelling. During the subsequent straining, a increases slightly and then decreases. This is due in part to the fact that the sample deswells.

A separate series of experiments were done to measure the stress relaxation in unswollen and swollen samples. The results of these experiments are shown in Figure 10. From the data, it is obvious that although the same strain rates and final strain were approximately equivalent, the stress is not the same. This effect is caused by nonequivalent swelling ratios and different degrees of plasticization of the swelling liquid. However, in general, it appears that swelling does cause faster relaxation. Another effect noted was an increase of stress around 100 sec. which appeared to be caused by deswelling of the samples, since, as the solvent is removed, the sample contracts. Thus, if the rate of contraction is faster than the stress

relaxation, then the stress will increase. Finally, a comparison of $\bar{\eta}^2$ and stress as a function of time for unswollen samples shows them to behave in a similar manner, and in fact, the ratio of these quantities is independent of time, similar to the stress optical coefficient in rubbers.

Conclusions

It was suggested previously that when a film of polyethylene was deformed uniaxially, that the crystallites would both rotate and translate.[2] Evidence has been previously offered which indicated that orientational relaxation times of crystallites are approximately .032 sec.[8] Our current data suggests that after the orientation of the crystals has stopped, that a subsequent translational motion of both crystalline and amorphous material takes place from approximately 1 sec. to more than 100 sec. This motion is in some way related on a molecular scale to the simultaneous relaxation of stress which occurs within the material as indicated by the constancy of the Rayleigh scattering optical coefficient in this region of time. Finally, the data shows that long-time relaxation in this material occurs over very large distances and is related to the mobility of the crystalline and amorphous material.

References

1. Erhardt, P. F., and D. G. LeGrand, *J. Polymer Sci.*, **62**, 547 (1962).
2. Erhardt, P. F., and D. G. LeGrand, *J. Appl. Phys.*, **34**, 68 (1963).
3. Erhardt, P. F., D. G. LeGrand, and R. S. Stein, unpublished results.
4. Wilson, P. and R. S. Stein, *J. Appl. Phys.*, **33**, 1914 (1961).
5. Stein, R. S., *J. Polymer Sci.*, **62**, 52 (1961).
6. Norris, F. and R. S. Stein, *J. Polymer Sci.*, **27**, 87 (1958).
7. Stein, R. S., "Morphology of Crystalline Aggregates in Polyethylene" in *Growth and Perfection of Crystals*, R. H. Doremus, B. W. Roberts, and D. Turnbull, eds., Wiley, New York, 1950, p. 549.
8. Erhardt, P. F. and D. G. LeGrand, *Trans. Soc. Rheol.*, **6**, 301 (1962).

Résumé

On a déterminé la relaxation de la lumière diffusée dans des films minces de polyéthylène sous tension. Des résultats pour des films gonflés et nongonflés ont été présentés. Des études simultanées de relaxation de tension montrent que le mécanisme par lequel a lieu la relaxation est associé à des changements dans la fluctuation moyenne de l'indice de réfraction du produit. Le rapport entre le changement de la fluctuation de l'indice de réfraction et la tension semble être indépendant du temps.

Zusammenfassung

Die Lichstreuungsrelaxation in dünnen gedehnten Polyäthylenfilmen wurde bestimmt. Ergebnisse an gequollenen und ungequollenen Filmen werden vorgelegt. Eine gleichzeitig durchgeführte Untersuchung der Spannungsrelaxation zeigt, dass der Relaxationsmechanismus mit einer Änderung der mittleren Brechungsindexschwankung des Materials verknupft ist. Das Verhältnis der Änderung der Brechungsindexschwankung zur Spannung scheint von der Zeit unabhängig zu sein.

JOURNAL OF POLYMER SCIENCE: PART C NO. 5, PP. 163–177

Morphological and Rheological Studies of Polyethylene by Light Scattering

ROBERT S. MOORE and SHIRO MATSUOKA, *Bell Telephone Laboratories, Incorporated, Murray Hill, New Jersey*

Synopsis

The technique of photographic light scattering was employed to study films of medium and high molecular weight linear polyethylene. Results on the high molecular weight polymer show that secondary crystallization is severely restricted, that oxidation induces further crystallization, and that annealing may lead to tilted chain lamellae. Results of experiments conducted on films of the medium molecular weight polymer while subjected to tensile stress indicate that spherulite deformation occurs at very small strains in agreement with proposed theories.

Introduction

The technique of photographic light scattering[1–4] has been shown to be an excellent method for observing differences in the structure of polyethylene spherulites. Modification of this technique has permitted us to obtain light scattering patterns from films subjected to tensile stress as well as scattering patterns from undeformed films. During these experiments it was found that scattering was not readily observed from films of very high molecular weight linear polyethylene whereas the usual scattering patterns were observed from films of lower molecular weight. Because this meant that crystallization was restricted in the high molecular weight polyethylene further studies were carried out by the technique of photographic light scattering. This paper presents the results of these studies as well as an interpretation of the light scattering measurements and the mechanical behavior of a sample of lower molecular weight polyethylene subjected to tensile stress.

Experimental

Some of the characteristics of the materials used in these experiments are listed in Table I. As can be seen from the table both the medium molecular weight linear polyethylene, MMWL (Philips Petroleum Co.) and the high molecular weight linear polyethylene, HMWL (Allied Chemical Co.) were extremely linear with fewer than three methyl groups/1,000 carbon atoms. The values of the density and x-ray degree of crystallinity of the HMWL polyethylene correspond to the values observed in a branched polyethylene

TABLE I

Polymer	Density,[a] g./cc.	X-ray % crystallinity	Melting point, °C.	CH_3/100 C[b]	Weight-average molecular weight
DYNH (Union Carbide Co.)	0.932	65	112.0	2.4	4×10^5
Marlex 6000-60 (Philips Pet. Co.)	0.960	80	137.5	<0.3	4×10^4
ACX Lot 13 (Allied Chem. Co.)	0.933	67	138.5	<0.3	$>10^6$

[a] As determined at room temperature.[5,6]

[b] Methyl groups/100 carbon atoms.[6]

of medium molecular weight with about 24 methyl groups/1,000 carbon atoms.

In these experiments a pulsed optical maser with a 90° oriented ruby crystal was used as the source of coherent, collimated, plane-polarized light (6943 A.) (see Fig. 1). The emitted energy ranged from 0.2 to 0.5 joules and the pulse duration was about 0.5 msec. The beam from the 5 by 0.6 cm. ruby rod was passed through the circular aperture to remove uncollimated fluorescent radiation and onto the vertically mounted sample. The scattered radiation was transmitted to the photographic film (ASA speed 400) via the analyzer whose plane of polarization was kept either parallel or perpendicular to the horizontal plane of polarization of the incident beam. The sample to film distance ranged from 12–39 cm. for these experiments. Those samples subjected to tensile stress were held in the tensile creep apparatus shown schematically in Figure 1. This consisted of a platform with two vertical rods to which were mounted two horizontal cross bars, the upper of which was clamped. The lower bar was mounted on two linear movement bearings by means of which the bar moved with slight friction on the vertical rods. As shown in Figure 1 a weight could be attached to vary the sample stress. The sample, of nominal dimensions 7.6 by 0.76 by 0.005–0.02 cm., was clamped at the upper and lower ends between the bars. The lower bar was held on a

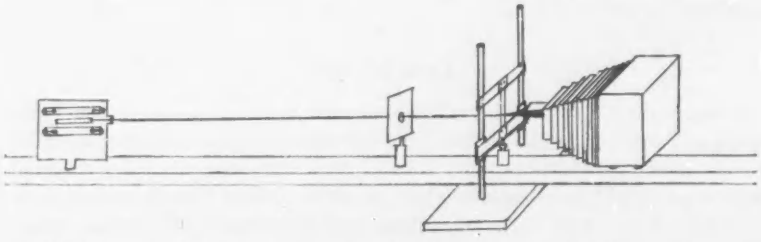

Fig. 1. Light scattering apparatus showing the light source, the defining aperture, the tensile creep apparatus, and the camera bellows.

platform which could be rapidly lowered to start the experiment. Not shown in Figure 1 is a direct current differential transducer by means of which sample elongation was recorded on a strip chart recorder. For static experiments the creep apparatus was replaced by a holding frame to which were attached samples melted between cover slides to reduce surface scattering. For both types of experiments samples of the MMWL polyethylene were prepared from films molded at 160°C., while samples of the HMWL polyethylene were prepared from films molded at 190°C. between sheets of polyethylene terephthalate to facilitate release. Samples for the static experiments were melted between cover slides at 260°C. for 20 sec. and quenched to room temperature on a metal block. These samples were subsequently annealed under various conditions as described in the next section.

Results

Shown in Figure 2 are the scattering patterns from a quenched MMWL polyethylene sample and the scattering patterns from a quenched HMWL polyethylene sample after it had been annealed at 125°C. for 90 min. For the MMWL sample the pattern observed with parallel polarizers is elon-

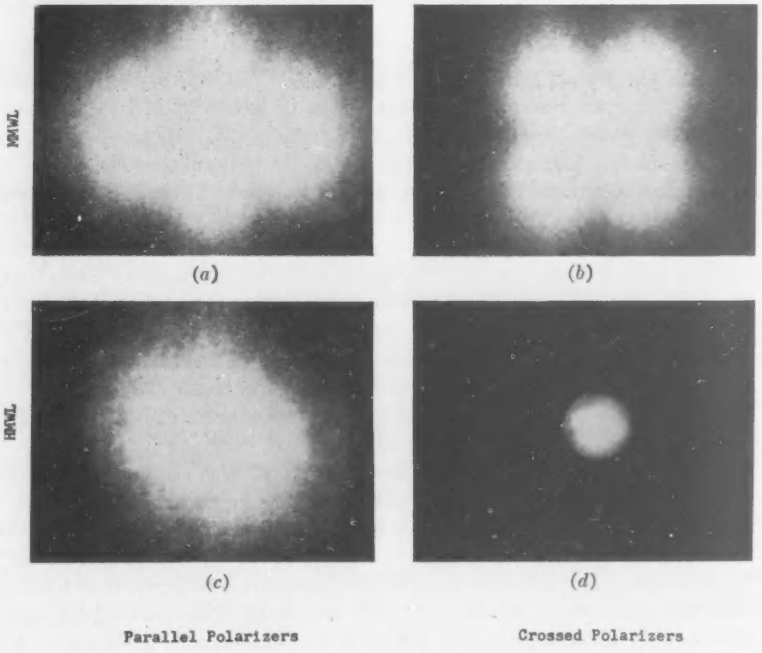

Fig. 2. Scattering patterns from (*a,b*) quenched MMWL polyethylene and (*c,d*) annealed HMWL polyethylene.

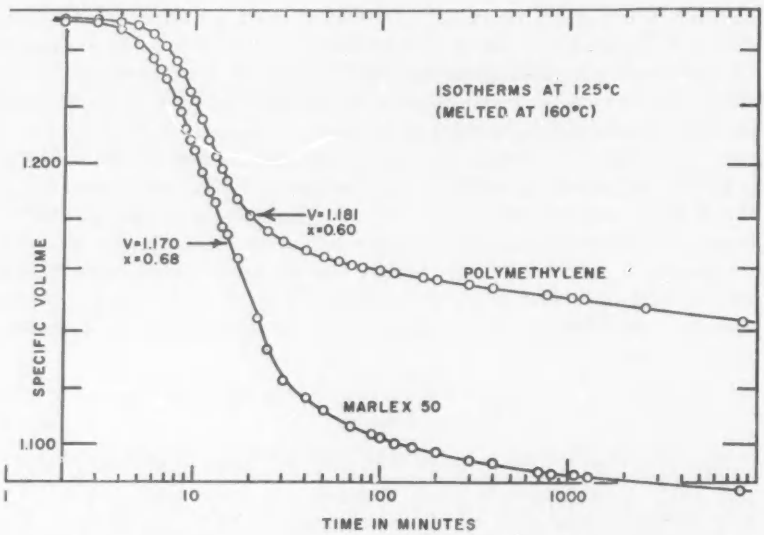

Fig. 3. Dilatometric measurements of the time dependence of the specific volume of two polyethylenes at 125°C. The arrows indicate the calculated time for spherulite impingement.

gated in the direction of polarization, while the pattern observed with crossed polarizers resembles a clover leaf with leaves at 45° to the horizontal and vertical axes, as observed previously.[2] The distance to one of the maxima is related to the average size of the spherulites,[2] the radius of the average spherulite being about 5.0 μ as determined from this scattering pattern.

During the primary stage of crystallization of spherulitic polymers the lamellar fibrils branch out from the center until they impinge on fibrils from other growing spherulites.[7] After this the secondary stage of crystallization predominates and the degree of crystallinity continues to increase.[8] The latter phenomenon has been attributed to crystallization of the material between fibrils[7] and to thickening and perfection of the fibrils themselves.[9,10] In polyethylene the c or chain axis and the a axis are tangential while the b axis lies in the direction of the radial fibrils.

It has been shown[2] that the development of the clover leaf pattern (see Fig. 2) occurs at about the same time that the pattern under parallel polarizer conditions changes from a circular pattern to one elongated in the direction of polarization. These changes occur during the secondary crystallization process when most of the chains are incorporated into fibrils with the chains lying tangential. The scattering observed under crossed polarizer conditions depends entirely on the existence of a difference between the tangential and radial refractive indices within the spherulites, and no observable pattern exists unless sufficient anisotropy is present.

Experimentally, a large increase in the intensity of scattering was observed subsequent to spherulite impingement[3] and was interpreted as arising from secondary crystallization of the material in the interfibrillar regions.[2] Thickening and perfection of the fibrils would also lead to enhanced scattering.

The lower pictures shown in Figure 2 are for the HMWL polyethylene under similar conditions. It can be seen that essentially no secondary crystallization has occurred as evidenced by the absence of a clover leaf scattering pattern even though the sample had been annealed at 125°C. for 90 min. A low intensity scattering pattern was obtained from this sample with the effective exposure about an order of magnitude higher indicating that the secondary crystallization was severely restricted.

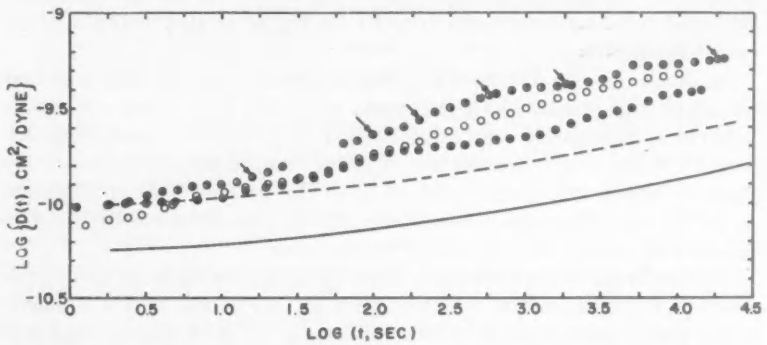

Fig. 4. Comparison of the tensile creep compliance at various stresses with data derived from dynamic mechanical measurements. Stress in units of 10^8 dynes/cm.^{2}: (●), 0.40; (○), 0.94; (◑), 1.2. (——), derived data; (- - -), derived data displaced vertically; (→), times at which scattering patterns in Figure 8 were taken.

In Figure 3 are shown plots of the specific volume against the logarithm of time obtained from dilatometric measurements at 125°C. for two polymers comparable to the HMWL and MMWL polyethylenes. The arrows indicate the time at which spherulite impingement was calculated to occur. The time of impingement was determined from knowledge of the radial growth rate and the average spherulite size obtained by microscopy.[7] These dilatometric measurements indicate a marked difference in the behavior of HMWL and MMWL polyethylene during crystallization. The difference is more pronounced after impingement has occurred when the specific volume of the MMWL polyethylene changes rapidly, but the specific volume of the HMWL polyethylene changes much more slowly and to a much lesser extent. Other evidence for restricted crystallization has been obtained from studies of the oxidative annealing,[5] the permeability,[6] and the dynamic mechanical properties of HMWL polyethylene[11] and will be referred to in a latter section of this paper dealing with static light scattering experiments.

Since interpretation of scattering from samples of HMWL polyethylene subjected to tensile stress was complicated by the lack of secondary crystallization, MMWL polyethylene was chosen from simultaneous creep and light scattering studies. The results of the creep measurements were converted to logarithmic plots of the tensile creep compliance D against time in seconds t as shown in Figure 4 for the MMWL polyethylene. The lower solid line in Figure 4 was calculated with the method of Hopkins and Hamming[12] from dynamic mechanical data obtained on a modified Maxwell Dynamic Tester.[6,11] These results were shifted vertically to more easily compare the shape of the curve with the results obtained from the creep measurements. The creep compliance is observed to increase gradually from about 10^{-10} to $10^{-9.2}$ cm.^{2}/dyne over about four decades at room temperature. The samples subjected to creep were more compliant than those subjected to dynamic stressing, due to the higher strains involved in the creep experiments.

As can be seen in Figure 4 the compliances are not coincident at long times and high strains which indicates a departure from linear viscoelastic behavior. Though the nature of the two experiments is somewhat different because simple tension occurs in the creep experiments and simultaneous tension and compression occur in the flexing of the rotating rod in the Maxwell Dynamic Tester,[13] the effect of this difference on the compliance and modulus is expected to be quite small.

The nonlinear behavior is more likely to arise from slippage and micro-yielding within spherulites. (This is not to be confused with the macroscopic phenomenon commonly called necking.) Micro-yielding would arise from the difference in the response of the fibrils perpendicular and parallel to the direction of stress in a manner similar to that observed by Horio[14] in cast films of polyethylene. The behavior of the load versus elongation curves for this cast polyethylene indicated that a large increase in stress occurred for a sample stretched in the a direction, the direction of casting, whereas the stress remained almost constant as the sample yielded when strained at right angles to the direction of casting, the b direction.[14] The stress at small strain required to produce this behavior[15] was about 10^8 dynes/cm.^{2} However, the actual stress required to cause yielding in our experiments would be below this value because there are fewer fibrils per unit volume and because the required stress level decreases with increasing time and strain. It can be seen from Figure 4 that under a stress of 1.2×10^8 dynes/cm.^{2} the compliance reaches a value of about $10^{-9.5}$ cm.^{2}/dyne in $10^{2.5}$ sec.; whereas at a stress level of 4×10^7 dynes/cm.^{2}, a value well below that believed necessary to cause micro-yielding at low strains, a compliance of $10^{-9.5}$ cm.^{2}/dyne is reached only after $10^{3.7}$ sec. Thus, the results of our creep experiments, which encompass the required stress level, probably reflect micro-yielding. While micro-yielding would be likely to cause spherulite deformation in a sample under the required stress such deformation could occur at small strains for other reasons as discussed below.

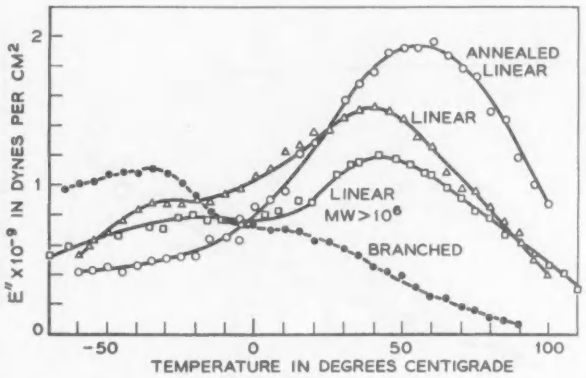

Fig. 5. Temperature dependence of the tensile loss modulus at one cycle per second for four polyethylenes.

Results of dynamic mechanical experiments on these polymers are presented in Figure 5 in which the loss modulus at one cycle per second as determined on a modified Maxwell Dynamic Tester is plotted as a function of temperature. Two maxima are observed: the α transition which occurs from 30 to 80°C., and the β transition which occurs at about −30°C. The height of the β peak is observed to increase with an increase in the amorphous content of the polymer, indicating that the transition is sensitive to the amorphous regions. (The lower peak height of the HMWL polyethylene, due to restricted segmental motion is discussed in a later section.) Further evidence that the β transition is influenced by the amorphous regions is obtained from the temperature dependence of the a_T shift factors used to superpose dynamic measurements obtained at different temperatures.[11] Determination of the coefficients of the WLF equation in the usual manner[16] resulted in a value for c_1^0 of 17.5 for a reference temperature of −27.5°C. This indicates that the mechanical behavior of polyethylene in the vicinity of the β peak is similar to the behavior of an amorphous polymer in the vicinity of its glass transition. The experiments of Nielsen[17] indicate that the crystalline regions also influence the β transition, and it is concluded that this transition involves motion of crystalline and amorphous regions coupled in series.[18] Though the height of the β peak has sometimes been related to the degree of branching it can be seen from Figure 5 that annealing of the MMWL polyethylene causes a drastic reduction in the height of the β peak.

The height of the α peak increases with increasing crystallinity and the maximum shifts to higher temperatures. This shift of the maximum with temperature is associated with an increase in the degree and perfection of the crystals, making motion more difficult until the temperature is increased. More important however is the fact that the α peak is due to a primary transition within the crystalline lamellae. The temperature

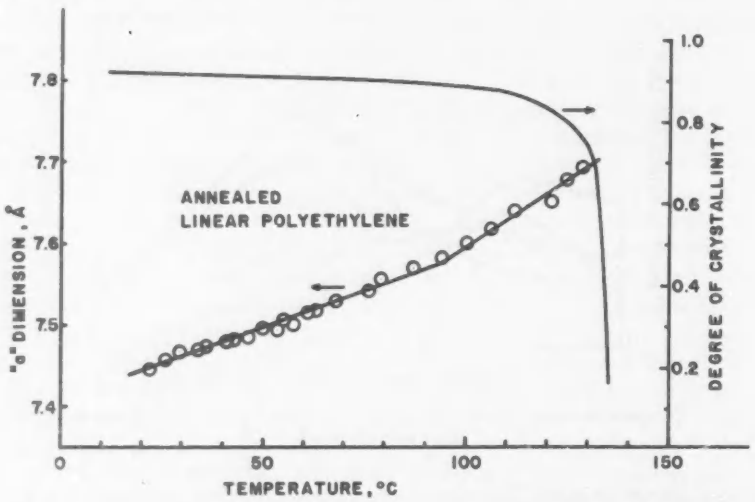

Fig. 6. Temperature dependence of the a dimension of the unit cell and of the degree of crystallinity for MMWL polyethylene. (Initially annealed at 125°C. for 5 hrs.)

of the maximum in the α peak for each of the polyethylenes is comparable with the temperature at which the thermal expansion coefficient of the crystals undergoes a change as observed by the change in the a dimension with temperature as shown in Figure 6. The a dimension and the degree of crystallinity are plotted here as a function of temperature. The change in the slope of the plot of the a dimension versus temperature occurs at about 100°C., which is comparable with the maximum in the α peak, as has also been observed by Takayanagi.[19] It can be seen that there is little change in the degree of crystallinity until well beyond the α peak of Figure 5, and the peak cannot be due to partial melting of the crystals. Rather, the peak must be due to a primary transition within the crystalline lamellae which has been transmitted throughout the sample.

One would not expect to observe the effect of the intralamellar transition unless mechanical continuity existed from one spherulite to another. By this it is meant that the polymer is made up of spherulites which have impinged upon their neighbors with little or no amorphous material in the regions between the spherulites. This would result in the transmission of any change within the lamellae from one spherulite to another, and so on throughout the sample. In contrast to this, an amorphous polymer loaded with rigid spheres would not be expected to reveal a transition within the spheres since the effect of the transition would be taken up by the amorphous material because the spheres would lack mechanical continuity.

The fact that two peaks are observed over a comparatively narrow temperature range (−30 to +20°C. for some branched polyethylenes) indicates

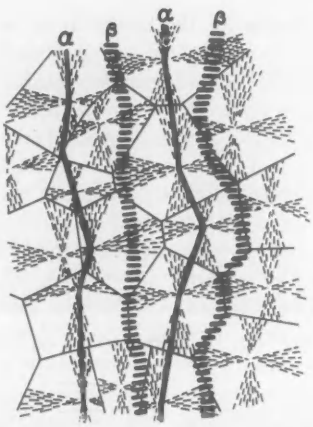

Fig. 7. Schematic diagram of a cross section of a spherulitic polymer under crossed polarizers subjected to vertical stress. The α and β lines represent parallel viscoelastic response mechanisms discussed in the text.

that there are two viscoelastic response mechanisms acting in parallel. A fringed micelle or series model would give one broad peak (unless the responses occurred at widely different temperatures) since the strains would be additive from the crystalline and amorphous portions. Moreover, a series model would show the compliance of the amorphous regions by a low-frequency storage modulus characteristic of a rubbery material, about 10^6 dynes/cm.^{2}. Because a low frequency storage modulus of 10^9–10^{10} dynes/cm.^{2} is observed even for 60% crystalline polyethylene[11] the response mechanisms must be coupled in parallel in order for the high modulus of the crystalline fibrils to be observed.

Any morphological model would have to be consistent with all of the above observations. The model proposed is shown in Figure 7 and is similar to one proposed by Takayanagi.[20] The diagram in Figure 7 represents a schematic cross section of a spherulitic polymer under crossed polarizers with the sample stressed in the vertical direction. The two viscoelastic response mechanisms are represented by the vertical solid lines α, and the vertical dashed lines β. The α lines represent the mechanical continuity from one spherulite to another through the vertical crystalline fibrils. These crystalline fibrils would transmit the effect of the primary intralamellar transition throughout the system and would give rise to a high storage modulus. The amorphous regions and the crystalline regions at right angles to the vertical fibrils, designated by the dashed lines in Figure 7, would reflect the large compliance of the amorphous regions and are to be associated with the β mechanism which must include motions of both regions in series. Because of the low compliance of the fibrils and because of the difference in the viscoelastic responses parallel and perpendicular to the direction of stress, spherulite deformation would have to

occur at very small strains for the model to be correct.[18] Experimental determination of spherulite deformation is discussed in the next section.

Photographs of the light scattering patterns taken at the times indicated in Figure 4 are shown in Figure 8 for the sample of MMWL polyethylene. Since the direction of sample elongation was vertical one would expect a horizontally elongated scattering pattern. In fact, Stein and co-workers observed an abrupt change from an elongated scattering pattern to two horizontal streaks at about 200% elongation which indicated that complete disruption of the spherulitic structure had occurred.[2] Two effects can be seen in Figure 8 as the amount of strain is increased. The patterns gradually become more diffuse and the clover leaves gradually compress toward the horizontal axis, until at about 6% strain the effect is quite marked. (The effects are more easily seen if the pattern at zero strain is

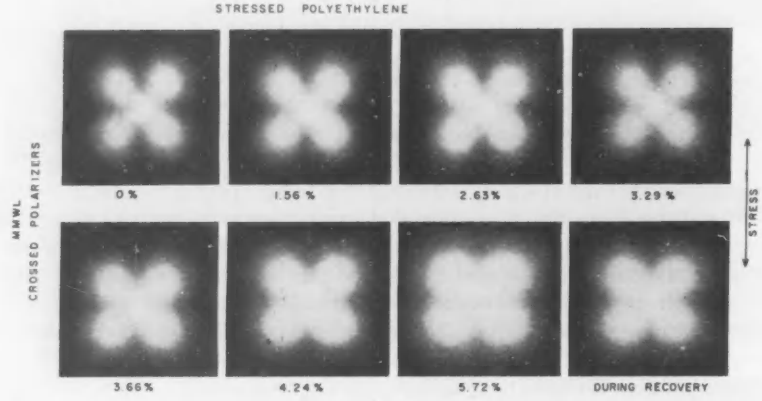

Fig. 8. Scattering patterns for MMWL polyethylene subjected to a tensile stress of 1.2×10^8 dynes/cm.^{2}. The per cent strain is indicated.

compared with each of the other patterns.) The first indication of deformed spherulites is detected at about 3% strain, though some deformation probably occurs before this. Thus, as would be expected from the theory, spherulite deformation occurs at very small strains.

The picture on the lower right in Figure 8 was taken shortly after the sample was released from stress. As can be seen the clover leaves are not as compressed and the picture is less diffuse. Pictures taken at later times show essentially complete recovery of the spherulites despite the fact that the strain has not returned to zero. This might arise from a process in which strained crystals unfold and reform within the spherulites during sample elongation, the rate of recrystallization not being fast enough to keep up with the increasing strain. Upon release of stress the reforming process would dominate and recovery of the light scattering pattern would occur. Residual strain would then be taken up in a nonrandom dis-

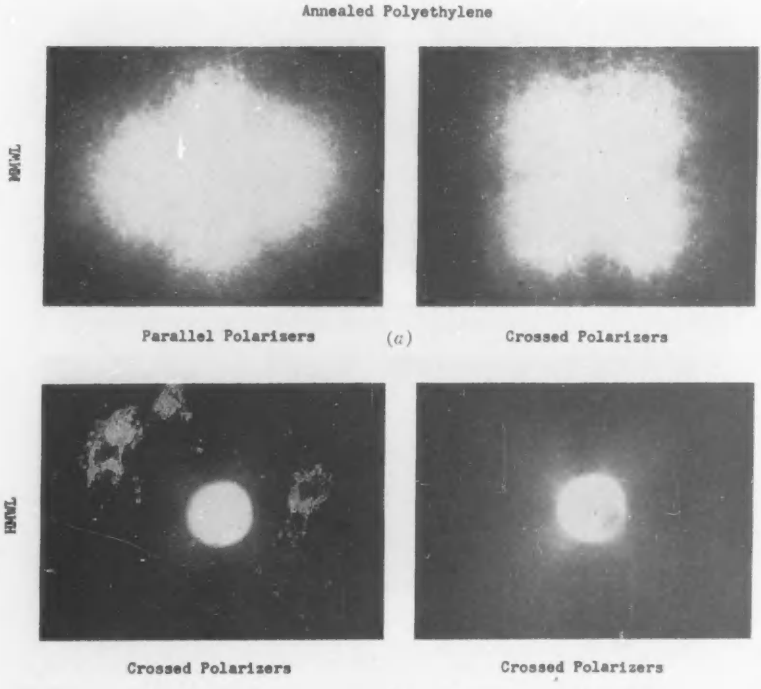

Fig. 9. Scattering patterns (*a*) from annealed MMWL polyethylene and (*b*) from HMWL polyethylene after further annealing.

tribution of amorphous material between fibrils. The amorphous material would be rather insensitive to light scattering, however.

In order to further investigate the restricted crystallization in the HMWL polymer the sample of Figure 2 was further annealed at 130°C. for about three hours. The scattering patterns from this sample are compared in Figure 9 with the patterns from the sample of MMWL polyethylene after annealing at 125°C. for 90 min. in the same air oven. The distribution of scattering in the upper pictures of Figure 9 for MMWL polyethylene is narrower than the distribution for the quenched MMWL polyethylene, as shown in Figure 2, indicating that the spherulites are more uniform in size and that they are slightly larger. The lower pictures in Figure 9, the one on the right being at a slightly higher output of the maser, show that a clover leaf pattern has developed in this sample of HMWL polyethylene upon annealing, though the weak intensity of the pattern indicates that the extent of secondary crystallization is still small.

In order to determine the effect of oxidation, a sample of HMWL polyethylene was melted between cover slips, quenched, and subjected to an

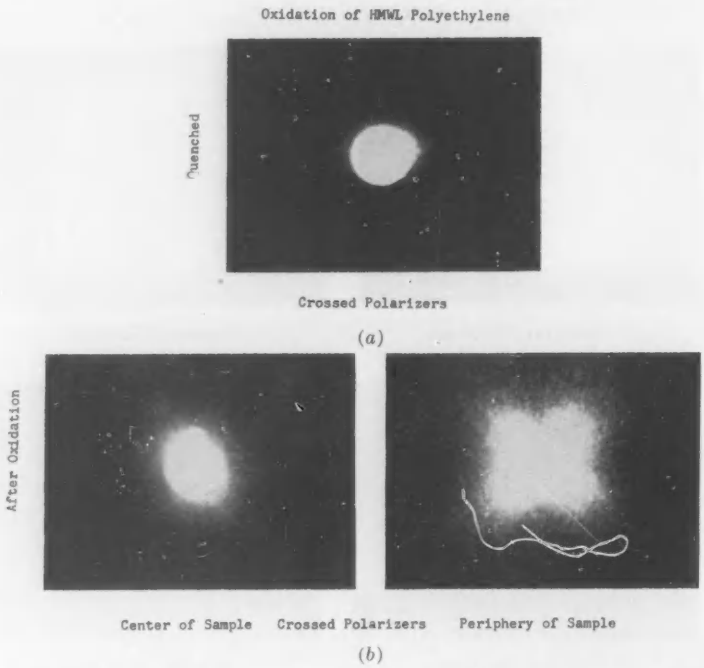

Fig. 10. Scattering patterns from (*a*) a quenched and (*b*) oxidized sample of HMWL polyethylene.

oxygen atmosphere for 17 hr. at 113°C. At this temperature little recrystallization would be expected to occur. Any effect would then be due mainly to crystallization of previously uncrystallized material. Scattering patterns from this sample are shown in Figure 10. The top picture of the quenched sample shows no scattering characteristic of secondary crystallization. The lower photographs were taken after oxidation, the picture on the left being of the scattering from the center of the sample while the picture on the right is of scattering from the periphery of the sample. The edge of the sample became whitened indicating that oxidation had occurred. From the striking difference in the two patterns it is clear that oxidation greatly enhanced the secondary crystallization, probably through scission of polymer chains imbedded in more than one lamella.[11]

The sensitivity of HMWL polyethylene to oxidative annealing has been observed by Winslow and co-workers.[5,21] A large increase in density occurred with a small amount of oxidation in the HMWL polyethylene whereas much more oxidation was required to achieve the same density and degree of crystallinity in lower molecular weight linear polyethylenes.[21] Branching and crosslinking were found to impede the ordering process which proceeded rapidly, however, in the HMWL polyethylene with an

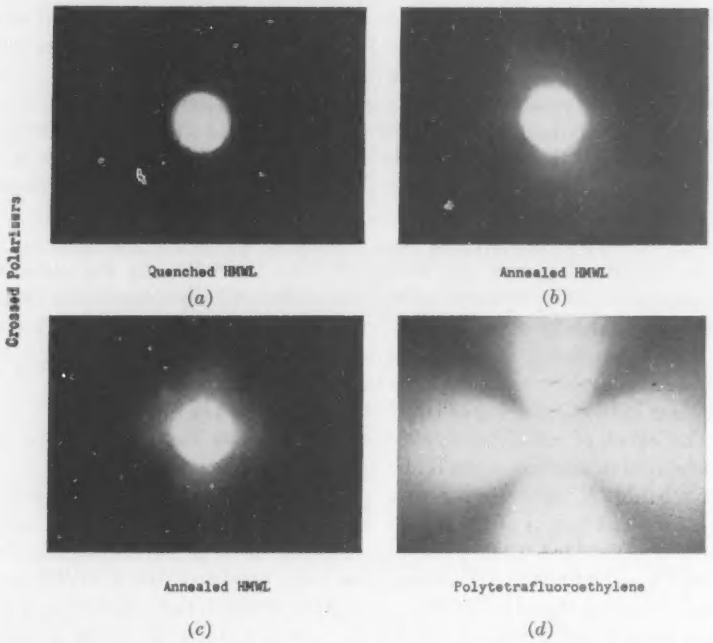

Fig. 11. Scattering pattern from a quenched (*a*) and vacuum-annealed (*b*, *c*) sample of HMWL polyethylene; scattering pattern from a sample of polytetrafluoroethylene film (*d*).

accompanying increase in the x-ray degree of crystallinity[5] from 67–95%. The similarity in total oxygen uptake was attributed to crystallization upon chain scission.[5] Evidence for the orderly packing of chains upon oxidation was observed by Winslow and co-workers in electron photomicrographs of the replicated fracture surface of a sample of oxidized HMWL polyethylene. Long banded structures were visible with striations perpendicular to the length of the bands.[21] These banded structures are similar to those observed in low molecular weight polyethylene by Anderson[22] in which the chains are believed to be parallel to the striations. Oxidation might be expected to lead to similar bands in the case of HMWL polyethylene.

To observe the effect of annealing without oxidation a sample of HMWL polyethylene was melted between cover slips and quenched to room temperature. It was then heated in a vacuum oven preflushed with nitrogen at 130°C. for 24 hr. and allowed to come to room temperature under vacuum. Shown in Figure 11 are the scattering patterns obtained with crossed polarizers for this sample. No scattering characteristic of secondary crystallization can be observed for the quenched sample. Scattering under the same conditions for the annealed sample are shown in the picture

at the upper right and at a higher intensity of the maser beam but at a further distance from the sample to film in the picture on the lower left. Both of these pictures show a cross rather than a clover leaf pattern. This is similar to the scattering pattern observed from films of polytetrafluoroethylene as shown on the lower right in Figure 11. Stein and co-workers have shown that this cross type scattering can occur if the scattering is from aggregates of crystals stacked at an angle to the direction of maximum polarizability, believed to be the case in polytetrafluoroethylene, or else it can occur if the scattering is from lamellae in which the chains are tilted at an oblique angle to the surface.[23] The scattering in the annealed samples of HMWL polyethylene could arise from tilting of the folded chains within the fibrils in a manner similar to that observed by Baltá Callejá, Bassett, and Keller in solution-grown single crystals of polyethylenes of lower molecular weight.[24] This tilting might arise in the HMWL polyethylene in the thickening of lamellae having chains in common.

The effect of restricted crystallization has also been observed in the mechanical properties of the HMWL polyethylene[6,11] in the behavior of the loss modulus E'' at one cycle per second as a function of temperature (see Fig. 5). The height of the β peak increases with an increase in the amorphous content for branched polyethylene and for annealed and unannealed MMWL polyethylene. However, the peak height of the HMWL polyethylene is less than that of the unannealed MMWL polyethylene and less than that of the branched polyethylene even though the latter material and the HMWL polyethylene have the same density and x-ray degree of crystallinity.[11] Chains tied to more than one lamella would be quite restricted in their motion and would be expected to cause a reduction in the height of the β peak of the HMWL polyethylene.

Summary

Through the use of photographic light scattering from thin films of high molecular weight linear polyethylene we have shown that secondary crystallization is severely restricted in this polymer, that oxidation induces further crystallization, and that annealing may lead to tilted chain lamellae. The restricted crystallization and the restricted motion observed in dynamic mechanical experiments probably have a common origin in the occurrence of lamellae with chains in common. Light scattering experiments conducted on films of medium molecular weight linear polyethylene subjected to tensile stress indicated that spherulite deformation occurred at very small strains, as predicted by Matsuoka[18] for a system with two quite different viscoelastic responses acting in parallel.

The authors wish to thank Dr. D. W. McCall for his helpful counsel during preparation of the manuscript. The help provided by Mr. C. J. Aloisio in performing the dilatometric and dynamic mechanical measurements is gratefully acknowledged. The sample of polytetrafluoroethylene film was kindly provided by Dr. H. W. Starkweather, duPont de Nemours and Company.

References

1. Plazá, A., and R. S. Stein, *J. Polymer Sci.*, **40**, 267 (1959).
2. Stein, R. S., and M. B. Rhodes, *J. Appl. Phys.*, **31**, 1873 (1960).
3. Rhodes, M. B., and R. S. Stein, *J. Polymer Sci.*, **45**, 521 (1960).
4. Rhodes, M. B., D. A. Keedy, and R. S. Stein, *J. Polymer Sci.*, **62**, S73 (1962).
5. Winslow, F. H., C. J. Aloisio, W. L. Hawkins, W. Matreyek, and S. Matsuoka, *ACS Polymer Preprints*, Vol. 4 (No. 1), 336 (1963).
6. Rogers, C. E., S. Matsuoka, and C. J. Aloisio, *ACS Polymer Preprints*, Vol. 4 (No. 1), 341 (1963).
7. Padden, F. J., Jr., and H. D. Keith, *J. Appl. Phys.*, **30**, 1479 (1959); and private communication.
8. Matsuoka, S., *Bull. Amer. Phys. Soc.*, **7**, 202 (1962).
9. Peterlin, A., *J. Appl. Phys.*, **34**, 102 (1963).
10. Weeks, J. J., *Bull. Amer. Phys. Soc.*, **8**, 243 (1963).
11. Matsuoka, S., and C. J. Aloisio, *Bull. Amer. Phys. Soc.*, **8**, 243 (1963); S. Matsuoka and C. J. Aloisio, to be published.
12. Hopkins, I. L., and R. W. Hamming, *J. Appl. Phys.*, **28**, 906 (1957).
13. Maxwell, B., *J. Polymer Sci.*, **20**, 551 (1956).
14. Horio, M., *Rheol. (Japan)*, **11**, 265 (1962).
15. Horio, M., private communication.
16. Ferry, J. D., *Viscoelastic Properties of Polymers*, Wiley, New York, 1961, chapter 11.
17. Nielsen, L. E., *J. Polymer Sci.*, **43**, 357 (1960).
18. Matsuoka, S., to be published.
19. Takayanagi, M., *J. Polymer Sci.*, **46**, 531 (1960).
20. Takayanagi, M., *Mem. Fac. Eng., Kyushu Univ.*, **23**, 41 (1963).
21. Winslow, F. H., C. J. Aloisio, W. L. Hawkins, W. Matreyek, and S. Matsuoka, *ACS Polymer Preprints*, Vol. 4 (No. 2), 706 (1963).
22. Anderson, F. R., *J. Appl. Phys.*, to be published.
23. Rhodes, M. B., and R. S. Stein, *J. Polymer Sci.*, **62**, S84 (1962).
24. Baltá Callejá, F. J., D. C. Bassett, and A. Keller, *Polymer*, **4**, 269 (1963).

Résumé

La technique de la diffusion lumineuse a été employée pour l'étude de films de polyéthylène linéaire de poids moléculaire moyen et élevé. Les résultats de l'étude du polymère de poids moléculaire élevé montrent que la cristallisation secondaire est fortement empêchée, que l'oxydation induit une cristallisation ultérieurement et que le recuit peut conduire à des lamelles enchevêtrées. Les résultats expérimentaux obtenus pour des films de polymère de poids moléculaire moyen indiquent qu'il y a dans le polymère, soumis à des tensions d'élongation, une déformation des sphérulites pour de très faibles tensions ce qui est en accord avec les théories proposées.

Zusammenfassung

Das photographische Lichtstreuungsverfahren wurde zur Untersuchung von Filmen aus linearem Polyäthylen mittleren und hohen Molekulargewichts herangezogen. Die Ergebnisse an hochmolekularen Polymeren zeigen, dass die Sekundärkristallisation stark eingeschränkt, ist, dass Oxydation eine weitere Kristallisation induziert und dass Temperung zu gekippten Kettenlamellen führen kann. Versuchsergebnisse an Filmen aus Polymeren mittleren Molekulargewichts unter Zugspannung zeigen, dass, in Übereinstimmung mit der Theorie, eine Sphärolithdeformation be sehr kleiner Verformung eintritt.

JOURNAL OF POLYMER SCIENCE: PART C NO. 5, PP. 179–190

Studies of Rates of Spherulite Deformation by Low-Angle Light Scattering*

PETER ERHARDT,† K. SASAGURI,‡ and R. S. STEIN, *Polymer Research Institute, University of Massachusetts, Amherst, Massachusetts*

Synopsis

The rates of spherulite deformation accompanying the elongation and contraction of polyethylene and the elongation of polybutene-1 samples have been observed using a low-angle light scattering technique. The light scattering pattern is obtained using a ruby pulsed laser which is flashed a predetermined time after the extension of the sample. It is found that spherulite deformation occurs in times less than 40 msec. which is less than the time required for the birefringence increase following deformation. Upon retraction, the light scattering pattern becomes symmetrical before the sample length has returned to its initial value. With quenched polybutene-1, the rapid change in shape of the light scattering pattern is accompanied by a slower change in intensity occurring over times comparable with that for the birefringence change. This is associated with changes in the crystal structure, orientation, and density within the spherulite following deformation.

In previous publications,[1,2] it was postulated that the initial orientation of crystals accompanying the deformation of a crystalline polymer is a consequence of the deformation of the spherulitic or crystalline superstructure within which they reside. A mechanism for such a deformation was proposed[1] which accounted for the change in birefringence and crystal orientation functions upon stretching the polymer. The crystal orientation was found to be time dependent giving rise to time dependent birefringence changes that have been studied in experiments involving relaxation at constant length or periodic straining. This paper represents an attempt to directly demonstrate this spherulite deformation and to establish whether the time dependence of crystal orientation is related to a time dependence of spherulite deformation.

The direct microscopic observation of spherulite deformation and its time dependence is difficult. A photomicrograph illustrating the changes seen between crossed polars upon deforming a polyethylene spherulite is shown in Figure 1. The birefringence signs (determined from interference

* Supported in part by contract with the Office of Naval Research and in part by Grants from the Air Force Office of Scientific Research and the Petroleum Research Fund.

† On leave from the General Electric Research Laboratory, Schenectady, New York.

‡ On leave from the Asahi Chemical Company, Japan.

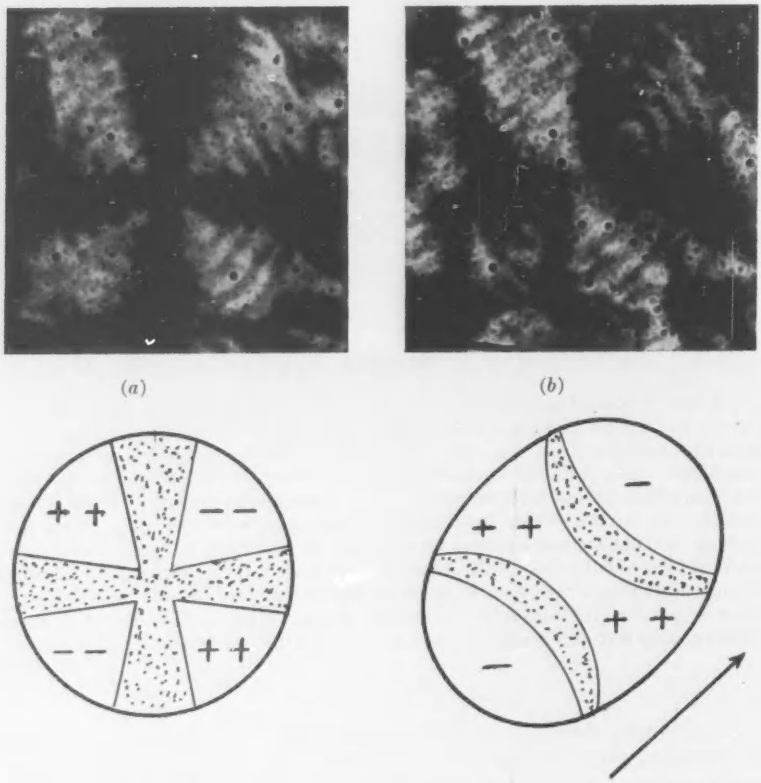

Fig. 1. Spherulites in (*a*) unstretched and (*b*) 6% stretched polyethylene. Polar directions are at ±45° to the stretching direction which is indicated by an arrow. The sketch under the pictures indicates the sign of birefringence, where a (+) sign indicates that the greatest refractive index is for light polarized in the stretching direction. (=) indicates a more negative birefringence than (−).

colors using a first-order red plate) are shown in the sketch below, where (+) signifies that the highest refractive index in that location is in the stretching direction and (−) the perpendicular direction. For polymers of practical interest, the spherulite size is usually too small to be easily resolvable by a light microscope, especially under conditions of samples being subjected to rapid strain. Consequently, low-angle photographic light scattering techniques were used.

The relationship between the low-angle light-scattering pattern and spherulite size and anisotropy has been described.[3–5] The deformation of the scattering pattern accompanying the stretching of the sample has been observed.[3] The initial change in the scattering pattern (at elongations up to 25–50% for low density polyethylene) may be associated with spherulite

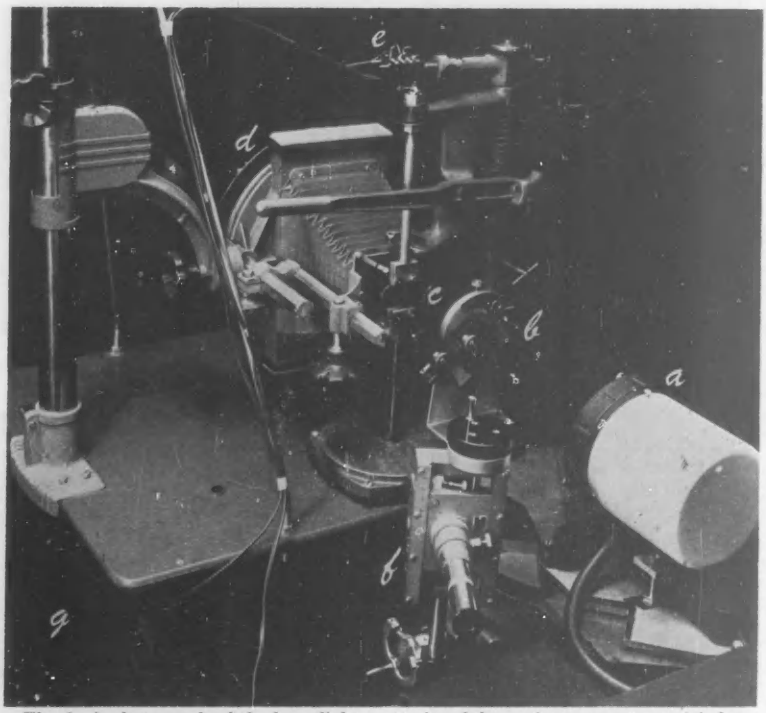

Fig. 2. A photograph of the laser light-scattering deformation apparatus: (*a*), laser head; (*b*) adjustable pinhole for elimination of stray light; (*c*) sample held in deformation apparatus; (*d*) photographic film holder and bellows; (*e*) microswitch which closes upon completion of sample deformation; (*f*) traveling microscope for measuring sample strain, and (*g*), electronic timing circuit.

deformation while the changes at higher elongation may be associated with the reorganization of the crystal structure to fibrillar morphology.[5] The use of a pulsed laser as a light source for these scattering measurements has been described.[6] This permits the obtaining of light scattering photographs in less than a millisecond. In this work, the laser technique was used for a sample subjected to rapid deformation and then relaxation at constant length.

The sample in the form of a film about 1 in. × 1/2 in. × 5 mil. was held between clamps in a lever operated manual deformation apparatus (fabricated from a drill press attachment for a 1/4-in. power home-workshop drill) which permitted stretching the sample at elongations up to 20% in 80 msec. (Fig. 2.) A microswitch was tripped by the deformation apparatus which triggered an electronic timing circuit which controlled the flashing of a small ruby crystal pulsed laser (Maser Optics, Boston, Mass., Model 600). The time interval between completion of stretching and flashing of the laser was controllable from 40 msec. upward. An elongation,

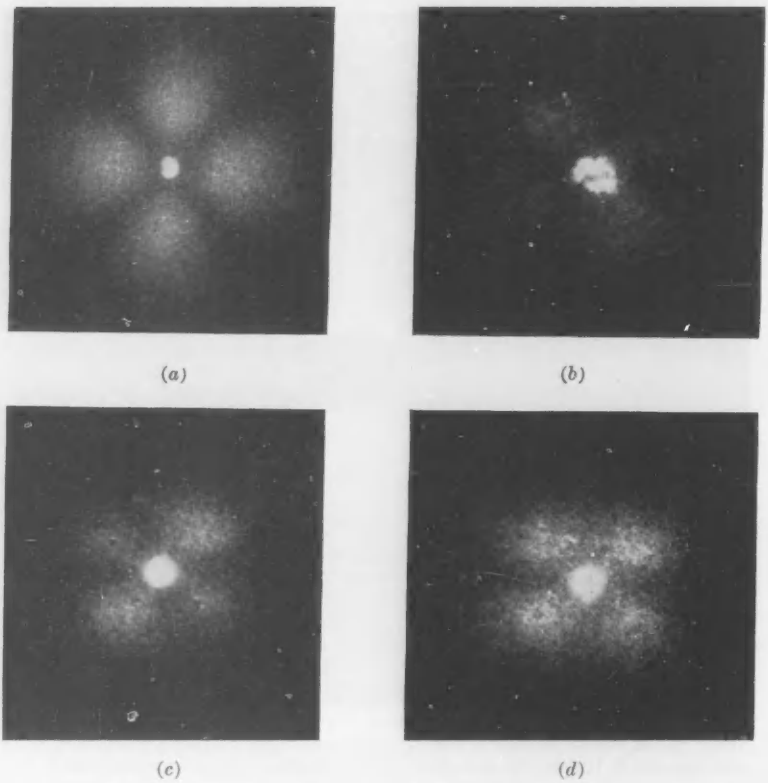

Fig. 3. H_v light scattering photographs for an undeformed polyethylene sample and for samples at varying time intervals after having rapidly been stretched 11–12%: (*a*) unstretched; (*b*) 0.042 sec.; (*c*) 0.082 sec.; (*d*) 40 min. The polarization directions are indicated by arrows at ±45° and the stretching direction is vertical.

using a new sample, must be carried out for each time interval for the short time range experiments. A polarized laser beam is obtained through use of a 90°-cut ruby crystal and a polaroid analyzer after sample is adjustable to either the V_V or H_V polarization conditions.[3]

The sample studied was a Monsanto experimental medium density polyethylene similar to that used in our previous work.[3,4] Films were press molded at 140°C. at 630 psi pressure. The heat was turned off and the sample was allowed to cool in the press at its natural cooling rate.

H_V scattering patterns for an unstretched sample and samples stretched 11–12%, where the picture is taken at varying time intervals following deformation, are shown in Figure 3. The polarization directions are ±45° and the stretching direction is vertical. It is seen that upon stretching, there is a deformation of the general shape of the pattern from circular to

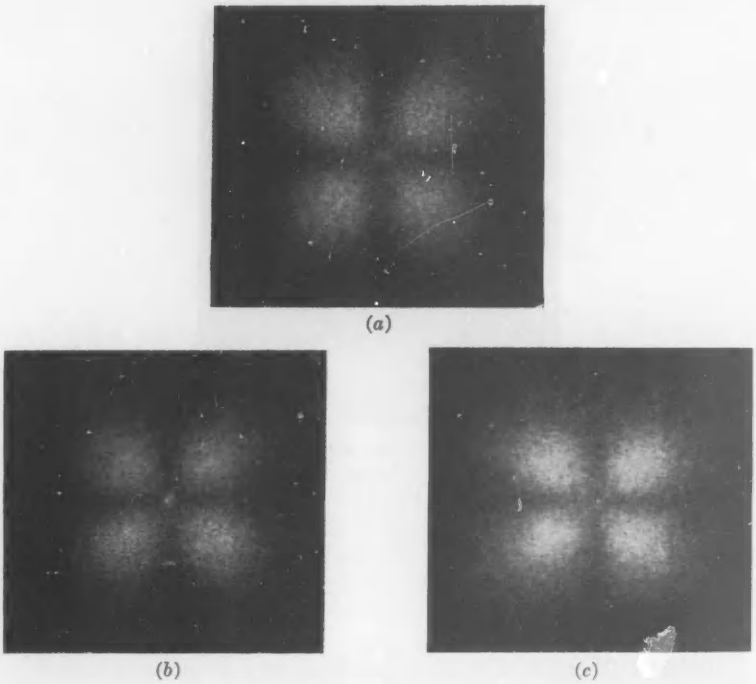

Fig. 4. H_v light scattering photographs for an undeformed polyethylene sample and for samples at varying time intervals after having rapidly been stretched at 15.2%. The polarization directions are vertical and horizontal and the stretching direction is vertical. (*a*) Unstretched; (*b*) 15.2% ϵ at 0.051 sec ; (*c*) 15.2% ϵ at 20 min.

elliptical accompanied by a decrease and then an increase in the intensity of the pattern. These changes are associated with (*a*) a deformation of the spherulite from spherical to ellipsoidal shape, and (*b*) a change in the anisotropy of the spherulite associated with reorientation of crystals within the spherulites. It is suggested that these two processes do not occur at equal rates. The deformation is indicated in the first picture obtained at 0.042 sec. after deformation while further changes are evident in the later picture at 0.080 sec. No appreciable changes are seen between 0.080 sec. and 4 min. The resulting pattern is extended in a direction perpendicular to stretching direction as has been proposed.[2]

Dynamic birefringence measurements show that the birefringence relaxation time is of the order of one second for this material at room temperature. Thus the time for spherulite deformation is less than that required for the birefringence change following stretching. The deformation of polyethylene appears to be a two stage process with the spherulite deformation occurring at very short times followed by an orientation process occurring at longer times.

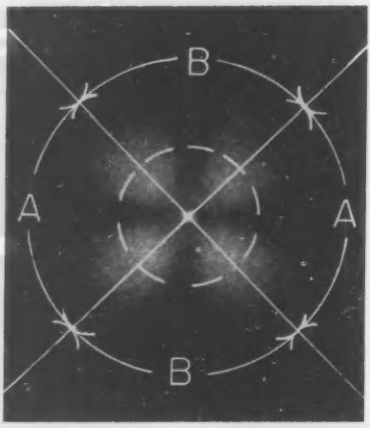

Fig. 5. H_r light scattering pattern for an unstretched polyethylene sample showing the relationship between A and B; and the path of the radial densitometer scan (- - -) The intensity maxima lie along the lines at $\pm 45°$.

One obtains photographs in which the changes are less apparent upon quick visual examination but which are more subject to quantitative interpretation, by having the stretching and polarization directions coincide (Fig. 4). The spherulites are again seen to deform very rapidly from spherical to ellipsoidal, with the ellipsoid extended in the stretching direction—with the scattering pattern extended perpendicular to the stretching direction. Radial scans (Fig. 5) using a microdensitometer reveal that the arc length B (in the vertical direction) between the intensity peaks increases from 90° in the unstretched case to 104° at 0.051 sec., and 109° at 20 min. The arc length A (in the horizontal direction) decreases from 90° to 76° to 71° over the same time interval. The uncertainty in the measurements is about $\pm 3\%$. The reduction in intensity at short times followed by an increase in intensity at longer times is also apparent.

Observations were made on the contraction of deformed polyethylene spherulites as the stretched polymer was allowed to retract freely. The sample was first rapidly stretched to 31.9% elongation and held at fixed length for one hour. Upon cutting the sample free and observing the changes in scattering pattern with time, the deformed pattern was found to approach that of unstretched polyethylene (Fig. 6). This result appears to be in agreement with that reported recently by Moore and Matsuoka.[9] The change in elongation of the sample on retraction was followed as a function of time, by observing the movement of bench marks on the sample using a traveling microscope (Fig. 7). The recovery of the deformed spherulite appears to be associated with the high rate of recovery portion of the curve.

It is noted, on comparing Figures 6 and 7, that the sample is still considerably strained when the spherulite pattern has returned to its unde-

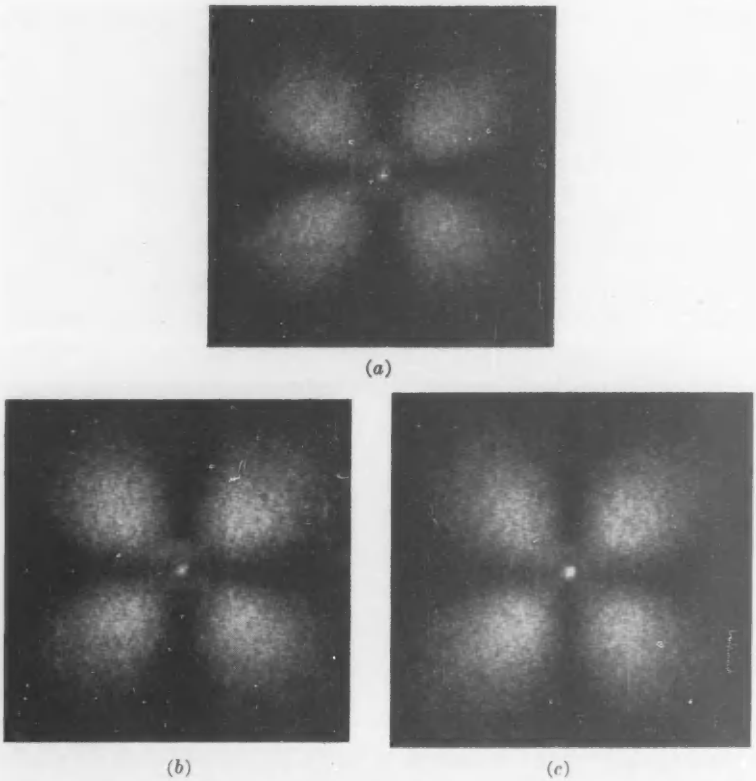

(a) (b) (c)

Fig. 6. H_v light scattering photographs for a polyethylene sample stretched 31.9% and for the sample at varying time intervals after the start of free retraction: (*a*) before retraction; (*b*) 4 sec.; (*c*) 10 min. The polarization directions are vertical and horizontal and the stretching direction is vertical.

formed shape. The mechanism by which this residual strain has occurred is not understood, and therefore further experiments are planned in an attempt to resolve this point.

Isotactic polybutene-1 has two crystalline modifications, one of which is stable at room temperature. The other form is that occurring at the time of crystallization.[10,11] This latter form is very unstable at room temperature. It spontaneously changes over to the stable form.

This transition rate is affected by such processes as aging, temperature, and mechanical stretching.[12]

Polybutene-1 samples were prepared by press molding between aluminum sheets at 156°C. at 400 psi pressure. The samples were quenched from the melt by waving them in air upon removal from the hot press.

The time dependence of low angle light scattering from quenched polybutene-1 was observed by the photographic technique. H_V light scattering

patterns for an unstretched quenched polybutene-1 sample (1 hr. after preparation) and for the sample held at 10% elongation after stretching are shown in Figure 8. After 0.041 sec. the spherulites are already deformed from spherical to ellipsoidal, with the ellipsoid extended in the direction of stretch, as was the case with polyethylene. The later pictures (at 1 hr. and 10 hr.) show a marked increase in the intensity of scattering while the pattern substantially retains its deformed shape. The birefringence of this stretched sample was found to be positive and to increase by a factor of about 2 over the time period concurrent with the increase in scattered intensity. This is in contrast to the observation[12] that the birefringence becomes negative upon stretching stable polybutene-1 which has

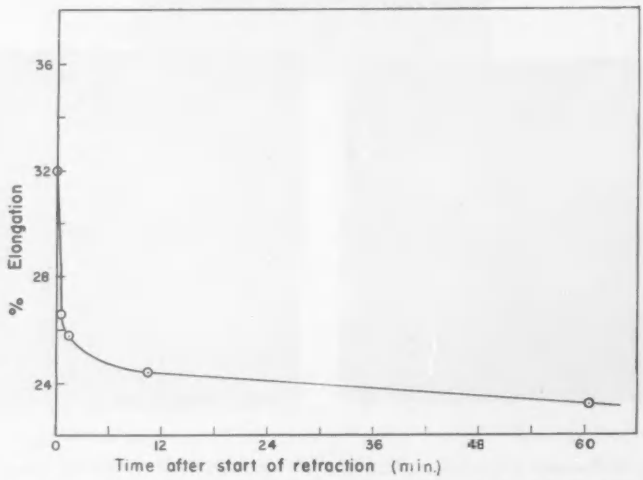

Fig. 7. The time-rate of retraction for the polyethylene sample for which light scattering photographs are shown in Figure 6.

been aged in the undeformed state. The shift from negative to positive values of the birefringence is not a result of the change in birefringence accompanying the transition, but rather results from a change in the orientation mechanism with aging. Evidence for this was obtained in the following manner.[12]

The mode of crystal orientation accompanying the stretching of a partly aged sample was studied by measuring the azimuthal dependence of x-ray diffraction. At high elongation, where the birefringence is positive, both the (110) and (300) reflections have maximum intensity at the equator, indicating that both the a and b axes orient perpendicular to the stretching direction.

At low elongations, where the birefringence is negative, the (110) reflection is more intense at the meridian, while the (300) reflection is more intense at the equator. Thus, the change from negative to positive

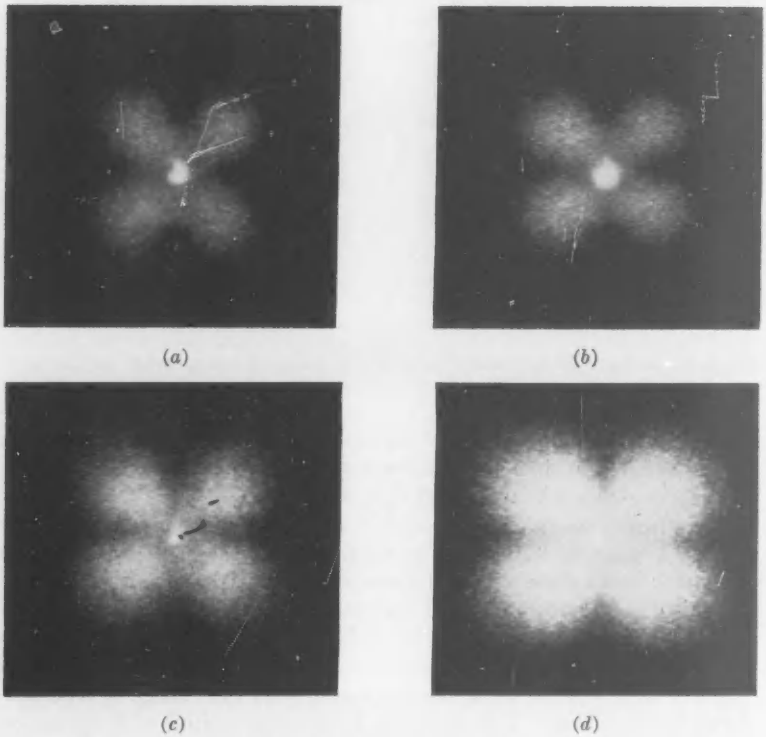

Fig. 8. H_v light scattering photographs for an unstretched freshly quenched polybutene-1 sample and for the sample at varying time intervals after being rapidly stretched 10%. The polarization directions are vertical and horizontal and the stretching direction is vertical. (*a*) 0% ϵ sec.; (*b*) 10% ϵ at 0.041 sec.; (*c*) 10% ϵ at 1 hr.; (*d*) 10% ϵ at 10 hr.

birefringence on stretching an aged sample is a result of the shift from a *b* axis to *c* axis orientation mechanism.

The crystalline contribution to the birefringence of a spherulite sample may be described by the equation[1]

$$\Delta = \int_{\theta=0}^{\pi} \Delta(\theta) \left[\frac{3\cos^2\theta - 1}{2}\right] N(\theta) \sin\theta \, d\theta \tag{1}$$

where $\Delta(\theta)$ is the spherulite birefringence per unit volume (difference between radial and tangential refractive index) contributed by those crystals in the volume element of width $d\theta$ lying on a spherulite radius making an angle θ to the stretching direction. In the unstretched state, $\Delta(\theta)$ is negative and independent of θ. If the spherulite deformation is a completely affine process (as is approximated in an aged polybutene-1 sample at low elongation), $\Delta(\theta)$ remains negative on stretching and the

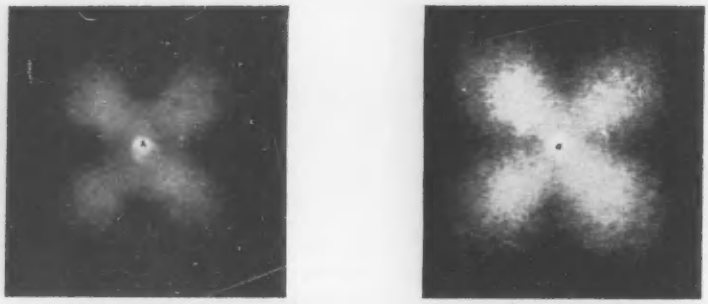

(*a*) (*b*)

Fig. 9. H_v photographic light scattering patterns for unstretched quenched polybutene-1: (*a*) fresh; (*b*) aged. The polarization directions are vertical and horizontal.

negative sample birefringence is a consequence of the change in the distribution function $N(\theta) \sin \theta \, d\theta$ (representing the number of spherulite radii in the volume element $N(\theta) \sin \theta \, d\theta$) with elongation.

For a freshly quenched polybutene-1 sample, $\Delta(\theta)$ changes with elongation as a result of the change in orientation of the crystals within the spherulite from a state where their *c*-axis is tangential to one where their *c*-axis is radial accompanying the transformation of their structure from that of modification II to modification I. This transformation is induced by the internal strain of the spherulite and results in a change of $\Delta(\theta)$ from a negative to a positive value simultaneously with the change in $N(\theta)$ produced by stretching. This results in Δ becoming positive with elongation of such a sample.

The transformation from modification II to I is time dependent and will not be complete at the time of completion of stretching. Hence, if the sample is held in this stretched state, $\Delta(\theta)$ continues to become more positive while $N(\theta)$ remains constant, resulting in Δ becoming more positive as observed.

An increase in the scattered intensity was also observed in the spontaneous transition of unstable to stable polybutene-1, in the unstretched case (Fig. 9). The transition in the unstretched state occurs at longer times after sample preparation, indicating that mechanical deformation enhances the transformation from unstable to stable polybutene-1, as has been observed from x-ray diffraction measurements. Densitometer scans of the photographic light scattering patterns of Figure 9 show a general rise in the overall level of intensity rather than an increase of amplitude of the intensity peaks. This indicates, that, in the unstretched state, the increase in the intensity of scattering is due to density rather than orientation fluctuations.

This would appear to be in agreement with the reported observation[13] that the conversion of unstable to stable polybutene-1 occurs with a change of crystalline form of lower density to one of higher density. Assuming the

volume of the unstretched sample to remain constant, such a redistribution of density within the sample would give rise to an increase in density fluctuations as has been observed.

References

1. Sasaguri, K., S. Hoshino, and R. S. Stein, *J. Appl. Phys.*, in press; presented before the Division of High Polymer Physics, American Physical Society, St. Louis, Missouri, March, 1963.

2. Wilchinsky, Z. W., paper presented before the Division of Polymer Chemistry, American Chemical Society, 142nd National Meeting, Atlantic City, September, 1962.

3. Stein, R. S., and M. B. Rhodes, *J. Appl. Phys.*, **31**, 1873 (1960).

4. Rhodes, M. B., and R. S. Stein, *J. Appl. Phys.*, **32**, 2344 (1961).

5. Stein, R. S., M. B. Rhodes, P. R. Wilson, and S. N. Stidham, *Pure and Applied Chemistry, Vol. 4*, Butterworths, London, 1962, p. 219.

6. Rhodes, M. B., D. A. Keedy, and R. S. Stein, *J. Polymer Sci.*, **62**, S73 (1962).

7. Stein, R. S., S. Onogi, and D. A. Keedy, *J. Polymer Sci.*, **57**, 801 (1962).

8. Stein, R. S., S. Onogi, K. Sasaguri, and D. A. Keedy, *J. Appl. Phys.*, **34**, 80 (1963).

9. Moore, R. S., and S. Matsuoka, paper presented before 4th International Congress on Rheology, Brown University, Providence, R. I., August 1963.

10. Natta, G., P. Corradini, and I. W. Bassi, *Makromol. Chem.*, **21**, 240 (1956).

11. Miller, R. L., and L. E. Nielsen, *J. Polymer Sci.*, **55**, 643, (1961).

12. Stein, R. S., S. Hoshino, and K. Sasaguri, papers presented before Division of Polymer Chemistry, American Chemical Society, 142nd National Meeting, Atlantic City, New Jersey, September 1962.

13. Jones, A. Turner, *J. Polymer Sci.*, **B1**, 455 (1963).

Résumé

Les vitesses de déformation des sphérulites, qui accompagne l'élongation et la contraction du polyéthylène et l'élongation d'échantillons de polybutène–1, ont été observées au moyen d'une technique de diffusion lumineuse à petit angle. L'image de la lumiere diffusée est obtenue au moyen de la lumière provenant d'un laser au rubis envoyée pendant un temps très court et prédeterminé après l'extension de l'échantillon. On a trouvé que la déformation du sphérulite a lieu dans un temps inférieur à 40 msec., ce qui est inférieure au temps requis pour que la biréfringence puisse faire augmenter la déformation subséquente. Lors de la rétraction, l'image de la lumière diffusée devient symétrique avant que la longueur de l'échantillon ne soit revenue à sa valeur initiale. Avec le polybutène-1 refroidi brutalement, le changement rapide de la forme de l'image de la lumière diffusée s'accompagne d'un plus faible changement de l'intensité qui a lieu dans des temps comparables a celui necessaire pour le changement de la biréfringence. Cela s'accompagne de changements dans la structure du cristal, l'orientation et la densité du sphérulite après déformation.

Zusammenfassung

Die Geschwindigkeit der Sphärolithdeformation bei der Elongation und Kontraktion von Polyäthylen und der Elongation von Polybuten-1-Proben wurde mit einer Kleinwinkel-Lichtstreuungsmethode gemessen. Das Lichtstreuungsdiagramm wird mit einem Rubinlaser erhalten, der zu einer vorbestimmten Zeit nach der Dehnung der Probe gezündet wird. Die Sphärolithdeformation erfolgt in Zeiten kürzer als 40 msec, was weniger als die für die Doppelbrechungszunahme nach der Deformation notwendige, Zeit ist. Beim Zusammenziehen wird das Lichstreuungsdiagramm vor der Rückkehr der Probenlänge auf ihren ursprünglichen Wert symmetrisch. Bei abgeschrecktem Polybuten-1 wird die rasche Gestaltsänderung des Lichtstreuungsdiagramms von einer

langsameren Intensitätsänderung begleitet, die sich über vergleichbare Zeiten wie die Doppelbrechungsänderung erstreckt. Sie steht in Beziehung zu Änderungeu der Kristallstruktur, Orientierung und Dichte innerhalb des Sphärolithes nach der Deformation.

AUTHOR INDEX

Amba-Rao, C. L.: 75
Andrews, R. D.: 101
Augstkalns, V. A.: 55
Chappelear, D. C.: 55
Dill, E. H.: 67
Erhardt, P.: 179
Haaf, W. R.: 153
Hammack, T. J.: 101
Hayashi, C.: 123
Honeycutt, E. H., Jr.: 37
Horio, M.: 123
LeGrand, D. G.: 153
Lindsey, E. E.: 55
Matsuoka, S.: 163
Minami, S.: 113
Moore, R. S.: 163
Onogi, S.: 123
Peebles, F. N.: 37
Philippoff, W.: 1
Prados, J. W.: 37
Read, B. E.: 87
Sasaguri, K.: 139, 179
Stein, R. S.: 139, 179
Sullivan, D. M.: 55
Takayanagi, M.: 113
Uemura, S.: 113
Wayland, H.: 11
Yamada, R.: 123

SUBJECT INDEX

Birefringence, dynamic, amorphous polymers, 87
polyolefins, 179
several high polymers, 123
orientation, polymers in the glassy and rubbery states, 101
streaming, of polymer solutions, 1
as a rheological research tool, 11
Birefringent properties, of milling yellow suspensions, 37
Creep, stress-strain-time-birefringence relations, 75
Dynamic rheo-optical properties, of crystalline polymer, 113
Equivalent model method, application to dynamic rheo-optical properties of crystalline polymers, 113
Light scattering, low-angle, studies of spherulite deformation, 139
particle size distribution, 55
studies of polyethylene, 163
Liquid/liquid dispersions, dilute, particle size distribution, 55
Milling yellow suspensions, birefringent and rheological properties, 37
Morphological studies, of polyethylene, 163
Particle size distribution, in dilute liquid/liquid dispersions, 55
Phenomenological rheo-optic constitutive relations, 67
Photoelastic plastics, stress-strain-time-birefringence relations with creep, 75
Polyethylene, morphological and rheological studies, 163
Polymers, amorphous, dynamic birefringence, 87
crystalline, dynamic rheo-optical properties, 113
glassy and rubbery states, orientation birefringence, 101
high, dynamic birefringence, 123
rheo-optical properties, 153
solutions, streaming birefringence, 1
Polyolefins, dynamic birefringence, 179
Rheological properties, of milling yellow suspensions, 37
Rheological research tool, streaming birefringence, 11
Rheological studies, of polyethylene, 163
Rheo-optical properties, of polymers, 153
Spherulite deformation, studies of rates by low-angle light scattering, 139
Stress-strain-time-birefringence relations, in photoelastic plastics, 75
Temperature dependence, of orientation birefringence, 101

TRANSACTIONS OF THE SOCIETY OF RHEOLOGY

Edited by BRYCE MAXWELL, *Plastics Laboratory, Princeton University;* R. D. ANDREWS, *Massachusetts Institute of Technology; and* E. H. LEE, *Brown University*. Containing the papers presented at annual meetings of the Society of Rheology, this series provides indispensable source books for up-to-date data in the field. An Interscience Series.

Vol. I *edited by* BRYCE MAXWELL. 1957. 224 pages.
Vol. II *edited by* R. D. ANDREWS. 1959. 316 pages.
Vol. III *edited by* R. D. ANDREWS. 1960. 218 pages.
Vol. IV *edited by* E. H. LEE. 1960. 370 pages.
Vol. V *edited by* E. H. LEE. 1961. 384 pages.
Vol. VI *edited by* E. H. LEE. 1962. 394 pages.
Vol. VII *edited by* E. H. LEE. 1963. 425 pages.

VISCOELASTIC PROPERTIES OF POLYMERS

By JOHN D. FERRY, *University of Wisconsin*. This book provides a uniform treatment of the viscoelastic properties and behavior of polymers. It develops the phenomenological theory of viscoelasticity, presents a wide variety of experimental methods, and appraises their applicability to polymeric materials of different characteristics. 1961. 482 pages.

VISCOSITY AND FLOW MEASUREMENT

A Laboratory Handbook of Rheology

By J. R. VAN WAZER, J. W. LYONS, K. Y. KIM, *and* R. E. COLWELL, *all of the Monsanto Chemical Company*. Here is a presentation of modern rheological theory in an easily assimilable form that can be immediately applied to experimental data. The book develops the fundamentals of rheology, discusses rotational viscometry and then reviews the present commercially available instruments used to measure viscosity and flow—including the interpretable results obtained from them. It concludes with a full discussion of viscoelasticity and its measurement. An Interscience Book. 1963. 406 pages.

INTERSCIENCE PUBLISHERS
a division of JOHN WILEY & SONS
New York • London • Sydney